GOETHE UNIVERSITÄT FRANKFURT AM MAIN

GEORG SPEYER HAUS
INSTITUT FÜR TUMORBIOLOGIE
UND EXPERIMENTELLE THERAPIE

Characterizing Conditional Knockout Mouse Models to Unravel the Physiological Function and Oncogenic Potential of Apoptosis Regulators AVEN and FUBP1

Dissertation

zur Erlangung des Doktorgrades
der Naturwissenschaften

vorgelegt beim Fachbereich Biochemie, Chemie und Pharmazie
der Johann Wolfgang Goethe-Universität
in Frankfurt am Main

von
Marlene Sophie Steiner
aus Seeheim-Jugenheim

Frankfurt am Main, 2018
(D30)

creative commons

vom Fachbereich Biochemie, Chemie und Pharmazie (FB 14) der
Johann Wolfgang Goethe-Universität als Dissertation angenommen.

Dekan:

Gutachter:

Datum der Disputation:

Erklärung

Ich erkläre hiermit, dass ich mich bisher keiner Doktorprüfung im Mathematisch-Naturwissenschaftlichen Bereich unterzogen habe.

Frankfurt am Main, den..... .....
(Unterschrift)

Eidesstattliche Versicherung

Ich erkläre hiermit an Eides statt, dass ich die vorgelegte Dissertation mit dem Titel

"Characterization of Conditional Knockout Mouse Models to Unravel the Physiological Function and Oncogenic Potential of Apoptosis Regulators AVEN and FUBP1"

selbstständig angefertigt und mich anderer Hilfsmittel als der in ihr angegebenen nicht bedient habe, insbesondere, dass alle Entlehnungen aus anderen Schriften mit Angabe der betreffenden Schrift gekennzeichnet sind.

Ich versichere, die Grundsätze der guten wissenschaftlichen Praxis beachtet, und nicht die Hilfe einer kommerziellen Promotionsvermittlung in Anspruch genommen zu haben.

Frankfurt am Main, den..... .....
(Unterschrift)

Table of Content

1 Zusammenfassung

Tumore entstehen in einem mehrstufigen Prozess, und die Mechanismen, die der Transformation einer gesunden Zelle in eine Tumorzelle zugrunde liegen, sind hoch komplex. Die Forschung der letzten Jahrzehnte hat sich intensiv mit diesen Mechanismen beschäftigt und sogenannte „Merkmale von Krebszellen“ identifiziert. Bei diesen Krebsmerkmalen handelt es sich um charakteristische Veränderungen in biologischen Prozessen, die Tumorzellen von gesunden Zellen unterscheiden und ihre malignen Eigenschaften erklären. Die identifizierten Merkmale sind: Aufrechterhaltung proliferativer Signalgebung, Vermeidung von Wachstums-Repression, Ermöglichung „replikativer Unsterblichkeit“, krebsfördernde Entzündungen, Aktivierung von Invasion und Metastasierung, Induktion von Angiogenese, Genom-Instabilität und Mutationen, Widerstand gegen Zelltod und deregulierter Energiestoffwechsel. Die wachsende Erkenntnis darüber, welche molekularen Strukturen und die damit verbundenen Funktionen für diese Merkmale von Krebs verantwortlich sind, hat die Entwicklung gezielter Krebstherapien ermöglicht. Während einer gezielten Krebstherapie („targeted therapy“) werden die Zielstrukturen spezifisch inhibiert. Weite Bereiche der Tumorbiologie sind jedoch nach wie vor unverstanden, und nur eine begrenzte Anzahl von Tumorerkrankungen kann zum heutigen Zeitpunkt durch zielgerichtete Therapie erfolgreich behandelt werden. Aus diesem Grund müssen die pro-tumorigenen Mechanismen fortwährend weiter erforscht werden, um der immensen Diversität der neoplastischen Erkrankungen begegnen zu können.

AVEN und *FUSE* Binding Protein *1* (FUBP1) besitzen beide die Eigenschaften, apoptotischen Zelltod zu verhindern und den Ablauf des Zellzyklus zu kontrollieren. FUBP1 spielt außerdem eine Rolle bei der Migration von Zellen. Diese Fähigkeiten bringen die beiden Proteine gleich mit mehreren Krebsmerkmalen in Verbindung: der Vermeidung von programmiertem Zelltod, der anhaltenden proliferativen Signalgebung, der Umgehung von Wachstumsrepression und der Aktivierung von Invasion und Metastasierung. Tatsächlich konnte eine unnatürlich hohe Expression von AVEN und FUBP1 in verschiedenen Krebsarten nachgewiesen werden, darunter Brustkrebs, akute Leukämien und Gliome. Welche molekularen Mechanismen den potentiell tumorverursachenden Eigenschaften von AVEN und FUBP1 zugrunde liegen, ist jedoch größtenteils unbekannt. Um die veränderten Eigenschaften und Funktionen von Genen zu verstehen, die zur Entstehung von Tumoren führen, ist es wichtig, die natürliche Funktion der entsprechenden Gene im gesunden Organismus zu kennen. Über die physiologische Funktion von AVEN und FUBP1 ist nur sehr wenig bekannt. Die Analyse von konstitutiven *FUBP1*-Knockout Mäusen hat gezeigt, dass FUBP1 eine wichtige Rolle

für den Erhalt und das Überleben von hämatopoetischen Stammzellen spielen könnte. Die Differenzierung von hämatopoetischen Stammzellen in Erythrozyten und verschiedene Lymphozyten schien auch durch FUBP1 beeinflusst zu werden. FUBP1 könnte außerdem für die Differenzierung von Neuronen benötigt werden. Über die physiologische Funktion von AVEN ist noch weniger bekannt. Nur eine Studie berichtet, dass AVEN-Expression für die Spermatogenese relevant sein könnte. Üblicherweise werden physiologische Genfunktionen in Knockout-Mausmodellen untersucht. Im Fall von AVEN und FUBP1 ist der Informationsgewinn aus konstitutiven Knockout Mäusen, die bis jetzt beschrieben wurden, begrenzt. Grund dafür ist die embryonale Letalität der homozygoten Defizienz der Gene, und ein fehlender Phänotyp im Fall der heterozygoten Geninaktivierung.

In dieser Doktorarbeit beschreibe ich die Etablierung und Analyse von konditionalen *Aven*- und *Fubp1*-Knockout Mäusen. Mithilfe eines Reporter-Mausmodells, in dem β-Galactosidase unter der Kontrolle des endogenen *Aven*-Promotors exprimiert wurde, habe ich die Expression von *Aven* in verschiedenen Geweben und in verschiedenen Entwicklungsstadien untersucht. Ich konnte zeigen, dass *Aven*-Expression sowohl Zelltyp-spezifisch als auch zeitabhängig ist. Eine Aktivität des *Aven*-Promotors konnte ab Tag 13.5 der Embryogenese nachgewiesen werden und erreichte maximale Werte in 15.5 Tage alten Embryos. Zum gleichen Zeitpunkt trat embryonaler Tod als Folge der homozygoten Ausschaltung von *Aven* auf. Da eine Aktivität des *Aven*-Promotors in so verschiedenen Zellen wie Neuronen, Epithel- und Muskelzellen nachgewiesen werden konnte, war es schwierig, *Aven* Expression mit bestimmten Zelleigenschaften in Verbindung zu setzen. Immunhistochemische Analysen zeigten keine vermehrte Apoptose in *Aven*-Knockout Embryos, was auf eine andere Funktion von AVEN als Apoptose-Inhibition während der Embryogenese hinweist. Da AVEN die Translation von bestimmten mRNAs, die eine spezifische Sekundärstruktur aufweisen, aktivieren kann, könnte die Rolle von AVEN während der Embryogenese in der post-transkriptionalen Regulation von gewebsspezifischen Genen in der Phase der Organdifferenzierung liegen.
In adulten Mäusen war signifikante *Aven* Promotor Aktivität im Gehirn zu sehen. Außerdem konnte ich zeigen, dass AVEN in der Brustdrüse während der Schwangerschaft und des Stillens hochreguliert wird und anschließend, während der Involution, wieder heruntergefahren wird.
Basierend auf diesen Ergebnissen habe ich Mäuse gezüchtet, in denen die Expression von *Aven* spezifisch in Neuronen und Brustepithelzellen ausgeschaltet war. Der Verlust von AVEN in diesen Zellen führte bemerkenswerterweise nicht zum Tod des Embryos, und die Histologie der betroffenen Gewebe war augenscheinlich unverändert. Offenbar

war AVEN für die (histologische) Entwicklung des Gehirns sowie für die Expansion und Involution der Epithelzellen während der Entwicklung der Brustdrüse verzichtbar.
Da eine erhöhte AVEN-Expression mit hämatologischen Krankheiten in Verbindung gebracht werden konnte, habe ich außerdem Mäuse mit einem spezifischen *Aven*-Knockout im hämatopoetischen System hergestellt. Die fehlende AVEN-Expression im blutbildenden System hatte keinen Einfluss auf die Häufigkeit von hämatopoetischen Stamm- und Vorläuferzellen oder auf die Expression von Differenzierungsmarkern in verschiedenen Blutzelllinien.
Da weder der Knockout von *Aven* im Nervensystem, noch in der Brustdrüse oder dem hämatopoetischen System die Gesundheit der Mäuse und die Integrität bzw. Homeostase der jeweiligen Gewebe beeinträchtigte, muss die genaue Funktion von AVEN, die für das Überleben der Embryos essentiell ist, noch aufgedeckt werden.

AVEN wird während der Entwicklung der Brustdrüse hoch- und wieder herunterreguliert. Des Weiteren konnte in einer nicht veröffentlichten Studie gezeigt werden, dass die Herunterregulation von AVEN in einer Brustkrebszelllinie das Tumorwachstum in einem Xenograft Experiment vollständig verhinderte. Ausgehend von diesen Ergebnissen habe ich die Rolle von AVEN in einem Mausmodell für Brustkrebs untersucht. Obwohl die Expression von AVEN in den Brusttumoren verglichen mit gesundem Gewebe erhöht war, entwickelten die Mäuse mit einem Brust-spezifischen *Aven*-Knockout zum gleichen Zeitpunkt Tumore wie ihre Geschwister mit normaler *Aven*-Expression. Auch hinsichtlich des Tumorwachstums konnte kein Unterschied zwischen den untersuchten Gruppen festgestellt werden. In Einklang mit diesen Ergebnissen konnten in den *Aven*-Knockout Tumoren weder mehr apoptotische Zellen noch eine verminderte Zellproliferation nachgewiesen werden. Zur Analyse der Rolle von AVEN im Kontext von Brustkrebs habe ich weitere, ergänzende Experimente *in vitro* durchgeführt. In Zellkulturexperimenten konnte ich zeigen, dass AVEN-Expression durch Östrogen hochreguliert wird. Die Herunterregulation von AVEN durch *short hairpin* RNAs (shRNAs) in der Brustkrebszelllinie MCF-7 führte zu leicht vermehrtem Zelltod nach UV-Bestrahlung-induzierter DNA-Schädigung im Vergleich zu Zellen, die vorher mit Kontroll-shRNA transduziert wurden. Gleichzeitig war der Metabolismus in Zellen mit verminderter AVEN-Expression leicht beschleunigt, verglichen mit Zellen mit unveränderter AVEN-Expression. Beide Effekte, vermehrte Apoptose und erhöhter Metabolismus, wurden in der Vergangenheit auch nach verminderter Expression des anti-apoptotischen Proteins BCL-x_L beobachtet. Eine anti-apoptotische Funktion von AVEN wurde bereits mit einer Protein-Protein-Interaktion mit BCL-x_L in Verbindung gebracht. Passend zu diesem Modell lassen sich die beschriebenen Beobachtungen durch verminderte Stabilisierung von BCL-x_L durch AVEN erklären.

Zusammenfassend lässt sich sagen, dass eine erhöhte AVEN-Expression in Brusttumoren vermutlich nicht die Entstehung oder das Voranschreiten der Krankheit in Mausmodellen begünstigt. Eine Überexpression des anti-apoptotischen BCL-x_L trägt zur Resistenz von Krebszellen gegenüber Chemotherapie bei. Durch die Stabilisierung von BCL-x_L könnte AVEN an Resistenzen gegenüber Chemotherapie beteiligt sein. Damit stellt die gezielte Inhibition von AVEN in Kombination mit DNA-schädigender Chemotherapie eine mögliche neue Strategie in der Krebsbehandlung dar. Da die Expression von AVEN durch Östrogen hochgefahren wird, könnte eine Inhibition von AVEN vor allem in Östrogenrezeptor-positiven Brusttumoren wirksam sein.

Um die physiologische Funktion von FUBP1 zu untersuchen, habe ich in Kooperation mit dem Deutschen Krebsforschungszentrums (DKFZ, Heidelberg) ein konditionales *Fubp1*-Knockout-Mausmodell etabliert. Während die Insertion von *loxP* Sequenzen in den *Fubp1* Lokus in einigen der generierten Mäuse bereits embryonale Letalität zur Folgen hatte, wurden andere Mäuse mit einer zelltypspezifischen Deletion von *Fubp1* entweder allgemein im hämatopoetischen System oder in EPO-Rezeptor exprimierenden Zellen lebend geboren. In diesen Mäusen war die Anzahl der hämatopoetischen Stamm- und Vorläuferzellen unverändert. Auch bei der Expression von linienspezifischen Differenzierungsmarkern, repräsentativ für die Bildung reifer Blutzellen, konnte kein Effekt des *Fubp1*-Knockouts beobachtet werden. Der fehlende Phänotyp in diesem Mausmodell stellt in Frage, ob FUBP1 für embryonale und adulte Hämatopoese essentiell ist, wie zuvor berichtet wurde. Es muss allerdings berücksichtigt werden, dass kompensierende Mechanismen, darunter Effekte eines gemischten genetischen Hintergrundes und transkriptionale Anpassungen, den Phänotyp beeinflussen können. Solche Effekte würden die Diskrepanz zwischen den beobachteten Phänotypen und den publizierten Funktionen von FUBP1 in ubiquitär konstitutiven Knockout-Mausmodellen und in Kockdown-Zellen erklären.
In einem weiteren Mausmodell, in dem ein durch die Exone 4 bis 7 codiertes Fragment in der zentralen Domäne von FUBP1 entfernt wurde, konnte ich ebenfalls keinen auffälligen Phänotyp feststellen. Aus diesem Mausmodell lässt sich schließen, dass der deletierte Bereich, der die erste KH-Struktur innerhalb der DNA-bindenden Domäne von FUBP1 umfasst, für die Proteinstruktur und Funktion von FUBP1 verzichtbar ist.
T cell acute leukemia 1 (TAL1) wurde kürzlich als ein Regulator der Transkription von FUBP1 identifiziert. Mithilfe von *Luciferase Assays* konnte ich zeigen, dass diese Regulation der *FUBP1*-Transkription durch TAL1 stark von der Integrität einer *GATA* Sequenz 340 bp oberhalb des Transkriptionsstarts von *FUBP1* abhängt. Mit Hilfe von

Chromatin-Immunpräzipitationen (ChIPs) in Lysaten primärer humaner hämatopoetischer Vorläuferzellen konnte ich außerdem nachweisen, dass der Transkriptionsfaktor GATA-1 an diese *GATA* Sequenz innerhalb des *FUBP1* Promoters bindet. Weitere ChIP Experimente zeigten, dass die Bindung von GATA-1 im *FUBP1* Promotor zunahm, wenn die primären Vorläuferzellen in die erythroide Linie differenziert wurden. Diesen Ergebnissen zufolge könnte die beschriebene Hochregulation von *FUBP1* während der Erythropoese durch einen Komplex aus Transkriptionsfaktoren und Co-Aktivatoren, der GATA-1 und TAL1 enthält, verursacht werden. GATA-1 wird im Moment der Festlegung von Vorläuferzellen auf die Magakaryozyten/Erythrozyten-Linie hochreguliert. Eine Hochregulation der FUBP1-Expression wurde nur für die erythroide, aber nicht während der megakaryozytäre Differenzierung beschrieben. Damit könnte die Hochregulation der Transkription von *FUBP1* durch einen GATA-1/TAL1-Komplex Teil eines molekularen Schalters sein, der den Weg zur erythroiden Differenzierung einleitet. Um neue Zielgene von FUBP1 zu identifizieren, die für die Erythropoese relevant sein könnten, habe ich differenzielle Genexpressions-Analysen in Zellen mit normaler und durch RNA-Interferenz verringerter *FUBP1*-Expression durchgeführt. RNA-Sequenzierungen und PCR-Arrays konnten allerdings nur geringfügig veränderte Genexpression in den Zellen mit verminderter FUBP1-Expression feststellen. Unter den Genen, deren Expression verändert war, waren Komponenten des PI3K- und NFκB-Signalweges, die beide durch Aktivierung des EPO-Rezeptors angeschaltet werden. Die Deregulation dieser Gene nach *FUBP1*-Knockdown war allerdings abhängig vom untersuchten Zelltyp. Weitere Gene, deren Expression verändert wurde, regulieren die Anzahl hämatopoetischer Vorläuferzellen und reifer Blutzellen. Zu diesen Genen gehören unter anderem *CYBB*, *RICTOR*, *TCF4* und *TXK*. Durch die transkriptionale Regulation dieser Gene könnte FUBP1 zur effizienten Differenzierung und dem Erhalt einer ausreichenden Anzahl von Erythrozyten beitragen.

FUBP1 ist Mitglied einer Familie von Transkriptionsfaktoren. Die Zielgene dieser Transkriptionsfaktoren (FUBP1, 2 und 3) überschneiden sich teilweise. Es wurde bereits vorgeschlagen, dass die verschiedenen FUBP-Proteine eine Feinregulation der gemeinsamen Zielgene ermöglichen. Die in dieser Arbeit beschriebenen Analysen der physiologischen Funktion von FUBP1 passen in ein Modell, in dem FUBP1 mit FUBP2 und 3 kooperiert, um Genexpression im Allgemeinen stabil zu halten. Sowohl die beobachteten geringen Veränderungen in der Genexpression nach *FUBP1*-Knockdown, als auch die verschiedenen beobachteten Phänotypen in *Fubp1*-Knockout Mäusen sprechen dafür, dass FUBP1 unter anderem dafür verantwortlich ist, Genexpression zu stabilisieren. In diesem Fall werden die Konsequenzen eines FUBP1 Verlusts von verschiedenen Faktoren, wie dem Mikromilieu, dem genetischen Hintergrund und dem Proliferationsstatus einer Zelle abhängen: Je nach dem Zustand einer Zelle wird die Zelle

mehr oder weniger auf die Genexpression-stabilisierende Wirkung von FUBP1 angewiesen sein. Zu den Phasen, die durch substantielle Veränderungen in der Genexpression gekennzeichnet sind, gehören Differenzierungsentscheidungen während der Embryogenese, aber auch während der adulten Hämatopoese. In eben diesen Prozessen wurde eine essentielle Rolle von FUBP1 beschrieben.

Weitreichende Veränderungen in der Genexpression kommen nicht nur bei physiologischen Prozessen während der Differenzierung von Zellen, sondern auch bei der Entstehung von Krankheiten vor. In Krebszellen führen Mutationen in einem oder mehreren Genen zu dramatischen Abweichungen in der Genexpression, die unter anderem vermehrte Proliferation, verlängertes Überleben der Zelle und verminderte Differenzierung zur Folge haben. Eine Überexpression von FUBP1 konnte in verschiedenen Krebserkrankungen wie dem hepatozellulären Karzinom (HCC) und dem Kolonkarzinom nachgewiesen werden. Die Ergebnisse meiner Doktorarbeit bekräftigen die Theorie, dass Krebszellen in einem gewissen Maß von signifikanter FUBP1-Expression abhängen, da FUBP1 der Zelle dabei hilft, die veränderten Genexpressionen zu tolerieren. Ebenso kann eine deregulierte FUBP1-Expression eine Störung der allgemeinen Genexpression zur Folge haben, die dann zur Entstehung von Tumoren beiträgt. Damit stellt die Inhibition von FUBP1 eine vielversprechende Strategie in der Krebstherapie dar – nicht nur um die entarteten Zellen selbst anzugreifenn, sondern auch in Kombinationstherapie, um die Wirkung von anderen Medikamenten zu verstärken. Eine von Forschern initiierte klinische Studie ergab bereits vielversprechende Ergebnisse bei der Behandlung von HCC-Patienten mit einem Standard-Chemotherapeutikum und dem potentiellen FUBP1-Inhibitor Irinotecan. Aktuell wird nach einem FUBP1-spezifischen Inhibitor gesucht. Die Untersuchung der Wirkung eines solchen Inhibitors alleine und in Kombination mit anderen Medikamenten wird zeigen, welches Potential FUBP1 als Zielstruktur in der Krebstherapie hat.

2 Summary

The mechanisms that underlie the transformation of a normal cell into a tumor cell are extremely complex. These mechanisms have been extensively studied in the past decades, leading to the identification of “hallmarks of cancer”. They represent characteristic changes in biological processes that discriminate tumor cells from healthy cells and rationalize their malignant transformation. Increasing knowledge about the molecular structures and the associated functions that are responsible for the hallmarks of cancer allowed their specific inhibition in targeted anti-cancer therapy. However, tumor biology is in large part still elusive, and successful targeted anti-cancer therapy is only available for a limited subset of diseases. Consequently, the continuous investigation of tumorigenic mechanisms is required to tackle the immense diversity of neoplastic entities.

AVEN and FUSE binding protein 1 (FUBP1) both display the abilities to regulate apoptotic cell death and cell cycle progression. These functions associate the two proteins with two hallmarks of cancer: resisting cell death, and uncontrolled proliferation. Indeed, aberrant expression of AVEN and FUBP1 could be demonstrated in multiple cancers. However, there is only little knowledge about their physiological function. Genetic knockout mouse models constitute a valuable tool to study gene functions. In the cases of AVEN and FUBP1, information gained from the characterizations of constitutive knockout mouse models had been limited due to embryonic lethality resulting from the homozygous knockout of both genes, while the heterozygous inactivation did not show phenotype.

In this study, I generated and analyzed constitutive and conditional *Aven* and *Fubp1* knockout mouse models to investigate their physiological function. By analyzing reporter mice expressing β-Galactosidase under the control of the endogenous *Aven* promoter, I identified *Aven* expression as both cell type-specific and dependent on the developmental stage. Maximal *Aven* promoter activity was detected in 15.5 days old embryos, a time point correlating with embryonic death in constitutive homozygous *Aven* knockout mice. Immunohistochemistry did not reveal increased apoptosis in *Aven* knockout mice, suggesting a functional role of AVEN besides apoptosis inhibition during embryogenesis.

Based on the significant *Aven* promoter activity detected in the adult brain and dynamic AVEN expression during the development of the mammary gland, I generated and characterized conditional *Aven* knockout mice with *Aven* deletion restricted to neurons or the epithelial cells of the mammary gland. AVEN depletion in these tissues did not result in embryonic lethality and the affected tissues displayed a normal histology. Since

aberrant *Aven* expression had been associated with hematologic malignancies, I also analyzed mice with an *Aven* knockout in the hematopoietic system. Loss of AVEN in the blood cells had no effect on hematopoietic stem and progenitor cell frequencies or lineage marker expression. As Loss of AVEN in the hematopoietic system, in the mammary gland or in the peripheral and central nervous system did not affect the viability of the mice and integrity of the respective tissues, the exact role of AVEN that is essential for embryo survival remains to be identified.

An unpublished study showed that knockdown of *AVEN* in a breast cancer cell line led to complete abrogation of tumor growth in a xenograft experiment. Encouraged by these results I investigated the role of AVEN in a mouse model for breast carcinogenesis. While AVEN expression seemed to be increased in breast tumors, tumor onset and progression were not altered in mice with depleted AVEN expression in the mammary gland. Consistently, *Aven* knockout tumor cells were neither less proliferative nor more prone to undergo apoptotic cell death than *Aven* wildtype tumor cells. Cell culture experiments demonstrated that AVEN expression is upregulated by estrogen. Knockdown of *AVEN* in the breast cancer cell line MCF-7 slightly increased UV irradiation-induced apoptosis and accelerated metabolism. Both effects can be explained by reduced BCL-x_L stabilization by AVEN. In conclusion, increased AVEN expression in ER^+ breast cancers seems to have no effect on tumorigenesis but might contribute to chemotherapy resistance, potentially by stabilizing BCL-x_L.

To study the physiological role of FUBP1, I generated a conditional *Fubp1* knockout mouse model in cooperation with the German Cancer Research Center. While the insertion of *loxP* sites into the *Fubp1* locus alone was embryonic lethal in some mice, other mice with a cell type-specific deletion of *Fubp1* in the hematopoietic system or EPO receptor-expressing cells were born alive. In these mice, frequencies of hematopoietic stem and progenitor cells as well as erythrocytes were unaltered. These results questioned the reported requirement for FUBP1 in embryonic and adult hematopoiesis. However, compensating mechanisms including background effects and transcriptional adaption might be responsible for the discrepancies between the observed phenotypes and reported FUBP1 function.

In cell culture studies, I could demonstrate that the previously reported upstream regulation of *FUBP1* by TAL1 depended on an intact *GATA* sequence 340 bp upstream of the transcription start of *FUBP1*. Furthermore, chromatin immunoprecipitation experiments demonstrated that GATA-1 binds to the FUBP1 promoter in primary hematopoietic progenitor cells, and this binding increased when erythroid differentiation of the cells was induced. Thus, a complex of TAL1 and GATA-1 and possibly other transcription factors and co-activators could induce the upregulation of FUBP1 during

erythropoiesis.

To identify new FUBP1 target genes with relevance for erythropoiesis, I performed differential gene expression analysis in cells with wildtype and depleted FUBP1 expression. RNA-sequencing and PCR-arrays revealed only moderately altered gene expression in *FUBP1* knockdown cells. However, among the differentially expressed genes were components of the EPO receptor signaling pathway as well as genes associated with apoptosis and proliferation of hematopoietic cells. By regulating the transcription of these genes, FUBP1 could contribute to efficient erythropoiesis.

The described analyses on the physiological function of FUBP1 support a model in which FUBP1 cooperates with FUBP2 and 3 to stabilize gene expression. This gives FUBP1 an important role in cells that experience substantial changes in gene expression. These cells include embryonic and adult stem cells, but also transforming cancer cells. Consequently, targeting FUBP1 constitutes a potential strategy in anti-cancer therapy.

3 Introduction

3.1 Apoptosis

The specific removal of cells that are not required, irreversibly damaged or potentially harmful for the organism is essential to sustain homeostasis in a multicellular organism. Controlled cell death allows to deplete dispensable and non-functional cells during organogenesis and cell differentiation. Infected, mutated or otherwise altered cells are equally eliminated to protect an organism from disease. The appearance of controlled cell death was first described in developmental studies in toads by Carl Vogt, already in the 19th century [1]. Over 100 years later, the “mechanism of controlled cell depletion” was termed “apoptosis”, derived from the ancient Greek “άποπίπτειν” = “falling off” [2]. Apoptosis is characterized by the chronological appearance of defined morphological cell features: the process begins with the rounding and shrinkage of a cell, which eventually detaches from the surrounding tissue. Concomitantly, a condensation of both the nucleus and the cytoplasm is observed, along with DNA fragmentation. The cell dissipates in small membranous vesicles which are called apoptotic bodies. The apoptotic bodies are readily engulfed and degraded by surrounding healthy cells and macrophages, avoiding inflammatory reactions [3]. A broad range of stimuli and elicitors can activate different pathways that finally initiate the described processes of apoptosis. A classification according to the molecular and other essential aspects of apoptosis initiation, execution and propagation is extensively described in the recommendations of the nomenclature committee on cell death [4]. In brief, apoptosis is discriminated into intrinsic and extrinsic apoptosis, as described in the following section.

3.1.1 The intrinsic pathway of apoptosis

Intrinsic apoptosis is mostly, but not exclusively, initiated by intracellular perturbations including DNA damage, starvation, ROS and ER stress. These perturbations lead to the irreversible mitochondrial outer membrane permeabilization (MOMP). MOMP results from the activation of BAX and BAK, pro-apoptotic members of the BCL-2 protein family. Upon activation, BAX and BAK oligomerize to form a pore in the mitochondrial outer membrane, which causes altered permeability and mitochondrial structure [4]. Consequently, “apoptogenic” factors that usually reside in the mitochondrial intermembrane compartment are released in the cytosol. The most prominent apoptogenic factor is Cytochrome c, which binds to APAF-1 to induce conformational changes under ATP consumption that result in the formation of the so-called apoptosome

complex consisting of 7 APAF-1 and CASP9 molecules [5]. In this multiprotein complex, induced proximity allows the proteolytic activation of pro-CASP9 dimers. CASP9, as it is the first activated caspase in a cascade of following proteolytic activations, is termed an initiator caspase. Cleaved CASP9 in turn activates CASP3 and CASP7, both executioner caspases that are responsible for the morphological changes observed during apoptosis (**Fig. 3.1**, right) [4].

Anoikis, apoptosis induced by the loss of integrin-dependent attachment to the extracellular matrix, constitutes a special form of intrinsic apoptosis. In this case, a perturbation of the extracellular matrix triggers MOMP, followed by CASP9 and CASP3/7 activation [4].

The intrinsic pathway of apoptosis is controlled at all stages by apoptosis promoting or inhibiting factors. An extensively studied mechanism of control is the regulation of MOMP by BCL-2 family members. Anti-apoptotic BCL-2 family members including BCL-2 itself and BCL-xL counteract MOMP by binding to BAX and BAK, thereby interfering with their oligomerization. Besides this inhibition, anti-apoptotic BCL-2 proteins can prevent MOMP by association with pro-apoptotic BH3-only activators. The most prominent representatives of these proteins are BID, BIM, PUMA and NOXA. They all transiently interact with BAX and BAK, which induces conformational changes and lead to the activation of BAX and BAK. Thus, by sequestering BH3-only activators, BCL-2, BCL-xL and others indirectly inhibit MOMP (**Fig. 3.1**, right) [4], [6].

3.1.2 The extrinsic pathway of apoptosis

The extrinsic pathway of apoptosis is initiated by extracellular perturbations that are signaled into the cell via cell surface receptors. Pro-apoptotic receptor signaling is either activated by ligand binding to so called death receptors or insufficient ligand binding to so called dependence receptors [4]. Ligand binding to death receptors, among them FAS and members of the TNF receptor superfamily, induces conformational changes that result in the formation of death inducing signaling complexes (DISCs) at the intracellular tail of the receptors [7]. Within these multiprotein complexes, initiator Caspase 8 or Caspase 10 are assembled and activated. The exact composition of the DISCs depends on the activated receptor and influences the degree of caspase activation – even the inhibition of caspase activation is possible [4]. Following CASP8 and CASP10 activation, apoptosis is propagated in two different pathways. One pathway requires the cleavage BH3-only protein BID, leading to MOMP and CASP9-dependent CASP3 and CASP7 activation. The other pathway cleaves and activates the executioner caspases MOMP-independently (**Fig. 3.1**, left) [4].

Dependence receptors comprise, amongst others, Netrin1 receptors, the neurotrophin receptor NTRK3 and sonic hedgehog receptor patched 1 (PTCH1). Under physiological

conditions, sufficient ligand binding activates pro-proliferative, pro-survival and pro-differentiation signaling, but if the level of ligands falls below a certain threshold, the dependence receptors induce apoptosis. The propagation of apoptosis follows various pathways, depending on the initiating receptor: initiator and executioner caspases can be directly activated, following MOMP, a p53-dependent regulated cell death can be induced and cell death may occur as a consequence of transcriptional upregulation of pro-apoptotic genes (**Fig. 3.1**, left) [4].

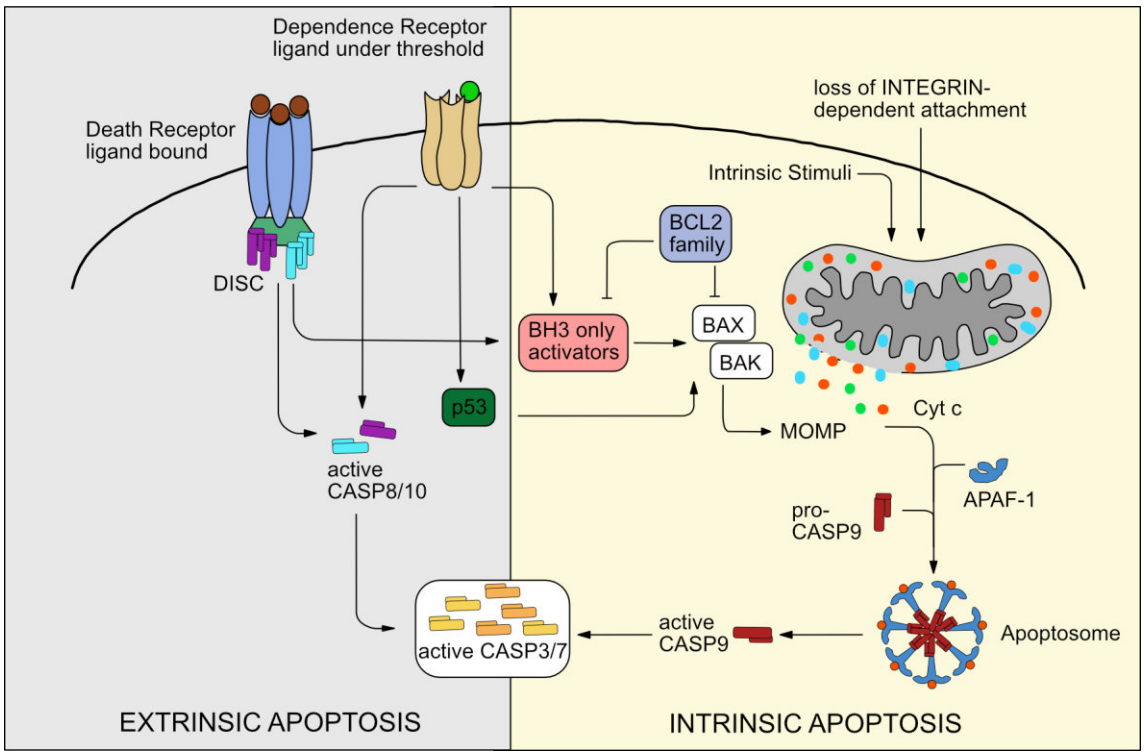

Figure 3.1: Apoptotic signaling pathways
According to the Nomenclature Committee on Cell Death, the extrinsic pathway of apoptosis is triggered by perturbations of the extracellular microenvironment and detected by plasma membrane receptors. Receptor signaling activates CASP8 and/or CASP10, which in turn activate executioner caspases (mainly CASP3 and CASP7). The intrinsic pathway of apoptosis is induced either by loss of INTEGRIN-mediated attachment (Anoikis) or alternatively, upon intrinsic perturbations like DNA damage, starvation and reactive oxygen species (ROS) signaling. Mitochondrial outer membrane permeabilization (MOMP) activates Casp9 in the so-called apoptosome and results in the activation of the same executioner caspases as used by the extrinsic pathway. For details see text. Cyt c: Cytochrome c; DISC: Death receptor induced signaling complex.

3.2 The apoptosis and cell cycle regulator AVEN

3.2.1 Apoptosis regulation by AVEN

AVEN has first been identified in a yeast-two-hybrid screen that was performed by Chau

and colleagues [8] as an interaction partner of BCL-xL. The assay was performed using a BCL-x_L mutant, which is unable to bind pro-apoptotic BAX and BAK, with the intention to isolate anti-apoptotic proteins acting downstream of BCL-x_L. Further analysis revealed that the interaction of AVEN with BCL-x_L not only enhanced the anti-apoptotic effect of BCL-x_L, but BCL-x_L mutants without anti-apoptotic potential simultaneously lost their ability to bind AVEN together with their anti-apoptotic potential.

Besides BCL-x_L, the apoptotic protease-activating factor APAF-1 also interacted with AVEN. This interaction interfered with the oligomerization of APAF-1, inhibiting Caspase 9 (CASP9) activation in the apoptosome. Thus, two possibly independent mechanisms of action for the anti-apoptotic function of AVEN were suggested: AVEN prevents apoptosis by interacting with and enhancing the function of BCL-x_L, and/or AVEN protects cells from apoptosis by binding to APAF-1, thereby inhibiting the formation of the apoptosome. The results of following studies, in part contradictory, provided further evidence for both mechanisms.

In Chinese hamster ovary (CHO) cells, the protective effect of AVEN alone was limited but seemed to be synergistically enhanced in combination with BCL-x_L, at least in the context of certain apoptosis stimuli [9]. In 2010, AVEN was reported to require BCL-x_L for the inhibition of DNA damage-induced apoptosis in various breast cancer cell lines [10]. As AVEN prevented the DNA damage-induced decrease of BCL-x_L levels, the authors concluded that the anti-apoptotic potential of AVEN relied on its ability to stabilize BCL-x_L.

In contrast, apoptosis in MCF-7 and RKO cells could only be reduced by AVEN after proteolytic procession by Cathepsin D (CATHD), which removed the N-terminus of AVEN [11]. CATHD cleavage is predicted to occur between AVEN amino acids (aa) 196 and 197 and, to a certain extent, also between aa 144/145. The truncated ΔN-AVEN was not able to interact with BCL-xL, consistent with a BCL-x_L interaction domain at aa 74-104, however, ΔN-AVEN co-precipitated with APAF-1. An interaction between ΔN-AVEN and BCL-xL could also be mediated by a potential BH3 domain consisting of aa 141-153, which was identified in a computational approach searching for novel BH3-only proteins [12]. Concluding from these publications, AVEN can prevent apoptosis by more than one molecular mechanism, probably depending on the cell-type and particular conditions.

3.2.2 Cell cycle regulation by AVEN

In 2008, AVEN was found to play a role in cell cycle regulation. Guo et al [13] demonstrated that AVEN was able to interact with and activate ataxia telangiectasia mutated (ATM) kinase in response to DNA damage. ATM senses DNA double strand breaks and, by phosphorylating its substrates, activates DNA damage responses, including cell cycle arrest at the G2/M stage [14]. In *xenopus laevis* oocytes, ATM-

induced cell cycle arrest was dependent on AVEN. Following activation, ATM phosphorylates AVEN, thereby increasing the ATM-activating potential of AVEN. Thus, ATM regulates AVEN activity in a positive feedback loop. A similar role in cell cycle regulation was shown for dAven, the *Drosophila melanogaster* orthologue of AVEN [15]. The dual role in regulating the mitochondrial pathway of apoptosis and DNA damage-induced cell cycle arrest enables AVEN to regulate cell fait: as with APAF-1 and pro-apoptotic BID, AVEN might be involved in the translation of the signals “low DNA damage” into cell survival and “extensive DNA damage” into apoptosis [16].

3.2.3 Regulation of translation by AVEN

In 2015, a third function of AVEN was revealed, as the protein was found to bind G-quadruplexes (G4) in mRNA in a methylation-dependent manner [17]. G4s represent highly stable secondary structures found in both DNA and RNA [18] that are formed by stacks of planar guanine tetrads. When present in RNA, they can stall or slow down translation. A complex of AVEN and the helicase DHX36 bound to G4 structures within mRNA was demonstrated to elevate translation of the respective mRNAs, adding the regulation of translation as another AVEN functions (**Fig. 3.2**).

3.2.4 Upstream regulation of AVEN

For the upstream regulation of AVEN, both transcriptional and post-translational mechanisms have been identified. Inhibition of nuclear export of AVEN, which depends on an intact leucine rich nuclear export signal (LR-NES) at aa 282 – 293, and which involves the nuclear exporter Exportin-1/CRM1, resulted in altered cell cycle regulation by AVEN [19]. Apparently, the cell cycle regulation by AVEN is, at least in part, regulated by its subcellular distribution. O´Shea et al [20] reported that apoptosis inhibition by AVEN is equally affected by its subcellular distribution. In bovine oocytes, progesterone (P4) stimulates a cytoplasmic localization of AVEN, which correlates with increased BCL-x_L protein levels and effective apoptosis inhibition. Although the authors assume a non-transcriptional regulation of AVEN by P4, the *Aven* promoter contains a potential progesterone binding element consensus sequence, so that transcriptional control of *Aven* by P4 appears also possible. Interestingly, hormonal regulation of *Aven* transcription could be demonstrated for 17β-estradiol (E2), which increased *Aven* mRNA expression in rat seminiferous tubules [21].

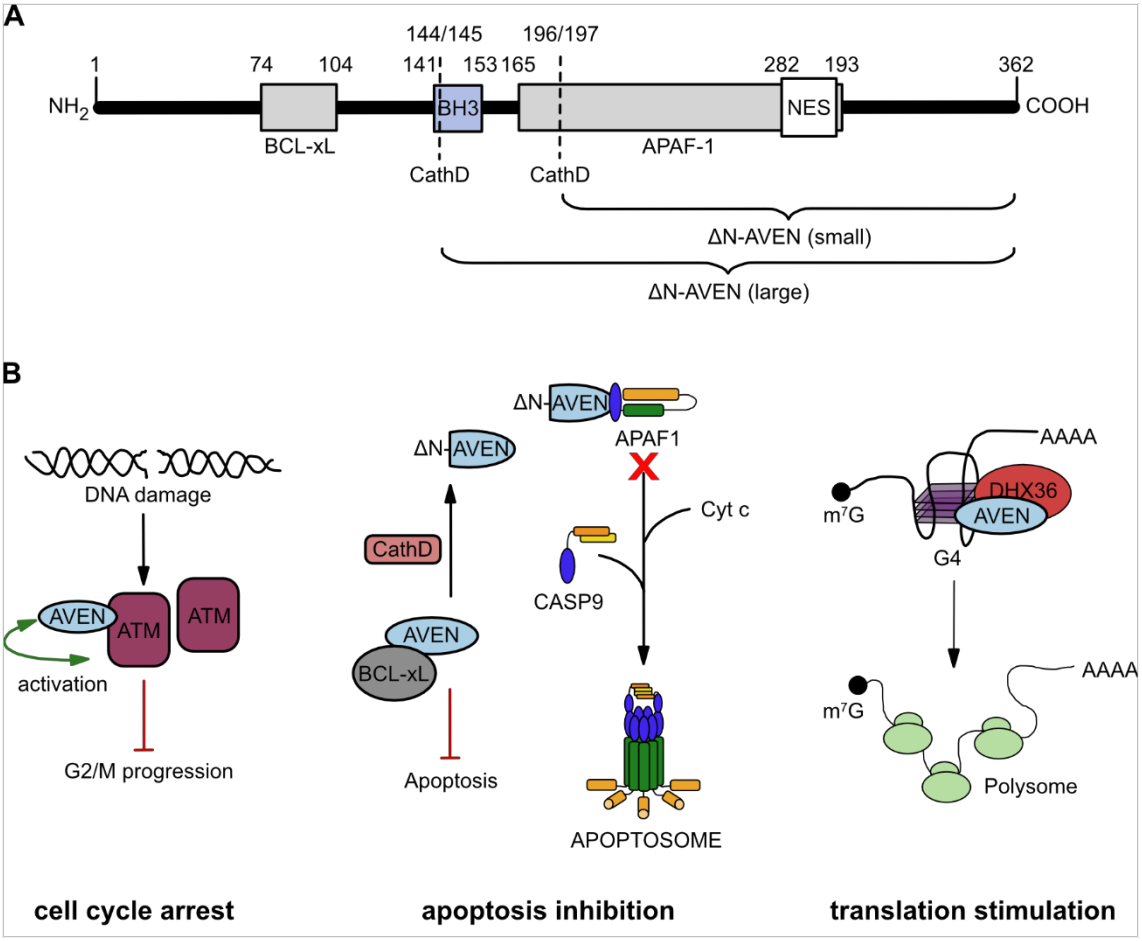

Figure 3.2: AVEN: structural features and models of action
A. Schematic representation of AVEN proteins. Processing by Cathepsin D removes the N-terminus, building a small or large truncated ΔN-AVEN dependent on the precise cleavage site. Protein section that are required for BCL-x_L and APAF1 binding are indicated. Numbers represent the position of amino acids. BH3: BCL2 homology domain 3. NES: Nuclear Export signal. B. Scheme of AVEN functions. AVEN regulates cell cycle progression by activating the DNA damage response machinery after DNA double strand breaks (left). Both, stabilization of BCL-x_L and interference with the formation of the apoptosome, inhibit apoptosis (middle). Together with the helicase DHX36, AVEN stimulates translation of mRNAs with G4 secondary structures. ATM: ataxia telangiectasia mutated kinase. m^7G: 7-methylguanolyte cap. AAAA: polyadenylation tail. G4: guanine quadruplex secondary structure.

3.2.5 The physiologic and pathologic role of AVEN

So far, little is known which of the identified functions of AVEN are required for normal life processes in cells, tissues and organs. A widespread expression of *Aven* was firstly reported by Chau [8]. A specific expression of a short *Aven* mRNA was found in post-meiotic murine spermatids. In these cells, AVEN is thought to control apoptosis together with BCL-x_L and APAF-1, which is essential for normal spermatogenesis [22]. Consistently, insufficient AVEN expression is associated with defective spermatogenesis in rats and humans [21]. Apoptosis control by AVEN is thought to be required to protect bovine oocytes and *xenopus* oocytes from cell death during maturation [20]. In regulatory T cells, AVEN could cooperate with Foxo-1 to mediate its proliferation promoting and

apoptosis inhibiting effects [23].

Apoptosis deregulation is associated with cancer development and progression, as well as with cancer therapy resistance. Resisting cell death has indeed been defined as a hall mark of cancer [24]. Identification of the exact mechanisms that control apoptosis and the involved players represents a prerequisite to understand tumor biology. This was the original purpose of screens looking for anti-apoptotic genes that resulted in the identification of *AVEN*. Consistently, deregulated AVEN expression has been associated with various cancers. Increased *AVEN* expression has been found in acute leukemias and correlated with poor prognosis in childhood acute lymphoblastic leukemia [25], [26]. In a transgenic mouse model, overexpression of *Aven* accelerated leukemogenesis in cooperation with the heterozygous loss of *p53*. Furthermore, knockdown of *Aven* in mouse xenograft experiments significantly decreased tumor growth [27]. These studies demonstrate the oncogenic potential of AVEN, especially in the context of hematopoietic malignancies. Implication of aberrant AVEN function in solid tumors was suggested by Kutuk et al. [10] who reported an altered AVEN localization in breast cancer tissues, and Ouzounova [28] who found elevated *AVEN* expression in breast cells with high tumor initiating potential. Furthermore, high AVEN expression levels were found in lung metastasis of osteosarcoma patients. In these patients, AVEN expression also correlated inversely with metastasis-free survival [29]. The same publication suggested that AVEN contributes to chemotherapy resistance in osteosarcoma. This hypothesis is strengthened by the report that AKT-regulated overexpression of *AVEN* in MCF-7 cells led to reduced sensitivity to anti-cancer drugs [30]. Finally, a combination treatment of glioma cells effectively reduced *AVEN* expression and induced apoptosis [31].

3.3 Apoptosis and cell cycle regulator FUBP1

3.3.1 Transcriptional regulation by FUBP1

Far upstream element (FUSE) binding protein 1 (FUBP1) was identified as a factor binding to the *FUSE* sequence in the promoter of the proto-oncogene *c-MYC*, 1.5 kb upstream of the transcription start [32]. FUBP1 specifically binds the single stranded (ss) non-coding strand of *FUSE* via its central domain, while its C-terminal domain interacts with the basal transcription machinery, leading to an upregulation of *c-MYC* expression. The N-terminus of FUBP1 is able to interfere with this C-terminal-mediated transactivation [32], [33], [34]. Further detailed analysis of the transcriptional activation

of *c-MYC* transcription activation by FUBP1 led to the following model:

FUBP1 requires an open chromatin structure of the *c-MYC* promoter to induce peak transcription. The open chromatin structure is found in cells actively expressing *c-MYC* at a basal level. Loading of the transcriptional machinery and movement of RNA polymerase II (POLII) cause negative supercoiling in the upstream promoter region. This torsional stress facilitates DNA melting of the AT-rich *FUSE* DNA double strand and allows FUBP1 to bind [35]. FUBP1 might generate a single stranded *FUSE* in the destabilized supercoiled DNA itself as it possesses an ATP- and Mg^{2+}-dependent helicase activity [36]. The single stranded *FUSE* is bound by the central domain of FUBP1, which consists of four RNA and ssDNA binding hnRNP K-homology (KH) domains [32]. Each of the KH domains forms a contact point with *FUSE*, but KH3 and 4 are sufficient for DNA binding, constituting the minimal binding motif [37]. The length and base pair composition of the spacers between the contact points contribute to minimal secondary structure and high flexibility of the ssDNA, which mirrors structure variability of DNA-bound KH domains. This flexibility is thought to enable interaction with moving and conformationally changing proteins like POLII [38]. *FUSE*-bound FUBP1 interacts with the basal transcription factor IIH (TFII(H), part of the transcription complex) via three tyrosine rich motifs in its C-terminal domain, causing a looping of DNA [39]. This interaction stimulates the helicase activity of TFIIH and promotes promoter escape of the associated POLII complex. As a result, *c-MYC* transcription is upregulated [33], [40]. The FUBP1-induced peak expression of *c-MYC* is repressed by FIR (FUBP1 interacting repressor). FIR binds *FUSE* and FUBP1 in a stable tripartite complex. *FUSE*/FUBP1-bound FIR dimerizes, forming a quaternary complex. The N-terminal repression domain of FIR interacts with TFIIH, thereby replacing the C-terminal FUBP1 transactivation domain and inhibiting helicase activity. In this manner, *c-MYC* transcription is downregulated back to basal levels. Upon transcriptional repression, FUBP1 is removed from the complex, while the FIR dimer remains bound for a certain period of time. FIR eventually dissociates from *FUSE*, probably induced by the re-annealing of *FUSE* upon termination of transcription [39], [41]. The features of the FUBP1 protein and the model of translational regulation of *c-MYC* are shown in **Fig. 3.3**.

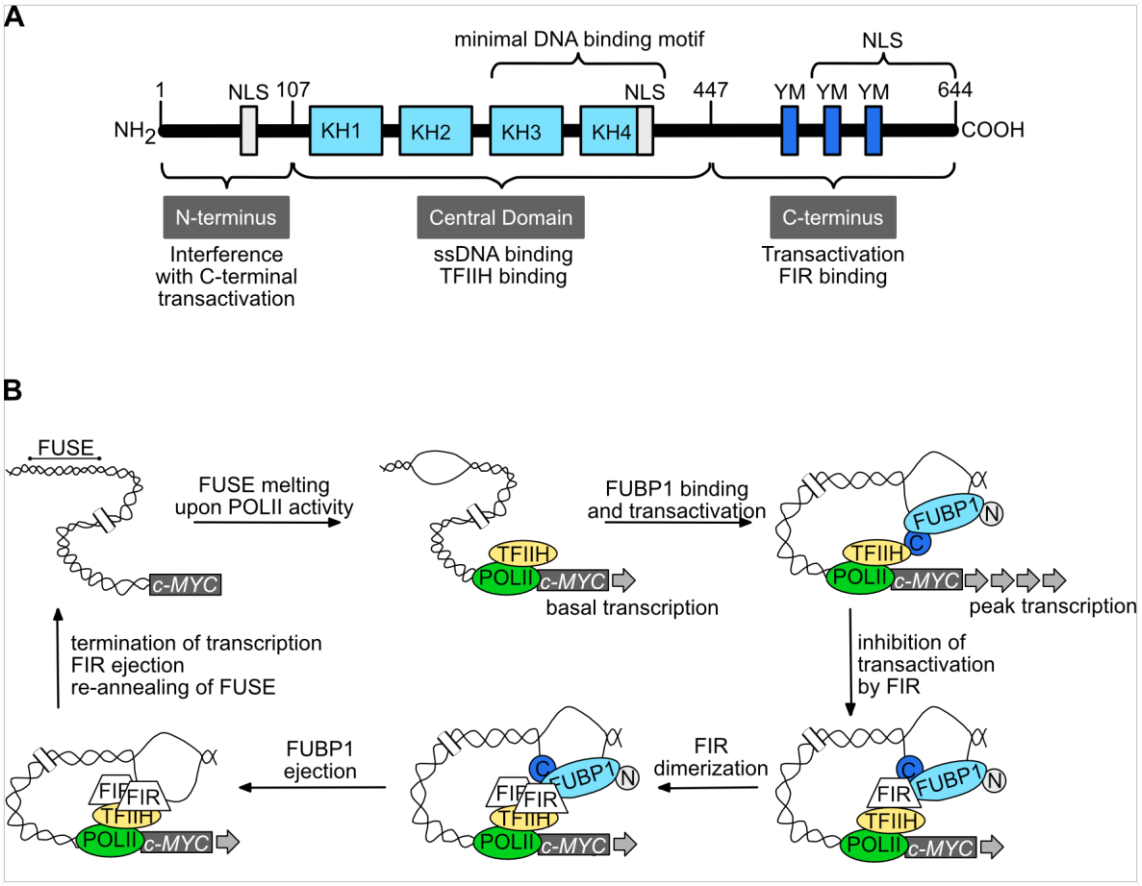

Figure 3.3: FUBP1: structural features and model of transcriptional *c-MYC* regulation
A. Scheme of the FUBP1 protein domains. Numbers represent the position of amino acids. The model is not true to scale. Adapted from [42]. NLS: nuclear localization signal. KH: hnRNP K-homology domain. YM: tyrosine-rich motif. B. Mechanism of *c-MYC* transcriptional regulation by FUBP1. During basal transcription of *c-MYC*, RNA polymerase II (POLII) binding and movement at the promoter cause torsional stress, leading to the unwinding of the *FUSE* sequence, 1.5 kb upstream of transcription start. FUBP1 binds the single-stranded *FUSE* via its central domain and interacts with TFIIH of the basal transcription machinery via its C-terminus, causing DNA looping. This interaction enables peak expression of *c-MYC*. FIR eventually replaces FUBP1 from TFIIH, thereby reducing *c-MYC* expression back to basal levels. Dimerization of FIR is followed by ejection of FUBP1 from *FUSE*. Upon termination of *c-MYC* transcription, FUSE re-anneals and FIR leaves the promoter site. Adapted from [43].

Further *FUSE* motifs have been identified in the promoters of cell cycle inhibitor *p21*, ubiquitin hydrolase *USP29* and apoptosis inducer *BIK* [44], [45], [46]. In contrast to *c-MYC* regulation, FUBP1 downregulates the transcription of these genes. The exact mechanism of this transcriptional repression remains to be elucidated. Of note, the *FUSE* sequence within the USP29 promoter better matches the “perfect binding sequence” that was proposed by Benjamin and colleagues [37] than does the *FUSE* sequence in the *c-MYC* promoter. Consequently, FUBP1 might bind more tightly to the *USP29 FUSE*, demonstrating how sequence composition could modulate binding site specificity of FUBP1.

3.3.2 Regulation of RNA by FUBP1

Binding of single-stranded nucleic acids is rather associated with RNA binding than DNA binding proteins – most transcription factors recognize double strand motifs. Indeed, RNA binding by FUBP1, associated with various effects, has been demonstrated:

FUBP1 confers increased stability to *GAP43* mRNA which plays an important role in neuronal development [47]. In contrast, FUBP1 destabilizes the mRNA of *p21.* Regarding the *FUSE* motif in the *p21* promoter, too, FUBP1 has the potential to target this gene on both the transcriptional and the post-transcriptional level [44], [48]. Similar to stability regulation, the effects of FUBP1 on translation are opposing: *nucleophosmin* mRNA translation is downregulated by FUBP1, while it promotes translation of *p27* mRNA [49], [50]. The same is true for the role of FUBP1 in viral replication: FUBP1 facilitates the replication of Hepatitis C virus and Enterovirus 71 but interferes with the replication of Japanese encephalitis virus [51], [52], [53], [54]. More recently, the potential of FUBP1 to modulate mRNA splicing was revealed, as FUBP1 is required for the alternative splicing of the oncogenes *MDM2*, *DMD* and *LSD1+8a* [55], [56], [57]. In summary, FUBP1 is a regulator of mRNA stability, translation, splicing and viral replication.

3.3.3 Upstream regulation of FUBP1

While several FUBP1 downstream targets have been identified, knowledge about the upstream regulation of FUBP1 is limited. However, control of FUBP1 levels on both mRNA and protein levels, as well as extracellular molecules that induce up- or downregulation of FUBP1 levels, have been presented. On the transcriptional stage, T cell acute lymphocytic leukemia protein 1 (TAL1) binds the FUBP1 promoter in cell lines and primary $CD34^+$ donor cells, resulting in an activation of the FUBP1 promoter [58]. The protein level of FUBP1 is regulated via ubiquitin-dependent degradation. FUBP1 is a substrate of the E3 ubiquitin ligase PARKIN and it is bound by p38/JTV-1, a subunit of the multi-aminoacyl-tRNA synthetase (ARS) complex. Both interactions promote ubiquitination of FUBP1 and subsequent proteasomal degradation [59], [60]. FUBP1 ubiquitination is counteracted by ubiquitin specific protease 22 (USP22) [61]. TGF-β signaling induces FUBP1 degradation by activating p38/JTV-1 but is repressed by prostaglandin E3 signaling [59], [62].

FUBP1 action also seems to be controlled by the localization of the protein. FUBP1 contains three nuclear localization signals (NLS): a classical bipartite NLS in the N-terminal domain, an alpha-helical NLS in KH3 within the central domain, and a tyrosine rich NLS in the C-terminal domain. Mutations of any of the NLSs result in changes in the nuclear localization [63]. CASP7 cleavage of FUBP1 disrupts the NLS in the N-terminal domain and causes cytoplasmic retention [64].

3.3.4 The physiological role of FUBP1

FUBP1 expression is widely spread throughout cells, tissues and organisms [65]. Already the first publications about FUBP1 reported a correlation of *FUBP1* expression with highly proliferative phases of undifferentiated cells, mirroring *c-MYC* expression [32] [34]. Consistently, FUBP1 has been shown to regulate the expression of several cell cycle regulators: besides *c-MYC*, FUBP1 also activates *Cyclin D2* (*CCND2*) [44] and *TCTP*, an inhibitor of cell cycle repressor p53. Concomitantly, FUBP1 inhibits expression of p53 activator *BCCIP* and cell cycle inhibitors *p21* and *p15* [66], [44]. FUBP1 also interacts with and thereby interferes with p53 on protein level [66]. By controlling p53 levels, FUBP1 also impacts apoptosis, as accumulation of p53 over a certain threshold induces regulated cell death. Further apoptosis-related genes that are also regulated by FUBP1 include *BIK*, *NOXA*, *TRAIL* and *TNF-α* [44]. They all are pro-apoptotic and repressed by FUBP1. FUBP1 also regulates apoptosis on another level. In staurosporine-treated MCF-7 cells, FUBP1 is cleaved by CASP7, which results in redistribution of FUBP1 to the cytoplasm. This change in FUBP1 localization is associated with reduced *c-MYC* expression and apoptosis induction [64]. In the context of oxidative stress, FUBP1 activates USP29, which deubiquitinates and thus stabilizes p53, resulting in apoptosis induction [45].

The potential of FUBP1 to inhibit apoptosis while promoting proliferation is essential for the survival and functionality of long-term hematopoietic stem cells (LT-HSCs) [43], [67]. The constitutive knockout of *Fubp1* in mice proved to be embryonic lethal between 10.5 and 15.5 dpc. Living homozygous embryos were anemic and appeared smaller than their wildtype littermates. *Fubp1* knockout fetal liver cells had a dramatically reduced repopulation potential in competitive transplantation assays. The effect on lineage differentiation varied between the two studies: *Fubp1* knockout cells from gene trap models only showed impaired erythropoiesis, knockout cells from a germline deletion model also showed reduced granulocyte-macrophage and lymphoid lineage differentiation. An important role of FUBP1 for erythropoiesis was also suggested by an *in vitro* study that demonstrated decreased erythroid differentiation potential of murine embryonic stem cells after *Fubp1* knockout [68]. Furthermore, T-cell acute lymphocytic leukemia protein 1 (TAL1), a master regulator of erythropoiesis, activates enforced *FUBP1* expression during the erythroid differentiation of primary human $CD34^+$ stem and progenitor cells, which is required for efficient differentiation [58].

The question, whether disturbed numbers and function of FUBP1-deficienct LT-HSCs and/or impaired erythropoiesis account for embryonic lethality of constitutive *Fubp1* knockout mice still remains open.

Besides hematopoiesis, FUBP1 might play a role in neuronal development. Its RNA

regulating function is required for the stable expression of *GAP43* and *LSD1+8* [47], [57], the genes that are both essential for neuron differentiation.

3.3.5 FUBP1 in cancer

By regulating apoptosis and proliferation, FUBP1 controls biological processes whose deregulation is involved in three hallmarks of cancer: resisting cell death, sustaining proliferative signaling and evading growth repression [24]. Confirmed targets of FUBP1, including *c-MYC* and *p53*, further emphasizes an oncogenic potential of FUBP1. *c-MYC* is overexpressed or over-activated in more than 50% of all human cancers. Aberrant *c-MYC* expression is not always the result of mutations in the *c-MYC* gene but might also be a consequence of constitutive active signaling pathways inducing *c-MYC* expression [69]. Deregulation of the FUBP1/FUSE/FIR transcription machinery constitutes yet another possibility for carcinogenic *c-MYC* expression: FUBP1 overexpression and activity as well as FIR downregulation or inactivity would lead to increased *c-MYC* expression.

Loss of function mutations in *p53* have been identified in ~50% of all human cancers, and an otherwise impaired p53 function is actually found in almost all of them [70]. As previously described, FUBP1 controls *p53* expression at the transcriptional level via transcriptional activation of *TCTP* and repression of *BCCIP*. Direct interactions between FUBP1 and p53 interfere with p53 function and FUBP1 promotes splicing of p53 inhibitor *MDM-2* [66] [55]. MDM-2 overexpression occurs in many tumors and can alone be the trigger of malignant transformation [71].

Indeed, aberrant FUBP1 activity has been identified in several cancers, summarized in **table 3.1** [42]. In most cancer entities, FUBP1 is overexpressed, but deficient FIR function can also be responsible for deregulated FUBP1 action, namely in cases of hepatocellular carcinoma (HCC) and colorectal cancer [72], [73]. Interestingly, *c-MYC* overexpression or reduced p53 levels are not always detected in FUBP1 overexpressing tumors. Weber and colleagues [74] found increased *c-MYC* expression in clear renal cell carcinoma but not in bladder and prostate cancer. In HCC, strong FUBP1 expression, which is almost absent in healthy tissue, promotes tumor growth by downregulating the pro-apoptotic *BIK*, *NOXA*, *TRAIL* and *TNFα* genes as well as the cell cycle inhibitors *p21* and *p15*, while differential *c-MYC* or *p53* expression was not reported [44]. Dixit et al [54] described another mechanism of FUBP1 promoted liver tumorigenesis: FUBP1 facilitates the replication of HCV in hepatocytes – which already has a cancerogenic potential as HCV infection and secondary liver cirrhosis constitute a major risk to develop liver cancer [75]. Furthermore, HCV replication is supported by FUBP1 via interference with p53 transcription and function, generating another tumor promoting feature [54].

FUBP1 potentially plays a role in metastasis. Not only via controlling the expression of

c-MYC, which is known to regulate migration, but also via controlling the expression of stathmin family members, FUBP1 expression is associated with enhanced migration and metastasis formation [76].

Oligodendroglioma represents an exception, because in this entity, mutations predicted to inactivate FUBP1 function were detected [77]. The authors speculate that the inactivation of FUBP1 results in reduced negative regulation of *c-MYC* by FIR, giving FUBP1 the character of a tumor suppressor in this scenario. Two other mechanisms support a tumor suppressive function of FUBP1. As previously described, FUBP1 activates USP29, thereby stabilizing p53 and inducing apoptosis in the context of oxidative stress [45]. Additionally, FUBP1 is required for splicing of *LSD1+8*, a factor activating neuronal differentiation and preventing tumorigenesis. Thus, defective splicing of *LSD1+8* in FUBP1-deficient neurons could contribute to development of oligodendroglioma [57]. The role of FUBP1 in cancer is summarized in table 1.

***Table 3.1**: Deregulated FUBP1 activity in cancer*

Malignancy	Alteration	Downstream target	Reference
Bladder cancer	FUBP1 ⬆	NA	[74]
Clear cell renal cancer	FUBP1 ⬆	C-MYC ⬆	[74]
Colorectal cancer	FIR*	C-MYC ⬆	[72], [78]
Colorectal cancer	FUBP1 ⬆	NA	[79]
Gastric cancer	FUBP1 ⬆	NA	[42]
Glioma	FUBP1 ⬆	C-MYC ⬆	[80] [81]
Liver	FUBP1 ⬆	BIK ⬇, NOXA ⬇, P21 ⬇, p15 ⬇, TNF ⬇, TRIAL ⬇, Cyclin D2 ⬆	[44]
Liver	FUBP1 ⬆	Stathmin ⬆	[82], [83]
Liver	FIR ⬆	FUBP1 ⬆	[73]
Non-small cell lung cancer	FUBP1 ⬆	Stathmin 1/3 ⬆	[76]
Oligodendrogliome	FUBP1*	NA	[77]
Prostate cancer	FUBP1 ⬆	NA	[84]

Adapted from [42] and [43]. NA: not available. ⬆: upregulated expression. ⬇: downregulated expression. *: loss of function mutation.

3.3.6 FUBP1 as a proto-oncogene with tumor-suppressive function

Altogether, FUBP1 integrates well into the list of proto-oncogenes with particular tumor-suppressor functions (POTSFs), which also includes its target genes *c-MYC* and *p53*. POTSFs have been listed and characterized by Shen and Wang [85]. Although FUBP1 does not appear in this list, it shares most qualities of POTSFs: about 50% of POTSFs are transcription factors which can act both as activators or repressors of their targets.

They are ubiquitously expressed and are not exclusively associated with one cancer type but rather with several entities. The intracellular localization of POTSFs is predominantly nuclear. In cancer tissue, POTSFs likely acquire gain of function mutations which are associated with reduced protein expression of the tumor suppressors. This is represented by FUBP1 over-expression in the liver which is accompanied by downregulation of pro-apoptotic targets. A single mutations in POTSFs can potentially activate their proto-oncogenic function AND disrupt their tumor-suppressor function, making them, including FUBP1, particularly interesting targets in anti-cancer therapy. An investigator-driven HCC study already produced promising results using double treatment with standard chemotherapeutic Mitomycin C and the potential FUBP1 inhibitor Irinotecan: Among 6 treated patients, a response rate of 67%, including one complete remission was observed, while interruption of treatment-causing side effects were absent [46].

Interestingly, leukemia is over-represented among cancers that display POTSFs mutations. A leukemia-promoting role of FUBP1 could recently be demonstrated in our lab. Knockdown of *Fubp1* prolonged survival of mice in chronic and acute myeloid leukemia (AML and CML) mouse models. Increased FUBP1 expression was found in patient samples compared to healthy samples. In both malignancies, FUBP1 expression correlated with bad outcome, and in CML, FUBP1 expression also reflected the advance of disease [86].

3.3.7 The FUBP family

FUBP1 has two highly homologous siblings, FUBP2 and FUBP3, and a potential third one in *c. elegans* that together comprise the FUBP1 family. FUBP1 is not only the first identified member of the family, but also the oldest, as it shares higher homology with both FUBP2 and FUBP3 than do the latter ones among each other [34]. Chung et al. [87] compared the features of FUBP1, 2 and 3 in detail: located at different chromosomes within the human genome (1p31.1, 19913.3 and 9q34.11, respectively), all three genes share overlapping sequences and show a high degree of structural similarity. The central DNA binding domain comprising four KH domains and the C-terminal transactivation domain containing tyrosine-rich motives are found in all FUBP family members. However, only FUBP1 has been shown possess a helicase activity [36]. The N-terminus differs between the family members, causing decisive functional differences: only FUBP1 and 2 interact with and are repressed by FIR. Both proteins are also mostly localized in the nucleus. Because of a missing hydrophobic sequence motif and NLS in the C-terminus of FUBP3, this molecule does not interact with FIR and is distributed equally in the nucleus and cytoplasm. FUBP3 differs further from the other FUBPs as it moves

slower in the nucleus. Concerning the transactivation capacity, FUBP3 causes the strongest promoter activation, followed by FUBP1, while FUBP2 shows the least activating potential. Looking at the expression of FUBPs, all members are ubiquitously expressed, although at differing levels [34].

The function of FUBP3 has so far hardly been studied: there is one publication reporting translation activation of fibroblast growth factor 9 mRNA [88]. Of note, FUBP3 occupies the *c-MYC* promoter before FUBP1 is recruited [87].

A larger amount of investigation in the past dealt with the RNA-binding potential of FUBP2, which allows FUBP2 to regulate mRNA stability, trafficking, translation and splicing (reviewed in [89]).

Differential gene expression analysis after knockdown of each of the three FUBP family members revealed largely overlapping targets [87]. Concluding from similarities and differences, the FUBP family members regulate common targets but with member-specific effects resulting from variances in protein-interactions and promoter activating potential. The influence on a certain target and its outcome will likely depend on the interplay of availability, stoichiometry, affinity and mobility of the FUBPs. Functional redundancy of the FUBPs to a certain degree seems to allow compensating mechanisms. *FUBP2* knockdown results in increased FUBP1 expression. However, the knockdown and knockout of the distinct *FUBPs* generates specific phenotypes: while the constitutive knockout of *FUBP1* in mice is embryonic lethal, knockout of *FUBP2* and *3* is not [83], [43], [67]. The issue emphasizes the divergence of FUBP functions and suggests that all three are required to sustain cell homeostasis.

3.4 Hematopoiesis

The formation of mature blood cells, which fulfill functions as different as immunity, oxygen supply and clot formation, is termed hematopoiesis. Mature blood cells are short lived, with average life times of 13 to 120 days. Thus, they need to be continuously regenerated to allow homeostasis. This is achieved by hematopoietic stem cells (HSCs) which have the potential to differentiate into all the distinct lineages via sequential steps of commitment and specification. To allow sustained production of blood cells, HSCs need to balance between self-renewal (meaning the replication of stem cells with all its features) and differentiation [90]. This balance, as well as the steps of lineage differentiation, are highly regulated by factors including transcription factors, miRNAs and factors of the microenvironment, the so called “niche” of hematopoiesis. The factors

regulating hematopoiesis vary over time, resulting in age- and stage-specific characteristics of hematopoiesis [90], [91], [92]. Hematopoiesis has been extensively studied in mice, so the following sections refer to murine hematopoiesis. The described principles of murine hematopoiesis are largely conserved in human hematopoiesis [93].

3.4.1 Embryonic hematopoiesis

First blood formation in mice is detected around embryonic day 7 in the so-called blood islands of the extra-embryonic yolk sac. Here, primitive nucleated erythroid cells expressing fetal globins, are generated to allow oxygen supply in the growing embryo. Additionally, macrophages and megakaryocytes are detected [94], [95]. These cells originate possibly from so called hemangioblasts; cells giving rise to both blood and vascular cells. However, the presence of hemangioblasts has been challenged [90]. This first wave of embryonic hematopoiesis is designated primitive hematopoiesis and is observed until embryonic day 11. Definitive hematopoiesis, which replaces the primitive one and constitutes the second wave of embryonic hematopoiesis, starts around embryonic day 10.5 in the aorta-gonad-mesonephros (AGM). It is characterized by the appearance of multipotent LT-HSCs that are able to colonize the adult bone marrow in transplantation experiments. Significant numbers of HSCs can be detected in the umbilical veins, allantois and placenta shortly after. Whether these HSCs originate from these sites of hematopoiesis or derive from HSCs in the yolk sac is a topic of current debate [90], [96]. From embryonic day 11.5 on, HSCs are thought to colonize the fetal liver, the main site of embryonic hematopoiesis until birth, where adult hematopoiesis is established. For the maturation of lymphoid and myeloid cells, hematopoietic progenitors colonize the thymus and spleen, respectively [96], [97]. At 19.5 dpc, shortly before birth, the site of hematopoiesis changes from the liver to the bone marrow. HSC characteristics, such as their proliferative stage or their requirement of factors for survival, differ depending on the developmental stage [90]. HSCs in the fetal liver are highly proliferative and they keep fast cycling in the bone marrow until about three weeks after birth. Subsequently, HSCs are mostly quiescent, until they experience a challenge that induces enforced cycling. With advanced aging, HSCs become more proliferative again. Additionally, “old” HSCs show reduced homing capacity in transplantation experiments and myeloid differentiation is increased at the expense of lymphoid differentiation [90]. Regarding survival factors, TAL1 and RUNX1 are critical for embryonic hematopoiesis while they are not essential for HSC survival and maintenance in the adult bone marrow, to name just one example [98], [99].The variation in HSC features is partly attributed to different microenvironments, but intrinsic effects also seem to be involved [90].

3.4.2 Adult hematopoiesis

Differentiation of HSCs to mature blood cells is modelled in a hierarchical system, with long-term repopulating (LT) HSCs at the top (**Fig. 3.4**). Some of the LT-HSCs, the most immature cells and the only cells capable of long-term self-renewal, become intermediate and short term HSCs with limited self-renewal capacity. Both self-renewal and reconstitution potential is further reduced in multipotent progenitors (MPPs). In a next step of commitment, MPPs are thought to bifurcate in common myeloid and lymphoid progenitors (CMPs and CLPs, respectively). While CLPs differentiate to mature lymphocytes, CMPs further bifurcate in granulocyte-macrophage progenitors (GMPs) and bipotent megakaryocytic-erythroid progenitors (MEPs) before final maturation [100]. While the hierarchical model of hematopoiesis with a gradual loss of differentiation potential is in current use, it has been challenged by in vivo and *in silico* analysis that revealed commitment already at the stage of multipotent progenitors. Both MPPs and CMPs can already be destined to become an erythrocyte, for example [101], [102]. The described steps of hematopoiesis and the scheme in **Fig. 3.4** constitute an incomplete and over-simplified picture of hematopoiesis that serves only as an overview on the complex pathways of hematopoietic differentiation. Ongoing research constantly reveals increasing numbers of subpopulations and alternative routes to mature cells [103].
Populations at each stage of differentiation have been characterized by their specific cell surface marker expression, allowing their isolation by fluorescence activated cell sorting (FACS) [104]. Surface expression markers that are associated with specific cell populations that were used in this work are indicated in **Fig. 3.4**.

3.4.3 The role of transcription factors during hematopoiesis

Transcription factors hold a pivotal role in hematopoiesis, as they induce the final execution of fait decisions in the pathways of lineage differentiation. Certain transcription factors that are expressed at rather low levels in multipotent cells are upregulated upon lineage commitment. Upregulation of such a transcription factor promotes one specific differentiation pathway while it concomitantly may repress other differentiation fates. Antagonism of transcription factors that favor opposing differentiation pathways is a common mechanism in lineage differentiation, such as antagonism of PU.1 and GATA-1, which is decisive for the choice of MEPs versus GMPs and antagonism of EKLF and FLI, which is crucial for the decision between erythrocyte and megakaryocyte fait [90]. The competition of antagonizing transcription factors on the one hand and cooperativity between other transcription factors on the other hand, allows the translation of transiently different transcription factor expression into lineage commitment. The power of transcription factors in hematopoiesis is further emphasized by their potential to change the fate of an already committed cell: enforced expression of certain transcription factors

is sufficient to induce lineage interconversion [90], [105], [106], [107].

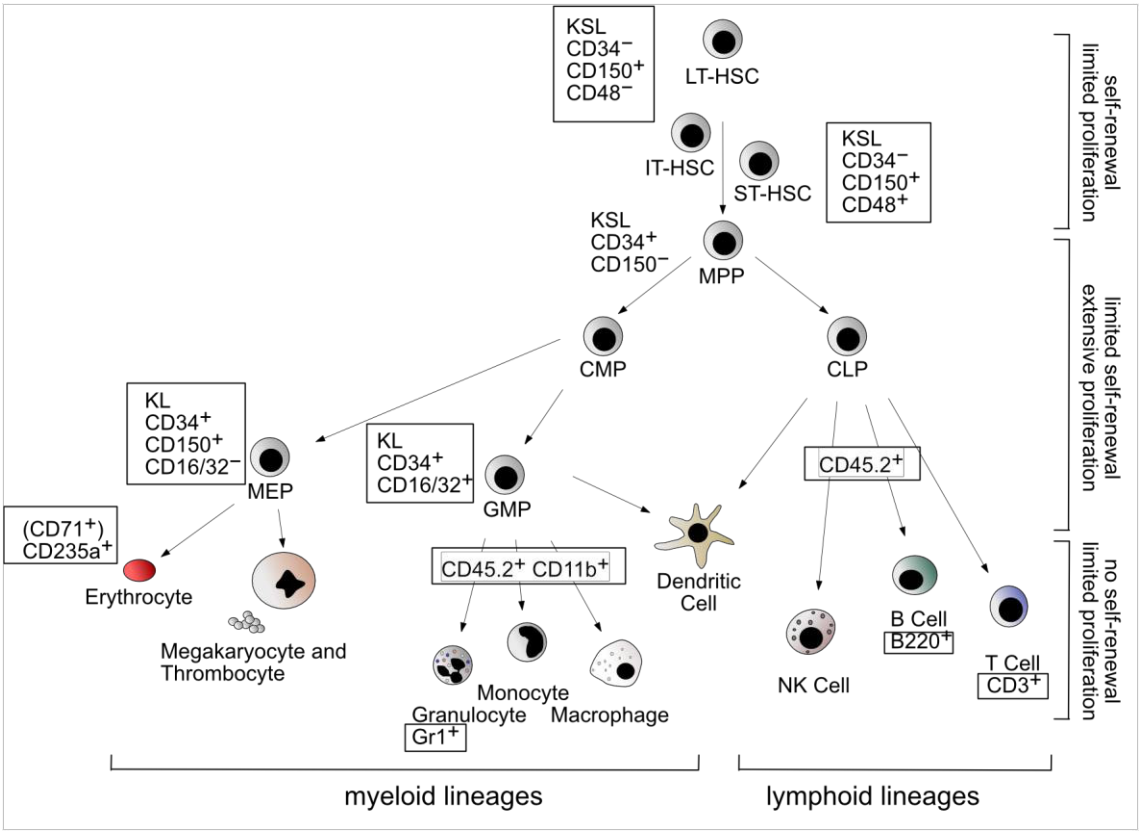

Figure 3.4: Hierarchical model of murine hematopoiesis
LT-HSCs possess full self-renewal capacity and differentiation potential, they represent the top of the hematopoietic hierarchy. With ongoing differentiation via multi- and bipotent progenitors these characteristics are lost. The scheme is over-simplified, and alternative differentiation routes and inter-lineage conversions have been described. Cell surface markers that were used in this study to identify specific populations are indicated in boxes. HSC: hematopoietic stem cell; LT: long-term repopulating; IT: intermediate-term repopulating; ST: short-term repopulating; MPP: multipotent progenitor; CMP: common myeloid progenitor; CLP: common lymphoid progenitor; MEP: megakaryocyte/erythroid progenitor; GMP: granulocyte/macrophage progenitor; NK cell: natural killer cell; KSL: c-Kit-positive, Sca1-positive, Lineage-negative cells; KL: c-Kit-positive, Sca1-negative, Lineage-negative cells.

3.4.4 Regulation of hematopoiesis

The maintenance of a sufficient number and function of HSCs, progenitors and mature cells is assured by the intricate interplay of cell intrinsic and extrinsic regulators. Extrinsic factors include growth factors, cytokines and other chemical modulators, such as NOTCH ligands and WNT proteins, BMPs, thrombopoietin, KIT-ligand, PGE_2 and retinoic acid [90], [108]. Furthermore, hematopoiesis is controlled by its specialized microenvironment, the hematopoietic niche. Here, cell-cell contacts and short-range secreted factors modulate the features of the residing hematopoietic cells. Intrinsic factors comprise CDX and HOX proteins and cell cycle regulators, amongst others [91]

[109], [90]. Epigenetic regulators that control the accessibility of the cis-regulatory elements which represent the targets of transcription factors, constitute another level of the intrinsic regulatory network [92].

3.5 Erythropoiesis

Like hematopoiesis, erythropoiesis, the formation of red blood cells (RBCs), is divided into a primitive and a definitive stage. Primitive erythropoiesis arises in the yolk sac. Putative hemangioblasts (see above) produce the so called EryP-CFC progenitor, which is unique for primitive erythropoiesis. This progenitor characteristically is not capable of self-renewal and runs highly aerobic glycolysis [94]. In the subsequent steps of maturation, the morphology of the cell changes: it decreases in size and the chromatin in the nucleus condenses, similar to the maturation of adult erythrocytes (described below) [110]. It was long thought that primitive erythrocytes do not enucleate, but the presence of enucleated red blood cells of primitive origin at later stages of embryogenesis suggest that enucleation is just retarded and uncoupled from morphologic remodeling [94]. Primitive erythroid progenitors can be distinguished from definitive progenitors by their differential gene expression. The most prominent difference is the expression of embryonic globin genes. With the onset of definitive erythropoiesis, which starts when HSCs colonize the fetal liver, globin expression switches to adult genes [111], [94].

The pathway of definitive erythropoiesis in both the fetal liver (first wave) and the adult bone marrow (second wave) starts with the differentiation of HSCs via MPPs and CMPs to lineage-committed MEPs. As already mentioned above, alternative routes of differentiation exist and the point of erythroid commitment can be detected as early as in MPPs or as late as in MEPs [101], [102]. The stages of erythroid maturation from MEPs to red blood cells comprise erythroid progenitors termed burst forming unit erythroid (BFU-E) and colony forming unit erythroid (CFU-E). The following precursor stages are named pro-, basophilic, polychromatophilic and orthophilic erythroblasts. Enucleation finally produces circulating reticulocytes and mature red blood cells. The distinct stages are characterized by the proliferation status of the cells, which drastically decreases with progressing maturation, and morphological features that result from accumulation of hemoglobin in the cytoplasm, shrinkage of the cell volume, nuclear condensation and reduction of RNA content [112]. The final step of maturation is the enucleation, leading to reticulocytes that are released in the blood stream, and pyrenocytes, which consist of the condensed nucleus surrounded by a thin layer of cytoplasm. Pyrenocytes are readily

taken up by macrophages. Reticulocytes reduce their volume and cell surface, undergo cytoskeletal rearrangements and remove their organelles by autophagy and exocytosis to form the disc-shaped mature red blood cells. The characteristic composition of plasma membrane and cytoskeleton and their special interconnection allows the high elasticity of red blood cells, which is required for the passage of even small capillaries [113].
During erythroid maturation in the fetal liver and adult bone marrow, erythroblasts attach to macrophages to form so-called erythroblastic islands. Macrophages fulfill various roles in erythropoiesis: in the erythroblastic islands, they support proliferation of the erythroid progenitors and precursors. Additionally, macrophages not only clear the blood from pyrenocytes, as mentioned above, but also remove senescent erythrocytes from the blood stream [114].

3.5.1 Regulation of erythropoiesis

Human erythrocytes have a life span of ~120 days. To sustain a number of $5x10^6$ erythrocytes per µl blood, about 2 million new reticulocytes need to be released in the blood circuit per day [111]. As both, decreased numbers of (functional) RBCs and elevated RBC counts, have serious consequences, the sufficient proliferation of erythroid progenitors and subsequent efficient differentiation need to be tightly regulated. The factors that regulate erythropoiesis are versatile and stage-specific, they include transcription factors, chromatin modifiers and miRNAs as well as growth factors, cytokines and glucocorticoids.

3.5.1.1 Extrinsic regulators of Erythropoiesis

The hormone erythropoietin (EPO) is the primary regulator of definitive erythropoiesis and is necessary and sufficient to promote survival and differentiation of pro-erythroblasts [115]. EPO also enhances cycling of CFU-Es but apart from that, its proliferative effect is limited. EPO receptor (EPOR) expression appears on the surface of BFU-Es and is upregulated on CFU-Es, followed by a subsequent downregulation resulting in reticulocytes and red blood cells without EPOR expression [116]. Consistently, EPO seems to be dispensable for the generation and survival of committed progenitors and primitive erythropoiesis while homozygous EPO and EPOR knockout mice die in utero because of inhibited erythrocyte development at the CFU-E stage [117] [118]. However, more recent studies showed that significant levels of *EPOR* mRNA could already be detected in the blood islands in the yolk sac of 7.5 to 8.5 days old embryos. At this stage, EPO produced by neuroepithelial cells could play a role in the regulation of primitive erythropoiesis [94]. Additionally, HSCs and MPPs also express minor levels of EPOR and Grover and colleagues [119] demonstrated that EPO acts on these cells

by repressing non-erythroid fate decisions, resulting in favored erythroid differentiation over myeloid and lymphoid lineage commitment. This mechanism is thought to increase production of red blood cells in the context of severe anemia [119].

The EPOR belongs to the type I family of single transmembrane cytokine receptors that dimerizes upon binding EPO. The intracellular domains of EPOR display no kinase activity, but exhibit binding sites for Janus kinase 2 (JAK2). EPOR activation results in JAK2 auto trans-phosphorylation and subsequent phosphorylation of tyrosines in the cytoplasmic tail of the EPOR. This generates docking sites for adapter proteins including Src family secondary tyrosine kinases. Subsequent complex formation and phosphorylations activate STAT5a/b signaling, Ras/Raf/MAPK, PI3K, and PLC-γ pathways. Thus, EPOR signaling activates gene expression profiles and pathways that inhibit apoptosis, induce proliferation and promote erythroid differentiation. Deactivation of EPOR signaling is achieved by dephosphorylation and proteasomal degradation of activated kinases [116].

Hypoxic conditions stimulate the production and release of EPO. As EPO promotes proliferation of CFU-Es, which possess limited proliferative potential, but fails to induce expansion of the highly proliferative BFU-Es, it is thought to be responsible for the short-term control of erythropoiesis, compensating moderate variation in mature red blood cell numbers. Under severe and/or chronic lack of oxygen, additional factors are required that induce proliferation and even self-renewal of BFU-Es. Among these factors that act on BFU-Es are stem cell factor (SCF), the ligand of c-KIT, interleukins 3 and 6, insulin like growth factor 1 (IGF-1) and glucocorticoids. The microenvironment might play a critical role in this context, as stress-induced erythropoiesis localizes to the spleen [120].

3.5.1.2 Intrinsic regulators of erythropoiesis

While EPO is known as the primary extrinsic factor regulating erythropoiesis, transcription factors are the best studied and most prominent intrinsic regulators of erythropoiesis. They can be divided into transcription factors critical for the erythroid commitment of progenitors, including TAL1, LMO2, GATA-2 and c-MYB, and factors restricted to erythroid committed cells that control further maturation and expression of genes which are essential for erythroid functions, among them GATA-1, FOG, KLF family members and NF-E2 [121], [120]. All these transcription factors act in concert with other transcription factors, antagonizing or cooperatively, and often within multi-protein complexes. Both GATA-1 and TAL1 can either activate or inhibit gene expression, depending on interaction with co-activators or co-repressors [122], [123]. They are often found together at enhancer sites of activated erythroid genes, in a pentameric complex which consists of the TAL1/E2A dimer, adapter molecules LMO2 and LDB1 and GATA-1 [124]. GATA-1, but not TAL1, also shares binding sites with KLF1, suggesting that

GATA-1 can form independent activating transcription factor complexes. The composition of GATA-1 and TAL1 complexes that inhibit gene expression is less clear. Repressive GATA-1 complexes could include FOG1, GFI-1b and/or chromatin modifiers EZH2 and EED, while TAL1 probably associates with ETO2 and MTGR4 to repress gene expression [120]. The interplay of different multiprotein complexes, their exact temporal and spatial composition and the consequent action on target genes still need to be identified. Transcription factors themselves are regulated by chromatin structure which defines the accessibility of transcription factor binding sites. EPOR signaling was reported to alter the histone mark signature at enhancers that are then occupied by erythroid-specific transcription factors, as one example [115]. Additionally, posttranslational modifications regulate transcription factor activity. Exemplarily, TAL1 phosphorylation interferes with its interaction with co-repressor LSD1 [125].

Besides transcription factors, miRNAs are important intrinsic regulators of erythroid lineage commitment, progenitor proliferation and terminal erythroid maturation. Among the miRNAs that have so far been identified to play a role in erythropoiesis are miR-123 and miR-150, which inhibit erythroid differentiation by downregulating MYB and LMO2, respectively. miR-221/miR222 have been found to inhibit proliferation of erythroid progenitors by downregulating c-KIT [120].

Just as in HSCs, erythroid maturation is controlled by cell cycle regulators. This kind of regulation is reflected by the role of c-MYC. C-MYC expression, which is associated with highly proliferative states, is required for the expansion of erythroid progenitors, but needs to be downregulated to allow the final maturation of erythrocytes [126]. One mechanism, by which the cycling state of a cell could influence differentiation, is that DNA remodeling, leading to differential gene expression, preferentially takes place during the S phase of the cell cycle [120]. The pivotal role of c-MYC, which not only acts as a cell cycle regulator but also as a transcriptional regulator of about 10% of all genes, was further emphasized when c-MYC, along with TAL1, GATA-1 and LMO2 was identified as the minimal factor which is required for lineage reprogramming of fibroblasts into erythroid progenitors [127].

3.5.2 Erythropoiesis in cell culture

The identification of specific cytokines and growth factors that act at different developmental time points to promote erythroid differentiation allowed the definition of cell culture media to differentiate hematopoietic stem and progenitor cells *in vitro*. These media contain factors that stimulate HSC proliferation, for example Fms-related tyrosine kinase 3 ligand (FLT3-L), SCF and thrombopoietin [128]. SCF as well as EPO and IGF-1 are added to expand erythroid committed progenitors, the latter two are also required to induce erythroid differentiation [128]. Further factors are granulocyte and granulocyte-

macrophage colony-stimulating factors G-CSF and GM-CSF as well as interleukins 1, 3, 4, 6, 9 and 11, which also induce differentiation of pluri- and multipotent progenitors [129]. All these factors also play a role in *in vivo* erythropoiesis. Media and supplements for the expansion and erythroid differentiation of hematopoietic stem and progenitor cells (HSPCs) are nowadays available from different companies, allowing reliable albeit expensive culture and erythroid differentiation of HSPCs.

3.6 Knockout mice

Understanding the physiological function of genes, i.e. how they impact the normal biological processes in an organism, is a prerequisite for the identification of aberrant gene functions that cause diseases. Characterizing the phenotype of gene inactivations represents a valuable if not the best method to depict gene functions within complex biological phenomena. Global consortia as the *International Mouse Phenotyping Consortium* (*IMPC*) and the *International Knockout Mouse Consortium* (*IKMC*) aim to produce a knockout mouse model for every coding gene and to catalog every gene function by phenotyping the respective mice [130]. The basis for this ambitious objective is the invention of gene targeting tools that allow modeling any alteration in the genome, including point mutations, micro-deletions and insertions as well as large chromosomal rearrangements [131].

3.6.1 Gene targeting

Early gene analysis studies characterized the outcome of naturally occurring variants in the genome of mouse strains or analyzed the consequences of mutations which were induced by radiation or chemicals. Micro-injections of exogenous DNA into single cell zygotes were used to create gene knock-ins as early as in the 1970/80s. However, these functional studies were limited as the sort and site of mutagenesis and DNA integration were random [132], [133]. Identification of the mammalian homologous recombination machinery and the establishment of embryonic stem cell (ESC) culture revolutionized the field of genetic engineering, allowing modern gene targeting that creates specific genetic modifications at exact genomic sites. Homologous recombination is a DNA damage repair mechanism that uses the presence of duplicated information in form of double chromosomes. The intact homologous DNA is melted to serve as a template for the repair of the broken complementary DNA. The structure of four intercrossed strands of homologous DNA is called a double Holiday Junction. Nucleolytic resolution of this structure can cause a crossover, meaning the exchange of DNA sections between

homologous strands [134]. By this mechanism, targeting vectors containing the desired mutations can be integrated at specific sites of the genome, if they comprise at least 2 kb of homologous sequence flanking the modified section [135]. The chance of random integration of the targeting vector is still 1000 fold higher than homologous recombination, demanding a sufficient number of cells to be targeted and selection mechanisms to isolate cells with correct integration [135]. The use of cultured ES cells instead of one-cell zygotes and electroporation instead of microinjections enable the modification of 10^7 cells in one experiment [133]. Antibiotic resistance genes, usually against neomycin, are included in the targeting vector for a positive selection of those cells, which integrated the vector. Several additional strategies exist to exclude cells that integrated the modified DNA at the wrong site. One approach is to clone the herpes simplex virus-thymidine kinase (*HSV-tk*) at the end of the targeting vector. In case of random integration of the vector, the intact tk gene is retained, so these cells can be eliminated by addition of the anti-viral tk substrate gancyclovir [136]. However, this strategy requires advanced cloning and increases the size of the vector, complicating the handling. For this reason, negative selection is often skipped and ESCs with correct integration are identified by PCRs and southern blotting as described in [137], [138]. Injected in blastocysts and transplanted in pseudo pregnant foster mice, the selected modified ESCs can contribute to all cells of the developing embryo, including the germline [133]. Successful germline transmission can easily be tested by using ESCs and blastocysts of mice that differ in their fur color [139]. The generation of genetically modified mice is summarized in **Fig. 3.5**.

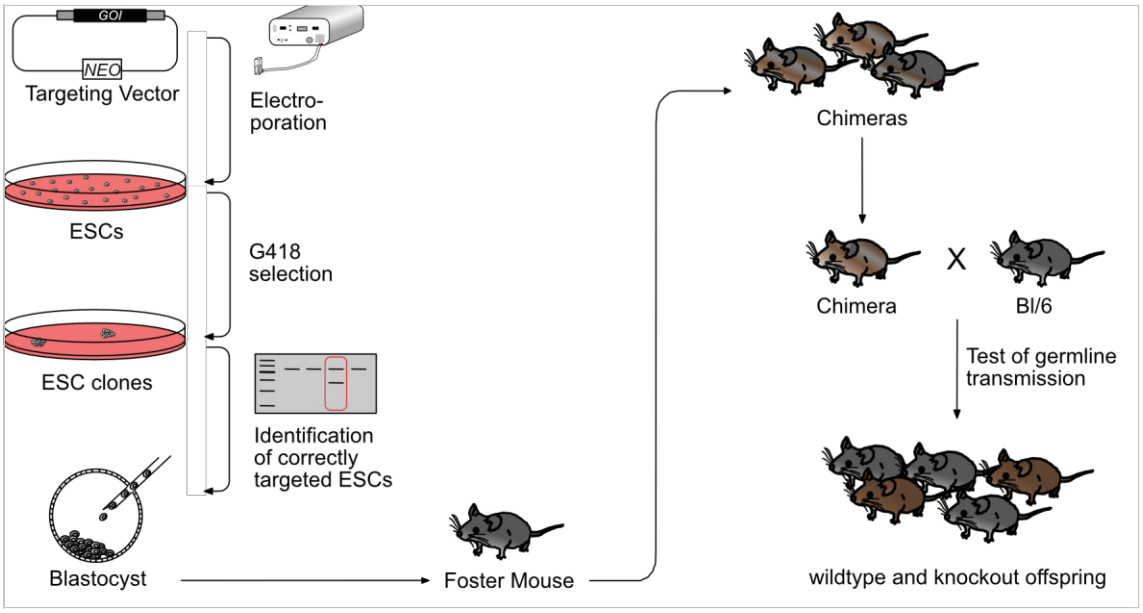

Figure 3.5: Generation of knockout mice
The targeting vector containing the modified gene and a Neomycin resistance gene is electroporated into ESCs. Successfully transfected cells are selected by culture in the presence

of G418. The correct integration of the targeting vector is tested by long-range PCR or southern blotting. Positively tested ESCs are injected in blastocysts and transplanted in the uteri of pseudo-pregnant mice. The resulting chimeric offspring is mated with Bl/6 mice (or other strains for backcrossing) to identify germline transmission of the targeted allele. Chimeras and germline transmission are identified by the fur color which differs between the ESC strain (here in brown) and the foster mother/mice for backcrossing (here in black).

3.6.2 Generation of gene knockouts

The disruption of genes, the most common form of gene targeting, can be achieved by different concepts. First knockout vectors were designed to replace the whole coding sequence of the target gene. These large-scale genetic modifications often had side effects on the regulation of other, both adjacent and distant, genes. Gene trap mutagenesis inserts cDNA in a gene, thereby disrupting normal transcription which often leads to functional inactivation of the gene. Gene trapping also provides the possibility to visualize promoter activity and the potential of conditional gene disruption. The different methods of gene trapping in mice are summarized in [140].

About 15% of the generated gene knockouts in mice had proven embryonic lethal, which led to a high interest in conditional knockout strategies that allow the spatial and temporal restriction of gene knockouts [135]. The “conditional knockout first vector”, which is extensively used by the IMPC, provides such conditional features. The unmodified conditional knockout first vector creates a null allele by a gene trap mechanism: the *LacZ* gene is inserted into the intron of the targeted gene. Via the splice acceptor of *mouse engrailed 2* (*En2*), *LacZ* is fused to preceding exons of the targeted gene and a polyadenylation signal ends translation of the mutated mRNA downstream of *LacZ*. *FRT* sites that are recognized by *Saccharomyces cerevisiae* flippase FLP, flank the *LacZ* reporter cassette. Thus, breeding with *Flp* deleter strains removes the reporter cassette from the modified locus, but leaves *loxP* sites (locus of crossing (X-ing) over) at both ends of critical exons within the target gene. The *loxP* sites are positioned in a way that deletion of the floxed (flanked by *loxP* sites) exons leads to a frame shift mutation and probably nonsense-mediated decay of the mutant mRNA. Thus, breeding with mice expressing CRE recombinase from the P1 bacteriophage cause a knockout deletion. As the expression of CRE can be controlled by promoters that act cell type-specific or contain transgenic sequences that repress CRE expression until binding of a particular ligand (e.g. tamoxifen binding to the estrogen receptor), gene knockout can be directed to distinct cells and tissues and can be induced at distinct developmental stages [131] [130], [135]. Such conditional knockout mice allowed the investigation of gene functions in adult organisms and other defined conditions that were inaccessible previously because of embryonic lethality in constitutive knockout mice.

The invention of CRISPR/Cas9 technology expanded the options of gene targeting even

further [141]. The CRISPR/Cas9 machinery is used for gene manipulation to induce double strand breaks at specific sites of the genome, which then constitute the origin of insertions, deletions and more complex modifications. The generation of knockout mice via targeted CRISPR/Cas9 is possible in a one step process, when the components of the CRISPR/Cas9 machinery are directly injected in the blastocyst of mice. Even multiple DNA modifications can be induced at the same time. This makes the CRISPR/Cas9 method faster and cheaper than the traditional technology: generation of knockout mice by homologous recombination in ES cells usually takes 12-18 months and costs ~100,000 $, not considering additional breeding to combine multiple mutations. CRISPR/Cas9 generated knockout mice can be produced within 8 months, with costs reduced to 35,000 $ [142], [143]. However, the CRISPR/Cas9 technology has some critical drawbacks. Insertion of transgenic sequences larger than 5 kb is difficult. Even more relevant is the appearance of mosaicism, i.e. variation of CRSIPR/Cas9 activity in different cells within one organism and thus incomplete gene targeting. Finally, there are off-target effects, altering the genome in an unintended way. Although refinement of the CRISPR/Cas9 technology has reduced mosaicism and off-target effects, disadvantages persist, legitimating the continuous use of “conventional” technology as homologous recombination in ESCs [143], [132], [144].

3.6.3 Relevance of knockout mouse models

So far, the IMPC has described 5,000 mutant mice, contributing to the discovery of gene function of a significant portion of all identified murine coding genes. The murine and human genome show a high level of homology: Almost every human protein-coding gene comes with a murine homologue, and the sequence identity of coding regions is almost 85%. 95% of the genes display identical numbers of exons, and 73% show identical exon lengths [145]. Consistently, 40% of the described phenotypes in IMPC correlate with disease states in humans, demonstrating the value of knockout mouse models [132].

Still, limitations of the conclusions that can be drawn from knockout mice studies must be taken into consideration. Not all gene functions found in the mouse can be translated to human gene function. Although humans and mice share a high amount of coding DNA sequence, they also show substantial differences in gene expression profiles, resulting, at least in part, from divergence of cis-regulatory elements [146]. The huge difference in life span complicates the comparison between humans and mice in age-dependent contexts. Obvious and more hidden discrepancies between murine and human gene function demonstrate that the laboratory mouse still is a “model” rather than an exact copy of men. Additionally, phenotypes of knockout mice cannot (always) be assigned one-to-one to single gene functions. Pleiotropy, meaning multiple functions of one gene, will likely cause phenotypes that are the result of a mixture of affected biological

processes. In this case, extensive and detailed characterization of the mice, including physiology, biochemistry, development and behavior, is required to delineate the complete functions of a gene [132] (Brown 2018). Furthermore, genetic engineering, even as precise and minimal as it is possible today, can result in target gene-unrelated effects. *LoxP* sites inserted in non-coding intronic regions might disrupt the integrity of so far unknown non-coding regulatory RNAs, for example. Finally, a broad range of compensatory mechanisms can impact mouse phenotypes and obscure gene function [147], [148], [149].

Concluding, genetically engineered knockout mice are an essential and so far irreplaceable tool to study the physiological and pathological impact of genes, as long as phenotypes are interpreted carefully and limitations of mouse models are respected.

3.7 Aim of this thesis

Deregulation of apoptosis is implicated in a broad range of diseases, including cancer and anti-cancer therapy resistance. The Zörnig lab established a functional yeast survival screen for anti-apoptotic genes with potential oncogenic function. The screens identified *AVEN* and *FUBP1* as candidate genes [44], [11]. Until now, a quite limited number of publications involving AVEN and a substantially larger number of studies dealing with FUBP1 confirmed the involvement of both proteins in cancer [27], [29], [42]. However, the exact mechanisms underlying the tumorigenic functions of AVEN and FUBP1 are in large part unclear. This is related to the incomplete knowledge of the physiologic function of these genes. Gene knockout mouse models constitute an important, currently also the most valuable tool, to study gene functions. As for AVEN and FUBP1, characterizations of established constitutive knockout mouse models are conclusive only to a limited extent. This is due to embryonic lethality which resulted from the homozygous inactivation of both genes, while heterozygous expression did not result in obvious phenotypes [150], [67], (unpublished data). Thus, the so far identified roles of AVEN and FUBP1 for normal development and cell function base on *in vitro*/*ex vivo* and knockdown experiments, and on the phenotyping of knockout embryos. Aim of this thesis was to generate and characterize conditional *Aven* and *Fubp1* knockout mouse models. By means of phenotyping mice with an *Aven* or *Fubp1* knockout that is restricted to distinct cell types, the impact of these genes on physiology was analyzed. For AVEN, the oncogenic potential of this molecule in the context of breast cancer was further tested in mouse models as well as in cell culture experiments.

In case of AVEN, a mouse strain with conditional knockout potential already existed. This model was used to identify the exact sites of endogenous *Aven* expression in the adult mouse and during embryogenesis. Subsequently, conditional knockout mice lacking AVEN in tissues that showed significant *Aven* promoter activity were generated. A special focus was laid on the characterization of mice with AVEN deficiency in the mammary gland and the hematopoietic system, as aberrant *Aven* expression had been associated with breast cancer and acute leukemias [10], [27]. To further investigate the role of AVEN in breast cancer, the consequences of *Aven* knockout in the mammary gland on the onset and progression of tumors in endogenous breast cancer mouse models were analyzed. The *in vivo* studies were complemented by *in vitro* studies regarding cellular functions of AVEN in breast cancer cell lines.

In case of FUBP1, I generated a novel strain with conditional knockout potential. Originating from this strain, mice with an FUBP1 deficiency restricted to the hematopoietic or erythroid compartment were bred and analyzed. These studies aimed to unravel the cause of embryonic lethality in constitutive *Fubp1* knockout mice and to define the role of FUBP1 in adult hematopoiesis and erythropoiesis *in vivo*. Additionally, the recently described upstream regulation of FUBP1 by TAL1 was analyzed in more detail *in vitro*.

4 Results

4.1 Analyses of the physiological and pathological role of AVEN

4.1.1 The constitutive knockout of *Aven* is embryonic lethal.

AVEN has originally been identified as an inhibitor of the mitochondrial pathway of apoptosis [8]. Besides apoptosis inhibition, cell cycle and translation regulation have been attributed to AVEN later on [13], [17]. While aberrant *AVEN* expression has been associated with cancer and defective spermatogenesis [25], [10], [27], [29], [21], nothing is known about the physiological function of AVEN during normal development and functionality of the organism. As a first step to understand the physiological role of AVEN, endogenous *Aven* promoter activity was analyzed in mice.

To identify the sites of endogenous AVEN expression, *Aven* promoter activity was visualized in *AvenLacZ* mice. The basis of this mouse strain is a conditional "knockout first" allele. Recombination catalyzed by the CRE recombinase deletes *Aven* exon 2 but leaves a reporter cassette containing the *LacZ* gene under the control of the endogenous *Aven* promoter, allowing the visualization of endogenous *Aven* promoter activity by X-Gal staining. The deletion of exon 2 leads to a frameshift mutation and thus to a constitutive knockout of *Aven* (**Fig. 4.1A**). Absence of *Aven* mRNA, probably as a consequence of nonsense-mediated decay of the frame-shifted *Aven* mRNA could be confirmed: No PCR product of *Aven* exons 3 and 4 could be detected (**Fig. 4.1B**). Also, no AVEN protein was detected in organs of homozygous *AvenLacZ* knockout mice in contrast to their wildtype littermates (**Fig. 4.1C**). Homozygous functional inactivation of AVEN by a GFP knock-in had previously been shown to result in embryonic lethality (unpublished data). The same phenotype was observed in the *AvenLacZ* mice. With ongoing backcrossing of the described *AvenLacZ* mice into the C57Bl/6J background, the number of living homozygous *AvenLacZ*$^{d/d}$ embryos decreased. In the fifth generation of backcrossing, no *AvenLacZ*$^{d/d}$ offspring was born anymore, which is in accordance with embryonic lethality of the homozygous deletion of *Aven* (**Fig. 4.1D**). The living *AvenLacZ*$^{d/d}$ embryos of the earlier generations used for X-Gal staining were smaller than their wildtype litter-mates and seemed to be developmentally retarded, as in some of them the eye-anlage was missing (**Fig. 4.1E**). Apart from this macroscopic phenotype, the histology of frozen sections showed no difference between homozygous *Aven* knockout and wildtype embryos and adult organs (data not shown).

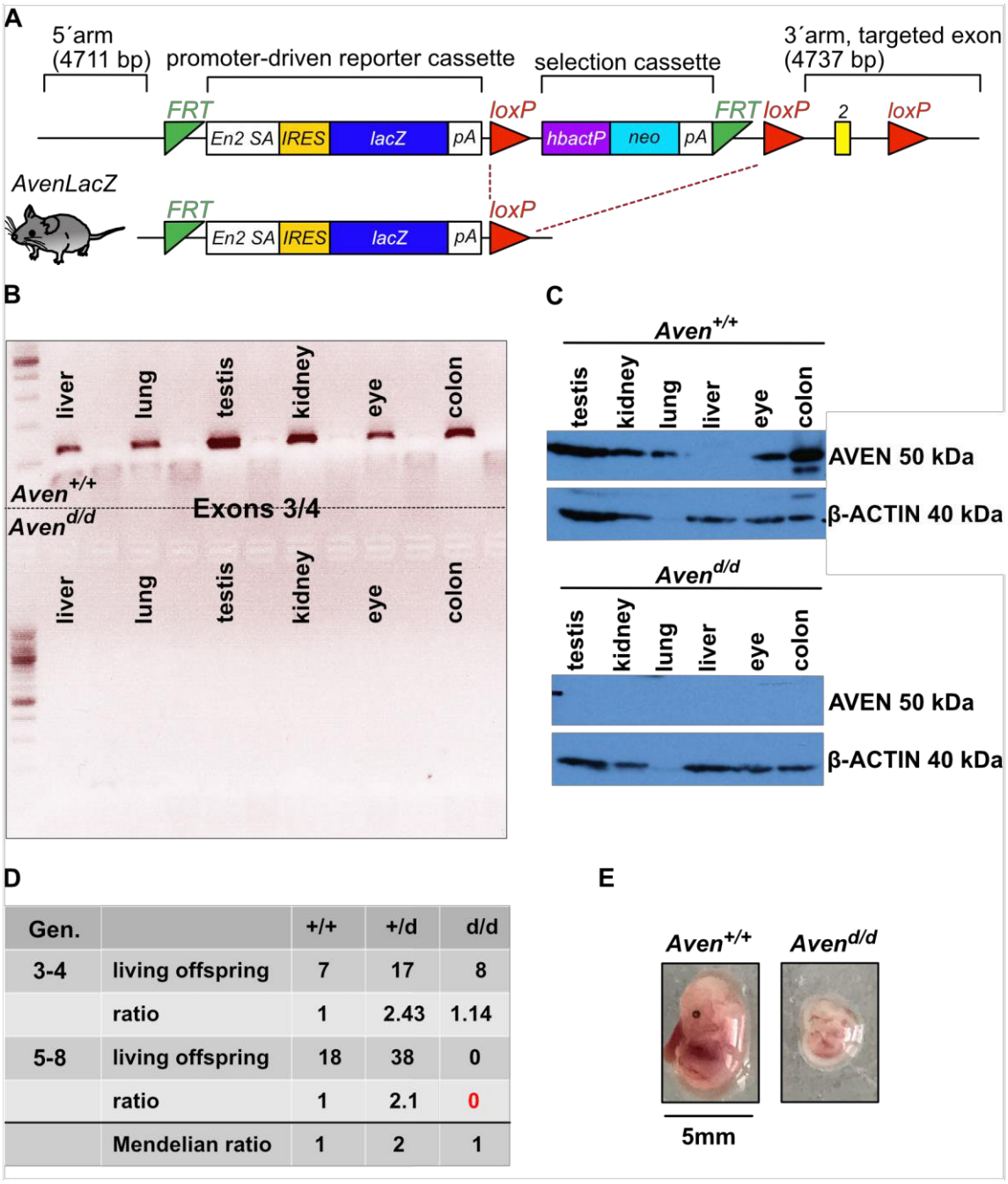

Gen.		+/+	+/d	d/d
3-4	living offspring	7	17	8
	ratio	1	2.43	1.14
5-8	living offspring	18	38	0
	ratio	1	2.1	0
	Mendelian ratio	1	2	1

Figure 4.1: The constitutive knockout of *Aven* is embryonic lethal. At 13.5 dpc, *Aven* knockout embryos are smaller than their wildtype littermates and display an anemic phenotype

A. Schematic presentation of the *Aven* conditional "knockout first" allele (upper part) and the allele of *AvenLacZ* mice resulting from Cre-mediated recombination (lower part). En2: mouse *engrailed 2* exon. IRES: internal ribosomal entry site. SA: splice acceptor. PA: polyadenylation. HbactP: human *β-ACTIN* promoter. Neo: neomycin resistance gene. **B**: In homozygous *AvenLacZ* mice (*Aven*$^{d/d}$), no *Aven* mRNA containing exons 3 and 4 can be detected in contrast to mice with a wildtype *Aven* allele (*Aven*$^{+/+}$). The gel shows PCR products after amplification of a cDNA fragment spanning *Aven* exons 3 to 4. **C**. AVEN protein expression detected in the indicated organs of mice with wildtype AVEN expression (Aven$^{+/+}$) is absent in homozygous *AvenLacZ* mice (*Aven*$^{d/d}$) as demonstrated by western blotting. β-ACTIN expression was used as a loading control. **D**: Offspring statistics of the mating of parents that were both heterozygous carriers of the *AvenLacZ* allele. Homozygous offspring was still born until the 4th generation of backcrossing, but not any more from the 5th generation on of backcrossing. Gen.: generation of backcrossing. **E**: At 13.5 dpc, homozygous *AvenLacZ* mice are smaller and paler than their wildtype litter mates.

4.1.2 Neuron-specific *Aven* expression in the adult mouse brain

To identify the exact sites of *Aven* promoter activity, organs of adult *AvenLacZ*$^{d/d}$ mice born earlier than the fifth backcrossing generation were dissected and frozen sections were stained with X-Gal. The staining appeared as blue dots of subcellular size and was detected in the brain, heart, lung, kidney, testis and colon. No staining was detectable in the spleen, the liver, and the thymus.

In the brain, the X-Gal staining appeared in a very specific pattern, with no staining in the white matter, regions in the grey matter of low staining density and regions of high staining density. In all areas, the staining could be associated to the cell bodies of the neurons. An overview of the analyzed areas of the adult brain is given in **Fig. 4.2**.

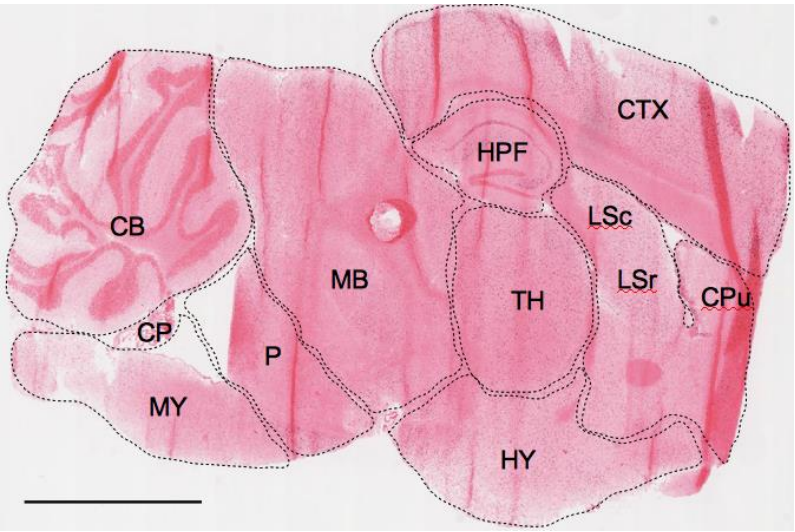

Figure 4.2: Areas within the adult mouse brain that were analyzed for *Aven* Promoter activity
Frozen section of the brain of an *AvenLacZ*$^{d/d}$ adult mouse. The indicated areas were analyzed for *Aven* promoter activity by X-Gal staining. The section was counter-stained with Eosin. CB: Cerebellum, CP: Choroid plexus, Md: Medulla, P: Pons, MB: Midbrain, HPF: Hippocampal formation, TH: Thalamus, HY: Hypothalamus, CTX: Cortex, LSc: Lateral septal nucleus, caudal part, LSr: Lateral septal nucleus, rostral part, CPu: Caudoputamen. Scale bar: 1 mm.

The Cerebral Cortex (CTX) shows an evenly distributed staining throughout the layers, with the exception of the outermost molecular cell layer, which contains very few neuronal cell bodies (**Fig. 4.3A** and **B**). Most cells of the external granular and external pyramidal cell layers (II/III) are stained, with scattered single cells without staining. The same staining pattern is found in the internal granular (IV) and multiforme (VI) layer. In contrast, all the cells of the internal pyramidal layer (V) are stained.

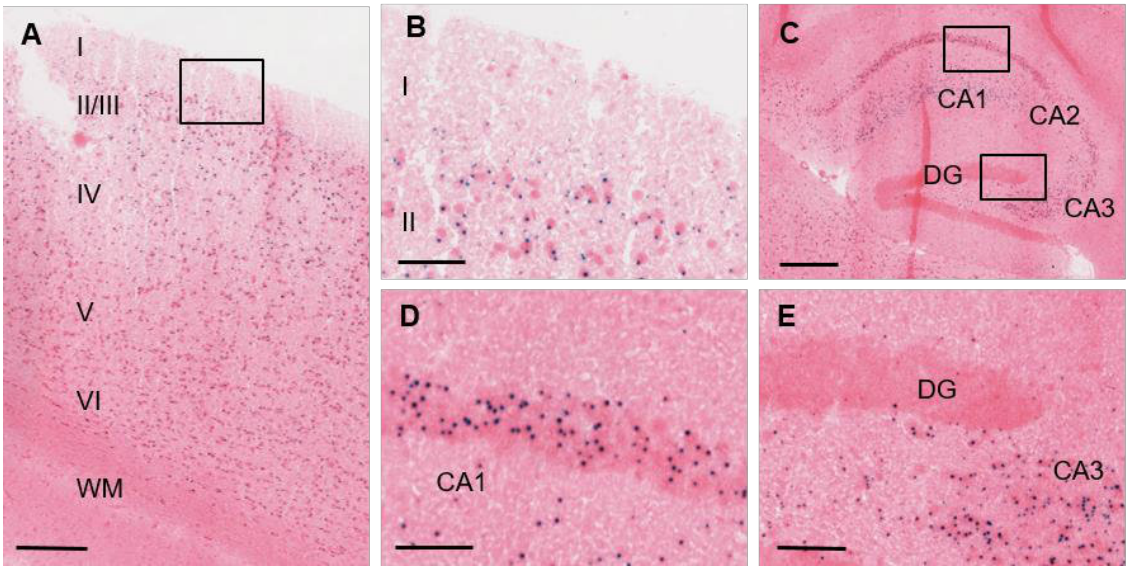

Figure 4.3: *Aven* promoter activity is prominently detected in the Cortex and in the CA1 and CA3 regions of the Hippocampus
A: X-Gal staining for Aven promoter activity in the cerebral cortex, layers I to VI are indicated. WM: white matter. **B**: Amplification of the staining in the molecular layer (I) and external granular/pyramidal cell layer (II/III). The area corresponds to the rectangle in A. **C**: Regions within the Hippocampus. DG: Dentate Gyrus. **D**: Amplification of the pyramidal cells in the CA1 region. The detail corresponds to the upper rectangle in C. **E**: Amplification of the granular cells in the Dentate Gyrus and the pyramidal cells in the CA3 region. The detail corresponds to the lower rectangle in C. The sections were counterstained with Eosin. Scale bar: 300 µm in A and C, 50 µm in B, D, E.

The pyramidal neurons of the Hippocampus are prominently stained in the CA1 and the CA3 region, there is a less intense staining in the CA2 region and remarkably no staining of the granule neurons in the Gyrus dentate (**Fig. 4.3C, D, E**).

A similarly distinct staining is detectable in the Cerebellum. Here, cell bodies within the molecular layer are stained and the cells of the Purkinye layer show a strong staining, while in the granular layer, staining is absent (**Fig. 4.4A** and **B**). A significant staining also appeared in the Choroid plexus (**Fig. 4.4C**).

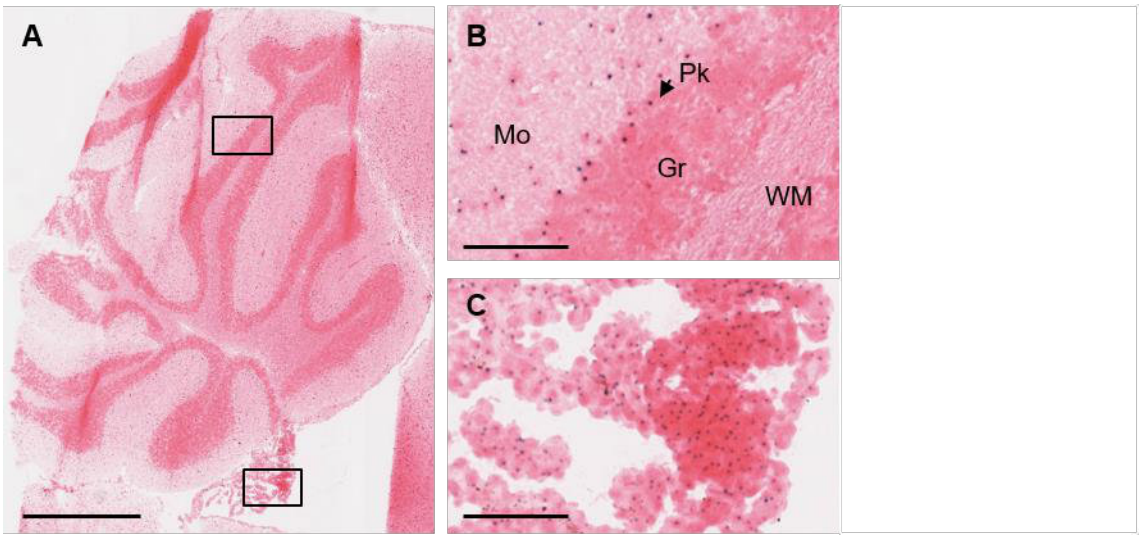

Figure 4.4: High levels of *Aven* promoter activity in the Purkinye cells
A: X-Gal staining for *Aven* promoter activity in the Cerebellum and Choroid plexus. **B**: X-Gal staining in the Molecular cell layer and Purkinje Cells. The amplification corresponds to the upper rectangle in A. Mo: molecular cell layer, Pk: Purkinje Cells, Gr: granular cell layer, WM: white matter. **C**: X-Gal staining in the cells of the Choroid plexus. The amplification corresponds to the lower rectangle in A. The sections were counterstained with Eosin. Scale bar: 1 mm in A, 100 µm in B, C.

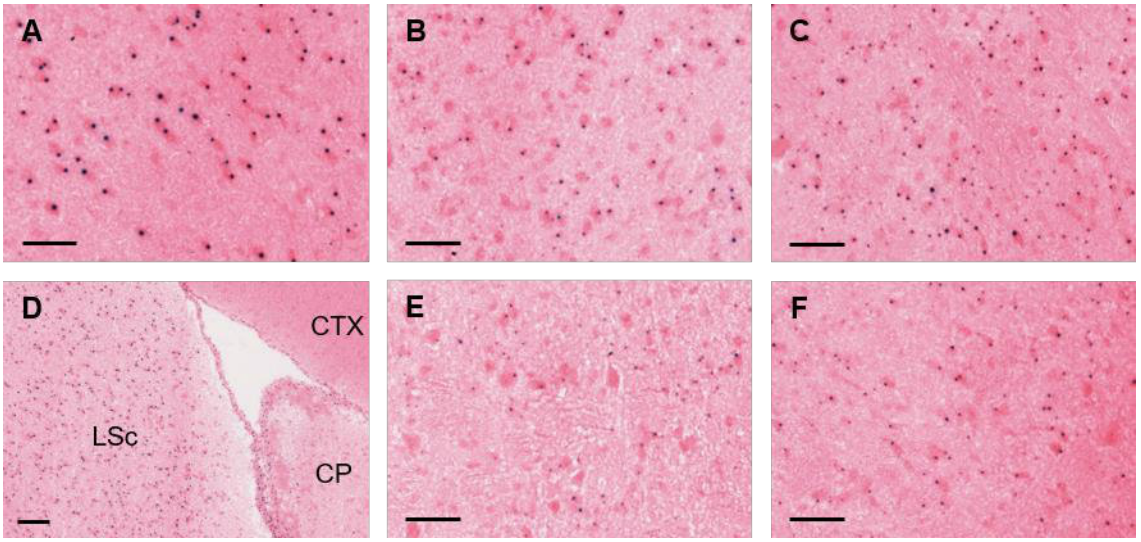

Figure 4.5: Significant *Aven* promoter activity in the Striatum, in the Midbrain, Interbrain and Hindbrain
X-Gal staining in the **A**: Thalamus, **B**: Hypothalamus, **C**: Midbrain, **D**: Striatum, a part of the cortex is also shown (LSc: Lateral septal nucleus, caudal part), **E**: Medulla, **F**: Pons. The sections were counterstained with Eosin. Scale bar: 100 µm

Within the brain stem, both the Midbrain and the interbrain which is composed of Thalamus and Hypothalamus, show a significant X-Gal staining, but the staining in the Thalamus is clearly stronger than in the Hypothalamus and Midbrain (**Fig. 4.5A, B, C**). In the Striatum, there is a difference in staining intensity between the Caudoputamen with low staining density and the lateral septal structures with high staining density **(Fig.**

4.5D). A significant staining is visible in the hind brain, both in the Pons and in the Medulla, but the staining is rather faint (**Fig. 4.5E, F**).

Altogether, *Aven* promoter activity in the brain is particularly detectable in pyramidal neurons, with activity levels varying between different brain regions. Remarkably, granular cells show no *Aven* promoter activity.

4.1.3 Endogenous *Aven* expression in other adult mouse organs

The X-Gal staining of neurons is not restricted to the brain; within the neuroretina, the neurons of the ganglion cell layer show the blue staining, whereas the other layers of the retina lack detectable X-Gal staining **(Fig. 4.6A, B**). The Harderian gland which is located within the scull behind the eyeball also shows the blue staining. In contrast to the staining in other tissues, the staining in the Harderian gland is not dot shaped but diffuse (**Fig. 4.6C**).

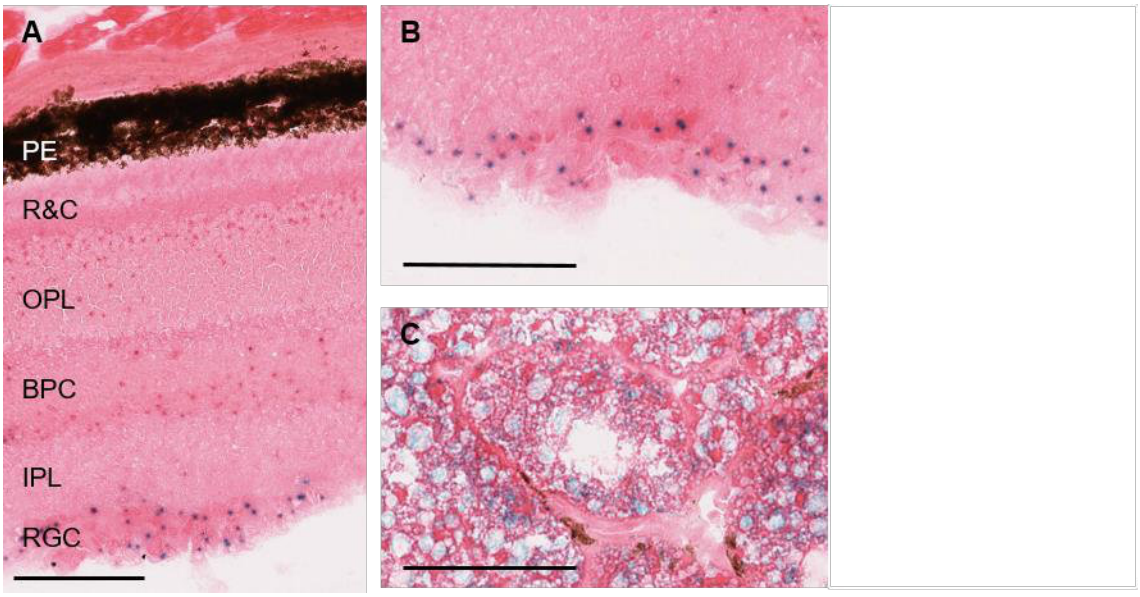

Figure 4.6: High lievels of *Aven* promoter activity in the retinal ganglion cell layer and in the Harderian Gland
A: X-Gal staining in the neuroretina. PE: Pigmentepithelium, R&C: rods and cones, OPL: outer plexiforme layer, BPC: bipolar cells, IPL: inner plexiforme layer, RGC: retinal ganglion cells. **B**: Amplification of the staining in the retinal ganglion cells. **C**: Harderian Gland. The sections were counterstained with Eosin. Scale bar: 100 µm.

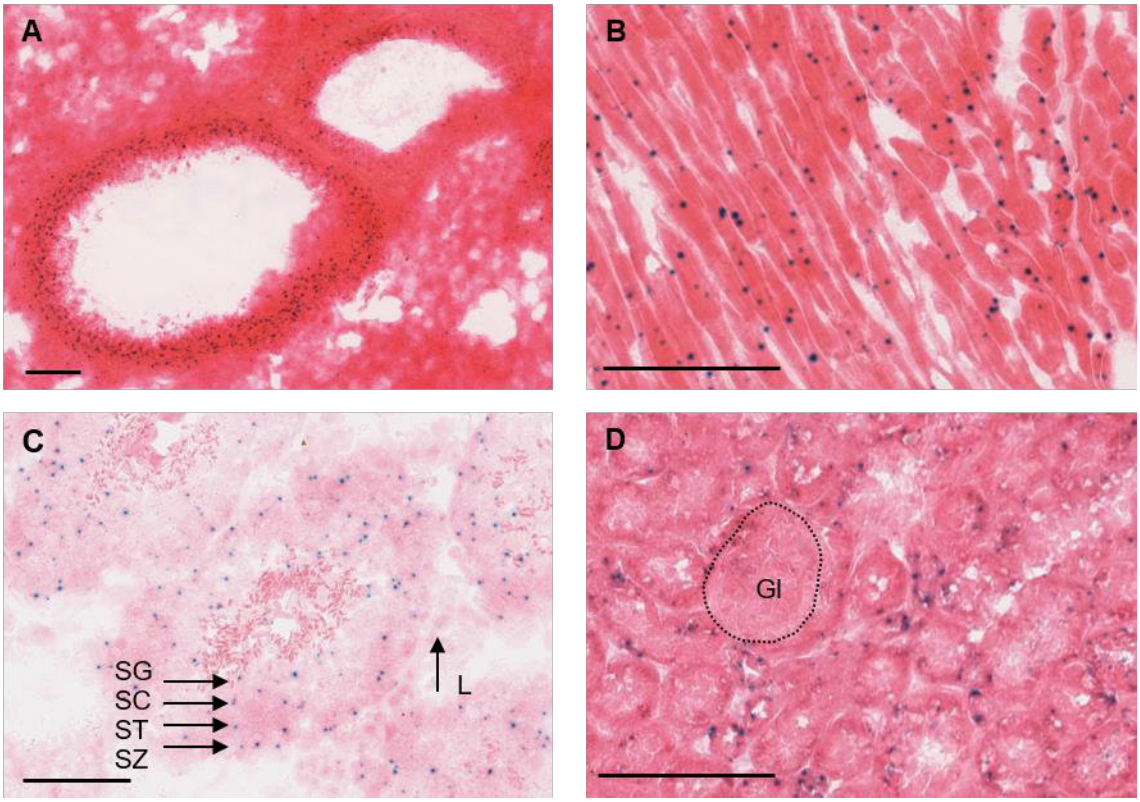

Figure 4.7: *Aven* promoter activity is detectable in the adult lung, heart, kidney and testis
A: X-Gal staining in the ciliated epithelial cells of trachea in the lung. **B**: X-Gal staining in heart muscle cells. **C**: X-Gal staining in the spermatogenic cells within the seminiferous tubuli. SG: Spermatogonia, SC: Spermatocytes, ST: Spermatids, SZ: Spermatozoa, L: Leydig cells (interstitial cells). **D**: X-Gal staining in the kidney. Gl: Glomerulum. The sections were counterstained with Eosin. Scale bars: 100µm.

In the lung, X-Gal staining appears in the epithelial cells of the bronchioli (**Fig. 4.7A**). There is no promoter activity in adjacent vessels or in the alveolar cells detectable. X-Gal staining of the heart shows an even staining of the cardiomyocytes (**Fig. 4.7B**). In the testis, the blue color is found in the seminiferous tubuli, but not in the Leydig cells within the interstitium between the seminiferous tubuli (**Fig. 4.7C**). The staining appears in spermatogenic cells of all maturation stages: from the spermatogonia at the base of the tubuli to spermatocytes, spermatids and mature spermatozoa at the lumina of the tubuli. In the kidney, X-Gal staining is found in the epithelial cells of the tubuli in the cortex, while there is no staining in the glomeruli (**Fig. 4.7D**). A very weak staining is also detectable in the epithelial cells in the colon. The small blue dots appear at the base of the crypts where the epithelial stem cells reside but also upwards of them in the dividing and differentiating cells. No staining could be detected in the spleen, the liver and the thymus (data not shown).

4.1.4 *Aven* promoter activity is restricted to distinct organs in 13.5 dpc embryos but spreads during further embryonic development

To find out whether *Aven* expression is dependent on the developmental stage of mice, X-Gal staining for *Aven* promoter activity was performed on frozen sections of embryos at 11.5, 13.5, 15.5 and 17.5 dpc.

No staining was detected in 11.5 days old embryos. The first staining appeared on sections of embryos at 13.5 dpc, most prominently in the heart, at the entrance of the nasal cavity and at the tips of the forepaws and hind paws (**Fig. 4.8A, B, C, D**). Some weaker staining was also observed in the cells of the anlagen of the stomach and the kidney (**Fig. 4.8E, F**). The liver showed no staining except for a few cells lining an intersection of the liver that is probably built of connective tissue (**Fig. 4.8G**).

At 15.5 dpc, the staining appeared more widespread and with a maximal staining intensity. Sections of homozygous carriers of the *LacZ* gene showed an overall dark blue staining. The reduced staining seen within the sections of heterozygous embryos allowed to differentiate between the levels of staining intensity in the different tissues. The most prominent staining was observed in the facial and cranial bone structures and in the Choroid plexus (**Fig. 4.9A, B, C**). Here, the staining appeared not dot-shaped but rather diffuse. The Choroid plexus was strikingly the only neuronal tissue that showed staining. Besides the heart and the lung, there was also an intense staining in the abdomen, namely in the kidney, stomach and adrenal gland anlagen (**Fig. 4.9E-I**). As at embryonic day 13.5, there was only a small fraction of stained cells in the liver (**Figure 4.9D**). Furthermore, the developing ribs and vertebra are stained, but in contrast to the scull anlagen which were completely stained, the staining was restricted to the outer cartilage cells and the periosteum. There was also staining in the brown fat tissue and the epithelium of the skin (**Fig. 4.9J-M**).

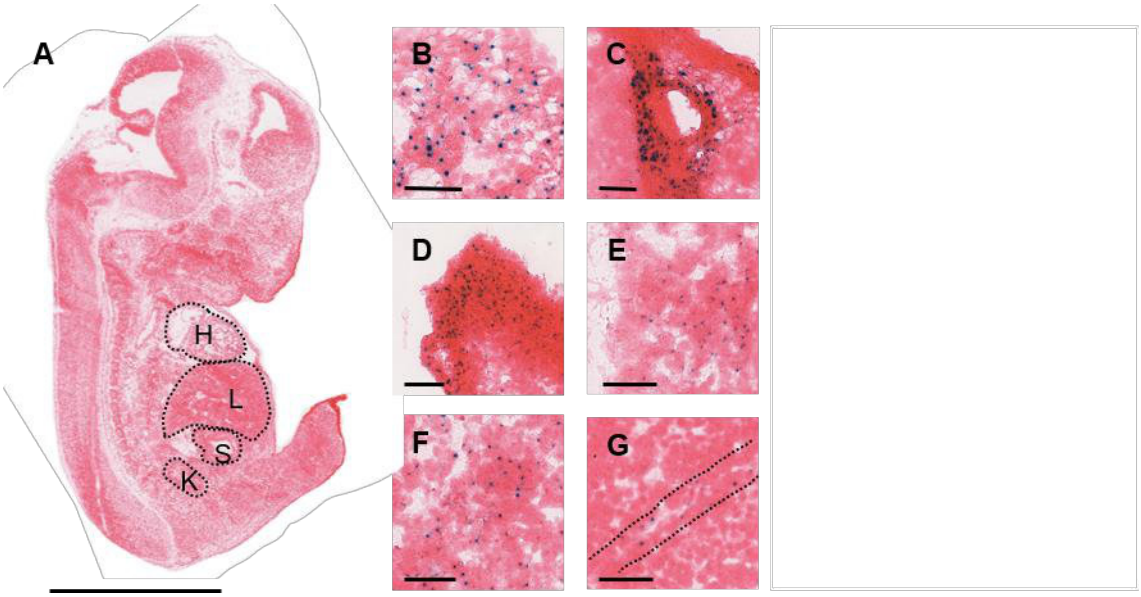

Figure 4.8: First detectable *Aven* promoter activity appears in 13.5 dpc embryos
A: Overview of the X-Gal-stained frozen section of an 11.5 dpc embryo. Tissues that showed X-Gal staining are indicated. H: heart, L: liver, S: stomach, K: kidney. Amplifications of the staining in this and other embryos are shown in B-G. **B**: heart. **C**: entry of the nasal cavity. **D**: tip of a hind paw. **E**: stomach. **F**: kidney **G**: liver. The section was counterstained with Eosin. Scale bars: A: 3 mm, B-G: 50 µm.

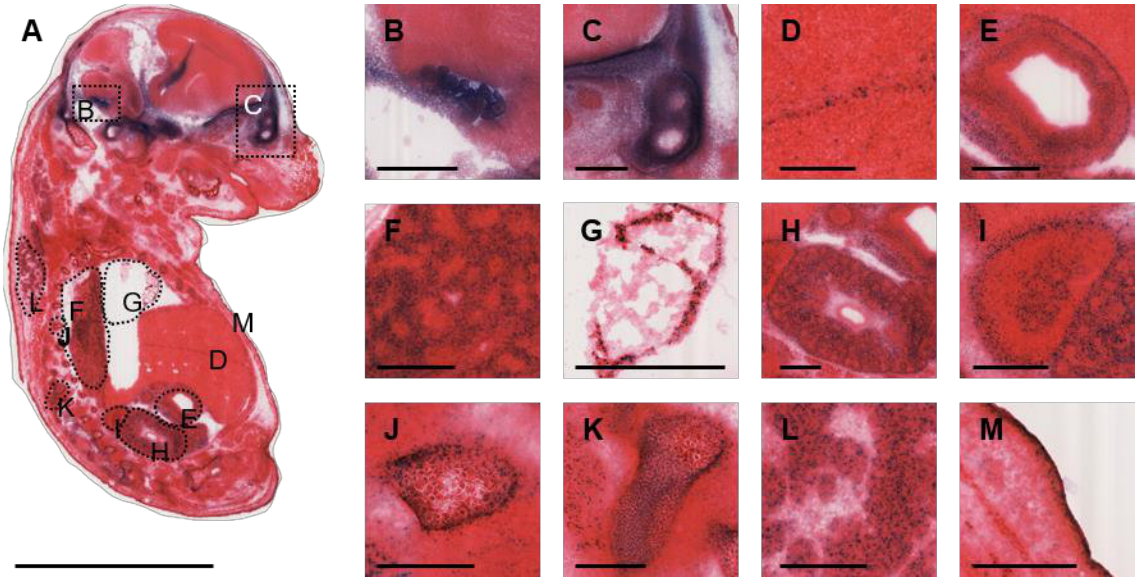

Figure 4.9: Maximal *Aven* promoter activity is detected within 15.5 dpc embryos
A: X-Gal staining of a frozen section of a 15.5 dpc *AvenLacZ*$^{+/d}$ embryo. Amplifications of the X-Gal staining in the different organs is shown in B-M. **B**: Choroid plexus. **C**: cartilage primordium with starting ossification of cranial/facial bones. **D**: liver **E**: stomach. **F**: lung. **G**: heart. **H**: kidney. **I**: adrenal gland. **J**: rib. **K**: vertebra. **L**: brown fat tissue. **M**: skin. The section was counter stained with Eosin. The section was counterstained with Eosin. Scale bars: A: 5 mm, B-M: 500 µm.

At day 17.5, the overall intensity of the staining appeared decreased compared to day 15.5, but was broadly present (**Fig. 4.10A**). The heart still showed a prominent staining. The staining of the Choroid plexus and cranial bone structures was still present but faint

at embryonic day 17.5 (**Fig. 4.10B, C**). The same was true for the vertebra, the lung, the line of connective tissue in the liver, the epithelium of the skin and the anlagen of the stomach and the kidney: they were significantly stained but at a lower degree of intensity than at day 15.5 (**Fig. 4.10D-H**). A new intense staining appeared in the vessels within the lung and in the large vessels next to the heart (**Fig. 4.10E, I**). The section of the 17.5 dpc embryo also showed a staining in the anlagen of the esophagus (**Fig. 4.10J**) and the seminiferous tubules (**Fig. 4.10K**), as well as in the mucous part of the salivary gland (**Fig. 4.10L**), in the ossification within the mandible and the primordium of a tooth **(Fig. 4.10M**). The most intense staining in the lumen of the intestine also appeared on wildtype sections and, thus, was unspecific.

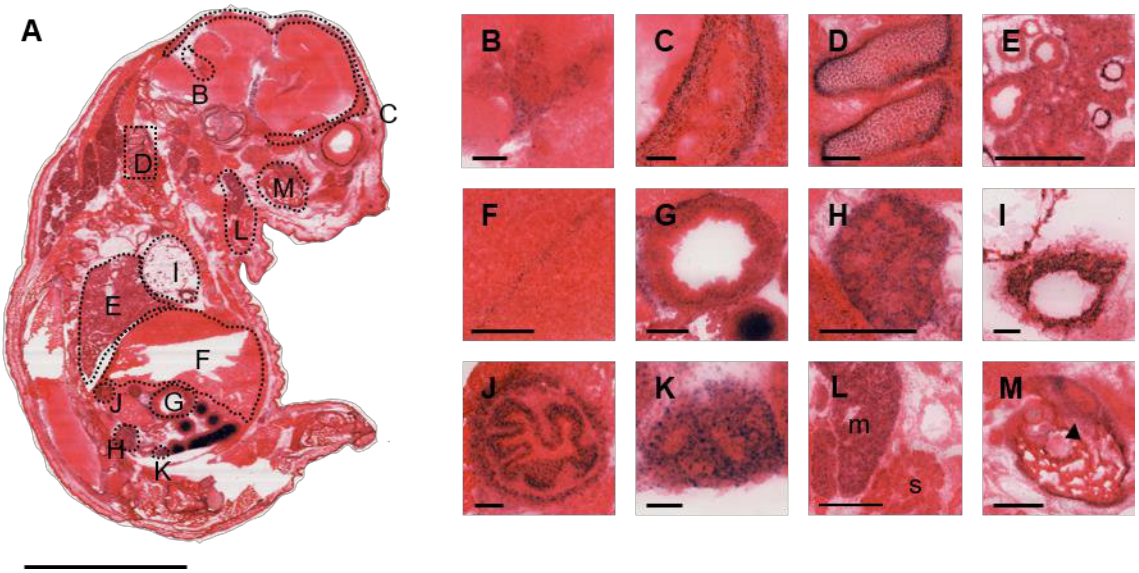

Figure 4.10: Widespread *Aven* promoter activity in 17.5 dpc embryos
A: X-Gal staining of the frozen section of a homozygous 17.5 dpc *AvenLacZ* embryo. Amplifications of the staining in different tissues is shown in B-M. **B**: choroid plexus. **C**: Ossification within cranial bone. **D**: vertebra. **E**: lung with vessels. **F**: liver. **G**: stomach, intestine in the lower right corner. **H**: kidney. **I**: vessel next to the heart at the upper left corner. **J**: esophagus. **K**: seminiferous tubules. **L**: salivary gland, m: mucous part, s: serous part. **M**: mandible with the primordium of a tooth (arrow head). The section was counterstained with Eosin. Scale bars: A: 5 mm, B, C, D, G, I, J, K: 100 µm, E, H, L, M: 500 µm.

In summary, the X-Gal staining of embryos at different developmental stages indicated that first *Aven* promoter activity arises at 13.5 dpc in heart, lung and abdominal organs. *Aven* promoter activity could be detected more widespread with ongoing maturation with maximal activity levels at 15.5 dpc in the Choroid plexus and facial and cranial bone structures. The *Aven* promoter activity in the 15.5 and 17.5 dpc embryos seemed to be higher than the promoter activity detected in adult organs.

AVEN had been described as an anti-apoptotic protein [8], so cells lacking AVEN in

homozygous knockout mice could be more prone to apoptosis. To test this hypothesis, paraffin sections of embryos and adult organs were immunohistochemically stained for cleaved Caspase 3, which is a marker of apoptosis. Comparison of *Aven* knockout and wildtype sections did not show any difference in the quantity of stained cells (**Fig. 4.11**). Obviously, the loss of AVEN did not lead to increased programmed cell death in the *Aven* knockout mice, which hints to a functional role besides apoptosis inhibition of AVEN during embryogenesis.

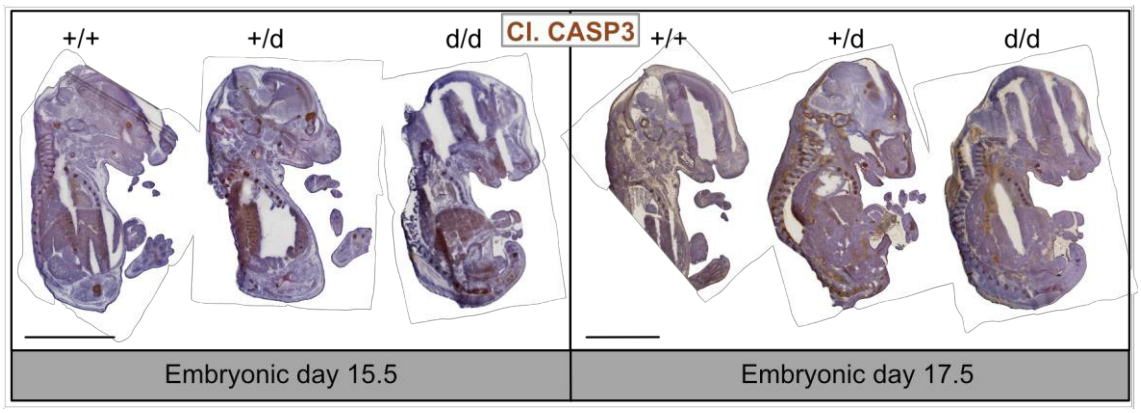

Figure 4.11: Depletion of AVEN does not increase cell death in 15.5 dpc and 17.5 dpc mouse embryos
Paraffin sections of fixed mouse embryos at 15.5 dpc and 17.5 dpc were stained for cleaved Caspase 3 (Cl. CASP3, brown color). There was no difference in the extent of staining between animals with wildtype AVEN expression (+/+) and depleted AVEN expression in heterozygous (+/d) and homozygous (d/d) *AvenLacZ* mice. Sections were counter-stained with hematoxylin (blue color). Scale bar: 5 mm.

4.1.5 Analysis of conditional *Aven* knockout mice

The constitutive knockout of *Aven* is embryonic lethal. Therefore, mice with a cell type-specific *Aven* knockout were analyzed to study the consequences of AVEN deficiency in distinct tissues. To generate conditional knockout mice, animals carrying a floxed *Aven* exon 2 were bred with deleter strains expressing CRE recombinase under the control of different, tissue-specific promoters. First, the efficiency of the deletion of *Aven* exon 2 was tested by mating floxed mice with a *CMV-Cre* deleter strain. The *CMV* promoter is active in all cells, already during the blastocyst-state [151], and therefore the CRE-expressing offspring carrying the targeted *Aven* allele display a constitutive knockout (**Fig. 4.12A**). As in the case of the constitutive knockout in the *AvenLacZ* mice, the constitutive knockout established from the conditional allele was embryonic lethal. While there was still some offspring with a homozygous *Aven* knockout in the first generations, backcrossing into a pure genetic Bl/6 background led to the complete loss of living homozygous offspring (**Fig. 4.12B**).

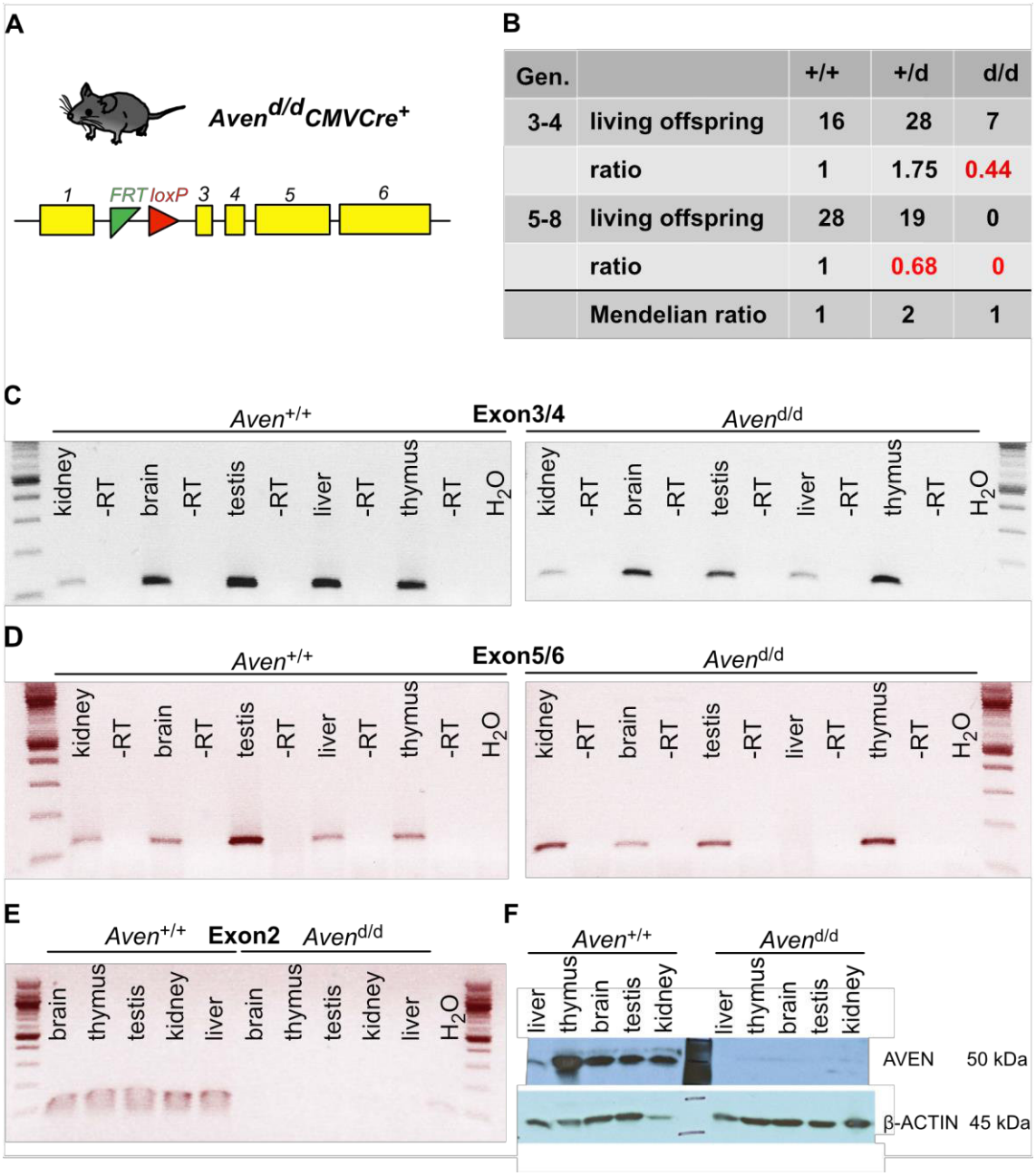

Gen.		+/+	+/d	d/d
3-4	living offspring	16	28	7
	ratio	1	1.75	0.44
5-8	living offspring	28	19	0
	ratio	1	0.68	0
	Mendelian ratio	1	2	1

Figure 4.12: Constitutive deletion of *Aven* exon 2 leads to a functional inactivation of AVEN and is embryonic lethal in mice
A. Scheme of the *Aven* allele in *Aven$^{d/d}$CMVCre^{+}* mice. **B**. Statistics of the *Aven* genotype of offspring from het:het mating (parents were *Aven$^{+/d}$CMVCre^{+}*). **C**-**E**. *Aven$^{d/d}$CMVCre^{+}* mice express *Aven* mRNA containing exons 3 (**D**) to 6 (**E**) but not exon 2 (**C**). RNA from different organs was isolated from *Aven$^{d/d}$CMVCre^{+}* and *Aven$^{+/+}$CMVCre^{+}* mice, reversely transcribed to cDNA and used for PCR. To exclude genomic DNA contamination, cDNA synthesis reactions were performed without reverse transcriptase (-RT) and used for PCR, too. **F**. AVEN protein was not detected by western blotting in organs lysates of *Aven$^{d/d}$CMVCre^{+}* mice in contrast to *Aven$^{+/+}$CMVCre^{+}*. β-ACTIN was detected as a loading control.

In contrast to the *AvenLacZ* mice, *Aven* mRNA could still be detected in the living homozygous knockout mice. No PCR product of *Aven* exon 2 could be amplified, since this exon had been deleted, but PCR products of exon 1 and exon transitions 3/4 and 5/6 were measurable (**Fig. 4.12C-E**). While an *Aven* mRNA lacking exon 2 sequence

was detectable, no AVEN protein was expressed in the mouse organs as tested by western blotting (**Fig. 4.12F**). It can be concluded that the deletion of *Aven* exon 2, which is predicted to result in a frameshift mutation, gave an mRNA product that escaped decay. However, the protein product of this mRNA (if produced at all) was not recognized by an anti-AVEN antibody and can be considered non-functional. Thus, the deletion of *Aven* exon 2 by cell type-specific CRE-recombinases in the conditional knockout mouse models was sufficient to functionally inactivate AVEN in the respective tissues.

4.1.6 AVEN expression is dispensable in developing neurons and mature hippocampal cells

Aven expression analysis in the *AvenLacZ* mice revealed a prominent *Aven* promoter activity in the hippocampal structure of the adult brain (**Fig. 4.3**). To test whether the loss of AVEN in these neurons was sufficient to cause embryonic lethality and to identify consequences of AVEN depletion in these cells of potentially living mice, animals with a floxed *Aven* locus were bred with *CamkIIα-Cre* deleters. CaMKIIα is a calcium channel, and the promoter is active only in mature specific cells of the brain [152], amongst them the pyramidal neurons of the hippocampus (**Fig. 4.13A**). The offspring of this breeding carrying the floxed *Aven* allele and expressing *CamkIIα-Cre* was alive and healthy. The brain region-specific knockout in these mice could be confirmed on mRNA and protein level: the front part of the brain consisting of cells that do express CaMKIIα showed an absence of AVEN. The hind region of the brain not containing CaMKIIa-positive cells had the same AVEN expression as the wildtype tissue, and the middle part, containing the hippocampus, displayed reduced levels of AVEN protein and *Aven* mRNA expression (**Fig. 4.13B, C, D**). Histological analysis of paraffin sections of the brains did not reveal any structural damage (data not shown). The lack of a phenotype of these mice showed that AVEN expression in CaMKIIα-positive adult neurons is not essential. However, behavioral studies need to be performed to reveal a potential requirement for AVEN for normal neuron function.

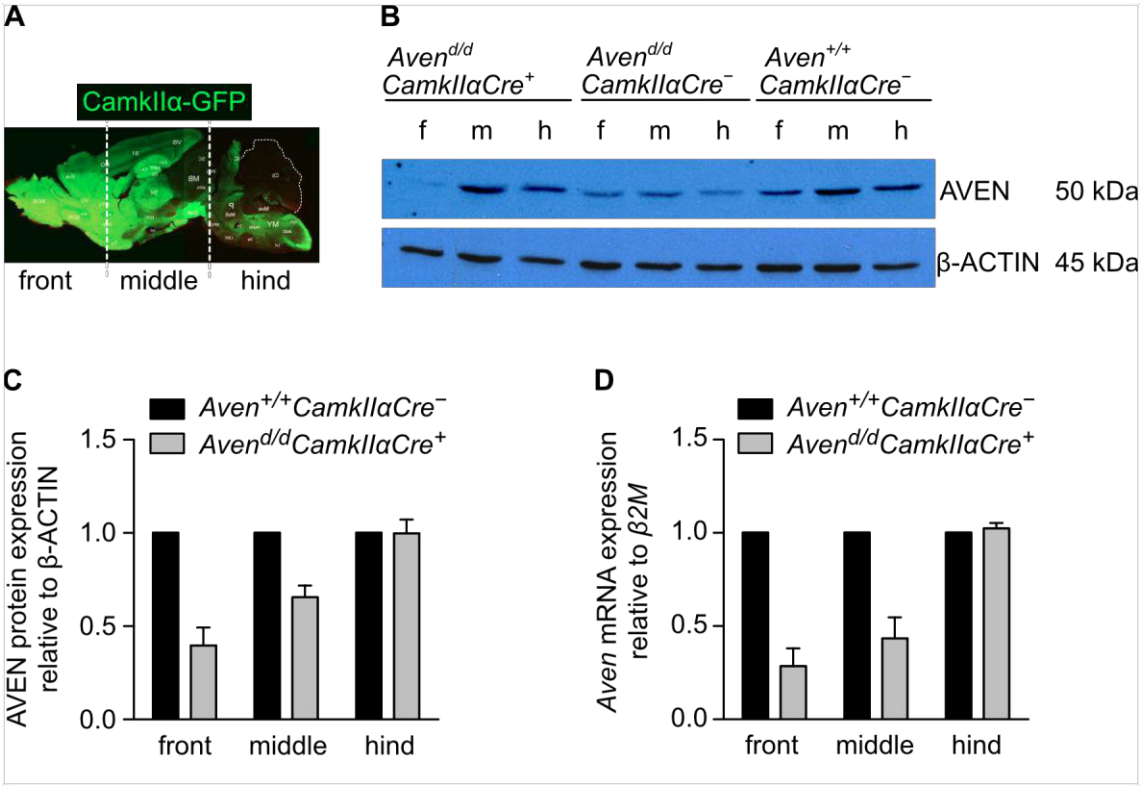

Figure 4.13: AVEN expression in the front and middle part of the brain is reduced in *Aven$^{d/d}$CamkIIaCre^{+}* mice
A. Sites of *CamkIIα* expression in the adult mouse brain, visualized by GFP expression (from Wang 2013). Sectioning of the brain into front (f), middle (m) and hind (h) part for western blotting in B is indicated. **B**, **C**. AVEN protein expression is strongly reduced in the front and moderately reduced in the middle part of the brain in *Aven$^{d/d}$CamkII*αCre^{+} mice compared to mice with wildtype AVEN expression (*Aven$^{d/d}$CamkII*αCre^{-} *and Aven$^{+/+}$CamkII*αCre^{-} mice). AVEN Protein signals in western blots (**B**) were quantified relative to β-ACTIN expression and normalized to expression of *Aven$^{+/+}$CamkII*αCre^{-} mice (**C**). **D**. The reduction of *Aven* expression in the front and middle part of the brain in *Aven$^{d/d}$CamkII*αCre^{+} mice could be confirmed on mRNA level. *Aven* mRNA expression was quantified by qPCR relative to *β2M* expression and normalized to expression of *Aven$^{+/+}$CamkII*αCre^{-} mice.

The knockout of *Aven* in CaMKIIα-expressing cells is restricted to distinct mature neurons. To test the requirements for AVEN in all developing neurons during embryogenesis, I bred mice carrying a floxed *Aven* allele with *Nestin-Cre* deleters. The *Nestin* promoter is reported to be active in neural stem cells the peripheral and central nervous system, detectable already in neuronal precursors at embryonic day 7 [153]. Consequently, homozygous carriers of the targeted *Aven* allele expressing *Nestin-Cre* should lack AVEN expression in all neurons from embryonic neurogenesis on. The *Aven* knockout in the whole brain could be confirmed on protein (**Fig. 4.14A, B**) and mRNA level (**Fig. 4.14C**). The conditional knockout mice were viable and fertile and the adult brains displayed no altered histology. Apparently, AVEN expression in developing neurons is dispensable.

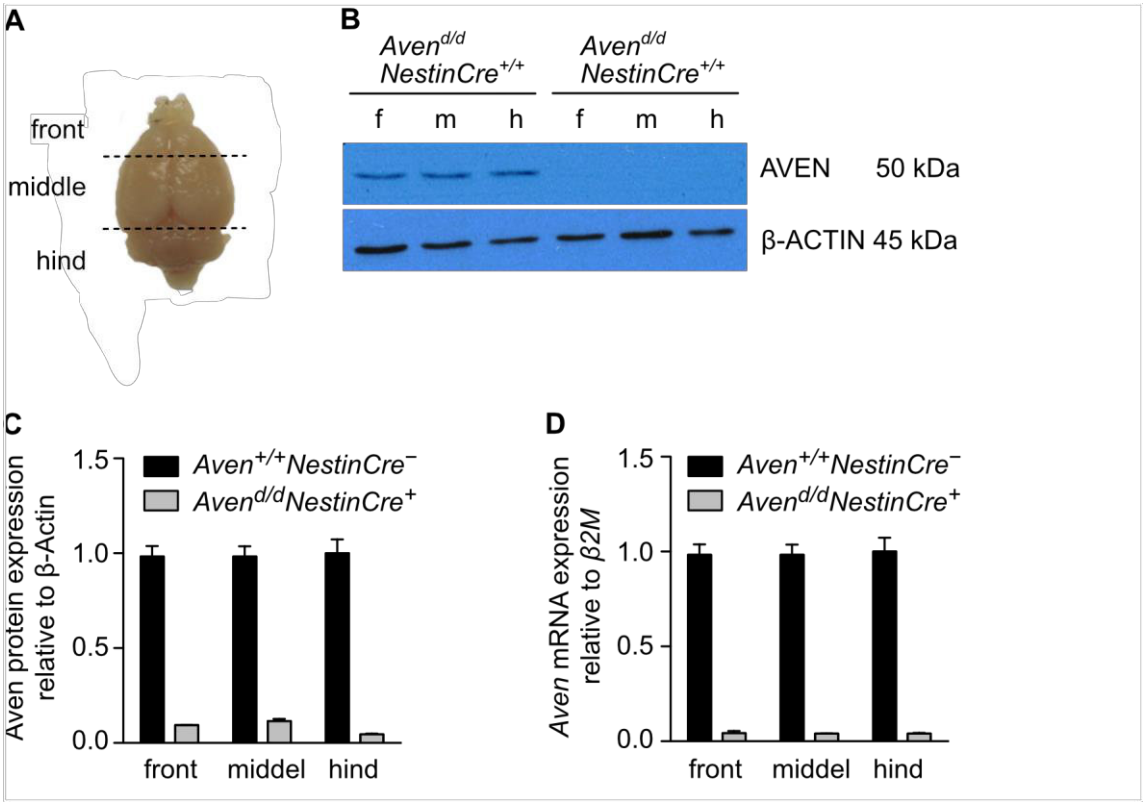

Figure 4.14: AVEN expression vanished in the whole brain of *Aven*$^{d/d}$*NestinCre*$^{+}$ mice
A. Sectioning of the brain into front (f), middle (m) and hind (h) part for protein lysates used in B. **B**, **C**. AVEN protein expression is missing in all parts of the brain in *Aven*$^{d/d}$*NestinCre*$^{+}$ mice. AVEN protein signals in western blots (**B**) were quantified relative to β-ACTIN expression and normalized to expression of *Aven*$^{+/+}$*Nestin*Cre^{-} mice (**C**). **D**. Knockout of *Aven* in the whole brain was also confirmed on mRNA level. *Aven* mRNA expression was quantified by qPCR relative to *β2M* expression and normalized to expression of *Aven*$^{+/+}$*CamkII*αCre^{-} mice.

4.1.7 Knockout of *Aven* in the hematopoietic system had no effect on stem and progenitor cell frequencies and lineage marker expression

Mice with a floxed *Aven* locus were bred with a transgenic *Vav-Cre* deleter strain to achieve an *Aven* knockout that is restricted to the hematopoietic system. Analyzing the effect of an *Aven* knockout in mature blood cells as well as in stem and progenitor cells seemed to be particularly interesting for the following reasons: First, aberrant expression of AVEN in blood cells has been associated with leukemia: high *AVEN* mRNA expression has been detected in AML, T-ALL and B-ALL patient samples [27]; high AVEN expression levels correlate with poor survival in childhood ALL [25], [26]. Overexpression of *Aven* in T-cells in a transgenic *p53*$^{+/-}$ mouse model induced T-ALL onset while knockdown of *Aven* in human T-ALL cell lines reduced tumorigenicity in in mouse xenograft model [27]. So increased *Aven* expression in leukocytes seems to exhibit oncogenic potential, but nothing is known about the function of physiologically expressed *Aven* in hematopoietic cells.

Second, the pale phenotype of homozygous constitutive *Aven* knockout embryos and embryonic lethality at a stage at which adult bone marrow hematopoiesis is established suggested an involvement of AVEN in hematopoiesis.

Mice that were heterozygous carriers of the floxed *Aven* allele (*Aven*$^{+/d}$) were crossed with *Aven*$^{+/d}$ animals that additionally expressed CRE under the control of the *Vav* promoter (*Aven*$^{+/d}$*VavCre*$^{+}$, **Fig. 4.15A**). The *Vav* promoter is active already in hematopoietic stem cells as well as in primitive and committed progenitors and mature blood cells [154]. Additionally, *Vav* promoter activity is reported in endothelial and germ cells [154]. Thus, *Aven* deletion mediated by CRE in *VavCre*$^{+}$ mice leads to an efficient knockout of *Aven* in the entire definitive hematopoietic compartment. The offspring statistics of these mice matched Mendel´s law which predicts a ratio of 1:2:1 of wildtype, heterozygous and homozygous *Aven* offspring. No AVEN protein was detected in *Aven*$^{d/d}$*VavCre*$^{+}$ spleenocytes and thymocytes, in contrast to the wildtype cells (**Fig. 4.15B**). Remarkably, no AVEN protein was detected in bone marrow cells of both *Aven*$^{d/d}$*VavCre*$^{+}$ and *Aven* wildtype (*Aven*$^{+/+}$*VavCre*$^{+}$) mice (**Fig. 4.15B**).

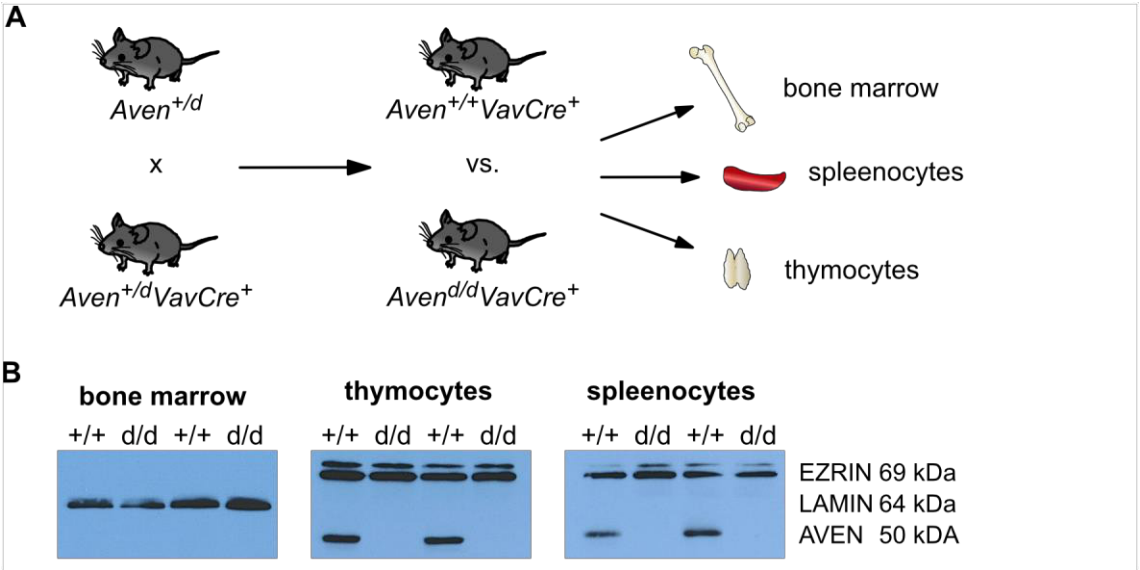

Figure 4.15: AVEN protein deficiency in the hematopoietic system of *Aven*$^{d/d}$*VavCre*$^{+}$ mice
A. Mice with a heterozygous floxed *Aven* allele (*Aven*$^{+/d}$) were crossed with *Vav-Cre* transgenic deleter animals (*VavCre*$^{+}$) to generate mice with an *Aven* knockout in the hematopoietic system (*Aven*$^{d/d}$*VavCre*$^{+}$). In analyses of these mice, litter mates with wildtype *Aven* alleles but *Cre* expression (*Aven*$^{+/+}$*VavCre*$^{+}$) were used as control group. **B**. AVEN protein expression was successfully depleted in bone marrow, thymocytes and spleenocytes of *Aven*$^{d/d}$*VavCre*$^{+}$ (d/d) mice as assessed by western blotting. No AVEN is expressed in the bone marrow of both *Aven*$^{d/d}$*VavCre*$^{+}$ and *Aven*$^{+/+}$*VavCre*$^{+}$ mice (+/+). EZRIN and LAMIN expression was detected as loading control.

To test whether the loss of AVEN had an effect on stem cell and progenitor frequencies and/or the efficiency of lineage differentiation, bone marrow mononuclear cells were

stained for stem and progenitor cell surface markers. Whole bone marrow cells and spleenocytes were tested for myeloid and lymphoid differentiation marker expression and thymocytes were analyzed regarding expression of T-cell differentiation markers. The frequencies of the stained cells were assessed by flow cytometry. Immature multipotent cells were defined as lineage marker negative, c-KIT- and Sca-1-positive (KSL cells). Within KSL cells, HSCs were discriminated as CD150-positive and CD34-negative cells. LT-HSCs were distinguished from ST-HSCs by the missing expression of CD48. The gating strategy is shown in **Fig. 4.16A** and **B**.

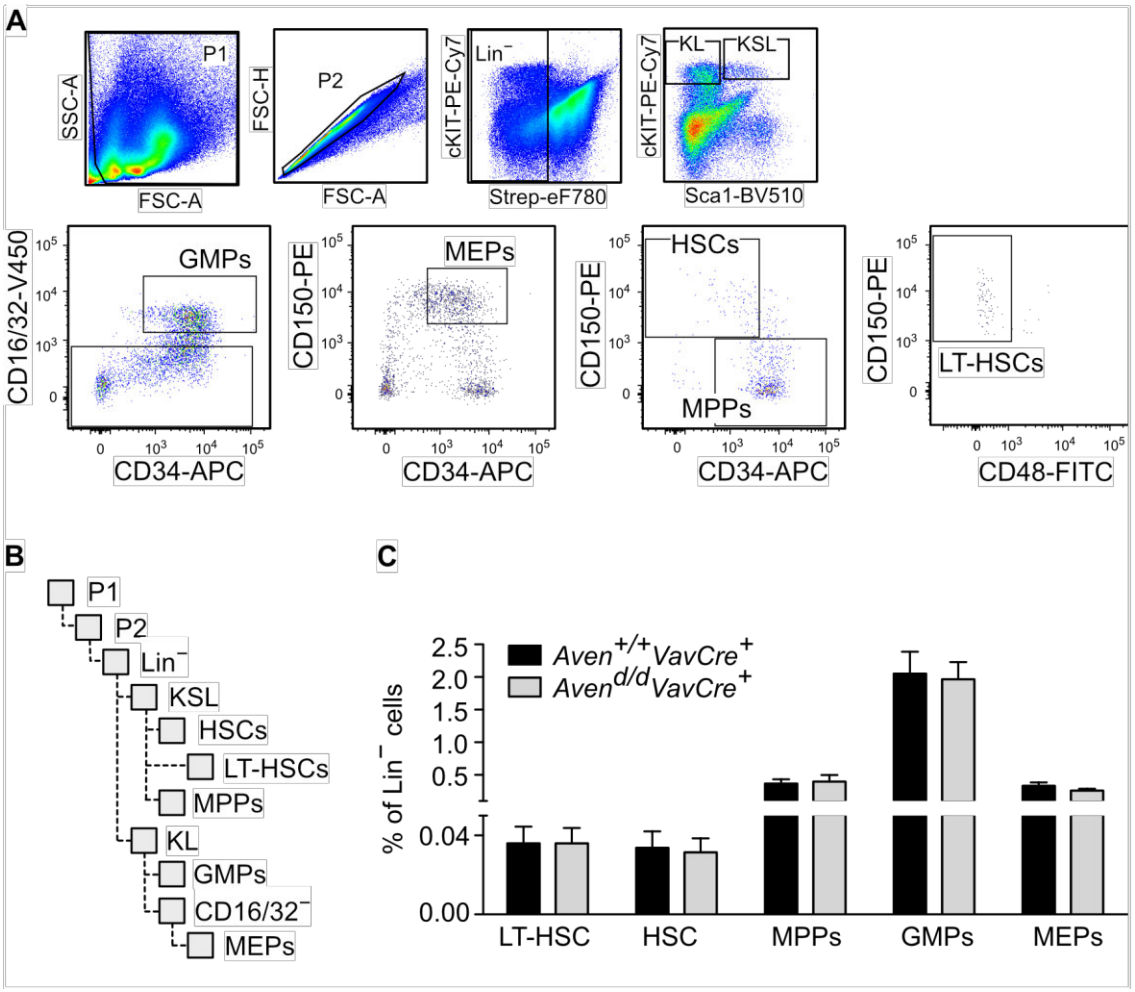

Figure 4.16: *Aven* knockout in the hematopoietic system has no effect on HSPC frequencies
A, **B**. Gating strategy in flow cytometry analysis of murine hematopoietic stem and progenitor cells after cell surface marker staining. **C**. No difference in hematopoietic stem and progenitor cell frequencies was observed between mice with an *Aven* knockout in the hematopoietic system (*Aven*$^{d/d}$*VavCre*$^{+}$, n=4) and control mice with wild type *Aven* expression (*Aven*$^{+/+}$*VavCre*$^{+}$, n=4). LT-HSCs: long term hematopoietic stem cells. MPPs: multipotent progenitors. GMPs: granulocyte macrophage progenitors. MEPs: megakaryocyte erythroid progenitors.

No differences between *Aven* knockout and control cell populations were observed (**Fig. 4.16C**). The frequencies of multipotent progenitors (MPPs, KSL cells that are CD150-

negative and CD34-positive), granulocyte macrophage progenitors (GMPs, lineage marker-negative, c-Kit-positive, Sca-1-negative cells (KL cells), CD34- and CD16/32-positive cells) and megakaryocyte-erythroid progenitors (MEPs, KL cells, CD16/32-negative, CD34-positive, CD150-positive cells) were also unaltered (**Fig. 4.16 C**). Concluding from these results, AVEN has no functional relevance for the generation and maintenance of stem and progenitor cells.

Frequencies of stained whole bone marrow cells, spleenocytes and thymocytes were assessed to test the differentiation potential of the *Aven* knockout progenitors. The gating strategy to identify different lineages is depicted in **Fig. 4.17A**. The percentage of CD45.2-positive leukocytes was unaltered between *Aven* knockout and control mice (**Fig. 4.17B, C**, left). Also, discrimination between B220$^+$ B cells and CD3$^+$ T cells did not reveal any abnormality in the *Aven* knockout tissue (**Fig. 4.17B, C**, right).

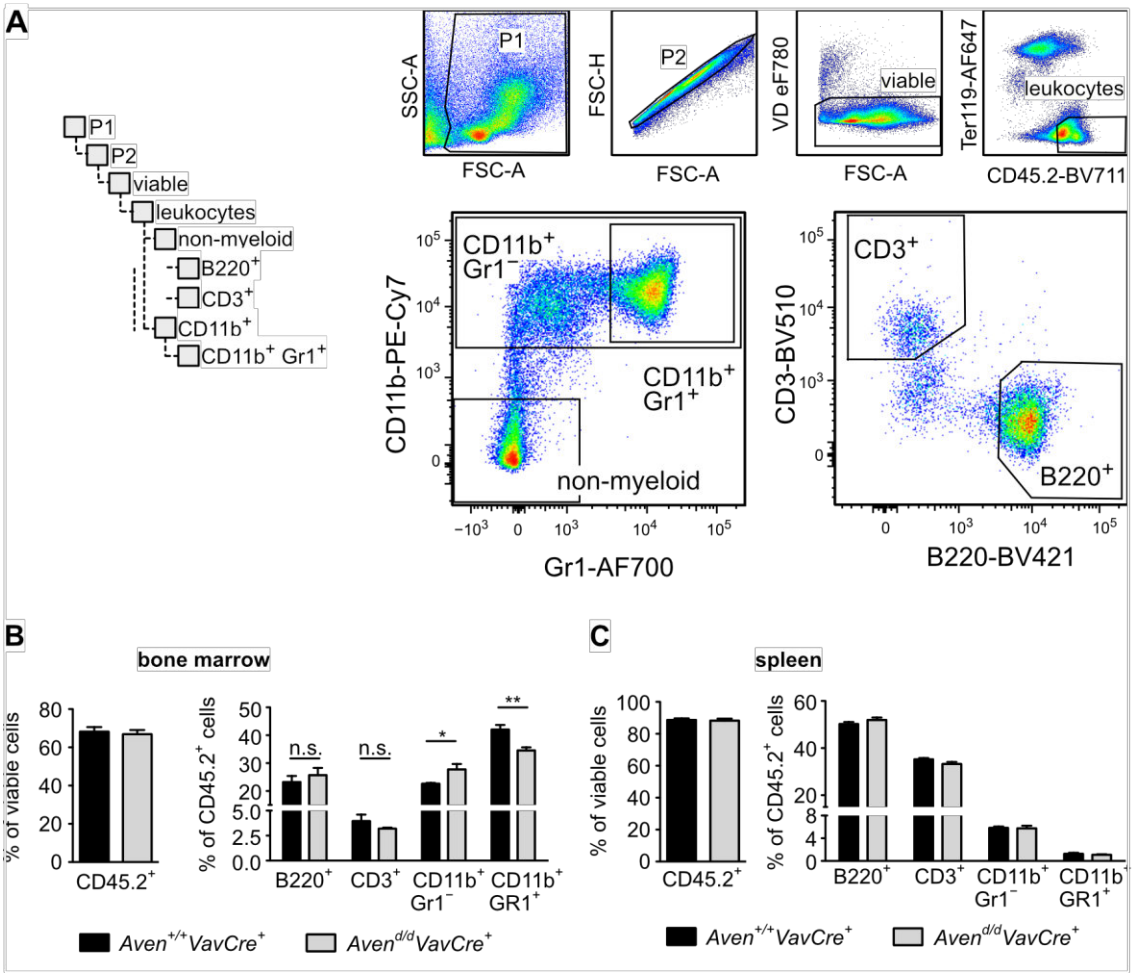

Figure 4.17: Knockout of *Aven* in the bone marrow microenvironment affects myeloid differentiation
A. Gating strategy for the analysis of lineage differentiation in the bone marrow and spleen by flow cytometry after cell surface marker staining. **B**. Knockout of *Aven* in *Vav* expressing hematopoietic and endothelial cells did not alter the percentage of overall leukocytes (CD45.2$^+$ cells) in the bone marrow but increased CD11B$^+$Gr1$^-$ myeloid cells on dispense of CD11b$^+$Gr1$^+$

cells. **C**. The effect of the *Aven* knockout in *Aven$^{d/d}$VavCre^{+}* mice on myeloid cell differentiation was not observed in the spleen. Cell population frequencies in *Aven* knockout mice (*Aven$^{d/d}$VavCre^{+},* n=4) were compared to frequencies in control mice with wildtype *Aven* expression (*Aven$^{+/+}$VavCre^{+},* n=4).

Interestingly, there was a significant reduction of CD11b, Gr1 double-positive myeloid cells in the *Aven* knockout bone marrow. In contrast, the percentage of only CD11b-positive but Gr1-negative macrophages was increased (**Fig. 4.17B** right). However, this alteration in myeloid cell frequencies was not observed in the spleen (**Fig. 4.17C**, right). As there is no AVEN expression in wild type bone marrow cells (**Fig. 4.15B**), the effect of *Aven* deficiency on myeloid cells has to arise as a consequence of the *Aven* knockout in the bone marrow microenvironment, namely the *Vav* expressing endothelial cells. The results suggest that AVEN deficiency in the bone marrow microenvironment shifts myeloid cell differentiation towards macrophages in the expense of granulocytes.

Looking at the thymocytes, no difference in the percentage of $CD3^{+}$ cells was detected (data not shown), complementing the results of $CD3^{+}$ cells in the bone marrow. Differentiation of T cells to mature T helper and naïve cytotoxic T cells can be monitored by the expression of cell surface markers CD4 and CD8. CD4 and CD8 double-negative (DN) lymphoid progenitors start to express both CD4 and CD8, constituting a double positive (DP) population. Continuing in differentiation, these cells reduce expression of both markers ($CD4^{low}$, $CD8^{low}$) before they increase first CD4 and then CD8 again ($CD4^{+}CD8^{low}$). Cells committed to become T helper cells reduce CD8 expression until they are CD4 single positive mature cells ($CD4^{+}$). Cells destined to become cytotoxic T cells reduce CD4 expression and increase CD8 expression ($CD8^{+}CD4^{low}$) to become CD8 single positive mature cells ($CD8^{+}$). Some of these cytotoxic committed cells also pass the $CD4^{+}CD8^{low}$ population before upregulation of CD8 [155]. All the described populations were identified in flow cytometry analysis (**Fig. 4.18A**), but in none of them a difference in the frequencies of *Aven* knockout and wildtype thymocytes was observed (**Figure 4.18B**). So, the loss of AVEN expression in thymocytes did not impact T cell differentiation in terms of differentiation marker expression.

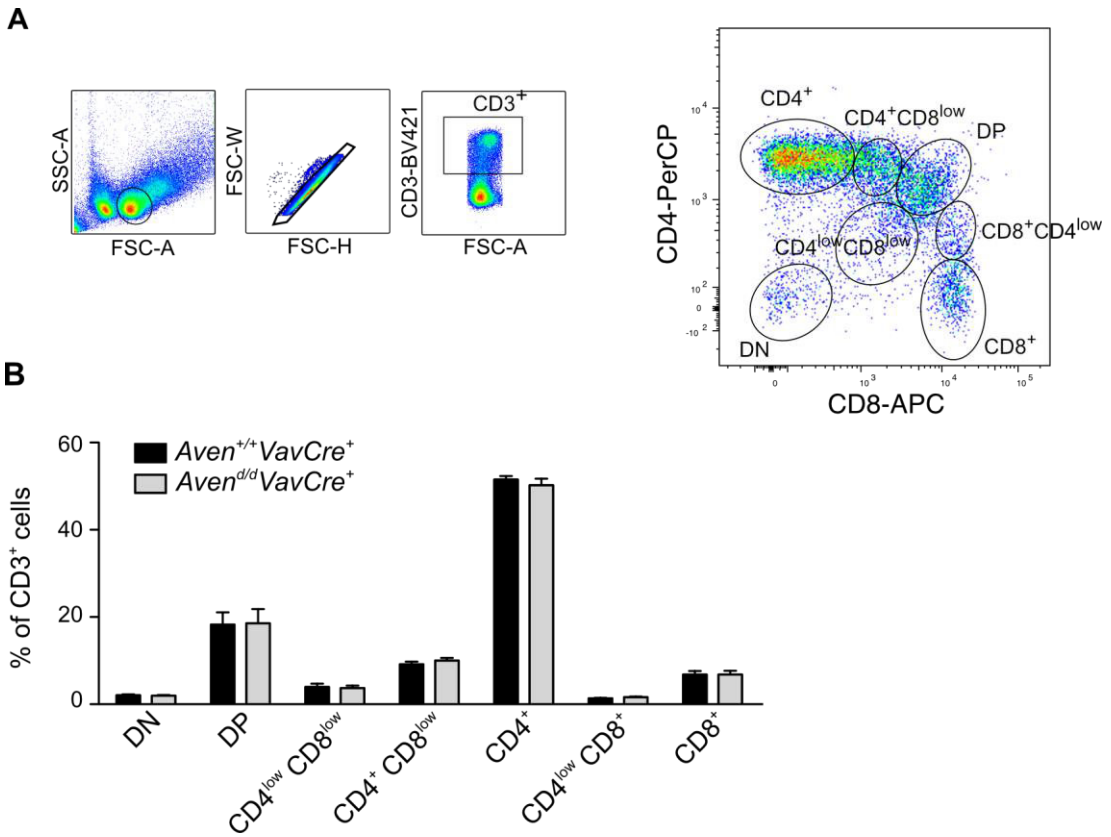

Figure 4.18: Knockout of *Aven* in the hematopoietic system has no effect on normal T cell development in the murine thymus
A. Gating scheme to identify T cell maturation stages of thymocytes by flow cytometry following CD3, CD4 and CD8 staining. **B**. No differences in the percentage of T cell differentiation stages were observed between *Aven* knockout (*Aven$^{d/d}$VavCre^{+},* n=4) and control mice (*Aven$^{+/+}$VavCre^{+},* n=4).

Finally, erythropoiesis in the bone marrow and in the spleen was investigated. Maturation of MEPs to enucleated red blood cells is characterized by the expression of transferrin receptor CD71 and murine glycopherin A (Ter119). Immature MEPs are negative for both markers, during erythroid differentiation, CD71 expression continuously increases, peaking at the stage of the early polychromatic erythroblast, followed by a subsequent down regulation. Increased Ter119 expression starts delayed compared to CD71 expression but stays at high levels until the end of erythroid differentiation [156]. Thus, progressing erythropoiesis is reflected by the following chronologically appearing populations: CD71^{-}Ter119^{-}, CD71^{+}Ter119^{-}, CD71^{+}Ter119^{m}, CD71^{+}Ter119^{+}, CD71^{m}Ter119^{+}, CD71^{-}Ter119^{+} (**Fig. 4.19A**). Evaluation of the percentages of these populations did not reveal any differences between *Aven* knockout and wildtype erythropoiesis (**Fig. 4.19B**).

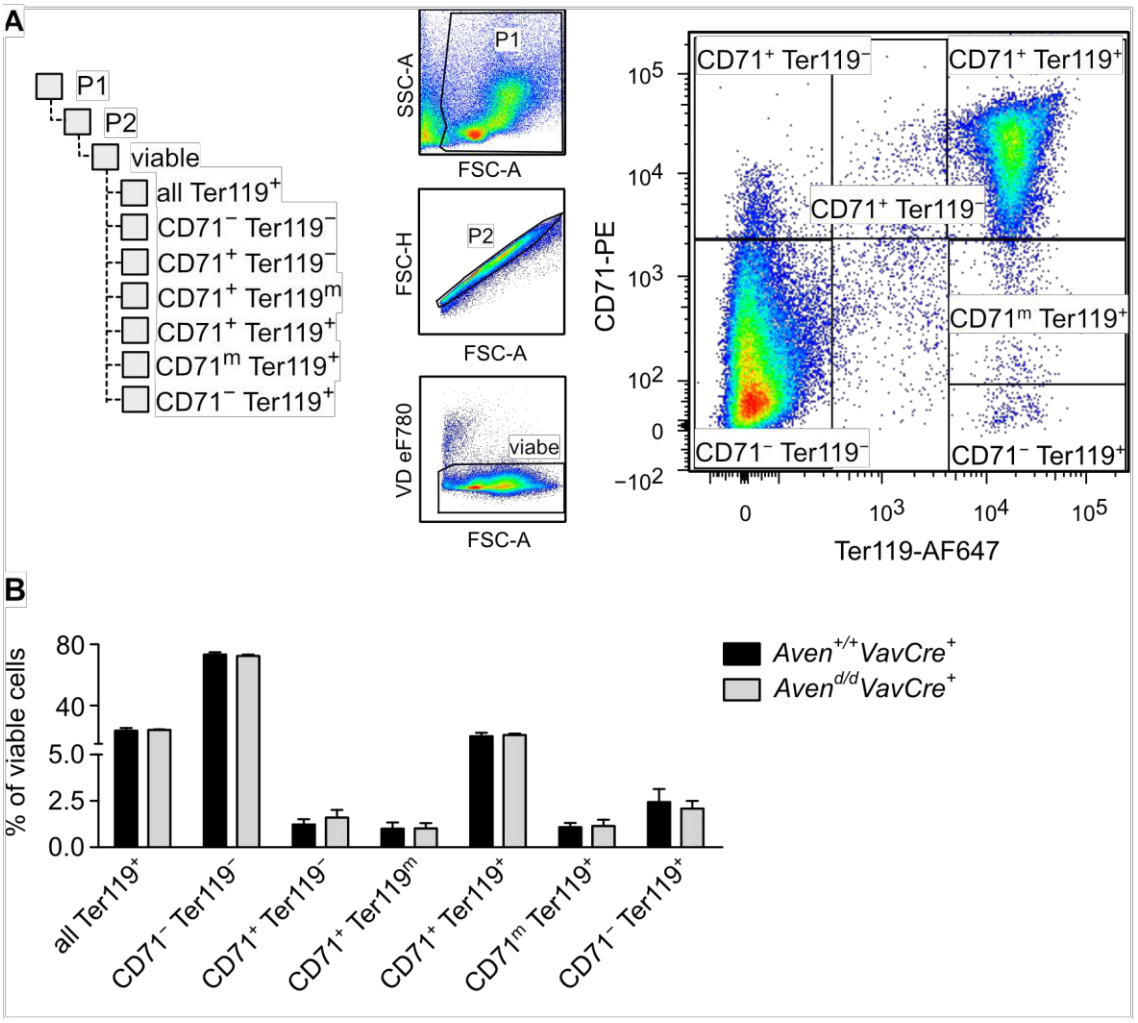

Figure 4.19: AVEN deficiency does not impact murine erythropoiesis
A. Gating scheme to discriminate erythroid differentiation stages by flow cytometry after cell surface marker staining. **B**. *Aven*$^{d/d}$*VavCre*$^{+}$ (n=4) mice showed no changes in percentages of erythroid populations compared to *Aven*$^{+/+}$*VavCre*$^{+}$ (n=4) mice.

All together, these results demonstrated that AVEN expression in hematopoietic cells was not required for the maintenance and differentiation of stem, progenitor and mature blood cells, at least not as far as the expression of particular differentiation markers was concerned. However, studies challenging the hematopoietic compartment need to be performed to test the functionality of *Aven* knockout blood cells. The observed effect of an *Aven* knockout in the bone marrow microenvironment on myeloid cell differentiation also warrants further examination.

4.1.8 Although AVEN expression is up-regulated in the mammary gland during pregnancy and lactation, it is dispensable for normal breast development in mice

Human AVEN has been reported to prevent DNA damage-induced apoptosis in breast

cancer cells [10]. The same publication shows reduced levels of nuclear localized AVEN in breast cancer tissues. In healthy breast tissue, a moderate AVEN signal is detected by immunohistochemistry in glandular cells and adipocytes, and a weak AVEN staining is detected in myoepithelial cells (the data is accessible in the Human Protein Atlas [157]). The same website provides AVEN expression analyses in breast cancer cell lines and patient samples: all breast cancer cell lines and 5 out of 11 patients displayed a medium to high AVEN expression. Preliminary analysis performed in the Zörnig lab (unpublished data) also confirmed that AVEN is moderately to highly expressed in various luminal and basal breast cancer cell lines. Furthermore, elevated levels of the endogenous anti-apoptotic ΔN-AVEN protein were detected in the luminal breast cancer cell line MCF-7. Xenograft experiments showed the complete prevention of tumor growth after *AVEN* knockdown in MCF-7 cells (**Fig. 4.20**). Interestingly, Cathepsin D over-expression has been described in breast cancer [158]. Since Cathepsin D activates AVEN by proteolytic removal of the inhibitory N-terminus, there is the possibility that enhanced proteolytic activation of AVEN might contribute to breast cancer development and progression.

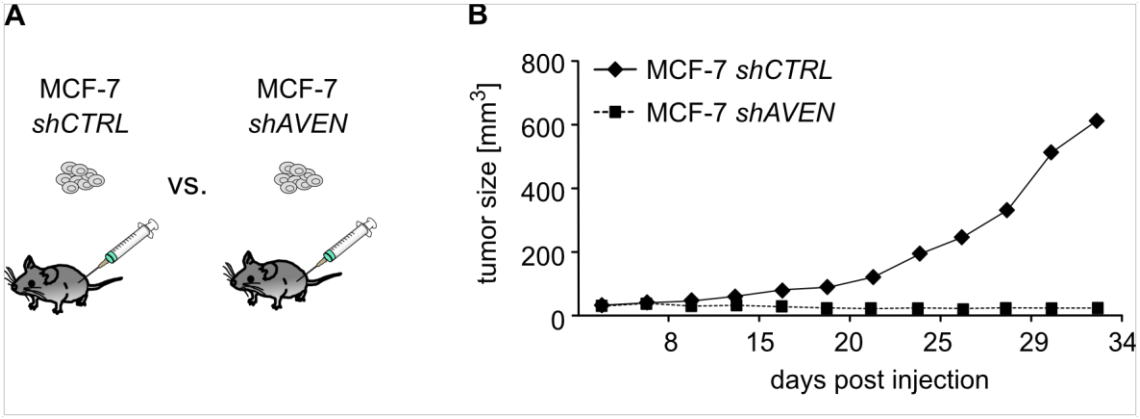

Figure 4.20: Tumor growth in a xenograft mouse model is abrogated after knockdown of *AVEN* in MCF-7 cells
A. MCF-7 cells were transduced with shRNA targeting *AVEN* or non-target shRNA as control and injected subcutaneously into the flanks of mice. **B**. In the xenograft experiment, tumor growth of *AVEN* knockdown cells was inhibited while the tumors formed of control cells showed a continuous growth. Data were generated by Inga Melzer.

To investigate the role of AVEN in normal and oncogenic breast development in more detail, histological analyses of the mammary gland were performed in *Aven* wildtype and conditional *Aven* knockout mice. Immunohistochemistry using an antibody that recognizes the C-terminus of AVEN and thereby detecting both full length and ΔN-AVEN confirms protein atlas data with AVEN expression in the luminal epithelial cells of the gland but not in the myoepithelial layer (**Fig. 4.21A**). The staining intensity seemed to

increase during pregnancy and lactation with the expansion of the epithelial cells and to decrease during involution (**Fig. 4.21A**). This observation was complemented by the results of western blot analysis also showing an increase in AVEN expression from virgin to lactating mice with a subsequent down-regulation during involution (**Fig. 4.21B**). Apparently, there is a dynamic regulation of AVEN expression during the development of the mammary gland.

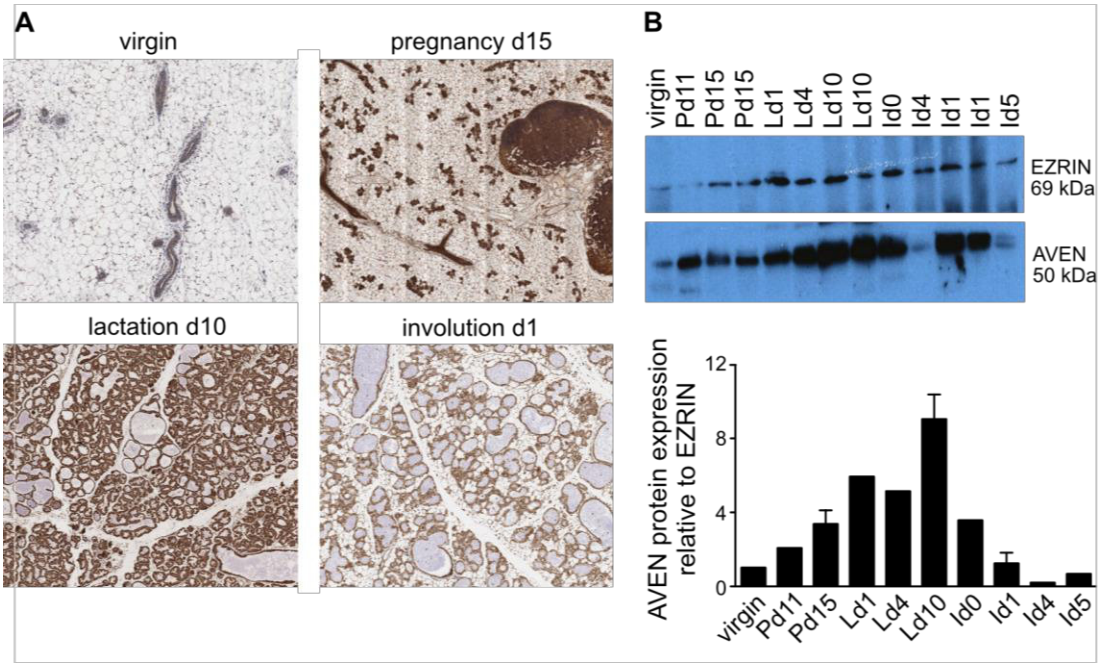

Figure 4.21: Dynamic regulation of AVEN expression during the development of the murine mammary gland
AVEN is expressed in the luminal epithelial cells of the murine mammary gland and the expression increases during pregnancy and lactation. A downregulation of AVEN expression is observed during involution. **A**. AVEN immunohistochemistry using paraffin sections of the mammary gland from Bl/6 mice at the indicated maturation stages. **B**. AVEN protein expression was detected by western blotting (upper part) and quantified using the *Fusion Fx* system (lower part). Protein expression was measured relative to EZRIN expression which served as a loading control. Expression levels were normalized to the expression in the virgin mammary gland. Bars represent the mean and standard deviation if more than one mouse was analyzed. P: pregnancy. L: lactation. I: involution.

To test the requirement of AVEN for the development of the mammary gland, mice with a floxed *Aven* allele were bred with *MMTV-Cre* deleters (**Fig. 4.22A**). The *mouse mammary tumor virus (MMTV)* promoter is active in breast epithelial cells as well as in a few other tissues (salivary gland, ovaries, epididymus and seminal vesicles [159]. As a consequence, offspring expressing CRE with homozygous floxed *Aven* alleles (*Aven*$^{d/d}$*MMTVCre*$^{+}$) are supposed to display an *Aven* knockout in the cells of the mammary gland. The knockout was verified by western blotting: there was only a weak AVEN signal in the samples of *Aven*$^{d/d}$*MMTVCre*$^{+}$ virgin and pregnant breast tissue while

there was a strong AVEN signal in samples derived from mice with wildtype *Aven* alleles (*Aven*$^{+/+}$*MMTVCre*$^{+}$) (**Fig. 4.22B**). Mice with a mammary gland-specific knockout of *Aven* showed the same normal histology of the breast in virgin mice (data not shown) and during pregnancy, lactation and involution (**Fig. 4.22C**) as their littermates with wildtype *Aven* expression. *Aven*$^{d/d}$*MMTVCre*$^{+}$ mice were able to nurse their pups, in consistence with the intact histology of the breast tissue. Concluding from these data, expansion and involution of epithelial cells during the development of the mammary gland is AVEN-independent.

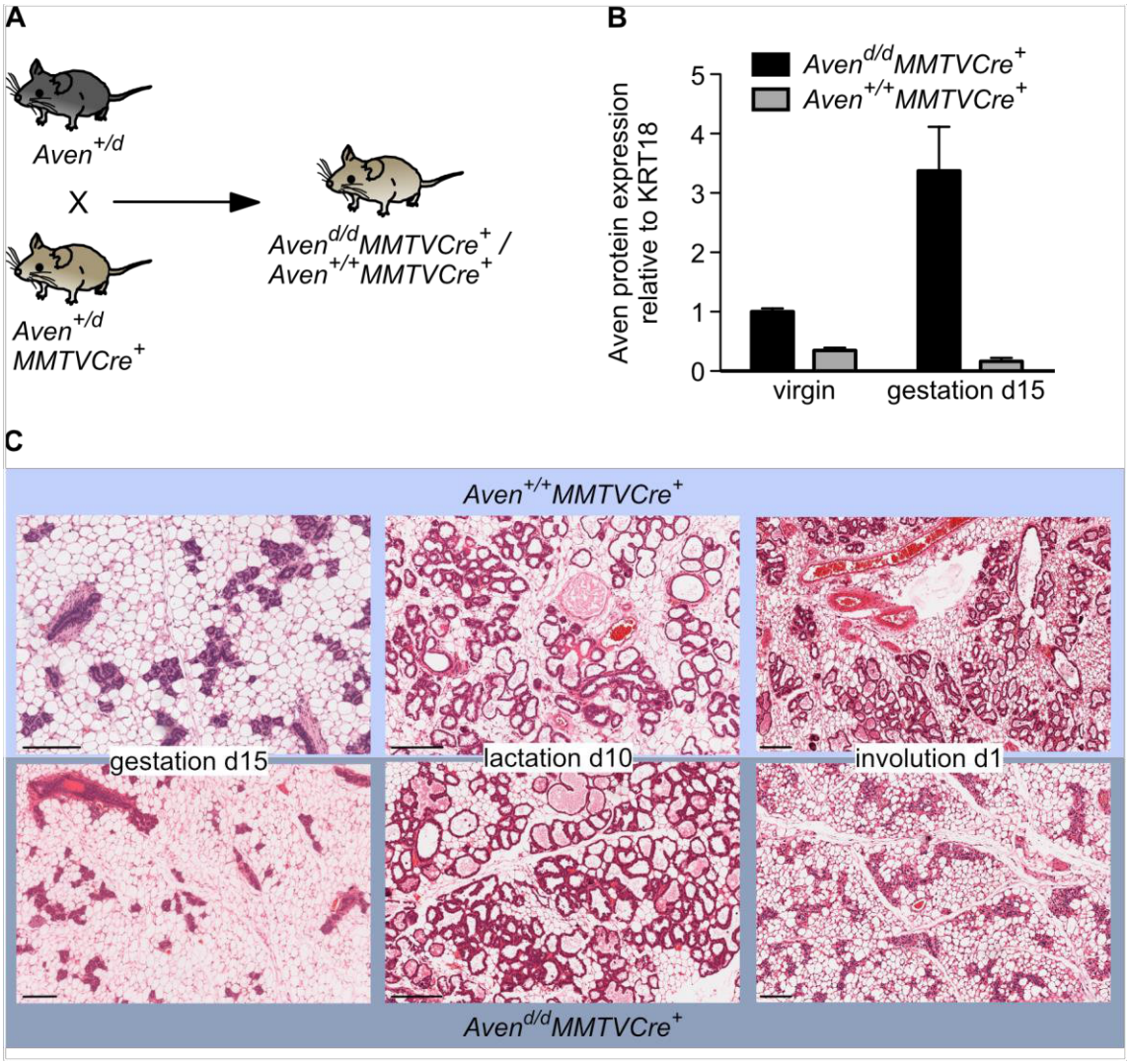

Figure 4.22: Knockout of *Aven* in the mammary gland does not interfere with tissue development during pregnancy, lactation and involution
A. Breeding scheme for the generation of mice with a homozygous knockout of *Aven* in the mammary gland (*Aven*$^{d/d}$*MMTVCre*$^{+}$) and control mice with wildtype AVEN expression (*Aven*$^{+/+}$*MMTVCre*$^{+}$). **B**. Knockout of *Aven* in the mammary gland of *Aven*$^{d/d}$*MMTVCre*$^{+}$ mice as detected by western blotting. AVEN signals on western blot membranes were quantified relative to Cytokeratin 18 (KRT18) which was detected as a loading control. Values were normalized to AVEN expression of virgin *Aven*$^{+/+}$*MMTVCre*$^{+}$ mice. Bars represent the mean and standard deviation of four values, generated by analyzing two mice per group and performing experiments in duplicates. **C**. Mice with a homozygous *Aven* knockout in breast epithelial cells show the same histology of the mammary gland as control mice with wildtype *Aven* expression. Paraffin sections

of mammary glands were stained with hematoxylin and eosin. Scale bar represents 200 µm.

4.1.9 Knockout of *Aven* expression in the mammary gland has no effect on breast tumor onset and progression

Knockdown of *AVEN* expression in the human breast cancer cell line MCF-7 completely abrogated tumor growth in a mouse xenograft model (**Fig.4. 20**). To test the impact of *Aven* expression on breast cancer onset and progression in an endogenous mouse model, heterozygous carriers of the floxed *Aven* allele expressing *MMTV-Cre* were bred with heterozygous carriers of the floxed *Aven* allele expressing the Polyoma virus middle tumor antigen (PyVT) under the control of the *MMTV* promoter (**Fig. 4.23A**). Expression of the PyVT transgene induces growth of breast tumors with a latency of 1 to 6 months [160]. Female offspring of these breedings carrying the PyVT transgene with either wildtype or deleted *Aven* expression in the mammary gland (*Aven*$^{d/d}$*MMTVCrePyVT*$^{+}$ vs. *Aven*$^{+/+}$*MMTVCrePyVT*$^{+}$) were monitored to assess tumor onset. When one tumor exceeded the mass of 1 cm^3 or 9 days after tumor onset at the latest, mice were sacrificed and the tumor burden was characterized by the total weight of all tumors. AVEN expression in the tumors and healthy mammary glands of these mice was analyzed by western blotting. Substantial AVEN expression was found in the *Aven* wildtype mammary gland which was even higher in the tumor tissue. There was significantly reduced AVEN expression in the *Aven* knockout mammary glands and tumors, confirming successful deletion of *Aven* in these mice (**Fig. 4.23B**). Mice without *Aven* expression in the breast epithelial cells developed tumors at the same age as mice with wildtype *Aven* expression and there was also no difference in the tumor burden between these two groups (**Fig. 4.23C**). Since AVEN can act as an inhibitor of apoptosis and as a regulator of cell cycle progression, proliferation and apoptosis in tumors with wildtype and knocked out *Aven* expression were analyzed. Immunohistochemically staining for Ki67 as a proliferation marker revealed no significant difference between *Aven* wildtype and knockout tumors (**Fig. 4.24A, B**), and staining for cleaved Caspase 3 showed no difference in the number of apoptotic cells between the two groups (**Fig. 4.24C, D**).

Thus, while AVEN expression seemed to be increased in MMTV-PyVT-induced breast tumors, knockout of *Aven* in the mammary gland did not increase latency time or tumor burden. Consistent with the similar tumor mass, *Aven* knockout tumor cells were neither less proliferative nor more prone to undergo apoptotic cell death than *Aven* wildtype tumor cells.

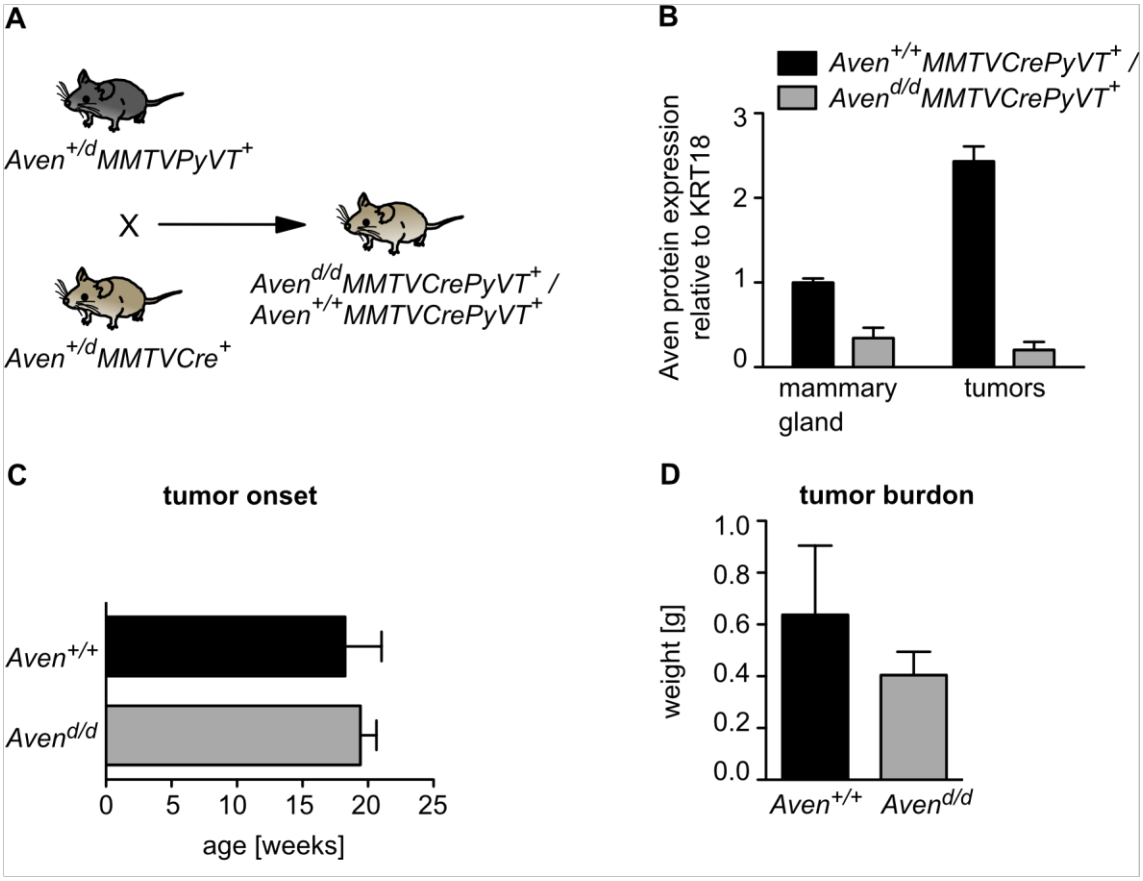

Figure 4.23: PyVT-induced tumor onset and progression in mice is not altered after knockout of *Aven* in the mammary gland
A. Breeding scheme to generate mice developing breast tumors as a consequence of MMTV-PyVT expression and an additional knockout of *Aven* in the mammary gland (*Aven$^{d/d}$MMTVCrePyVT^{+}*). Mice with wildtype *Aven* alleles were used as a control group (*Aven$^{+/+}$MMTVCrePyVT^{+}*). **B**. AVEN expression was efficiently depleted in *Aven$^{d/d}$MMTVCrePyVT^{+}* mammary glands and tumors. AVEN signals in western blots were quantified relative to Cytokeratin 18 (KRT18) which was detected as a loading control. Values were normalized to AVEN expression in *Aven$^{+/+}$MMTVCre^{+}* healthy breast tissue. **C**. Tumor onset was not altered in *Aven$^{d/d}$MMTVCrePyVT^{+}* mice (n=7) compared to the control group with wildtype AVEN expression (n=4). **D**. There was no difference in the tumor burden as measured by total tumor weight per mice between *Aven$^{d/d}$MMTVCrePyVT^{+}* and *Aven$^{+/+}$MMTVCrePyVT^{+}* mice.

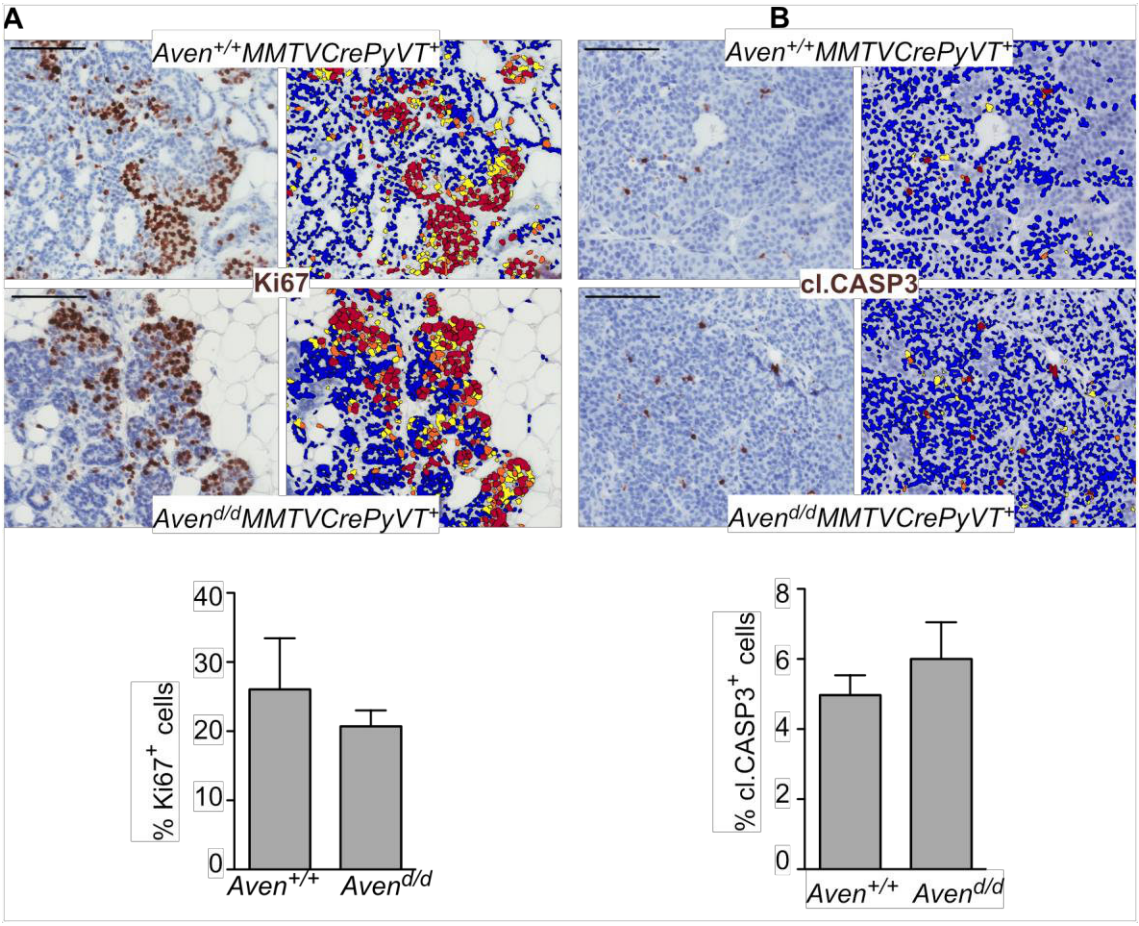

Figure 4.24: *Aven* knockout in the mouse mammary gland has no effect on proliferation and apoptosis in breast tumor cells
A. Immunohistochemical staining of Ki67 on paraffin sections of tumors from mice with wildtype and depleted AVEN expression (*Aven$^{d/d}$MMTVCrePyVT^{+}* (n=7) vs. *Aven$^{+/+}$MMTVCrePyVT^{+}* (n=4)). Ki67 stained cells (yellow, orange and red cells representing low, moderate and high staining intensity, respectively) were identified and quantified using *Aperio ImageScope software* (right panel). No difference in the percentage of Ki67^{+} proliferating cells was detected between *Aven$^{d/d}$MMTVCrePyVT^{+}* and *Aven$^{+/+}$MMTVCrePyVT^{+}* tumors. **B**. Immunohistochemical staining of cleaved Caspase 3 on paraffin sections of tumors from mice with wildtype and depleted *Aven* expression. Cleaved Caspase 3-stained cells (yellow, orange and red cells) were identified and counted using *Aperio ImageScope* software (lower panel). No difference in the percentage of cl. CASP3^{+} apoptotic cells was detected between *Aven$^{d/d}$MMTVCrePyVT^{+}* and *Aven$^{+/+}$MMTVCrePyVT^{+}* tumors. Scale bars: 100 µm.

4.1.10 Knockdown of *AVEN* in the breast cancer cell line MCF-7 has no effect on proliferation but could increase therapy-induced apoptosis

Analysis of mice with a knockout in the mammary gland did not show any effect of AVEN deficiency on the onset and progression of breast tumors. However, it has been shown that AVEN prevents apoptosis induced by DNA damaging irradiation and chemotherapeutic drugs [10], [29], [30]. Thus, targeting AVEN in combination with standard chemotherapy could represent a new strategy in anti-cancer therapy.

To test this theory, a possible protection of cells from apoptosis by AVEN was investigated. MCF-7 cells were transduced with two different shRNA constructs targeting *AVEN* and scrambled shRNA as a control. AVEN protein expression was efficiently knocked down in *shAVEN*-transduced cells compared to *shCTRL*-transduced cells (**Fig. 4.25A**). *AVEN* knockdown and control cells were used in alamar blue assays to monitor the metabolic activity. The knockdown of *AVEN* had no consequence for the metabolic activity of the cells, as no difference in alamar blue reduction between the groups was observed (**Fig. 4.25B**). Next, the transduced cells were either UV-irradiated or treated with Mitomycin C. Both treatments lead to DNA damage, causing the cells to undergo apoptosis. Consequently, alamar blue reduction was reduced in all analyzed groups compared to the untreated cells. Again, there was no difference in metabolic activity between *AVEN* knockdown and control cells (**Fig. 4.25C, D**).

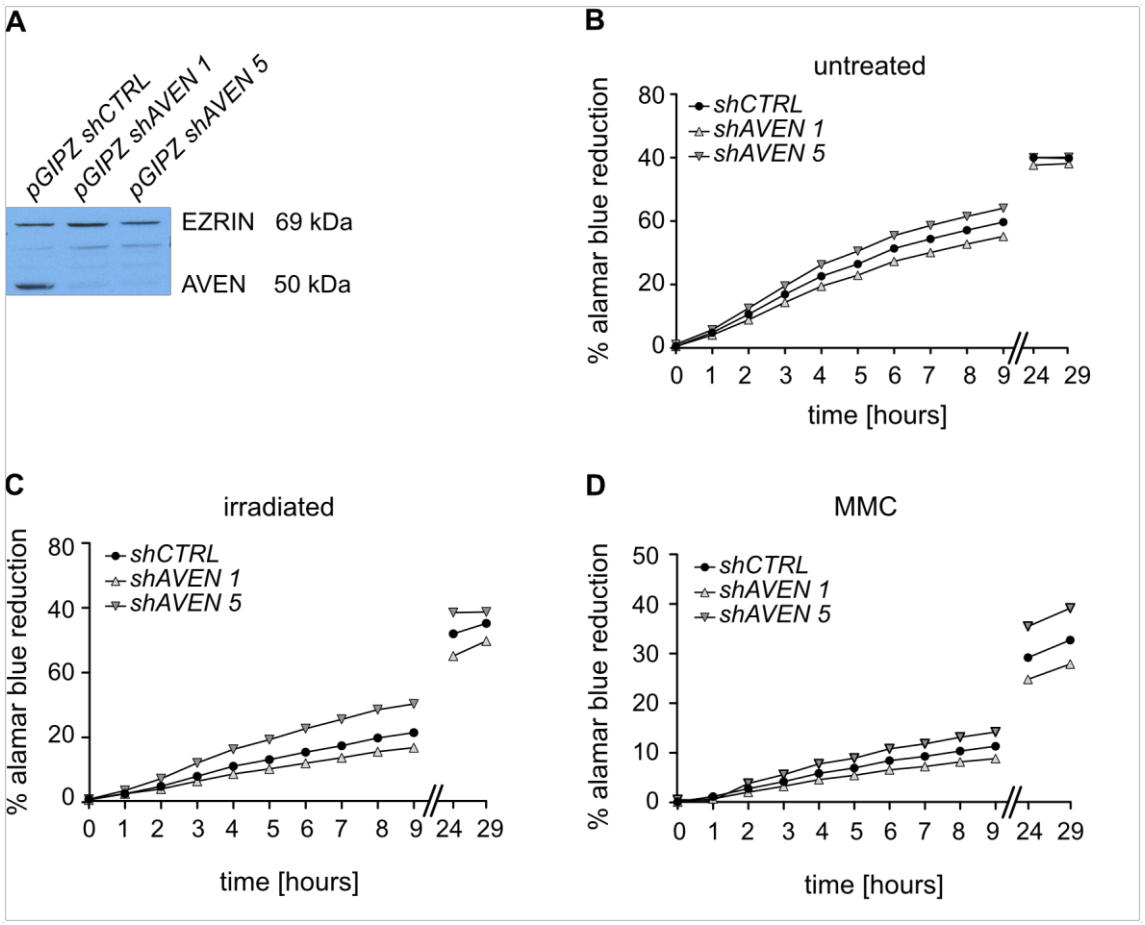

Figure 4.25: Breast cancer cell lines with wildtype *AVEN* expression display no growth advantage over *AVEN* knockdown cells
A. AVEN protein expression in MCF-7 cells was efficiently knocked down after transduction with shRNAs targeting *AVEN* compared to cells transduced with control shRNA. Successfully transduced cells expressing GFP were sorted by FACS. EZRIN was detected as loading control in western blots. **B**. Metabolic activity as measured by alamar blue reduction was not changed in *AVEN* knockdown cells compared to control cells. **C**, **D**. UV irradiation (20 mJ/cm^2, **C**) and Mitomycin C treatment (8 µg/ml, **D**) one and 24 h prior to alamar blue addition, respectively, reduced the metabolic activity compared to untreated cells (**B**). No difference between *shAVEN*-

and *shCTRL*-transduced cells was detected. Data points represent the mean and standard deviation (covered by data points) of three replicates, generated in one representative experiment out of three.

As the alamar blue assay measures oxidoreductive metabolic activity of cells, it only gives an indirect hint about the viability and apoptosis of the cells. For this reason, apoptotic cells in the MCF-7 *AVEN* knockdown and control groups were also directly quantified by a viability dye staining. To test the setup of the experiment, MCF-7 wildtype cells were irradiated prior to the staining, again to induce DNA damage and apoptosis. Additionally, another set of cells was starved for 24 hours by serum deprivation to activate a DNA damage-independent pathway of apoptosis. Apoptotic cells that were positive for the viability dye stain were recorded by flow cytometry. The percentage of stained apoptotic cells was significantly increased in the irradiated (25.18%) and starved cells (19.89%) compared to the untreated cells (7.25%) (**Fig. 4.26A**). The viability dye staining was repeated with the MCF-7 *AVEN* knockdown and control cells. The *AVEN* knockdown cells did not exhibit increased percentages of dead cells compared to the control cells in the untreated and starved group. However, the mean percentage of dead cells in the UV irradiated group was 30.93% and 32.08% in the *AVEN* knockdown cells compared to 24.26% in the control cells. This increase was not significant, though (**Fig. 4.22B**).

To further validate these data, cell death of *AVEN* knockdown and control cells in an untreated and in an irradiated group was assessed by another method, the Nicoletti Assay [161]. This assay uses propidium iodide (PI) to stain the DNA of permeabilized fixated cells. Thus, the intensity of the detected PI signal can be correlated with the stage of cell cycle in living cells, while dead cells are substantially less stained. The results of the Nicoletti assay in transduced MCF-7 cells showed no significant difference in cell cycle distribution between *AVEN* knockdown and control cells, in both untreated and irradiated groups (**Fig. 4.26D**). There were significantly more dead cells in the *AVEN* knockdown population compared to the control population after irradiation, but not in the untreated group (**Fig. 4.26D**). Interestingly, the opposite effect was observed in MDA-MB 453 cells, another luminal epithelial breast cancer cell line (**Fig. 4.26E**).

Summarizing the *in vitro* analysis, the cytoprotective function of AVEN in the context of DNA damage that has been reported by Kutuk et al. could only partially be confirmed in MCF-7 cells and not in MDA-MB 453 cells. The apoptosis-inhibiting effect of AVEN expression seems not to be a consequence of cell cycle control but might result from the stabilization of anti-apoptotic BCL-x_L, as it has been suggested by Kutuk [10].

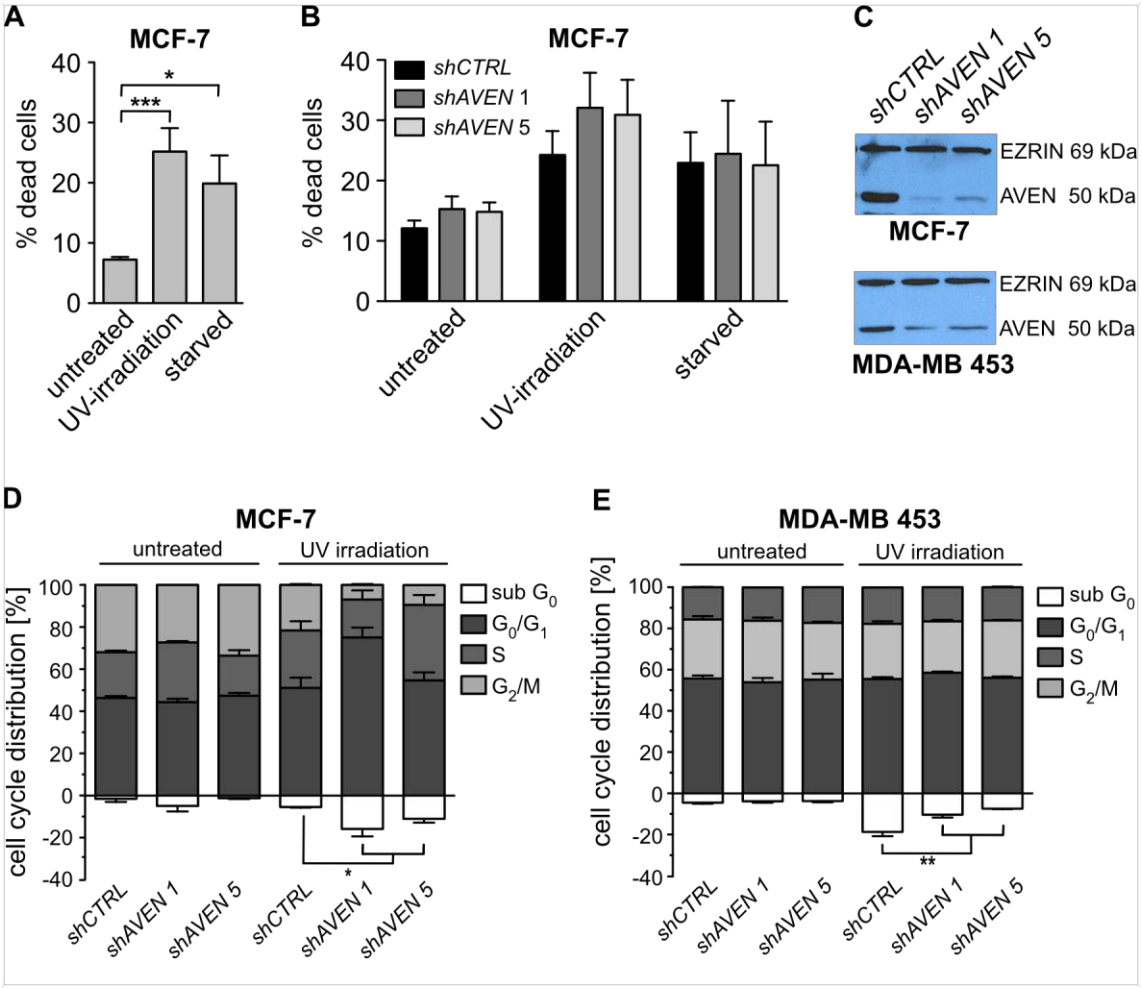

Figure 4.26: Increased irradiation-induced apoptosis in MCF-7 cells after *AVEN* knockdown
A. UV-irradiation (180 mJ/cm^2) and starvation for 24 hours significantly increased apoptosis in MCF-7 cells, as measured by viability dye staining and flow cytometry. **B**. UV irradiation- but not starvation-induced apoptosis is slightly increased in *AVEN* knockdown cells compared to pGIPZ *shCTRL* transduced cells. The percentage of dead cells was assessed by viability staining and flow cytometry. AVEN knockdown efficiency after transduction with pGIPZ *shAven* was demonstrated by western blotting. EZRIN was detected as a loading control. **C**. Efficiency of *AVEN* knockdown in MCF-7 cells (used in A, B and D) and MDA-MB 453 cells (used in E) was assessed by western blotting. EZRIN was detected as a loading control. **D**. Nicoletti assays show increased percentages of apoptotic (sub G_0) cells in *shAVEN*-transduced MCF-7 cells compared to *shCTRL*-transduced cells after irradiation. **E**. In MDA-MB 453 cells, the percentage of dead cells is significantly increased in the *shCTRL*-transduced group compared to *AVEN* knockdown cells. Bars represent the mean and standard deviation of three independent experiments.

4.1.11 Estrogen upregulates AVEN expression in human breast cancer cells but estrogen-induced proliferation and apoptosis inhibition is AVEN-independent

Paydas et al. [25] could show that *AVEN* is an estrogen target gene in mammalian testis. In the context of breast cancer, enhanced AVEN expression as a consequence of estrogen receptor activation could be of relevance for tumor growth and chemotherapy resistance. Estrogen receptor alpha (ER1) is expressed in 70% of all breast cancers and transcriptional regulation by the activated ER1 is known to control proliferation,

differentiation and migration [162], [163]. Thus, aberrant ER1 signaling is involved in the development of breast tumors [163]. The previously described results suggest apoptosis inhibition mediated by AVEN after irradiation. In osteosarcomas, AVEN expression might also contribute to chemotherapy resistance [29]. Thus, increased AVEN expression induced by ER1 activation in breast cancer cells could constitute a mechanism mediating therapy resistance.

To test a possible upregulation of *AVEN* expression by ER1 in breast cancer cells, AVEN protein levels were measured after application of 17β-estradiol (E2). $ER1^+$ MCF-7 cells were cultured in medium supplemented with charcoal-stripped FBS to deprive endogenous hormones. After five days of culture, cells were split in fresh medium supplemented with or without human recombinant E2. After 6, 28 and 96 hours of incubation, cells were harvested and AVEN protein expression was measured by western blotting and western blot signal quantification. At all three time points, AVEN expression was substantially higher in the E2 treated cells (**Fig.4. 27A, B**). Apparently, *AVEN* represents a direct or indirect estrogen target gene in MCF-7 cells, as it was shown in mammalian testis.

Interestingly, the E2 untreated cells also showed an upregulation of AVEN expression, followed by a moderate downregulation over time (**Fig. 4.27A, B**). To test whether AVEN expression correlated with the density of cells in the culture dish, AVEN protein expression was detected in MCF-7 cells grown at different confluence. The results showed the same tendency as observed in the previous experiments: AVEN expression first increased parallel to confluence but decreased when cells reached 90% confluence. However, the changes in AVEN expression were moderate and not statistically significant (**Fig. 4.27C**).

Next, AVEN-dependence of ER1-induced growth of MCF-7 cells was tested. MCF-7 cells were transduced with shRNA targeting *AVEN* and scrambled shRNA as control, with an *AVEN* overexpression construct and the corresponding empty vector as additional controls. Knockdown and overexpression of AVEN were verified by western blotting (**Fig. 4.27D**). Each of the four groups was cultured in estrogen-free or estrogen-containing medium, and the proliferation of the cells was measured via their metabolic activity in an alamar blue assay. Each cell group showed the expected accelerated alamar blue reduction when kept in estrogen-containing medium (**Fig. 4.27E, F**). Remarkably, the *AVEN* overexpressing cells showed a reduced metabolic activity compared to their control cells (**Fig. 4.27E**) and the *AVEN* knockdown cells exhibited increased metabolic activity compared to their control cells (**Fig. 4.27F**). According to these results, AVEN expression decelerates E2-induced cell proliferation.

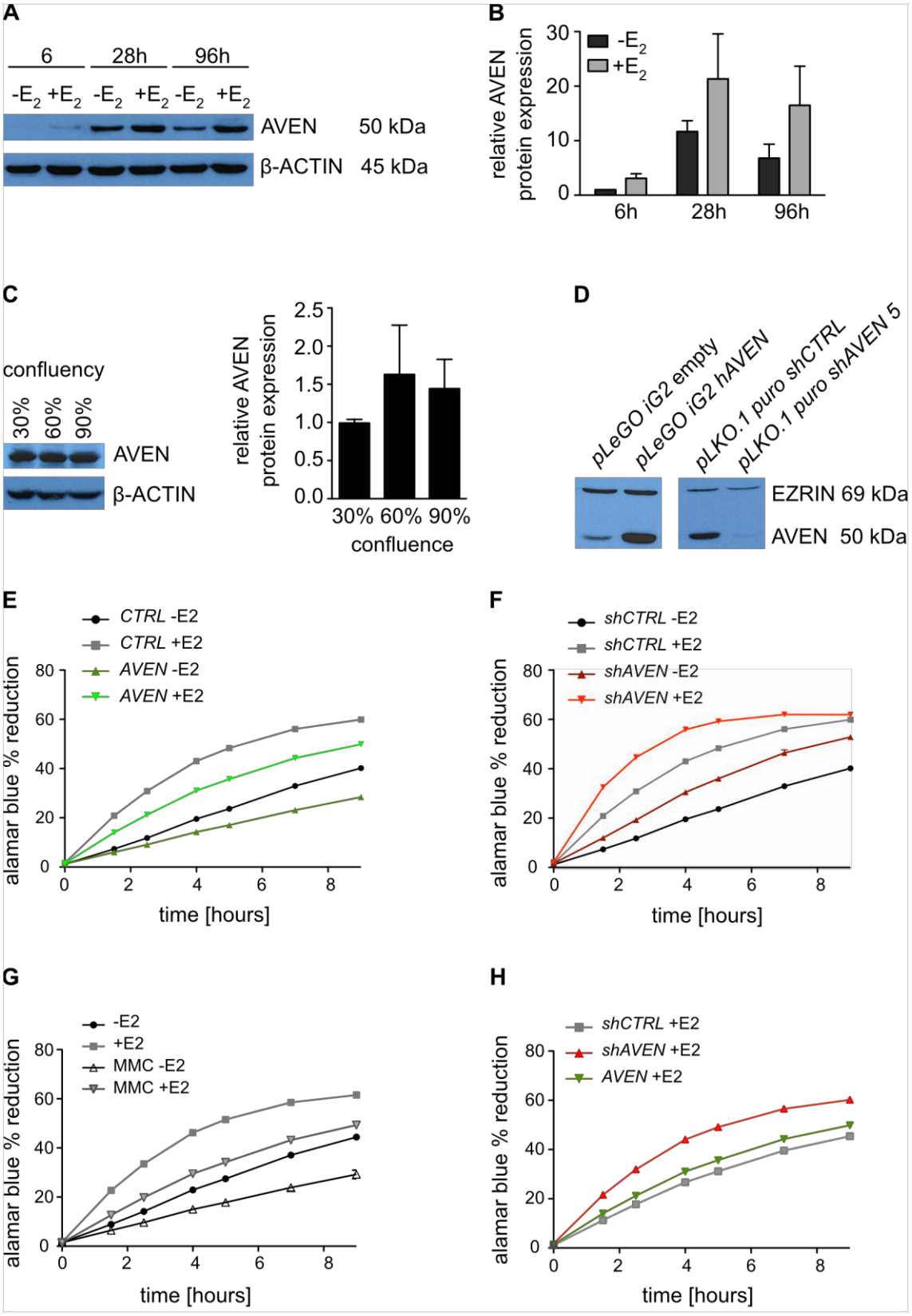

Figure 4.27: Estrogen induces AVEN expression in MCF-7 cells, but estrogen-induced proliferation is repressed by AVEN

A. Western blot results obtained with whole cell lysates reveal increased AVEN levels in MCF-7 cells after estrogen treatment (+100 nM E2) compared to cells cultured without estrogen (−E2). β-ACTIN was detected as loading control. **B**. Western blot signals in A were quantified using the *Fusion fx* system. AVEN expression was calculated relative to β-ACTIN expression. Values were normalized to AVEN expression of cells grown without E2 after 6h. Bars represent the mean and standard deviation of three independent experiments. **C**, AVEN expression does not change significantly with increasing confluence of the cells as assessed by western blotting. Western blot

signals in were quantified using the *Fusion fx* system. AVEN expression was calculated relative to β-ACTIN expression and normalized to AVEN expression of cells grown with 30% confluence. Bars represent the mean and standard deviation of four independent experiments. **D**. *AVEN* overexpression and *AVEN* knockdown in MCF-7 cells after transduction with *pLeGO iG2 hAVEN* and *shAVEN*, respectively, was verified by western blotting. β-ACTIN was detected as loading control. **E**, **F**. Alamar blue reduction representing metabolic activity of MCF-7 cells is decreased in *AVEN* overexpressing cells (**E**) and increased in *AVEN* knockdown cells (**F**). **G**. Treatment with 4 µg/ml Mitomycin C (MMC) for 24 hours decreases metabolic activity in MCF-7 cells. **H**. *AVEN* knockdown increases E2-induced proliferation of MCF-7 cells after MMC treatment. Data points represent the mean and standard deviation (covered by data points) of three replicates, generated in one representative experiment out of two.

Estrogen has been reported to inhibit apoptosis in MCF-7 cells [164]. This apoptosis inhibition could be mediated by AVEN. To test this hypothesis, proliferation of *AVEN* knockdown, *AVEN* overexpressing and control cells, was measured after Mitomycin C treatment. Proliferation was again assessed indirectly via an alamar blue assay. MMC-treated cells showed a clear reduction in metabolic activity compared to untreated cells (**Fig. 4.27G**). Overexpression of *AVEN* had no effect on alamar blue reduction, but knockdown of *AVEN* led to a slight increase in metabolic activity (**Fig. 4.27H**). These findings question the theory that estrogen-induced AVEN expression prevents cells from DNA damage-induced apoptosis. However, increased metabolic activity as a consequence of apoptosis inhibition could be compensated by AVEN-induced metabolic deceleration that was described above (**Fig. 4.27E, F**).

4.1.12 *ER1* translation is not regulated by AVEN

The mRNA of *ER1* contains a potential quadruplex forming sequence (**Fig. 4.28A**). This secondary RNA structure has been shown to regulate *ER1* translation by slowing down or stalling temporarily translation elongation [165]. Recently, AVEN has been found to bind to such quadruplex structures in mRNA and, in complex with a helicase, to facilitate translation of the bound mRNA (**Fig. 4.28B)** [17]. Thus, a positive feedback regulation of ER1 expression by AVEN was possible. The impact of AVEN expression levels on *ER1* translation was tested by western blotting. AVEN expression in MCF-7 cells was knocked down by two different shRNAs. A scrambled shRNA was used as control. Knockdown efficiency was tested by western blotting and revealed a reduction of AVEN protein levels by more than 75% in knockdown cells compared to the control cells (**Fig.4. 28C, D**). *ER1* mRNA levels were measured by qPCR and ER1 protein levels were measured by western blot experiments. On both, mRNA and protein level, there was no differences in ER1 expression between *AVEN* knockdown and control cells became detectable (**Fig. 4.28E, F**). Concluding from these results, *ER1* translation is not enabled by AVEN.

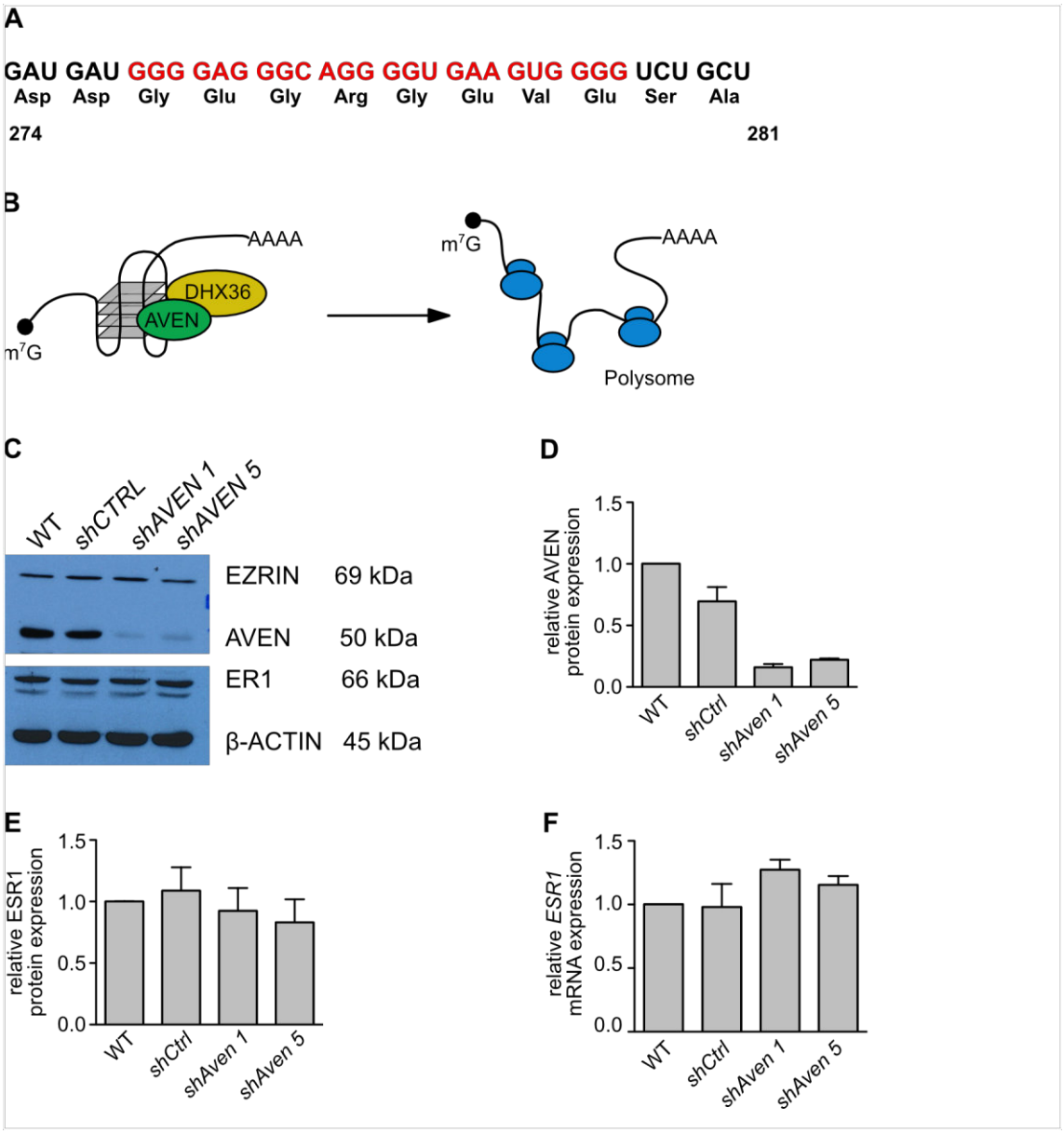

Figure 4.28: AVEN expression levels do not regulate ER1 mRNA translation
A. Potential quadruplex forming sequence in the mRNA of *ER1* [165]. **B**. AVEN binds quadruplex secondary structures in mRNA and enables translation of the bound mRNAs [17]. **C**. Efficient knockdown of *AVEN* in MCF-7 cells after transduction with *shAVEN* as measured by western blotting. ER1 expression was unaltered in AVEN knockdown cells. B-ACTIN was detected as loading control. **D**, **E**. Quantification of the western blot signals in **C**. AVEN (**D**) and ER1 (**E**) protein expression were calculated relative to β-ACTIN expression and normalized to the signal of untransduced cells (WT). **F**. *ER1* mRNA expression is unaltered in *AVEN* knockdown cells compared to control cells. mRNA levels were quantified by qPCR relative to *HPRT1* expression and normalized to expression of untransduced (WT) cells. Bars represent the mean and standard deviation of three independent experiments.

4.2 Analyses of the physiological role of FUBP1 in hematopoiesis

4.2.1 TAL1, an upstream-regulator of FUBP1 in erythroid progenitors, activates the *FUBP1* promoter in the context of an intact *GATA* sequence

Recent studies demonstrated that T cell acute lymphocytic leukemia 1 (TAL1) binds to the *FUBP1* promoter at an E-box -340 bp upstream of the *FUBP1* transcription start in human primary $CD34^+$ stem and progenitor cells [58]. This binding increased when the cells were induced to undergo erythroid differentiation, and the increased binding correlated with rising *TAL1* and *FUBP1* mRNA levels during the differentiation process. These data suggest an activation of *FUBP1* transcription upon binding of TAL1 to the *FUBP1* promoter at the -340 bp E-box. This hypothesis was strengthened by a reporter gene assay in K562 cells. After mutation of the -340 bp E-box in the *FUBP1* promoter sequence, the activity of the reporter gene which was controlled by the *FUBP1* promoter, decreased [166]. This assay demonstrated that an intact sequence of the -340 bp E-box was important for *FUBP1* promoter activation. However, the result allows no conclusion about the binding of which protein is prevented by a mutation within the E-box: besides TAL1, several other transcription regulators recognize this sequence (**Fig. 4.29A**).

To test whether indeed the binding of TAL1 to the *FUBP1* promoter was affected by the E-box mutation leading to the reduced activity of the reporter gene, another luciferase assay was performed. A construct containing *luciferase* cDNA under the control of a 0.5 kb *FUBP1* promoter fragment was used to measure *FUBP1* promoter activation via luciferase activity. The E-box at position -340 bp at which high TAL1 binding was observed in ChIP assays was included in the 0.5 kb promoter fragment (**Fig. 4.29B**, upper panel). The 0.5 kb *FUBP1* promoter construct already showed high activity when transfected on its own in HEK293T cells, compared to the activity of the empty construct (**Fig. 4.29C**, bars 1 and 2). The promoter activity was substantially increased when either *TAL1* or *E47* expression plasmids were co-transfected, and the strongest promoter activation was measured when both cDNAs were co-transfected (**Fig. 4.29C**, Bar 3, 4, 5). Point mutations within the -340 bp E-Box (**Fig. 4.29B**, second and third panel) did not reduce promoter activity (**Fig. 4.29C**, grey bars), which is inconsistent with previous results.

When analyzing the human *FUBP1* promoter, we detected a *GATA* motif 329 bases upstream of the *FUBP1* transcription start which is separated by five DNA bases from the -340 bp E-box (**Fig. 4.29A**). Such juxtaposed E-box and *GATA* motifs constitute cis-elements that are found in genes critical for erythroid differentiation. A concomitant binding of TAL1 and GATA-1 at these sites was demonstrated to activate erythroid gene expression [167]. Interestingly, TAL1 can be recruited to DNA in absence of an E-box as

binding site, possibly anchored to the genomic DNA by GATA-1 [168].

The luciferase assay was repeated with constructs containing point mutations within the *GATA* sequence (**Fig. 4.29B**, lower two panels) to test the relevance of an intact *GATA* motif for *FUBP1* promoter activation by TAL1. Both mutations introduced into the *GATA* sequence completely abolished luciferase activity (**Fig. 4.29C**, white bars). Hence, the TAL1/E47 dimer seems to play a functional role in the up-regulation of *FUBP1* transcription, and this function is highly dependent on an intact *GATA* motif. The underlying mechanism in HEK293T cells remains to be investigated, as this cell line does not express the likely interaction partner GATA-1.

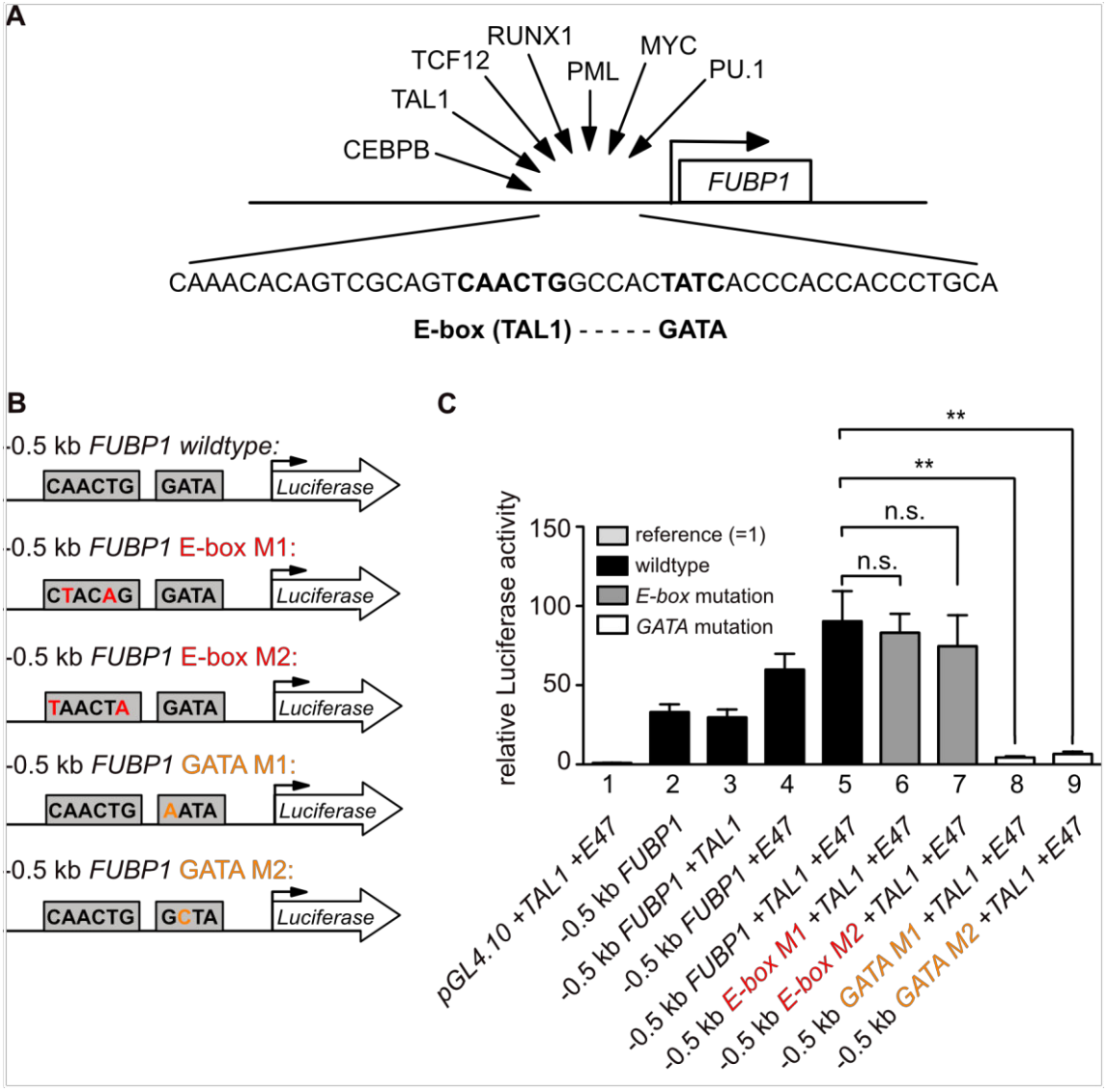

Figure 4.29: Activation of the *FUBP1* promoter by TAL1 is dependent on an intact *GATA* sequence motif

A.The *FUBP1* promoter contains, amongst other binding sites for several different transcription factors, a composite E-box/*GATA* motif that is recognized by TAL1 and GATA-1. **B**. Schematic representation of the *FUBP1* promoter constructs that were used in luciferase assays. A genomic *FUBP1* sequence 0.5 kb upstream of the transcription start was cloned upstream of the luciferase reporter gene (upper panel). Two different point mutations, either within the E-box -340 bp

upstream of the transcription start (middle panel) or within the *GATA* motif -329 bp upstream of the transcription start (lower panel) were introduced by PCR. **C**. HEK293T cells were transfected with the reporter constructs shown in B. Co-expression of TAL1 and E47 resulted in the highest luciferase activation (black bar 5) compared to expression of TAL1 or E47 alone or none of them (black bars 1-4). Point mutations within the *GATA* motif (white bars 8 and 9) but not within the E-box (grey bars 6 and 7) significantly reduced luciferase activity. Values for luciferase activities are presented relative to luciferase activity of cells transfected with the luciferase reporter vector without the *FUBP1* promoter region and normalized to β-Galactosidase activity. Bars represent the mean with standard deviation of three independent experiments, each measured in technical duplicates.

4.2.2 GATA-1 binds to the *FUBP1* promoter and GATA-1 recruitment to the *FUBP1* promoter increases during erythroid differentiation along with TAL1 and POLII recruitment

Since the transcriptional activation of *FUBP1* by TAL1 appears to depend on an intact *GATA* but not an intact E-box motif, TAL1 could be recruited to the *FUBP1* promoter as part of a complex consisting of GATA-1 or GATA-2. There is a switch from high GATA-2 to GATA-1 expression at the moment of erythroid commitment of progenitor cells [169]. Furthermore, TAL1/GATA1 complexes have been identified as activators of erythroid gene transcription [123] and therefore, an association of TAL1 with GATA-1 at the *FUBP1* promoter seemed likely for *FUBP1* activation during erythroid differentiation.

In such a scenario, GATA-1 should be found at the same sites within the *FUBP1* promoter as TAL1. To verify this assumption, GATA-1 chromatin immunoprecipitations (ChIPs) with subsequent qPCR quantification were performed in K562 cells using the same primer pairs that were previously used for TAL1 ChIPs [166]. All primer pairs showed an enrichment of *FUBP1* sequences after GATA-1 precipitation, but the most prominent signal was found using primer pair P2, amplifying a fragment containing the E-box/*GATA* composite motif (**Fig. 4.30A**, left). These results confirmed the presence of GATA1 protein at the *FUBP1* promoter at the same sites as TAL1 protein. The same *FUBP1* promoter sequence enrichment could be found after precipitating RNA polymerase 2 (POLII) (**Fig. 4.30A**, right), suggesting co-occupancy of the *FUBP1* promoter by TAL1, GATA-1 and POLII. Consequently, a TAL1/GATA-1 complex could physically interact with POLII to induce *FUBP1* transcription.

In the next experiment, it was tested whether an increased binding of GATA-1 to the *FUBP1* promoter during erythroid differentiation could be observed, as it had been detected for TAL1 and POLII [58]. Primary hCD34$^+$ donor cells were cultured in medium inducing erythroid differentiation. After 7 to 12 days of culture, the extent of differentiation was determined by measuring differentiation marker expression. High expression levels of *CD71* (*transferrin receptor*) and *CD235a* (G*lycophorine A*, *GYPA*) mRNA confirmed erythroid differentiation as well as CD235a surface expression staining showing that >

80% of the cells were positive for the erythroid surface marker (**Fig. 4.30B**). ChIP assays using either erythroid differentiated or undifferentiated hCD34$^+$ cells showed a considerable increase in the enrichment of the E-box/*GATA* containing fragment after GATA-1 precipitation (**Fig. 4.30D**, left). This increase correlated with the reported significant increase of TAL1 and POLII binding to the *FUBP1* promoter in erythroid differentiated cells, which could be confirmed (**Fig. 4.30D**, middle, right). No enrichment of a sequence within the intergenic region of chromosome 18 was detected in the GATA-1, TAL1 and POLII precipitates, excluding unspecific antibody binding (**Fig. 4.30C**).
These results suggest the presence of TAL1 and GATA-1, possibly in a complex, at an E-box/*GATA* composite motif near the *FUBP1* transcription start. Recruitment of TAL1/GATA-1 to the *FUBP1* promoter increased upon erythroid differentiation, most likely leading to previously described enforced *FUBP1* transcription.

4.2.3 FUBP1 expression might affect erythroid differentiation via transcriptional regulation of the EPO receptor signaling pathway

The upregulation of *FUBP1* expression which has been observed during erythroid differentiation of primary hCD34$^+$ cells seems to be important for efficient maturation of the cells. Knockdown of *FUBP1* in hCD34$^+$ cells led to reduced percentages of CD235a-positive cells after induction of erythroid differentiation, and the knockdown cells were limited in their potential to form erythroid colonies [58]. Proliferation, differentiation and survival of erythroid progenitors is mainly induced by erythropoietin (EPO) [94] [129]. Thus, inefficient erythroid differentiation could be a consequence of defective EPO receptor (EPOR) signaling. FUBP1 acts as a transcriptional regulator, and FUBP1 deficiency might interfere with EPOR signaling if the expression of components of the signaling pathway was dependent on FUBP1. To test a possible transcriptional regulation of EPOR components by FUBP1, qPCR-arrays were performed using the erythroleukemia cell lines HEL and K562. In these assays, the mRNA expression level of 92 components of the EPOR signaling pathway was quantified in *FUBP1* knockdown and control cells. Reduction of FUBP1 expression by over 90% as assessed on protein level (**Fig. 4.31**) only led to a moderate deregulation of EPOR signaling components. The 26 most deregulated genes in HEL cells after *FUBP1* knockdown are shown in **Fig. 4.31A**.

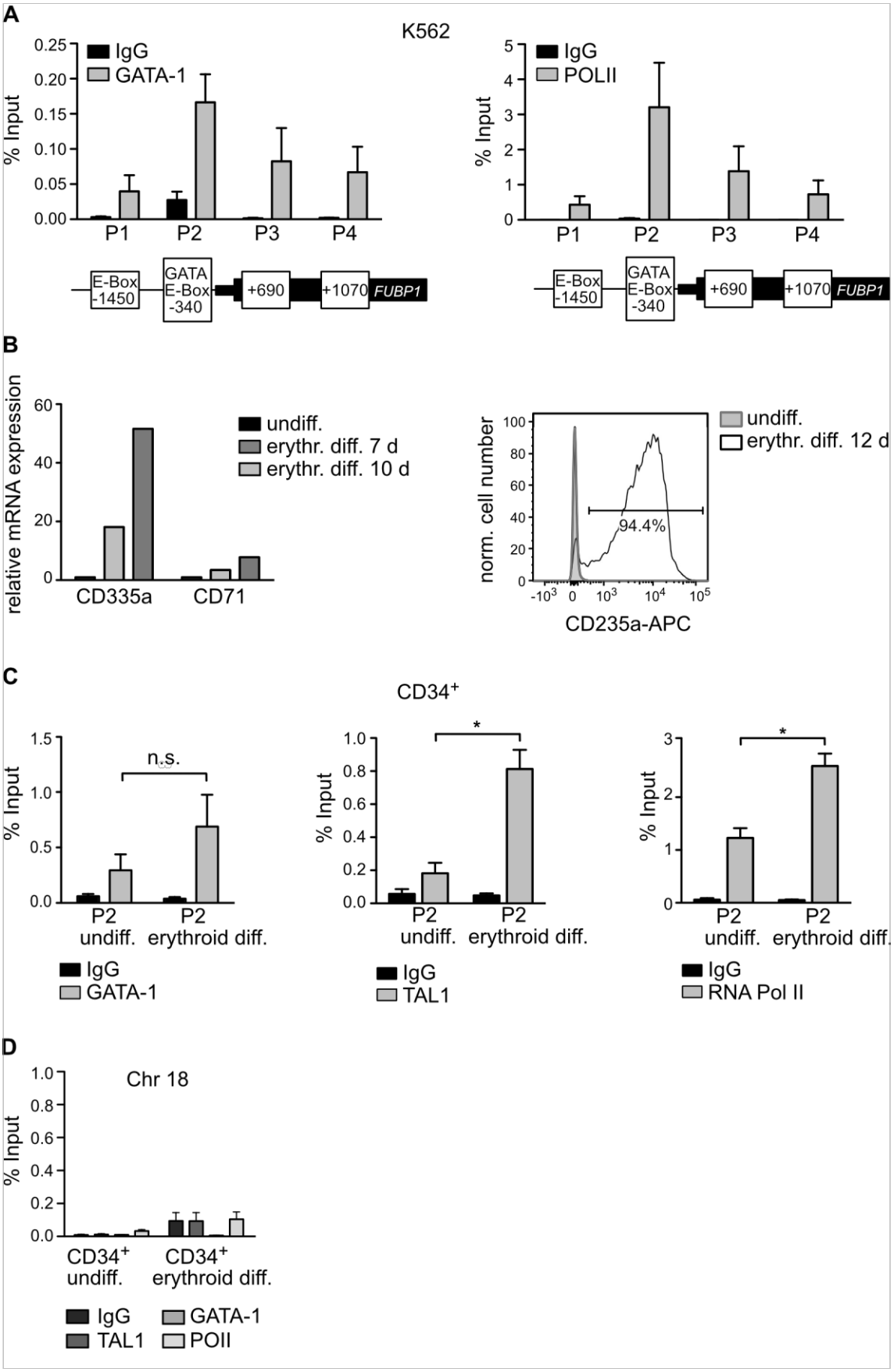

Figure 4.30: GATA-1 binds to the FUBP1 promoter and GATA-1 recruitment increases during erythroid differentiation along with TAL1 and POLII recruitment

A. ChIP analyses of GATA-1 and POLII binding to the *FUBP1* promoter in K562 cells using specific antibodies against GATA-1 (left) and POLII (right). ChIP-qPCR with primer pairs at distinct regions of the *FUBP1* promoter (P1 to P4, positions are outlined below the bars) indicate GATA-

1 and POLII binding in proximity to the transcriptional start site. **B.** Primary hCD34$^+$ cells were tested for erythroid marker expression after erythroid differentiation. MRNA expression was calculated relative to GAPDH expression and normalized to levels of undifferentiated cells (left). Staining for CD235a expression was measured by flow cytometry (right). **C**. Antibodies used in ChIP experiments showed no unspecific binding within an intergenic region of chromosome 18 (fragment from Chr18:65075058 to Chr18:65075181). **D**. TAL1, GATA-1 and POLII binding to the *FUBP1* promoter is increased upon erythroid differentiation of hCD34$^+$ cells. ChIPs were performed with an anti-GATA-1 antibody (left), anti-TAL1 antibody (middle) and anti-POLII antibody (right). IgG antibodies were used as an isotype-matched negative control in the ChIP experiments. Bars represent the mean results, with SD derived from four values generated in two independent experiments, each performed in technical duplicates.

Among the 18 down-regulated genes, four genes are part of the NFκB signaling pathway (RELB, REL, RELA, NFKB1), and one inhibitor of NFκB signaling is upregulated (NFKBIE). NFκB pathway activation via EPO can result in anti-apoptotic activity and is supposed to protect differentiating progenitors from cell death [170]. So FUBP1 deficiency could cause diminished NFκB pathway activation, and this in turn could lead to reduced numbers of mature erythrocytes because of increased apoptosis.

In K562 cells however, no components of the NFκB pathway were amongst the 23 most deregulated genes. In this cell line, four subunits of the PI3 kinase were upregulated (PIK3C3, PIK3R2, PIK3CD and PIK3R3) while one subunit was downregulated (PIK3CB) after *FUBP1* knockdown (**Fig. 4.31B**). EPOR-induced survival, proliferation and differentiation of erythroid progenitors is mediated by several different pathways, but PI3K/AKT signaling is critical for these effects [171]. Inhibition of PI3K also reduces GYPA expression, an effect that correlates with the consequences of *FUBP1* knockdown [171], [58]. Thus, *FUBP1* knockdown could interfere with erythropoiesis by deregulating the expression of PI3K pathway components.

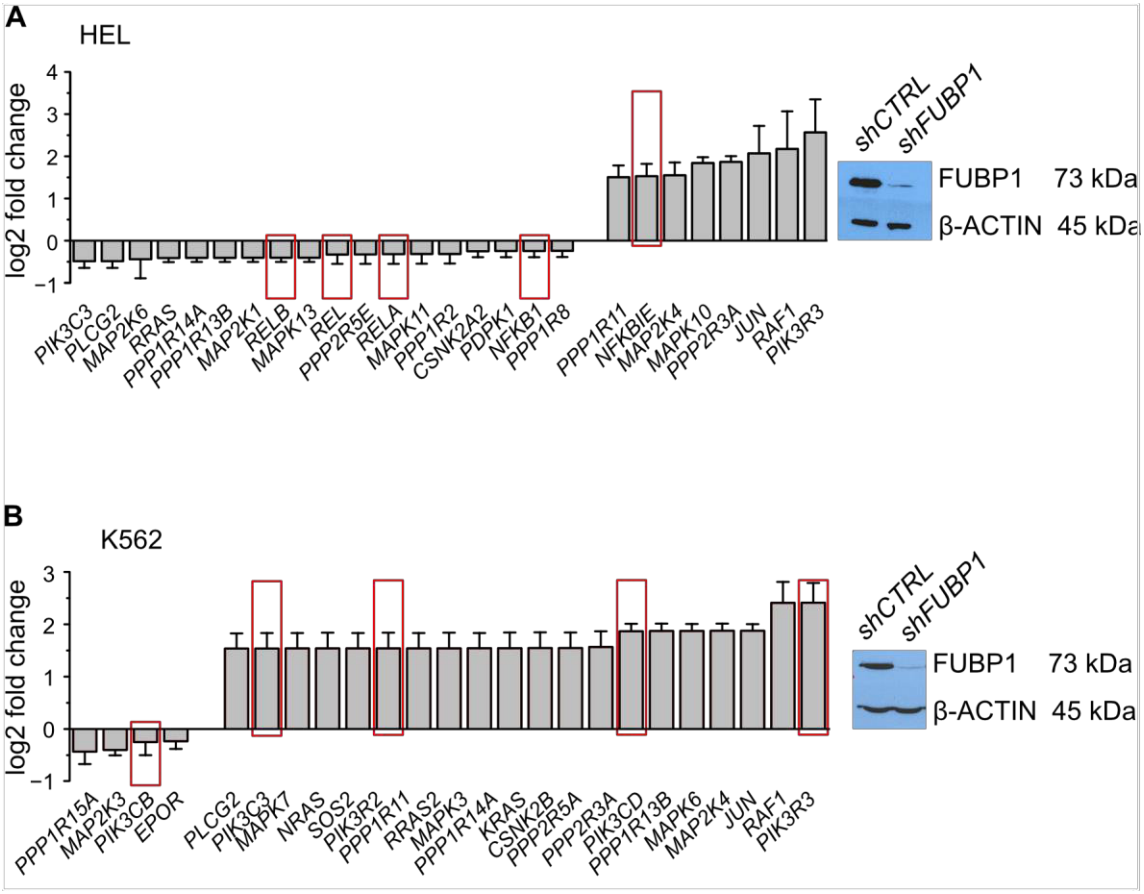

Figure 4.31: qPCR arrays with RNA obtained from *FUBP1* knockdown cells suggest FUBP1 target genes involved in NFkB- and PI3K-signaling
qPCR-arrays were performed with *FUBP1* knockdown and control cells to test the mRNA expression of 92 components of the EPO receptor signaling pathway. The knockdown was confirmed in western blot experiments. A representative blot of one experiment is shown on the right. β-ACTIN was detected as loading control. **A**. In HEL cells, among the 26 genes that were most deregulated after *FUBP1* knockdown, 5 are part of the NFκB signaling pathway (red boxes). **B**. In K562 cells, 5 components of the PI3K signaling pathway (red boxes) are among the most deregulated genes. Bars represent the mean and standard deviation of three independent experiments. Expression in *FUBP1* knockdown cells was calculated relative to the mean expression of three housekeeping genes (*18S, GUSB, HPRT1*) and is shown as log2 fold change over the expression of control cells with wildtype *FUBP1* expression.

4.2.4 RNA-Seq reveals possible new target genes of FUBP1 that are important for the development and function of the hematopoietic system

The results of the qPCR-arrays suggest a regulation of NFκB and PI3K signaling by FUBP1 that could be relevant for normal erythropoiesis. However, expression deregulation of the pathway components after *FUBP1* knockdown was only moderate and dependent on the cell lines used. For this reason, I also wanted to test whether transcription regulation by FUBP1 of genes apart from the EPOR pathway components affected erythropoiesis. A transcriptome-wide search for FUBP1 target genes was performed by RNA sequencing using K562 cells with and without *FUBP1* knockdown. The RNA sequencing was performed by the Transcriptome and Genome Analysis

Laboratory (TAL, University Medical Center Göttingen). Two different analysis approaches were used to identify up- and downregulated genes in the *FUBP1* knockdown cells compared to cells with *FUBP1* wildtype expression levels. 19 genes that showed the most prominent deregulation according to both analysis methods are shown in **Fig. 4.32A**. Among the most significantly downregulated genes was *FUBP1* itself, demonstrating and validating knockdown efficiency. Ingenuity® pathway analysis was performed to identify signaling and metabolic pathways as well as biological functions that were most affected by the gene expression deregulation. Furthermore, the software was used to predict the downstream effects of the deregulated biological processes. In *FUBP1* knockdown cells, expression of genes important for hematologic system development and function were altered in a way that was predicted to result in reduced numbers of hematopoietic progenitors as well as mature blood cells (**Fig. 4.32A**). Additionally, *FUBP1* knockdown was predicted to lead to increased cell death. These results support an important role of FUBP1 for erythropoiesis and confirm the role of FUBP1 as an apoptosis inhibitor. Validation of the deregulation of gene expression by qPCR analysis could only confirm deregulation of six out of 15 tested genes (**Fig. 4.32B**). Among those genes was *p21*, an already validated FUBP1 target gene. However, only one downregulation, the decreased expression of alpha fetoprotein (*AFP*), was statistically significant.

To summarize, while RNA-Seq data analysis suggest that FUBP1 is required to maintain a sufficient number of hematopoietic progenitor cells and blood cells, the data could not be validated by qPCR, questioning the reliability of the results.

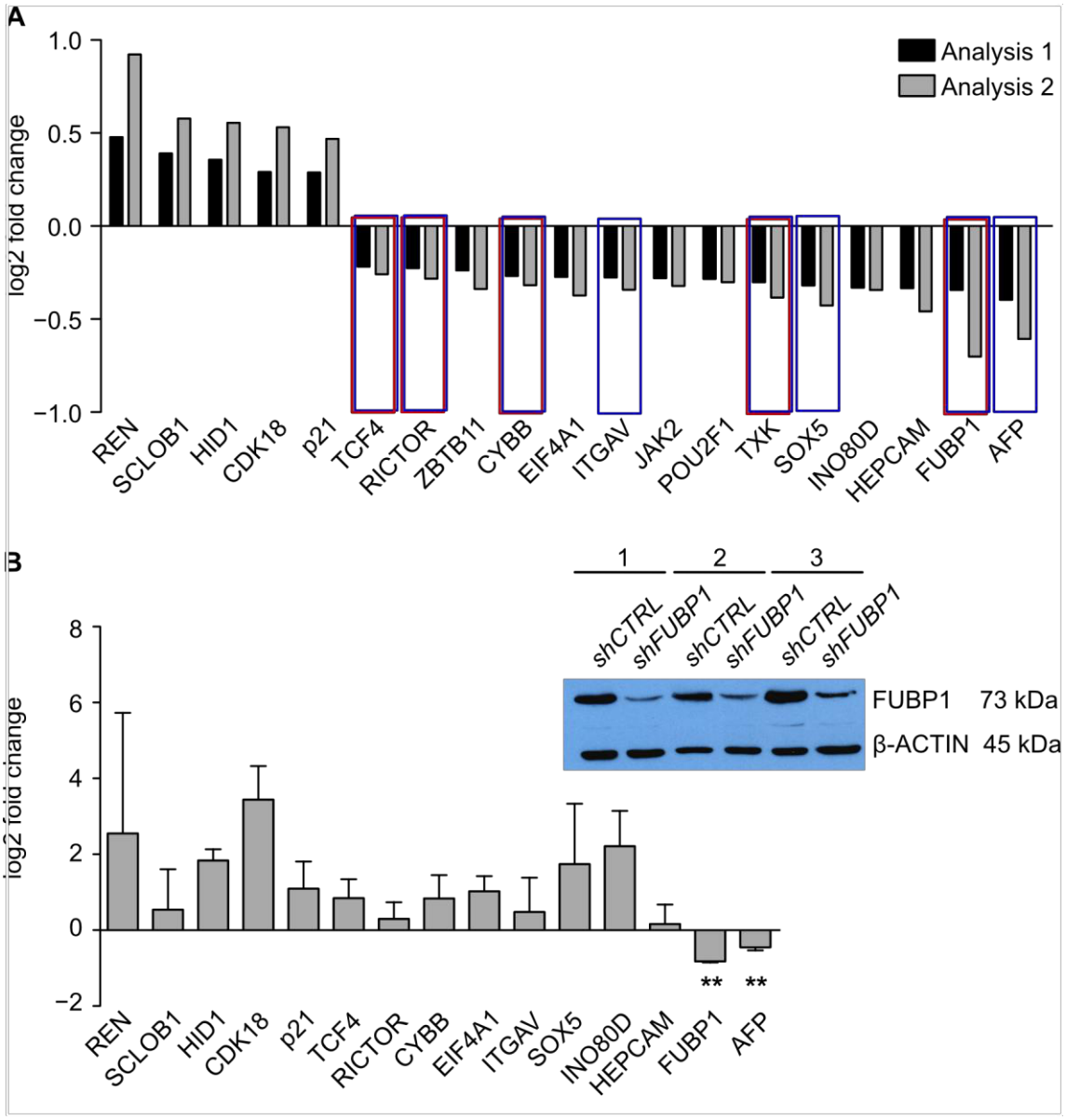

Figure 4.32: RNA sequencing analysis of *FUBP1* knockdown cells suggests FUBP1 target genes involved in hematopoiesis and cell death regulation

A. Deregulated gene expression following *FUBP1* knockdown in K562 cells, identified by RNA sequencing. RNA-Seq results were evaluated independently in the Georg-Speyer-Haus (Birgitta Michels, Analysis 1) and by the Transcriptome and Genome Analysis Laboratory Göttingen (Analysis 2). Genes involved in hematologic system development and function, as predicted by Ingenuity® Pathway Analysis (IPA), are marked in red, genes associated with cell death regulation are marked in blue. Gene expression in *FUBP1* knockdown cells is given as log 2 fold change over gene expression in cells transduced with scrambled shRNA. Bars represent the mean of three independent experiments. **B**. Gene expression analysis of a selected group of genes from **A** by qPCR only confirmed up-regulation of genes and down-regulation of *AFP*. Gene expression was calculated relative to *HPRT1* expression and expression in *FUBP1* knockdown cells is given as log 2 fold change over gene expression in cells transduced with scrambled shRNA. Bars represent the mean of three independent experiments. The efficiency of FUBP1 knockdown in all three experiments (1-3) was confirmed on western blots. β-ACTIN was detected as loading control.

4.2.5 Generation of a mouse model with conditional *Fubp1* knockout potential

All the presented results describing the role of FUBP1 for erythropoiesis were obtained in cell culture experiments. To test the relevance of FUBP1 for erythropoiesis *in vivo*, the consequences of an *Fubp1* knockout in mice were analyzed. Together with the transgenic unit of the German Cancer Research center (DKFZ) in Heidelberg, I established a conditional *Fubp1* knockout mouse model to allow the cell type-specific deletion of *Fubp1*. The conditional deletion of *Fubp1* was supposed to overcome embryonic lethality in constitutive knockout mouse models. A conditional knockout first vector purchased from the international mouse phenotyping consortium was used to target the *Fubp1* allele (**Fig. 4.33A**). The targeting strategy of this vector is the same as the one described for the conditional *Aven* knockout mice (sections **4.1.1** and **4.1.5**). *LoxP* sites flanking *Fubp1* exons 4 to 7 allow CRE-mediated deletion of these exons, leading to a frameshift that is supposed to activate nonsense-mediated decay of the resulting mRNA product. The integrity of the purchased vector was verified by sequencing. The results confirmed the presence and correct sequence of all critical vector components. Subsequently, the linearized vector was introduced into murine embryonic stem cells by electroporation. The neomycin resistance gene in the targeting vector allowed the selection of transfected cells by culture in G418-containing medium. Homologous recombination within the *Fubp1* gene that exchanged the wildtype *Fubp1* locus with the targeted one was verified by both long-range PCR and southern blotting. First, neomycin-resistant ESC clones were tested for the correct integration of the vector by PCR. In a first reaction, the presence of the targeted 3´arm upstream of wildtype exon 14 was demonstrated: a 4,332 bp PCR product that was only generated if the homologous recombination had occurred as intended at the 3´arm of the vector, was identified in 15 out of 288 clones (**Fig. 4.29B**, upper panel). The positively tested clones were screened for correct homologous recombination at the 5´arm of the vector by a similar strategy. 9 out of the 15 tested clones showed the 5,782 bp PCR product of the correctly recombined 5´arm (**Fig. 4.33B**, lower panel). The clones were further tested by southern blotting. Digestion of genomic DNA with restriction enzyme *SacI* gave a 12 kb DNA fragment of the wildtype *Fubp1* locus and a 4.4 kb fragment of the targeted locus, since the targeted DNA contained another cleavage site. Seven out of the nine preselected clones showed the corresponding 4.4 kb band in the southern blot, demonstrating the correct integration of the conditional knockout vector into the genome of the mESCs (**Fig. 4.33C**). Positively tested cell clones were injected into blastocysts that were transplanted in the uteri of pseudo-pregnant foster mothers. Chimeric offspring was identified by a mixed coat color and mated with wild type animals to secure germ line transmission of the targeted allele. Among the offspring of this mating were animals

with the corresponding coat color associated with the modified allele – indicating successful germ line transmission. Successful germline transmission was observed in two independently established mouse lines that had been derived from two different ESC clones. The presence of the *Fubp1* knockout allele in these mice was verified by PCR. The mouse strain with the targeted *Fubp1* locus was used to generate constitutive *Fubp1* knockout mice upon mating with *CMV-Cre* deleter animals and to generate tissue-specific *Fubp1* knockout mice upon mating with *Flp*-deleter animals first and then with cell type-specific *Cre*-deleter mice.

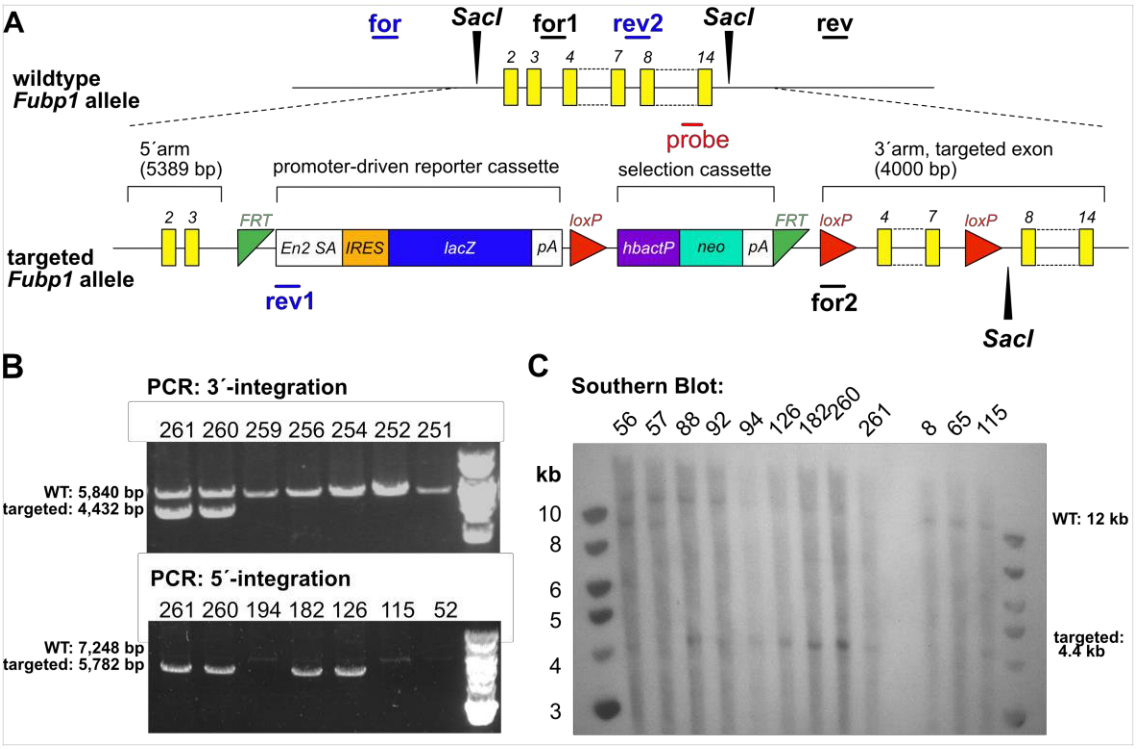

Figure 4.33: Integration of the conditional *Fubp1* knockout first vector in the genome of murine embryonic stem cells
A. Scheme of the murine *Fubp1* wildtype locus and the targeted *Fubp1* conditional knockout allele. The position of primers used to test the correct integration of the targeted allele into the genome are depicted in black (integration test at the 3´end) and in blue (integration test at the 5´end). Cleavage sites of *SacI* and the position of the probe used in southern blot analysis are indicated. **B**. Integration of the conditional *Fubp1* knockout first allele into the genome by homologous recombination was confirmed by PCR reactions. One PCR tested the correct integration at the 3´end of the linearized targeting vector (upper panel, 4,432 bp PCR product in case of correct integration, 5,840 bp product in case of wild type *Fubp1* locus), a second PCR tested the correct integration at the 5´end (lower panel, 5,782 bp PCR product in case of correct integration, 7,248 bp product in case of wildtype *Fubp1* locus. **C**. Southern blot analysis revealed the intended homologous recombination in samples 88 to 261 but not in samples 56 and 57. Samples 8, 65 and 115 were used as negative control (4.4 kb DNA fragments in case of correct vector integration, 12 kb fragments in case of the wildtype *Fubp1* allele following *SacI* digestion).

4.2.6 Constitutive deletion of *Fubp1* exons 4 to 7 leading to a shortened version of the FUBP1 protein is not embryonic lethal in mice

Mice carrying the targeted *Fubp1* allele were mated with *CMV-Cre* deleter animals to achieve a constitutive *Fubp1* knockout by deletion of *Fubp1* exons 4 to 7. Recombination catalyzed by CRE is supposed to remove the selection cassette and the target region, leaving the *LacZ* containing reporter cassette between *Fubp1* exons 2 and 8 (**Fig. 4.34A**). Genotyping of the offspring of mice that were heterozygous carriers of the *Fubp1LacZ* gene showed a drastically reduced percentage of homozygous carriers of the *Fubp1LacZ* gene (**Fig. 4.34B**) compared to expected number according to the Mendelian ratio. The absence of homozygous *Fubp1* knockout animals confirmed embryonic lethality that had been observed using three different *Fubp1* gene trap mouse models [43]. The question remained, why four constitutive *Fubp1* knockout mice were born alive at all. To answer this question, FUBP1 protein and mRNA expression in these mice was analyzed. Western blotting demonstrated the presence of a protein that was recognized by both anti-FUBP1 antibodies used – one binding to the N-terminus, one binding to the C-terminus of FUBP1. The protein detected in the *Fubp1LacZ* mice appeared at a lower molecular weight, at ~64 kDa compared to the band of ~68 kDa in the *Fubp1* wildtype mice (**Fig. 4.34C**). This result suggested that the *Fubp1LacZ* mice express a shortened version of FUBP1. Looking at the *Fubp1* mRNA, a PCR amplifying fragments of different *Fubp1* exons demonstrated the presence of exons 1, 9, 10, 14, 15, 19, 20 in both *Fubp1* wildtype and *Fubp1LacZ* mice. However, fragments spanning exons 2 to 4, 5 to 7 and 7 to 8 were not detected in the *Fubp1-LacZ* mice and the fragment spanning exon 3 to exon 8 was shorter than the wildtype equivalent (**Fig. 4.34D**). Concluding from these results, *Fubp1* exons 4 to 7 were deleted in the *Fubp1LacZ* mice, but a splicing process seemed to have joined *Fubp1* exon 8 to exon 3. Sequencing of the PCR product spanning exon 3 to 8 confirmed this theory and revealed a sequence which is part of the mouse *EN2* exon between *Fubp1* exons 3 and 8 (**Fig. 4.34E**). Remarkably, the inserted *EN2* sequence did not lead to a frameshift mutation. *EN2* is part of the targeted locus, it contains the sequence of a splice acceptor which is supposed to link the reporter cassette to *Fubp1* exon 3. The unintended splicing observed in the *Fubp1LacZ* mice did not cause a knockout of *Fubp1* but created a new version of FUBP1 shortened by exons 4 to 7, with an additional fragment of EN2. As these mice were alive and healthy, FUBP1 amino acids 80 to 154, which are encoded by exons 4 to 7, seem to be dispensable for the FUBP1 structure and function.

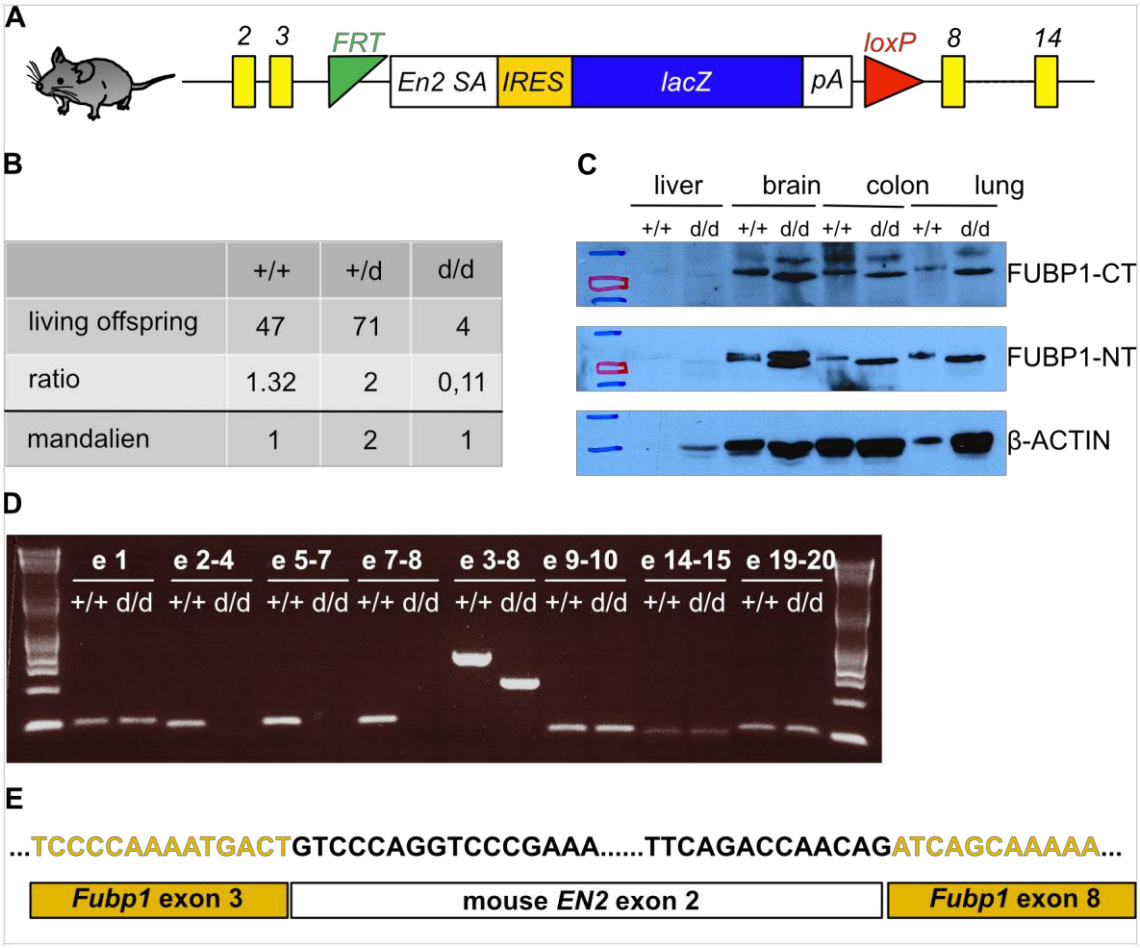

	+/+	+/d	d/d
living offspring	47	71	4
ratio	1.32	2	0,11
mandalien	1	2	1

Figure 4.34: Constitutive deletion of *Fubp1* exons 4 to 7 leading to a shortened version of FUBP1 is not embryonic lethal in mice
A. Scheme of the *Fubp1* allele in *Fubp1LacZ* mice. Exons 4 to 7 were replace by a *LacZ* containing reporter cassette. **B**. Offspring statistics of heterozygous *Fubp1LacZ* mice showed drastically reduced numbers of homozygous *Fubp1LacZ* mice. **C**. Western Blot analysis showed an FUBP1 protein in the organs of *Fubp1LacZ* mice (d/d) that was smaller than in organs of *Fubp1* wildtype mice (+/+). Two anti-FUBP1 antibodies, one binding at the C-terminus (CT), one binding at the N-terminus (NT) of FUBP1, were used. β-ACTIN was detected as loading control. **D**. qPCR analysis of *Fubp1* mRNA in *Fubp1LacZ* mice (d/d) and *Fubp1* wildtype mice (+/+). *Fubp1* exons (e) that were amplified are indicated. **E**. Sequencing of the PCR product spanning *Fubp1* exon 3 to 8 shown in **D** was sequenced. The identified sequence corresponds to *Fubp1* exons 3 and 8 that are linked by a sequence encoding exon 2 of mouse *engrailed 2* (*EN2*).

4.2.7 Insertion of *loxP* sites in the *Fubp1* locus causes embryonic lethality

To generate conditional *Fubp1* knockout mice, heterozygous carriers of the targeted *Fubp1* locus were mated with *Flp*-deleter animals. Recombination by FLP first removed both the reporter and the selection cassette, and only an *FRT* sequence and *loxP* sites remained as synthetic DNA in the *Fubp1* locus. Genotyping of the offspring confirmed recombination in most of the heterozygous carriers of the targeted *Fubp1* locus expressing FLP (**Fig. 4.35A, B**). Mice that were heterozygous for the successfully

recombined *Fubp1* locus were mated with constitutive or cell type-specific *Cre* deleter strains. Mating with *CMV-Cre* mice caused a constitutive *Fubp1* knockout that was embryonic lethal: among the 65 offspring of heterozygous parents, none showed a homozygous *Fubp1* deletion (data not shown). Genotyping prenatal offspring of heterozygous transgenic animals also demonstrated the absence of homozygous *Fubp1* knockout embryos at 13.5 dpc (10 embryos analyzed) and at 10.5 dpc (24 embryos analyzed, data not shown). Thus, a splicing event as observed in the *Fubp1LacZ* mice could be excluded in the animals whose genomic DNA was recombined with FLP first. Embryonic lethality of a constitutive *Fubp1* knockout as described in other mouse models could be confirmed, although embryonic death seemed to happen earlier than in the *Fubp1* gene trap mice [150], [67].

Mice carrying the floxed *Fubp1* locus were mated with *Alb-Cre* transgenic deleter mice to generate an *Fubp1* knockout in the liver. *Vav-Cre* transgenic mice were used to generate an *Fubp1* knockout in the whole hematopoietic system, and *ErGFP-Cre* transgenic animals were used to knock out *Fubp1* in EPO receptor-expressing cells. Progeny of this mating that was heterozygous for the floxed *Fubp1* locus ($Fubp1^{+/d}$) and expressed the respective CRE recombinase (Cre^{+}) was bred with $Fubp1^{+/d}$ mice (**Fig. 4.35C**). Half of the offspring of this mating should express CRE (Cre^{+}). Concerning the *Fubp1* locus, the expected distribution of genotypes was 25% $Fubp1^{d/d}$, 50% $Fubp1^{+/d}$ and 25% $Fubp1^{+/+}$ according to Mendel´s law if viability was not affected. The offspring statistics revealed that homozygous $Fubp1^{d/d}$ mice were completely absent after breeding with *Alb-Cre* deleters, numbers of $Fubp1^{d/d}$ mice were strongly reduced after breeding with *ErGFP-Cre* deleters and moderately reduced after mating with *Vav-Cre* deleters (**Fig. 4.35C**). The number of heterozygous offspring was also reduced after breeding with *ErGFP-Cre* and *Vav-Cre* deleters. A distortion of the Mendelian distribution could be the consequence of embryonic lethality after knockout of *Fubp1* in the respective cells. In this case, a normal distribution should be observed in the Cre^{-} offspring and a reduction of homozygous $Fubp1^{d/d}$ offspring should be restricted to the Cre^{+} population. However, the number of $Fubp1^{d/d}$ mice was equally decreased in Cre^{-} and Cre^{+} offspring. $Fubp1^{d/d}Cre^{-}$ mice were supposed to express wildtype levels of FUBP1. This could be confirmed by western blotting using the organs of living $Fubp1^{d/d}Cre^{-}$ mice (data not shown). The significant reduction of living $Fubp1^{d/d}Cre^{-}$ mice strongly suggested embryonic lethality as a result of the inserted *loxP* sites within the *Fubp1* locus. Survival of some of the $Fubp1^{d/d}Cre^{-}$ mice could be the consequence of some kind of compensation for the disturbance in the *Fubp1* locus. Hence, the action of compensating mechanism was kept in mind when the surviving conditional *Fubp1* knockout mice were analyzed as described in the following sections.

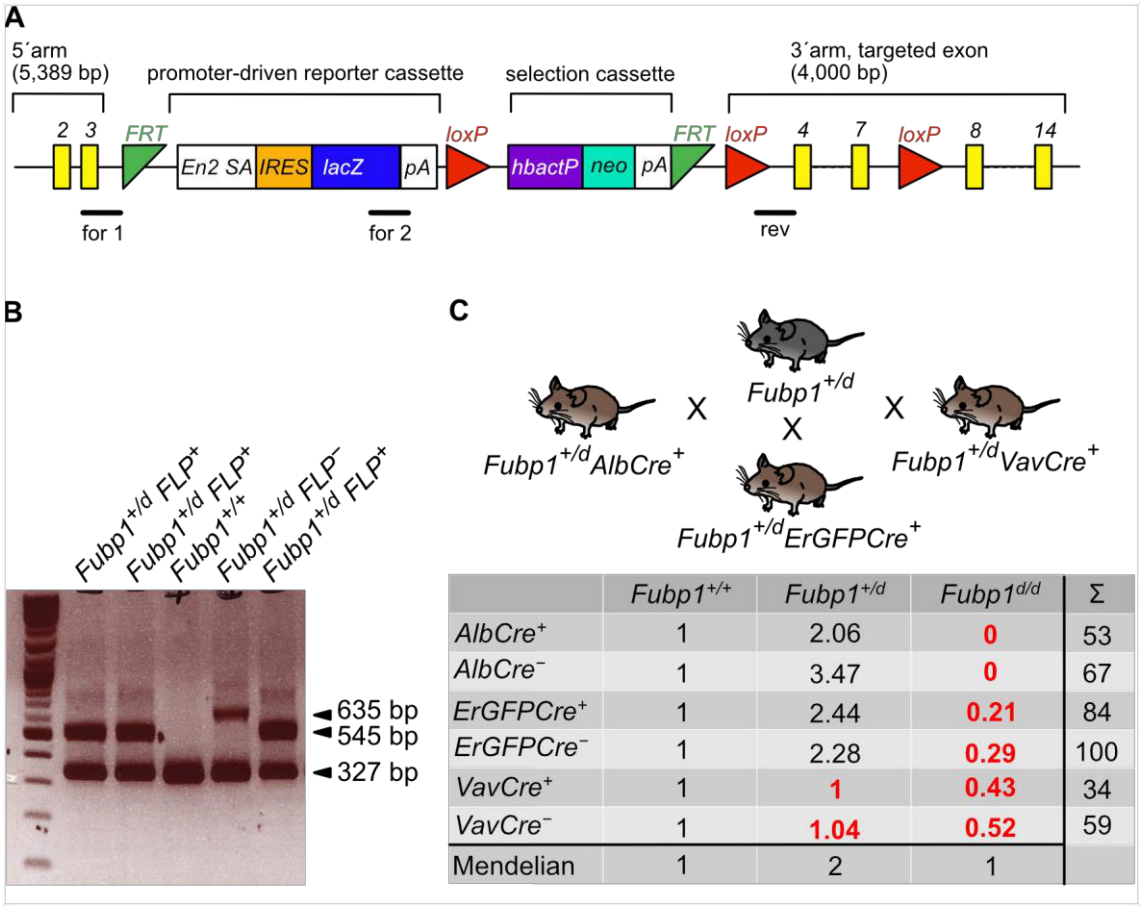

	Fubp1$^{+/+}$	*Fubp1*$^{+/d}$	*Fubp1*$^{d/d}$	Σ
AlbCre^{+}	1	2.06	**0**	53
AlbCre^{-}	1	3.47	**0**	67
ErGFPCre^{+}	1	2.44	**0.21**	84
ErGFPCre^{-}	1	2.28	**0.29**	100
VavCre^{+}	1	**1**	**0.43**	34
VavCre^{-}	1	**1.04**	**0.52**	59
Mendelian	1	2	1	

Figure 4.35: Targeting the *Fubp1* locus in conditional knockout mice may already be embryonic lethal before the cell type-specific deletion of *Fubp1*
A. Scheme of the targeted *Fubp1* locus in mice with conditional *Fubp1* knockout potential. Primers used to identify successful recombination mediated by FLP recombinase (B) are indicated. **B**. Genotyping of conditional *Fubp1* knockout mice that expressed FLP revealed successful recombination of the *Fubp1* locus (327 bp PCR fragment in mice with wildtype *Fubp1* locus, 545 bp PCR product in mice with targeted *Fubp1* locus after successful FLP-mediated recombination, 635 bp PCR product in mice with targeted *Fubp1* locus without FLP-mediated recombination). The PCR and gel electrophoresis was performed by Susanne Bösser. **C**. Breeding strategy to generate mice with a cell type-specific *Fubp1* knockout. Offspring statistics of the mating are shown below. The total number of analyzed animals is shown in the right column (Σ). Ratios deviating from the Mendelian distribution are marked in red.

4.2.8 Depletion of FUBP1 in the hematopoietic system does not change stem cell and progenitor frequencies or affect lineage differentiation in mice

In vivo studies on the physiological role of FUBP1 in murine hematopoiesis have so far been limited, as the constitutive *Fubp1* knockout in mice was reported to be lethal around 15.5 dpc [150]. A conditional *Fubp1* knockout mouse model was not available, and therefore characterization of *Fubp1* knockout mice was restricted to the embryonic stages. The new conditional *Fubp1* knockout mice presented here allowed further investigation of the endogenous function of Fubp1 *in vivo*, focusing on the following questions: Is the reported function of FUBP1 in HSC survival and self-renewal

responsible for embryonic lethality in constitutive *Fubp1* knockout mice? Which role does FUBP1 play in adult hematopoiesis? Can the effects of FUBP1 deficiency observed in *in vitro* and *ex vivo* studies – reduced viability and erythroid differentiation potential of HSPCs – also be observed i*n vivo*?

To tackle these questions, mice with an *Fubp1* knockout in VAV-expressing cells (*Fubp1*$^{d/d}$*VavCre*$^{+}$), i.e. in the hematopoietic system and endothelial cells, were produced by mating the available mouse strains. As discussed above, mice with this genotype were born and alive, but their number was clearly reduced (**Fig. 4.36C**). FUBP1 protein expression in the bone marrow, in the spleen and in the thymus was analyzed; these organs consist mostly of VAV expressing cells and thus should be depleted of FUBP1 protein in *Fubp1*$^{d/d}$*VavCre*$^{+}$ mice. Indeed, a knockout of *Fubp1* could be demonstrated in all three organs (**Fig. 4.36A, B**). Regarding the considerable number of these mice that were alive, lack of FUBP1 in the hematopoietic system does at least not seem to be the only reason for embryonic lethality observed in constitutive knockout mice.

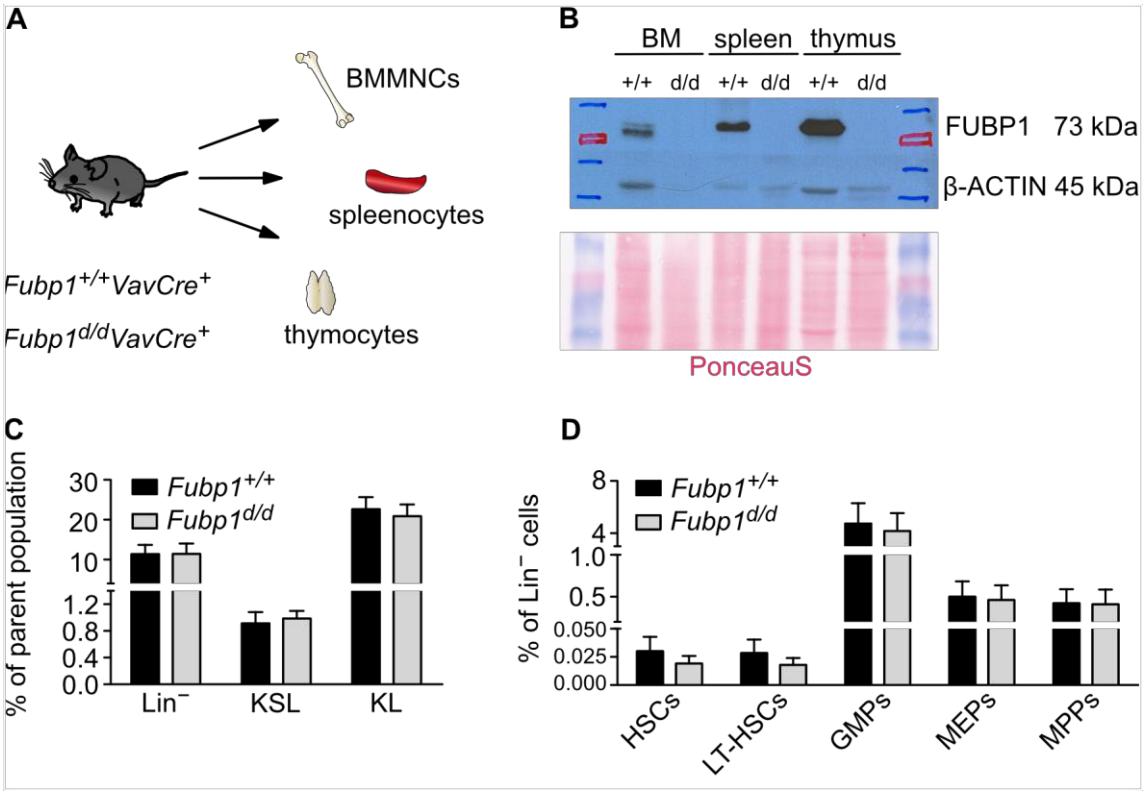

Figure 4.36: Depletion of FUBP1 in the hematopoietic system did not change stem cell and progenitor frequencies in mice
A. Bone marrow mononuclear cells (BMMNCs), spleenocytes and thymocytes of mice were analyzed in mice with a knockout of *Fubp1* in Vav-Cre expressing cells (*Fubp1*$^{d/d}$*VavCre*$^{+}$, n=7). Littermates with wildtype *Fubp1* expression (*Fubp1*$^{+/+}$*VavCre*$^{+}$, *n=7)* were used as control group. **B**. *Fubp1* knockout in the whole bone marrow (BM), spleen and thymus in *Fubp1*$^{d/d}$*VavCre*$^{+}$ mice (d/d) was confirmed by western blotting. β-ACTIN detection and PonceauS staining were performed as loading control. **C**, **D**. The percentages of naïve hematopoietic populations was not altered in *Fubp1*$^{d/d}$*VavCre*$^{+}$ mice compared to mice with wildtype FUBP1 expression, as shown by flow cytometry analysis.

To investigate the consequences of FUBP1 deficiency in adult stem and progenitor cells, bone marrow mononuclear cells (BMMNCs) were isolated, and frequencies of different naïve populations were measured by flow cytometry. No difference in the percentage of undifferentiated cells (Lin negative cells), immature multipotent cells (KSL cells) and committed progenitor cells (KL cells) was detected between *Fubp1* knockout and control mice (**Fig. 4.36C**). Further discrimination of the populations into HSCs, LT-HSCs, MPPs, GMPs and MEPs also revealed no significant differences, although the percentage of HSCs in *Fubp1*$^{d/d}$*VavCre*$^{+}$ mice was slightly reduced (0.019%) compared to *Fubp1*$^{+/+}$*VavCre*$^{+}$ mice (0.030%, **Fig. 4.36D**). A similar reduction was observed in the LT-HSC population (0.018% in *Fubp1*$^{d/d}$ vs. 0.028% in *Fubp1*$^{+/+}$ mice, **Fig. 4.36D**). Population definitions and gating strategy were the same as in section **4.1.7**. Apparently, the described reduction of LT-HSCs and increase of MPPs in the fetal liver of *Fubp1* gene trap mice [150] could not be reproduced in the conditional *Fubp1* knockout mouse model.

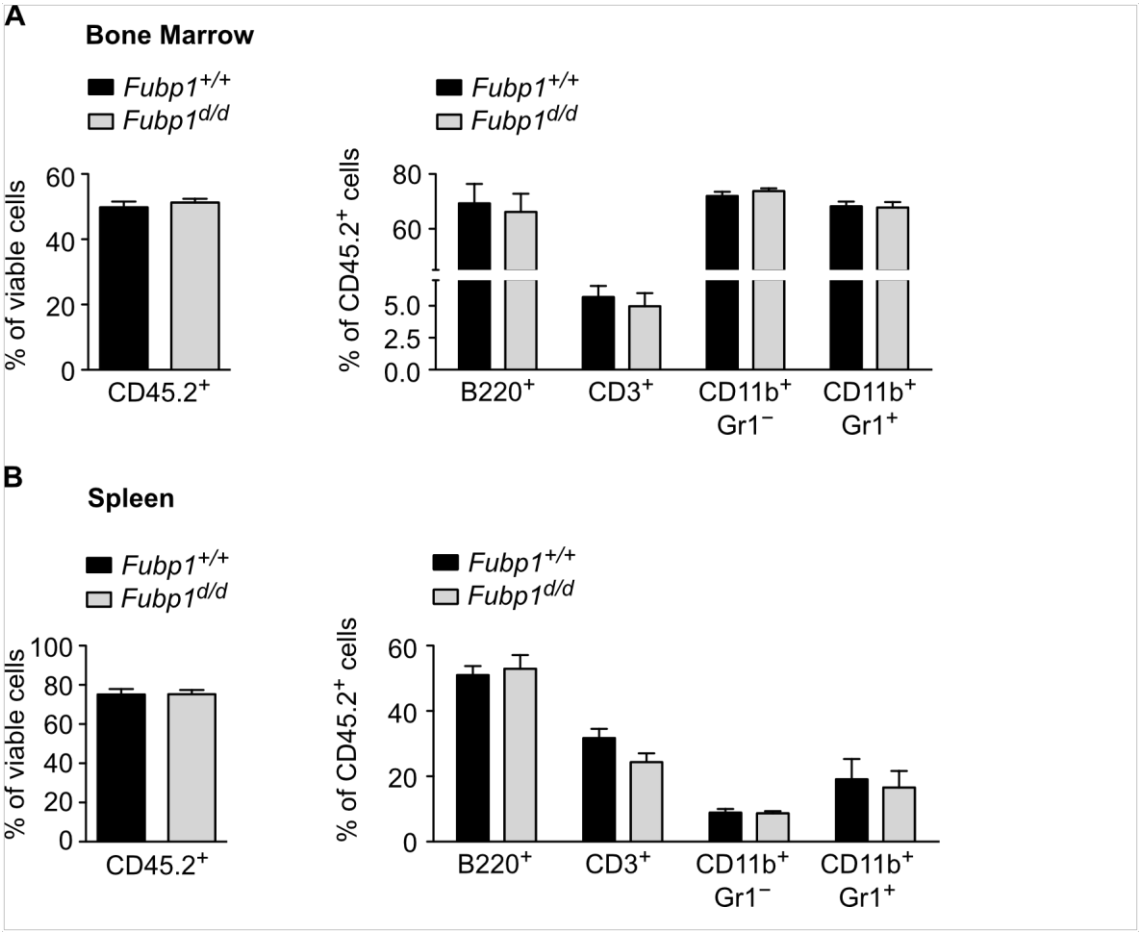

Figure 4.37: *Fubp1* knockout in the hematopoietic system has no effect on lineage differentiation in the murine bone marrow and spleen
Percentages of leukocytes (CD45.2^{+} cells, left), B cells (B220^{+}), T cells (CD3^{+}) and myeloid cells

(CD11b$^+$) (right) are not changed in the bone marrow (**A**) and spleen (**B**) of mice with an *Fubp1* knockout in the hematopoietic system (*Fubp1$^{d/d}$VavCre$^+$,* n=7) compared to mice with wildtype *Fubp1* alleles (*Fubp1$^{+/+}$VavCre$^+$,* n=7). Percentages of surface marker stained cells were recorded by flow cytometry. Gating and population definitions are shown in **Fig. 4.17**.

Staining for different lineages in the bone marrow and spleen as described previously for the *Aven$^{d/d}$VavCre$^+$* mice (see section **4.1.7**) demonstrated that differentiation into T, B and myeloid cells as well as erythropoiesis was not altered in *Fubp1$^{d/d}$VavCre$^+$* mice compared to mice expressing wildtype levels of FUBP1 (**Fig. 4.37**, **4.38**). Concluding from these results, FUBP1 seems to be dispensable for hematopoietic lineage differentiation. This is in contrast to previous findings, especially concerning erythropoiesis.

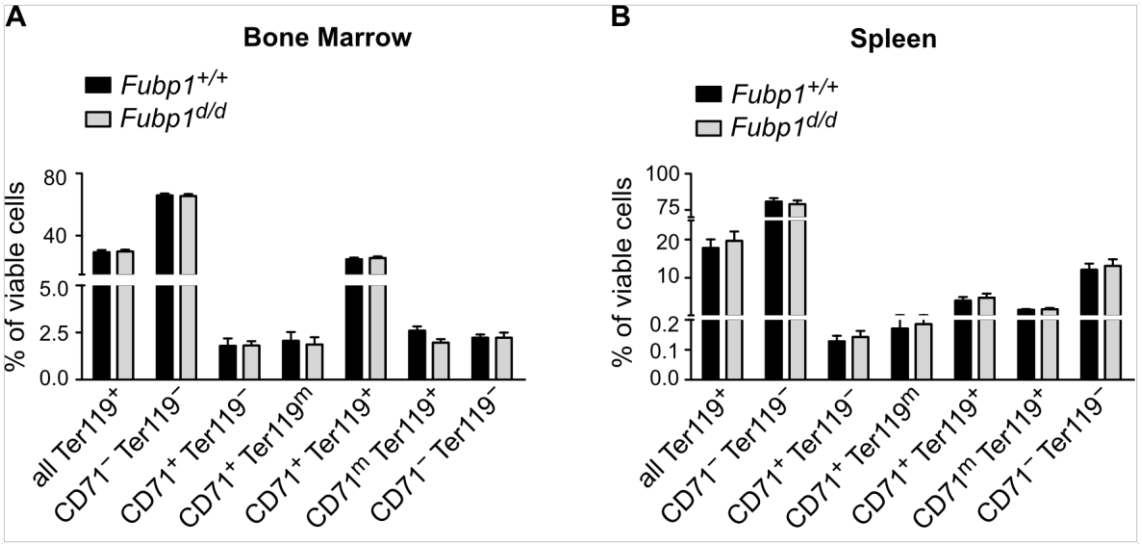

Figure 4.38: Normal erythropoiesis in mice with an *Fubp1* knockout in the hematopoietic system
All stages of erythroid differentiation were present at normal frequencies in the bone marrow (**A**) and spleen (**B**) of mice with an *Fubp1* knockout in the hematopoietic system (*Fubp1$^{d/d}$VavCre$^+$,* n=7) compared to mice with wildtype *Fubp1* alleles (*Fubp1$^{+/+}$VavCre$^+$,* n=7). Population frequencies were recorded by flow cytometry after cell surface marker staining. Gating and population definitions are shown in **Fig. 14.9**.

4.2.9 Knockout of *Fubp1* in the hematopoietic system leads to reduced numbers of mature T helper cells in the murine thymus

To complete characterization of the *Fubp1$^{d/d}$VavCre$^+$* mice, T cell development in the thymus was analyzed. Maturation stages of T helper and cytotoxic cells were assessed by CD4 and CD8 surface expression staining and quantification by flow cytometry was performed as described in section **4.1.7**. Additionally, a staining for T cell receptor (TCR,

CD3) surface expression was performed. Cell surface expression of the mature αβ TCR starts at the stage of CD4, CD8 double positive progenitors and is present in all following stages [172]. Anti-CD3 staining was used to exclude non-T cells from the analysis. Interestingly, the percentage of CD3 positive cells was significantly reduced in *Fubp1*$^{d/d}$*VavCre*$^{+}$ mice compared to the control group (*Fubp1*$^{+/+}$*VavCre*$^{+}$ mice, **Fig. 4.39A**). Looking at the distinct differentiation stages of the T cells, *Fubp1* knockout mice display higher percentages of immature populations (DP, CD4^{low}CD8^{low}, CD4^{+}CD8^{low}) while the frequency of mature T helper cells (CD4^{+}) is significantly decreased compared to mice expressing FUBP1 wildtype levels (**Fig. 4.39B**). There was no alteration in the frequency of mature cytotoxic T cells (CD8^{+}) in *Fubp1*$^{d/d}$*VavCre*$^{+}$ thymocytes. These data suggest that FUBP1 promotes final maturation of T helper cells in the murine thymus.

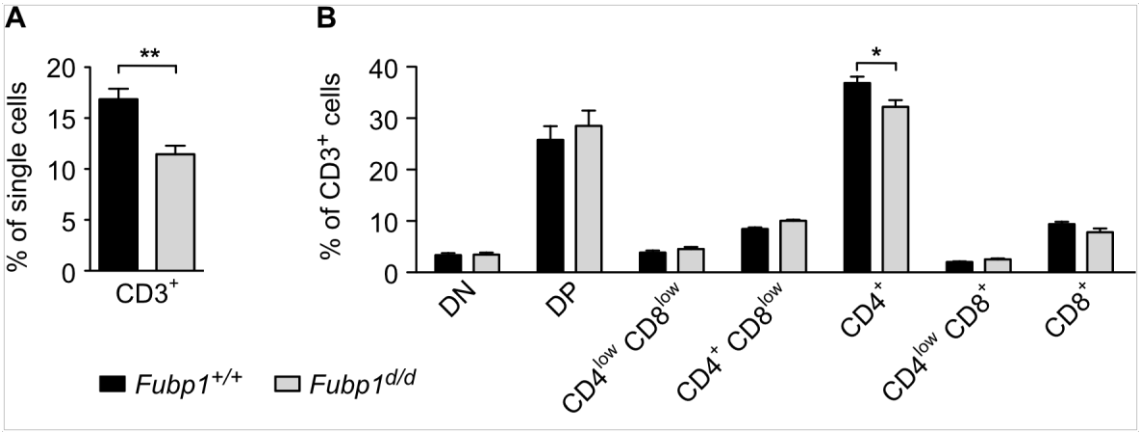

Figure 4.39: Knockout of *Fubp1* in the hematopoietic system leads to reduced numbers of mature CD4+ T helper cells in the murine thymus
A. The percentage of T cell receptor (TCR, CD3) expressing cells in the thymus was significantly reduced in *Fubp1*$^{d/d}$*VavCre*$^{+}$ (n=7) mice compared to the control group (*Fubp1*$^{+/+}$*VavCre*$^{+}$*, n=7*). **B**. The percentage of CD4^{+} mature T helper cells was significantly decreased in *Fubp1*$^{d/d}$*VavCre*$^{+}$ mice compared to animals expressing wildtype FUBP1 levels (*Fubp1*$^{+/+}$*VavCre*$^{+}$). Population frequencies were measured by flow cytometry following cell surface marker staining. Gating and population definitions are shown in **Fig. 4.18**.

In summary, the characterization of mice with an *Fubp1* knockout in VAV expressing cells showed that FUBP1 is required in the hematopoietic system only under certain conditions. The knockout of *Fubp1* in hematopoietic cells is only partially embryonic lethal and embryonic lethality could also be the consequence of the floxed *Fubp1* locus in cells apart from the VAV-expressing compartment. The frequencies of hematopoietic stem and progenitor cells were unaltered in *Fubp1*$^{d/d}$*VavCre*$^{+}$ mice, similar to lineage differentiation in the bone marrow and spleen. However, reduced percentages of CD3-positive and CD4-positive thymocytes in *Fubp1*$^{d/d}$*VavCre*$^{+}$ mice suggest a role for FUBP1 in T cell development.

4.2.10 Depletion of FUBP1 in EPO receptor-expressing cells does not change erythropoiesis in mice

Normal frequencies of erythroid progenitors and mature erythrocytes were observed in mice with an *Fubp1* knockout in the whole hematopoietic system. As an additional model to characterize erythropoiesis in the absence of FUBP1, mice with an *Fubp1* knockout in EPO receptor-expressing cells (*Fubp1*$^{d/d}$*ErGFPCre*$^{+}$ mice) were bred. This model was also produced for the case of embryonic lethality as a consequence of *Fubp1* deletion in HSCs in the *Fubp1*$^{d/d}$*VavCre* model. Genotyping tail tissue and bone marrow of *Fubp1*$^{d/d}$*ErGFPCre*$^{+}$ mice showed a clearly visible PCR product representing deletion of *Fubp1* exons 4 to 7 in the bone marrow but not in the tails of the analyzed mice (**Fig. 4.40B**). Bone marrow contains a considerable number of EPOR-expressing cells in contrast to the tail, so these results confirmed the cell type-specificity of the *Fubp1*$^{d/d}$*ErGFPCre*$^{+}$ knockout mice. Bone marrow, spleenocytes and peripheral blood were isolated to analyze erythropoiesis in *Fubp1*$^{d/d}$*ErGFPCre*$^{+}$ and control mice (*Fubp1*$^{+/+}$*ErGFPCre*$^{+}$ and *Fubp1*$^{d/d}$*ErGFPCre*$^{-}$ mice). The expression of CRE in the *ErGFPCre*$^{+}$ mice is coupled to the marker expression of GFP. Although GFP expression was quite weak, the percentage of GFP expressing cells in the bone marrow of *ErGFPCre*$^{+}$ mice, quantified by flow cytometry, was significantly higher than in *ErGFPCre*$^{-}$ mice (**Fig. 4.40C**, left). Significant GFP expression could not be detected in the spleen and peripheral blood of *ErGFPCre*$^{+}$ mice due to the restriction of *EPOR* promoter activity to erythroid progenitors before enucleation (**Fig. 4.40C**, middle and right). Nucleated erythroid cells are detectable only at negligible levels in the spleen and peripheral blood. The measured GFP expression is another evidence for the cell-specific CRE expression. Erythroid differentiation stages, as monitored by the surface expression of CD71 and Ter119, were present at normal frequencies in *Fubp1* knockout and control bone marrow (**Fig. 4.40D**) as well as in the spleen and peripheral blood (data not shown). So, this mouse model confirmed the finding of the *Fubp1*$^{d/d}$*VavCre*$^{+}$ model that FUBP1 is dispensable for normal adult erythropoiesis. However, the EPOR^{+}-specific homozygous knockout of *Fubp1* was embryonic lethal in over 70% (**Fig. 4.35**). If this embryonic lethality was caused by loss of FUBP1 in erythroid progenitors rather than unintended effects of the inserted *loxP* sites or other effects, FUBP1 could play a pivotal role already during embryonic erythropoiesis.

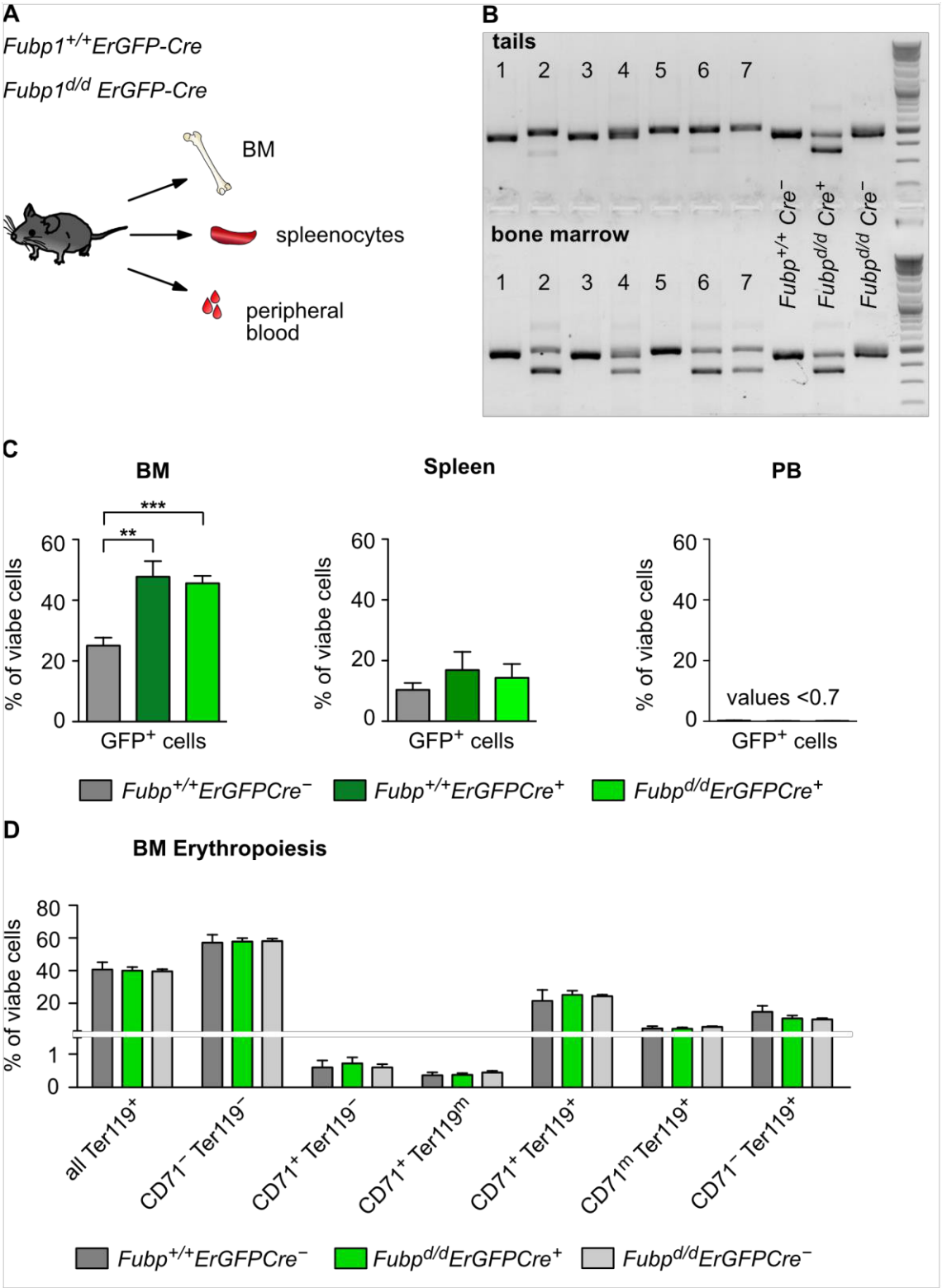

Figure 4.40: Living mice with and Fubp1 knockout in EPO receptor-expressing cells exhibit no aberrant phenotype

A. Bone marrow mononuclear cells (BMMNCs), spleenocytes and peripheral blood of mice were analyzed in animals with a knockout of *Fubp1* in EPO receptor-CRE expressing cells (*Fubp1$^{d/d}$ErGFPCre^{+},* n=5). Littermates with wildtype FUBP1 expression (*Fubp1$^{+/+}$ErGFPCre^{+}, n=3 and Fubp1$^{d/d}$ErGFPCre^{-}, n=2*) were used as control group. **B**. Genotyping of tail tissue from six *Fubp1ErGFPCre* mice showed hardly any PCR product of the deleted *Fubp1* locus (372 bp). This fragment was detected in the bone marrow, though. The 429 bp PCR product corresponds to the wildtype *Fubp1* allele, the 509 bp PCR product corresponds to the targeted *Fubp1* allele without ErGFP-CRE mediated recombination. The last three lanes were run as controls. **C**. Significant percentages of GFP-expressing cells were detected in the bone marrow of ErGFP-expressing mice (left), but not in the spleen and in peripheral blood (middle and right). GFP

expression was detected by flow cytometry. **D**. All stages of erythroid differentiation were present at normal frequencies in the bone marrow of mice with an *Fubp1* knockout in EPOR-expressing cells compared to mice with wildtype *Fubp1* expression. Population frequencies were recorded by flow cytometry after cell surface marker staining. Gating and population definitions are shown in **Fig. 4.19**.

5 Discussion

Characteristic changes in biological processes that discriminate tumor cells from healthy cells and rationalize their malignant transformation are defined as “hallmarks of cancer”. Resisting cell death, sustaining proliferative signaling and evading growth suppression, both leading to deregulated cell cycling, constitute three of ten identified hallmarks [24]. The identification of the molecular structures and their functions that underlie the hallmarks of cancer allowed their specific inhibition in targeted anti-cancer therapy. The inhibition of epidermal growth factor receptor (EGFR) in cancer treatment represents a prominent example [173], [174]. Research on EGFR signaling discovered its physiologic role in promoting cell growth, but also an involvement in the modulation of cell survival, differentiation, adhesion and migration. This research constituted the prerequisite for the association of aberrant EGFR activity in several cancer entities with the malignant traits of tumor cells. Multiple strategically developed EGFR inhibitors and antibodies targeting EGFR have been approved for the treatment of different diseases. EGFR-targeting therapy has been demonstrated to significantly increase the overall and progression-free survival and the overall response rate in a subset of patients. However, measures to predict anti-EGFR-therapy response are not available yet.

Targeting cell death resistance in anti-cancer therapy is less advanced, but some therapeutics show promising results in clinical trials, among them small molecule inhibitors of BCL-2 family members and inhibitor of apoptosis proteins (IAPs), and BH3 mimetics [175]. Just as EGFR-inhibitors, these therapeutic strategies successfully combat cancer only in a subset of patients. Consequently, tumorigenic mechanisms need to be continuously investigated to tackle the immense diversity of neoplastic entities.

As regulators of apoptosis and cell cycle progression, both AVEN and FUBP1 constitute potential targets in anti-cancer therapy [8], [13], [42]. An aberrant expression of both proteins could be demonstrated in multiple cancer entities [27], [10], [42]. Assessing their value as therapy target requires knowledge on their physiological function: Knowing how AVEN and FUBP1 impact normal biological processes will not only shed light on their role in tumorigenesis, but also help to estimate on-target toxicity of therapeutic interference with their function. The physiological role of AVEN and FUBP1 is elusive in large parts. FUBP1 has been reported to play an important role in the survival and maintenance of hematopoietic stem cells [150], [67] and might be required for neural development [57]. AVEN is potentially required for normal spermatogenesis [21]. Gene knockout mouse models constitute a valuable tool to study gene functions. Regarding AVEN and FUBP1, information gained from the characterization of constitutive knockout mouse models is limited due to embryonic death of homozygous knockout animals [43],

[150], [67], (unpublished data).

In this thesis, I presented the generation of novel *Aven* and *Fubp1* genetic mouse models. By characterizing *Aven* reporter mice, I identified *Aven* expression in specific cell types and developmental stages. Conditional *Aven* and *Fubp1* knockout mice were established to study the consequences of tissue-specific AVEN and FUBP1 depletion. The role of AVEN in the context of breast cancer was further investigated by analyzing a mouse model for tumorigenesis in the mammary gland in the presence and absence of *Aven* expression. The results obtained by the characterization of the mouse models and additional complementing *in vitro* studies are discussed in the following.

5.1 AVEN is essential for embryogenesis and might be required to enable translation of tissue-specific transcription factors during organogenesis

To gain insight into the physiological function of AVEN, *AvenLacZ* mice allowing the visualization of the exact sites of endogenous *Aven* promoter activity were analyzed. The results demonstrate that *Aven* promoter activity is on the one hand tissue- and cell type-specific and dependent on the developmental stage. On the other hand, *Aven* promoter activity is observed in cells as different as neurons, epithelial and muscle cells, making it difficult to associate *Aven* expression to a specific cell feature (**Fig. 4.3-4.10**). The biological processes that AVEN has been linked to so far – apoptosis, regulation of cell cycle and mRNA translation – are of general importance for all kind of cells at all developmental stages. Considering this, a widespread *Aven* expression is not surprising. It is rather remarkable that some tissues as the liver totally lack *Aven* expression.

Aven promoter activity changes with maturation. The overall *Aven* promoter activity is stronger in embryos compared to adult tissues (**Fig. 4.3-4.10**). While the embryonic brain shows no *Aven* promoter activity, there is a prominent and distinct staining for *Aven* promoter activity in many neurons of the adult brain. In contrast, the embryonic lung shows a strong staining for *Aven* promoter activity that is reduced in intensity and restricted to the ciliated epithelium of the bronchioles in the adult organ. A similar reduction in *Aven* promoter activity from the embryonic to the adult organ is found in the kidney. These results indicate that AVEN function is required for certain processes that are important and activated at specific points in time during development. The knockout of *Aven* in cells that showed high *Aven* expression only at the adult stage – the brain and the mammary gland – surprisingly showed no effect on viability of the mice or tissue integrity (**Fig. 4.13**, **4.14**, **4.22**). Also, the knockout of *Aven* in the hematopoietic system

did not cause embryonic lethality. In constitutive *Aven* knockout mice, a significant reduction of living homozygous *Aven* knockout offspring is observed at 15.5 dpc. At 13.5 dpc, living homozygous *Aven* knockout mice appeared behind normal development considering their reduced size and impaired eye anlagen development (**Fig. 4.12**). This is consistent with *Aven* promoter activity which is maximal at 15.5 dpc and first detected at 13.5 dpc. These findings suggest an essential role for AVEN during embryogenesis, particularly during the late stage of organogenesis taking place between 13.5 dpc and 15.5 dpc [60]. Interestingly, AVEN has been reported to play a role in blastocyst development. *Aven* expression was found increased in fertilized oocytes that failed to develop to blastocysts compared to fertilized oocytes that reached blastocyst stage [176]. So onset of considerable *Aven* expression might be repressed until mid-gestation to allow normal embryogenesis.

Apoptosis is an important process during embryogenesis: 50-70% of the neurons in the murine embryonic cortex die between embryonic day 14 and 18 [177]. In addition, apoptosis is an essential process during the morphogenesis of the four-chambered heart in the embryo [178]. These are just two of many examples. Thus, it stands to reason that AVEN acts as an inhibitor of apoptosis in the embryo to prevent those cells from cell death that must not die. However, increased apoptosis could not be detected in AVEN-deficient embryos (**Fig. 4.11**) and organs (data not shown). Furthermore, the anti-apoptotic function of AVEN has been attributed to the truncated ΔN-AVEN, a product of CathD procession, but not the full-length protein [11]. In contrast to the homozygous knockout of *Aven*, the *CathD* knockout in mice is not embryonic lethal [179]. This points to a different and essential function of full length AVEN besides apoptosis inhibition during embryogenesis, or alternative procession of AVEN in embryos. Regulation of translation by AVEN in the embryonic heart constitutes one possible function that warrants further investigation. AVEN binds quadruplex structures in mRNAs in a complex with helicase DHX36 [17]. This helicase is so far the only enzyme known to be able to resolve mRNA quadruplexes. During embryogenesis, DHX36 is required to enable *Nkx2-5* translation. NKX2-5 is a cardiac transcription factor that is essential for heart development [180]. Increasing DHX36 expression in the heart from embryonic day 14.5 to 16.5, followed by a downregulation, correlates with cardiac *Aven* promoter activity in *AvenLacZ* mice. Additionally, embryonic lethality as a consequence of DHX36 inactivation in cardiac progenitors at 14.5 dpc coincides with the observed embryonic lethality as a consequence of *Aven* knockout [180]. Thus, a complex of AVEN and DHX36 could be required for *Nkx2-5* translation activation.
Such post-transcriptional regulation of tissue-specific gene expression, especially during tissue differentiation, not only in the heart but also in other sites of high *Aven* promoter

activity, would constitute a pivotal function of AVEN in late organogenesis.

5.2 The regulation of apoptosis and metabolism by AVEN correlates with BCL-x_L function and could be targeted to sensitize ER^+ breast tumors to chemotherapy

AVEN apparently has the potential to regulate cell cycle progression and apoptosis [8] [13], [20], [10]. Thus, aberrant AVEN expression can be associated with two hallmarks of cancer. Indeed, high AVEN expression levels have been found in acute leukemias [25], [26], [27], osteosarcoma lung metastasis [29] and breast cancer cells with high tumor initiating ability [10]. To further investigate the role of AVEN in breast cancer development, an *MMTV-PyVT* conditional *Aven* knockout mouse model was characterized. An increased AVEN expression was detected in *MMTV-PyVT*-induced tumors compared to healthy tissue, but knockout of *Aven* in the mammary gland showed no effect on tumor onset and tumor burden (**Fig. 4.22**-**4.24**). In contrast to the *p53* knockout mouse model, in which enforced AVEN expression induced accelerated leukemogenesis [27], high *Aven* expression is not oncogenic in the *MMTV-PyVT* model for mammary carcinoma. The lack of the expected tumorigenic effect of AVEN in this mouse model could be the result of compensating background effects. Even after extensive backcrossing to generate a genetic background that is thought to be >99% “pure”, genetic variations originating from the ES cell strain that was used to introduce the transgenes may still be present [147], [148]. Such genetic variations can have substantial effects on the phenotypes of transgenic mice, including the complete absence of a phenotype [149]. The complete absence of a phenotype, most probably as a result of background effects, was observed in a *WAP_SV40Tt Aven* knockout mouse model. These animals showed a conditional knockout of *Aven* in the mammary gland and were expressing Semian Virus 40 small and large tumor antigen in *WAP* (Whey acidic protein)-positive cells to induce mammary tumors. The latency of tumor development in these mice is reported to vary between 3 and 8 months after at least one pregnancy [181], [182]. However, the *AvenWAP_SV40Tt* mice showed no tumorigenesis at all 12 months after pregnancy, independent of the genotype of the *Aven* allele (Data not shown). As these mice had a mixed background comprised of FVB, NMRI and Bl/6, it seems likely that the absent phenotype was a consequence of genetic variance. The *Aven$^{d/d}$MMTVPyVT* mice also had a mixed FVB and Bl/6 background. Consequently, oncogenic activity of AVEN could be reduced by genetic background effects. Background effects and other compensating mechanisms in transgenic mouse models are discussed in more detail in sections **5.5** and **5.6**. The effects of continuous backcrossing on the

Aven$^{d/d}$*MMTVPyVT* and *Aven*$^{d/d}$*WAP_SV40Tt* phenotypes *would have* to be analyzed to evaluate background effects in such mouse models.

Even though knockout of *Aven* had no effect on tumor onset and progression in the described mouse models, AVEN expression could still contribute to bad outcome in breast cancers by promoting resistance to chemotherapy. Knockdown of *AVEN* in MCF-7 cells significantly increased irradiation-induced cell death (**Fig. 4.26C**). This finding is in line with reported DNA damage-induced apoptosis inhibition by AVEN in breast cancer cells [10] and increased sensitivity to chemotherapy after (indirectly) targeting AVEN in osteosarcoma cells [29]. Interestingly, cell cycle arrest by AVEN after DNA damage, as reported in [10], was not observed. Instead, AVEN expression could be inversely correlated with metabolic activity of MCF-7 cells (**Fig. 4.25, 4.27**). An integration of apoptosis and metabolism regulation has recently gained special attention, in particular in the context of cancer. Pathways of apoptosis and metabolism intersect at the level of BCL-2 family members, amongst others. Besides their long-studied role as controllers of the mitochondrial outer membrane potential, BCL-2 family members have been found to modulate metabolism by enhancing or repressing distinct metabolic pathways [183], [184]. The anti-apoptotic function of BCL-x_L has long been attributed to its ability to bind its counterparts BAX, BAK, and several BH3-only proteins, thereby preventing pro-apoptotic signaling and pore formation in the outer mitochondrial membrane. However, its anti-apoptotic function is almost completely preserved in mutants that are not able to bind the pro-apoptotic family members [185]. Remarkably, over-expression of BCL-x_L decreases levels of the metabolite Acetyl-CoA [183], [184]. Consequently, protein N-α-acetylation is reduced, as it relies on Acetyl-CoA supply. As protein N-α-acetylation is required for efficient apoptosis induction, BCL-x_L seems to inhibit apoptosis by inhibiting protein acetylation [183], [184]. At the same time, reduced acetyl-CoA levels reflect a low energy state of the cells [186] and therefore, BCL-x_L could lead to decreased proliferation rates and overall metabolic activity. As AVEN has been reported to interact with and stabilize BCL-x_L, the observed inhibition of irradiation-induced apoptosis and the deceleration of metabolic activity by AVEN could be the consequence of BCL-x_L stabilization. Furthermore, DNA damage activates protein N-α-acetylation leading to apoptosis [184]. In this context, apoptosis inhibition by AVEN after DNA damage in particular fits well to an anti-apoptotic mechanism via BCL-x_L stabilization.

Inhibition of DNA damage-induced apoptosis by AVEN could contribute to chemotherapy resistance, as it has been suggested in osteosarcoma and MCF-7 cells [10], [29]. Again, this role of AVEN correlates with BCL-x_L: increased expression of BCL-x_L confers resistance to chemotherapy [187], [188] and a negative correlation between drug sensitivity and BCL-x_L levels has been reported [189], [190]. The overlapping role of

AVEN and BCL-x_L in chemotherapy resistance, together with a demonstrated interaction of both proteins raises the question whether the anti-apoptotic action of both was dependent on each other or synergistic. In this context, it would be interesting to check whether therapy-resistant tumors show elevated expression of BCL-x_L or AVEN alone or whether the tumors co-overexpress both proteins.

Summarized, *in vivo* and *in vitro* analysis of AVEN in breast cancer demonstrated that AVEN expression was increased in murine mammary tumors but irrelevant for tumor onset and progression. However, the oncogenic potential of AVEN in breast cancer following over-expression-inducing mutations remain to be investigated. The hypothesis that AVEN contributes to chemotherapy resistance was strengthened by the finding that knockdown of *AVEN* increased irradiation-induced apoptosis in MCF-7 cells. The concomitant finding that AVEN decelerated metabolism argues for a mechanism of apoptosis inhibition via BCL-x_L stabilization. Thus, targeting AVEN in combination with DNA damage-inducing chemotherapy might represent a promising strategy in anti-cancer therapy. As AVEN expression is activated by estrogen, targeting AVEN could be of special interest for ER^+ chemotherapy-resistant breast cancers.

5.3 Activation of FUBP1 transcription by TAL1 and GATA-1 is part of an erythroid molecular switch that initiates the final steps of erythroid-specific stable gene expression

In hematopoiesis, successive steps of specification, commitment and differentiation define the route of multipotent hematopoietic stem cells (HSCs) to mature functional blood cells. Lineage differentiation is controlled by transcription factors that act both cell type- and maturation stage-dependent. The precisely regulated activation and deactivation of transcription factors finally results in a lineage-specific chromatin structure that is translated in cell type-specific gene expression.

The transcriptional regulator FUBP1 (FUSE binding protein 1) has been reported to play an important part in the complex action of transcription factors during hematopoiesis [150], [67]. FUBP1 regulates gene transcription by binding to AT-rich *FUSE* sequences in the promoter region of target genes, melting DNA double strands into single strands and interacting with the basal transcription machinery positioned near the transcription start of genes. Target genes of FUBP1 include regulators of proliferation and cell death such as *HoxA10*, *p21*, *NOXA* and *c-MYC* [150], [42]. Regulating transcription of these genes by FUBP1 is essential for the self-renewal and expansion of long term HSCs [150]. However, factors that control the expression of FUBP1, especially during hematopoiesis,

are mostly unknown. Recent studies demonstrated that FUBP1 is not only required for LT-HSC survival and proliferation but also for efficient erythropoiesis [68], [58]. Furthermore, T cell acute lymphoblastic leukemia (TAL1) was identified as a direct regulator of FUBP1 transcription that activates increased FUBP1 expression observed during erythroid differentiation of primary hCD34$^+$ stem and progenitor cells. TAL1 was suggested to bind the *FUBP1* promoter at an E-box sequence (*CAACTG*) 340 bp upstream of transcription start [58], [166] . In the presented work, I could demonstrate that *FUBP1* activation by TAL1 is highly dependent on an intact *GATA* motif adjacent to the -340 bp E-box (**Fig. 4.29**). In contrast, mutation of the -340 bp E-box sequence had no effect on *FUBP1* promoter activation. These results correlate well with studies showing that TAL1 directly binds DNA most commonly at *CAGCTG* sequences but can also regulate gene expression in absence of an intact E-box motif [168], [191]. Activation of transcription after the concomitant binding of TAL1 and GATA-1 is predominantly found at genomic DNA sites that are associated with genes that represent master regulators of erythroid differentiation (such as *KLF1*) and with genes that fulfill key functions in erythrocytes (such as *HBB*) [123], [192], [193]. Indeed, ChIP assays proved increased binding of GATA-1 to the *FUBP1* promoter during erythroid differentiation, correlating with increased recruitment of TAL1 (**Fig. 4.30**). Thus, binding of TAL1 and GATA-1 (possibly in a multiprotein complex) to the E-box/*GATA* composite motif in the *FUBP1* promoter likely induces increased FUBP1 expression during erythropoiesis, integrating FUBP1 in the group of erythroid-specific genes that are controlled by TAL1/GATA-1.

FUBP1 transcription activation by TAL1 and GATA-1 during erythroid differentiation constitutes one of the final steps in the establishment of cell type-specific gene expression. In multipotent progenitor cells, chromatin structures are opened up for gene expression activation later in differentiation as a consequence of binding of transcription factors such as RUNX1. Further transcription factors are then recruited to the marked chromatin: TAL1 and RUNX1 occupy the promoters of erythroid and megakaryocytic genes in MEPs, contributing to a bivalent chromatin status [168]. In erythroblasts, TAL1 can then be recruited to genes by association with GATA-1, inducing lineage-specific gene expression. GATA-1 expression is strongly upregulated at the moment of erythroid and megakaryocytic commitment [194]. With increasing FUBP1 expression during erythroid but not during megakaryocytic maturation, activation of FUBP1 transcription by TAL1 and GATA-1 can be viewed as part of an erythroid molecular switch. This switch initiates the final steps of erythroid-specific stable gene expression.

5.4 FUBP1 seems to act in a coordinated network with other FBP family members to fine regulate gene expression of common target genes such as *c-MYC* during erythroid differentiation

FUBP1 functions as a transcriptional regulator, and the requirement of FUBP1 for efficient erythropoiesis is based on the control of a transcriptional network that allows erythroid progenitor survival, proliferation and differentiation. To identify FUBP1 targets within this network, differential gene expression in *FUBP1* knockdown cells was analyzed. Using RNA sequencing (RNA-Seq), the whole transcriptome was analyzed. Ingenuity® pathway analysis suggested that FUBP1 controls the expression of genes that are required to sustain a sufficient number of hematopoietic progenitor and mature blood cells. This hypothesis bases on differentially expressed genes that impact the quantity of hematopoietic cells, among them CYBB, RICTOR, TCF4 and TXK (**Fig. 4.32**). However, significantly deregulated expression of these potential new FUBP1 target genes could not be confirmed in qPCR analysis. Focusing on components of the EPO receptor signaling pathway as FUBP1 candidate target genes also demonstrated only a moderate deregulation of gene expression following *FUBP1* knockdown. In addition, the effects of *FUBP1* knockdown on expression of EPOR signaling components appears cell type-dependent: while in HEL cells, NFκB components were accumulated in the down-regulated gene set, in K562 cells, several PI3K signaling components were upregulated (**Fig. 4.31**). NFκB and PI3K pathway activation are both essential to translate EPOR signaling into survival, proliferation and differentiation of erythroid precursors [170], [171]. Therefore, both, altered NFκB and altered PI3K pathway signaling could account for the observed inefficient erythroid differentiation after *FUBP1* knockdown in $hCD34^+$ cells. However, the presented mRNA expression results need to be evaluated with special caution. First, both analyzed cell types display an unphysiological signaling pathway activation as a consequence of constitutive active Bcr-Abl (in K562 cells) and JAK2-V617F (in HEL cells) kinases [195], [196]. Any observed gene expression alterations in these cell lines may therefore not be present in healthy erythroid progenitors with physiological kinase signaling. Second, FUBP1 shares a set of target genes with its family members FUBP2 and FUBP3. It has been suggested that the interplay of all three FUBPs fine-regulates common target genes to adjust gene expression to different conditions [87]. In this case, target genes that are not exclusively regulated by FUBP1 but also by FUBP2 and 3 will only be slightly modulated (and not deregulated) after knockdown of just one member of the family. The observed moderate changes in gene expression after *FUBP1* knockdown argue for such a fine-tuning of transcription regulation by FUBP1. Keeping in mind that gene expression varies extensively depending on time, cell type and stimuli, it is hard to assign the observed differential gene expression to decreased FUBP1 expression alone rather than also to

unintended other effects. Finally, increasing evidence demonstrates the profound differences between transcriptome and proteome [197], [198], [199]. Consequently, the observed differential mRNA expression is not necessary translated into differential protein expression, which would be responsible for the predicted effects. Analysis of differential protein expression remains to be performed.

Although the first described FUBP1 target gene, *c-MYC*, was not among the significantly deregulated genes according to the results of RNA-Seq, regulation of *c-MYC* transcription constitutes one pathway by which FUBP1 could support erythropoiesis. c-*myc* expression is dynamically regulated during erythropoiesis in mice. In HSCs, *c-myc* is expressed at relatively low levels but is essential for inhibiting self-renewal and concomitantly inducing differentiation [200]. With ongoing differentiation, c-MYC protein levels increase, allowing the expansion of erythroid progenitors and inhibiting early maturation [201]. At the end of erythropoiesis, a down-regulation is essential for the final maturation of red blood cells [126]. A corresponding up- and downregulation of *c-MYC* transcription was observed during the erythroid differentiation of primary hCD34$^+$ cells and correlated with *FUBP1* expression [58]. “The FBP level generally parallels c-*myc* expression; both are associated with proliferative states and are down-regulated upon differentiation” was already stated in [87]. For erythroid differentiation, this hypothesis could be confirmed but downregulation appeared to be restricted to final maturation.

The pivotal role of c-MYC in erythropoiesis was emphasized when c-MYC was identified as one of the minimal factors required for direct lineage conversion to erythroid cells together with TAL1, GATA-1 and LMO2 [127]. This function of c-MYC in lineage reprogramming suggests a role of c-MYC in erythropoiesis in addition to and different from proliferation control. Indeed, the direct regulation of genes essential for erythrocyte function (such as proteins required for heme biosynthesis) by c-MYC could be demonstrated [202]. Interestingly, *c-MYC* mRNA expression is regulated by FUBP1 and GATA-1, with opposing effects: while FUBP1 activates *c-MYC* expression, GATA-1 represses *c-MYC* transcription [32], [203]. The same was observed for transcriptional regulation of FUBP1 and GATA-1 target genes *cyclin D2* and *c*-KIT [44], [203], [204], [205]. Inhibition of proliferation as a consequence of downregulation of these three genes by GATA-1 could be counteracted by FUBP1 during early erythroid maturation. This would allow the essential expansion of pro-erythroblasts. However, erythroblasts stop cycling before they enucleate, which is critical for final maturation. Proliferation inhibition results from c-MYC, CCND2 and c-KIT downregulation, possibly mediated by GATA-1. This repression by GATA-1 could be enabled by a concomitant down-regulation of FUBP1, which was observed at the end of erythroid differentiation [58]. The underlying mechanisms of reduced *FUBP1* expression at this developmental stage remain to be elucidated.

5.5 Embryonic lethality in conditional *Fubp1* knockout mice might depend on the genetic background of the animals

Embryonic lethality as a consequence of a constitutive *Fubp1* knockout has been demonstrated in three different mouse models so far. Insertion of a gene trap in *Fubp1* intron 18 produced a fusion protein, consisting of functionally inactive FUBP1 amino acids 1 to 589, β-Galactosidase and Neomycin Phosphotransferase. Homozygous inactivation of *Fubp1* in this model led to embryonic lethality around embryonic day 15.5 [43]. Death *in utero* at the same developmental stage was observed in a second gene trap mouse model. In this model, the gene trap was inserted in the first *Fubp1* intron, causing a complete abrogation of *Fubp1* expression [43]. In a third mouse model, floxed *Fubp1* exons 8 to 13 were deleted by CRE-mediated recombination. These exons encode the nucleic acid binding domain of *Fubp1* and their removal resulted in the complete loss of FUBP1 protein. These mutant mice died between embryonic day 10.5 and birth [67]. Both, the constitutive knockout of *Fubp1* in *Fubp1LacZ* mice, and in conditional *Fubp1* knockout first mice after FLP- and CRE-mediated recombination, which were presented in this work, were embryonic lethal (**Fig. 4.34**). The time point of embryonic death in the latter one laid before 10.5 dpc and in contrast to the model described in [67], no living embryos are found at later stages. The later incidence of embryonic lethality in the first gene trap mouse model could be referred to residual activity of the FUBP1 fusion protein. However, this explanation is not valid for the second gene trap model, for which complete loss of FUBP1 expression was demonstrated [43]. Apparently, genetic background effects are more likely to account for the inconsistent survival of the *Fubp1* knockout embryos. While the gene trap mice consisted of a mixed TBV-2/BL/6J background [43], the “Zhou model” had a mixed 129/BL/6 background [67], and the conditional knockout first models comprise a mixed C57BL/6N-A^{tm1Brd}/BL/6J background. Residual genetic material from the ES cells used to introduce the modified locus can be spread throughout the BL/6 genome which was used for backcrossing. Such mixed backgrounds can be responsible for variations in the phenotypes observed in genetically modified mouse models [147], [148].

Introduction of *loxP* sites flanking *Fubp1* exons 8 to 13 already caused embryonic lethality, and Zhou et al. [67] concluded that at least one of the *loxP* sites interfered with *Fubp1* expression. Mice with *loxP* sites flanking *Fubp1* exons 4 to 7 that were generated by the conditional knockout first model described in this thesis also died *in utero*, but the penetrance of this phenotype was clearly dependent on the genetic background (**Fig. 4.35**). While in *Fubp1*$^{d/d}$*AlbCre*$^{-}$ mice, embryonic lethality showed a penetrance of 100%,

in *Fubp1*$^{d/d}$*ErGFPCre*$^{-}$ animals, the penetrance was 83% and in *Fubp1*$^{d/d}$*VavCre*$^{-}$ mice, there was no embryonic lethality observed at all (**Fig. 4.35**). In living homozygous offspring with floxed *Fubp1* exons, *Fubp1* expression was not reduced compared to mice with wildtype *Fubp1* alleles (data not shown). Consequently, not the modification of the *Fubp1* locus *per se*, but rather genetic background effects again seem to be responsible for the phenotype observed. The targeting vector with the altered *Fubp1* locus was introduced in ES cells that were derived from the *BL/6N-A*^{tm1Brd} strain, and the *BL6/J* strain was used for backcrossing. By using ES cells of a *BL/6* strain, background effects are reduced compared to commonly used ES cells from the *129* strain that genetically differs significantly from the *BL/6* strain. However, a comparative analysis of *BL/6N* and *BL/6J* inbred mice has revealed a range of genetic differences between these strains that have the potential to influence the phenotypic outcome of genetic modifications: 34 SNPs, 2 small indels and 15 structural variants were identified within coding regions, leading to phenotypic differences in morphology, metabolism and hematology, amongst others [206]. At least 10 generations of backcrossing are required to generate a 99.9% pure congenic *BL/6* background and even then, ES cell background loci may still be found in the genome. The flanking regions of the targeted locus in particular are not likely to be exchanged by *BL/6* DNA without losing the knockout [147], [148]. Considering the fact that the analyzed conditional strains were backcrossed for six generation at maximum, there is a fair chance of background-dependent effects to appear. Especially, as conditional knockout mice were not bred with wildtype *BL/6* mice but with deleter strains which might contain genetic material of yet another origin. A closer look at the offspring statistics of the *Fubp1*$^{d/d}$*ErGFPCre*$^{+}$ mice confirmed the theory that background effects cause embryonic lethality: mating *Fubp1*$^{+/d}$ with *Fubp1*$^{+/d}$*ErGFPCre*$^{+}$ mice resulted in drastically reduced numbers of living *Fubp1*$^{d/d}$*ErGFPCre*$^{+}$ offspring. When this offspring was intercrossed, the number of *Fubp1*$^{d/d}$*ErGFPCre*$^{+}$ offspring met the Mendelian distribution (however, this observation needs to be verified, as only 30 mice of the second generation were analyzed). Obviously, the genetic trait causing embryonic lethality could be eliminated without affecting the *Fubp1* knockout. Genome sequencing of the three different conditional knockout mouse strains could identify genetic variants, in coding regions in particular, that correlate with the difference of embryonic lethality. Identification of such variants in the genetic background that cause embryonic death would be of high interest; they should be excluded to be phenotype-relevant in the previously described *Fubp1* mouse models as well as other knockout mouse models.

5.6 Multiple compensatory mechanisms can be responsible for different phenotypes in *Fubp1* knockout mouse models

The knockout of *Fubp1* in the *Vav* expressing compartment, including the hematopoietic system, showed no influence on the frequency of HSCs and progenitors (**Fig. 4.36**). Lineage differentiation seemed also unaffected (**Fig. 4.37**). For the process of erythropoiesis, this conclusion was consolidated in another conditional *Fubp1* knockout mouse model with deficient FUBP1 expression only in EPO receptor-expressing cells (**Fig 4.40**). The absence of a phenotype in these mouse models is in sharp contrast to the reported essential role of FUBP1 in LT-HSC function and erythroid differentiation [150], [68], [58]. Absence of an expected phenotype could be the consequence of incomplete protein deletion – this scenario could be excluded for the *Fubp1*$^{d/d}$*VavCre*$^{+}$ model, in which a complete loss of FUBP1 expression in the bone marrow, spleen and thymus was demonstrated (**Fig. 4.36B**). Another possible explanation for an absent phenotype could be the existence of compensating mechanisms. Compensation can result from different molecular reasons, which can be classified into three categories [149]:

1) Compensation can be the direct consequence of the functional inactivation of the knockout gene, e.g., the loss of a feedback inhibition of a compensating gene induces expression of the selfsame compensating gene.
2) Overexpression of a deleted gene does not always restore normal expression of compensating genes. Furthermore, phenotypic differences between gene knockouts and gene knockdowns have been reported, drawing attention to the possibility that not the non-functional protein, but DNA lesions and mutant mRNAs induce compensating gene expression. This kind of compensation is also referred to as transcriptional adaption [149].
3) Compensation can occur independently of both altered gene function and coding DNA integrity, induced either by environmental factors or genetic background effects.

How the three compensation categories might explain the absence of a phenotype in the analyzed conditional *Fubp1* knockout mouse models is described in the following.

5.6.1 Compensation induced by loss of gene function

Redundancy of protein function allows for the compensation of dysfunction of single proteins. This way, organisms can sustain viability and ensure normal development in case of gene perturbations arising during the process of evolution. Overlapping protein function is often found within the members of one protein family, resulting from the same ancestry and conserved structure elements [207]. The FBP family is indicative for such

overlapping function: all three members (FUBP1-3) are involved not only in transcriptional regulation but also in the control of RNA stability, splicing and translation, and they share common targets [87], [42]. Thus, a compensation for an *Fubp1* knockout by *Fubp2* and/or *Fubp3* upregulation seems likely. FUBP2 expression was unchanged in two different *Fubp1* knockout mouse models [67], [43]. However, recent research demonstrated that the knockdown of *Fubp2* in *Fubp1* knockout MEFs was lethal, while the knockdown of *Fubp2* in wildtype MEFs increased *Fubp1* expression [208]. This finding strongly suggests that FUBP1 and FUBP2 can, at least in part, compensate the loss of each other. FUBP3 could also buffer deficient FUBP1 activity, although the missing inhibition of FUBP3 by FIR and its considerable cytoplasmic localization limit its potential to fully substitute the loss of FUBP1 [87]. *Fubp3* expression in *Fubp1* knockout mice remains to be analyzed. Furthermore, consequences of concomitant *Fubp1* and *Fubp3* or *Fubp2* and *Fubp3* deficiencies should be analyzed to shed more light onto the coordinated expression and action of these proteins.

Besides FUBP family members, other proteins could compensate the loss of FUBP1. FUBP1 has the potential to inhibit the transcription of target genes. One or more (yet unknown) target genes inhibited by FUBP1 could take over missing FUBP1 function and their expression would be up-regulated in the absence of FUBP1. If insufficient FUBP1 expression or function induced the expression of compensating genes, the question remains to be answered why this mechanism could not rescue HSC function in the constitutive knockout mouse models. Again, background effects could be responsible for the differences in the mouse models. Possible genetic variants affecting FUBP family expression and regulation need to be further investigated.

5.6.2 Compensation by transcriptional adaption

Knockdown of *Fubp1* in sorted murine LT-HSCs significantly reduced cell cycling and increased cell death rates. This effect on LT-HSCs complemented the phenotype observed in *Fubp1* gene trap mouse models [150] but could not be observed in the Zhou model [67] and the presented conditional knockout mouse models. Similarly, the knockdown of *Fubp1* in primary human $CD34^+$ cells interfered with efficient erythroid maturation [58], another effect that was not present in the conditional knockout mice. Such discrepancy between gene knockout and knockdown has been described for a range of genes in different organisms. Compensatory gene expression that is activated by deletion mutations rather than loss of gene function was first demonstrated by Rossi et al, 2015. Similar cases of transcriptional adaption and potential underlying mechanisms have been reviewed in detail [149]. In short, the described underlying mechanisms can be discriminated into processes that depend on the decay of the mutant mRNA, processes that depend on a temporarily stable mutant mRNA and processes that

are mutant mRNA independent:

Lesions within DNA can cause chromatin remodeling, DNA looping or altered nuclear organization, all leading to the activation of compensatory genes at regulatory regions, enabling their transcription. Alternatively, deletion of genomic DNA sections can induce DNA damage responses leading to changes in interchromosomal interactions. Furthermore, exon deletion can generate the expression of a new transcription modulating non-coding RNA, again upregulating compensatory gene expression. These mechanisms are mutant mRNA independent. If a temporarily stable mutant mRNA is built, it can guide transcription factors to the regulatory region of compensatory genes itself or interact with the RNAi-machinery to do so. If the mutant mRNA is readily degraded, otherwise bound RNA binding proteins (RBPs) and miRNAs are free to stabilize the mRNA of compensatory genes. MiRNAs and RBPs often regulate genes of one family (because of sequence homology), so called RNA regulons or operons. Thus, stabilization of the mRNA of *Fubp2* or *Fubp3* could be of relevance for compensation in the conditional knockout mouse models.

Transcriptional adaption represents a sufficient explanation for differences between *Fubp1* knockdown and knockout phenotypes. Expression of mutant *Fubp1* mRNA in the conditional knockout mouse models as well as in the Zhou mouse model should be tested to identify the potential underlying mechanism.

Comparison of the potentially expressed mutant mRNAs in the four existing *Fubp1* mouse models, shown in **Fig. 5.1**, already helps to confine the type of underlying mechanism. In the two gene trap models, stable mutant mRNA expression could be demonstrated. In one of them, *Fubp1* mutant mRNA comprises of exons 1 to 18, followed by β-Galactosidase, in the other one, mutant mRNA only consists of *Fubp1* exon 1 followed by β-Galactosidase, while all other *Fubp1* exons are lost. In the Zhou mouse model, the presence and character of a mutant mRNA has not been tested. If a mutant mRNA was stably expressed, it lacked *Fubp1* exons 8 to 13. In the here presented conditional knockout models, a potentially expressed *Fubp1* mRNA lacked *Fubp1* exons 4 to 7. Thus, mutant mRNAs of all four mouse models have in common that they contain *Fubp1* exon 1. Apart from that, they differ critically. Consequently, redundant RBPs or miRNAs, in case of degraded mutant mRNA in the conditional knockout mouse model, could only be the source of compensation if they bound within *Fubp1* exon 1, the only exon still present in the second gene trap model. It seems to be more likely that the specific mutant mRNAs resulting from deletion of exons 4 to 7 compensate for the loss of *Fubp1*, as this exact deletion is only present in the conditional knockout model.

Concluding, multiple compensatory mechanisms of transcriptional adaption can sufficiently explain the difference in phenotypes of the four *Fubp1* knockout mouse models, even without the presence of further background effects.

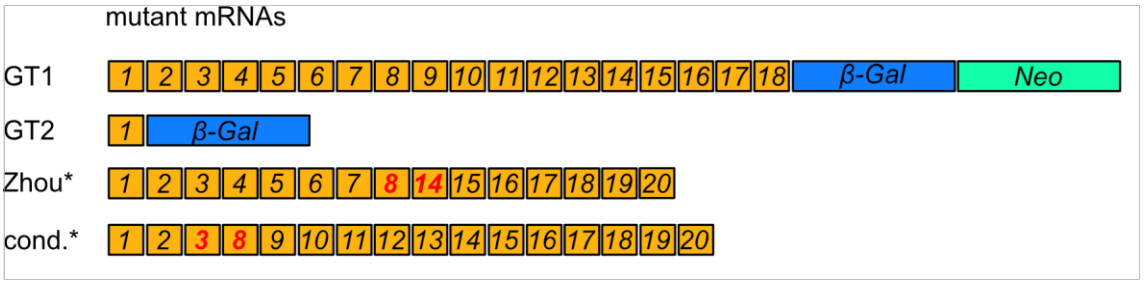

Figure 5.1: Mutant *Fubp1* mRNA in four genetically different mouse models
Schematic representation of the mutant *Fubp1* mRNAs resulting from different mutations in four genetic mouse models. GT1: gene trap mouse models. GT2: gene trap mouse model. Zhou: Germline deletion of *Fubp1* exons 9 to 13, the model was described by Zhou 2016. Cond: conditional germline deletion of *Fubp1* exons 4 to 7, the model is described in the presented thesis. The asterisks indicate that evidence for the presence of the mutant mRNA has not yet been provided. Exon transitions that arise from germline deletions are highlighted in red.

5.6.3 Compensating background effects

As already discussed in section **5.5**, all four *Fubp1* knockout mouse models that have been described so far are kept in different genetic backgrounds. A genetic variant present in the *BL/6N-A*^{tm1Brd} strain could lead to compensating gene expression, rescuing the effect of FUBP1 deficiency only in the conditional knockout mouse model but not in the other mouse models. Candidate genes that should be tested first for sequence variants in their exons or regulatory regions are FUBP family members as well as known FUBP1 target genes.

In summary, conditional *Fubp1* knockout mice that lack FUBP1 either in the whole hematopoietic system or only in erythroid cells do not show reduced numbers of HSCs, mature erythrocytes or B cells, in contrast results obtained in constitutive *Fubp1* knockout models and knockdown experiments. The different phenotypes may be the result of various compensatory mechanisms, including background effects and transcriptional adaption. Backcrossing to generate a pure congenic background is required to discriminate between phenotypes caused by missing FUBP1 function or genetic background effects. Rescue experiments, mutant mRNA characterization and detection of differential gene expression in conditional knockout mice can help to identify the exact compensating mechanisms that obscure phenotypes in conditional *Fubp1* knockout mice. Analyzing the consequences of FUBP1 inhibition on the protein level for LT-HSC function and erythropoiesis after treatment with the potential FUBP1 inhibitor Irinotecan [209] would also help to clarify the role of FUBP1 in these cells. Furthermore, functional assays need to be performed, to test the capacity/potential of *Fubp1*$^{d/d}$*VavCre*$^{+}$ LT-HSCs. HSC function could for example be evaluated in competitive transplantation experiments.

Analysis of lineage differentiation in conditional *Fubp1* knockout mice suggests that, besides erythropoiesis and B-cell differentiation, FUBP1 could play a role in the maturation of T helper cells (**Fig. 4.39**). Assays challenging the immune system need to be performed to test the consequences of significantly reduced T helper cells and potential functional deficiencies of T cells in conditional *Fubp1* knockout mice.

5.7 Conclusions about FUBP1 function during development and tumorigenesis

Substantial variance in both *Fubp1* knockout phenotypes and differential gene expression after *Fubp1* knockdown argues for a role of FUBP1 in "stabilizing" gene expression. Depending on factors like environment, genetic background or the metabolic/proliferative state of a cell, FUBP1 deficiency will result in different outcomes. In other words, depending on context, a cell will rely more or less on gene expression stabilization by FUBP1. The coverage of effective compensation, no matter if it is adoption of FUBP1 function by FUBP2 or 3 or other mechanisms, would then also depend on the state of the cell. Cell states that are characterized by dramatic changes in gene expression are states associated with cell fait decisions, as they happen at developmental checkpoints during embryogenesis [210] and also during adult hematopoiesis [92]. Consistently, *Fubp1* knockdown and knockout phenotypes (embryonic lethality and impaired hematopoiesis) are associated with exactly these cell states.

Of note, extensive changes in gene expression are not only associated with physiological conditions during development, but also with diseases, including cancer. In transformed cells, mutations of one or more genes activate dramatic changes in gene expression leading to enhanced proliferation and survival but decreased differentiation [211], [24]. Interestingly, overexpression of FUBP1 has been demonstrated in HCC [44], colorectal cancer [79] and prostate and bladder cancer [84], supporting the theory that cancer cells could rely to some extent on FUBP1 to cope with aberrant transcriptional regulation. Overexpression of FUBP1 in these cancers entities could also help the cells to escape therapy-induced apoptosis – in this case, FUBP1 could constrain up- and downregulation of gene expression which was activated by pro-apoptotic therapy-induced signaling. Thus, targeting FUBP1 in anti-cancer therapy appears promising not only because of direct effects on cancer cells, but also for synergistic effects with other agents. A combined treatment with the potential FUBP1 inhibitor Irinotecan and the standard chemotherapeutic agent MMC already proved an enhanced anti-tumor effect compared to single treatment in mouse xenograft models [46], [209] and provided promising results

in patients in an investigator-driven study [46]. Current research focuses on the development of a specific FUBP1 inhibitor. Analysis of its action alone and in combination with other chemotherapeutics will shed light on the potential of FUBP1 as an anti-cancer target.

Finally, FUBP1 function is not only able to support cancer cells in dealing with considerably changed gene expression but could also induce transformation of cells in case of loss-of-function. In oligodendroglioma, FUBP1 mutations have been reported, resulting in non-functional FUBP1 [80]. In this scenario, the resulting unsteady and labile gene expression of FUBP1 targets likely drives tumorigenesis.

6 Material

6.1 Cell Culture

***Table 6.1**: Cell lines*

Cell line	Description	Medium	Source
HEL	Human erythroleukemia cell line established from the peripheral blood of a 30-year-old man with erythroleukemia (AML M6) in relapse (after treatment for Hodgkin lymphoma)	RPMI 1640 10% FBS 4 mM L-Glutamine 100 U/ml Penicillin 100 µg/ml Streptomycin	B. Groner *Georg-Speyer-Haus*, Frankfurt DSMZ ACC 11
HEK293T	Human epithelial kidney cells derived from the HEK-293 cell line, which was transformed with the SV40 "large T"-antigen	DMEM 10% FBS 20 mM HEPES 4 mM L-Glutamine 100 U/ml Penicillin 100 µg/ml Streptomycin	M. Grez *Georg-Speyer-Haus*, Frankfurt DSMZ ACC 305
K562	Human leukemia cell line established from pleural effusion of a Caucasian 53 year old female with chronic myelogenous leukemia in terminal blast crisis	RPMI 1640 10% FBS 4 mM L-Glutamine 100 U/ml Penicillin 100 µg/ml Streptomycin	D. Krause *Georg-Speyer-Haus*, Frankfurt ATCC CCL 243
MCF-7	Human breast adenocarcinoma cell line, derived from pleural effusion	RPMI 1640 10% FBS 4 mM L-Glutamine 100 U/ml Penicillin 100 µg/ml Streptomycin	M. Zörnig *Georg-Speyer-Haus*, Frankfurt ATCC HTB-22
MDA-MB 453	Human breast carcinoma cell line, derived from pericardial effusion	DMEM 10% FCS 4 mM L-Glutamine 100 U/ml Penicillin 100 µg/ml Streptomycin	K. Strebhardt *University Hospital Frankfurt* ATCC HTB 131

***Table 6.2** Cell culture media and supplements*

Name	Description	Manufacturer
Dexamethasone	Dexamethasone – water soluble	*Sigma-Aldrich Chemie GmbH*, Steinheim
DMEM	Dulbecco's Modified Eagle Medium, 4.5 g/l glucose	*GIBCO*, Eggenstein
DMSO	Dimethyl sulfoxide, highly purified	*Merck*, Darmstadt

DPBS	Dulbecco's phosphate buffered saline	*GIBCO*, Eggenstein
E2	17-β-Estradiol	*Sigma-Aldrich Chemie GmbH*, Steinheim
EPO	Human erythropoietin	*Roche*, Mannheim
FBS	Fetal Bovine Serum	*PAA Laboratories*, Pasching
FLT3-L	Fms-related tyrosine kinase 3 ligand, 100 ng/µl aqueous solution with 0.1% BSA	*Miltenyi Biotec GmbH*, Bergisch Gladbach
IL-3	Interleukin-3, 100 ng/µl aqueous solution with 0.1% BSA	*Miltenyi Biotec GmbH*, Bergisch Gladbach
IL-6	Interleukin-3, 100 ngµ/l aqueous solution with 0.1% BSA	*Miltenyi Biotec GmbH*, Bergisch Gladbach
L-Glutamine	200 mM solution	*GIBCO*, Eggenstein
Pen/strep	10,000 U/ml penicillin, 10,000 µg/ml streptomycin	*GIBCO*, Eggenstein
RPMI 1640	Roswell Park Memorial Institute	*GIBCO*, Eggenstein
SCF	Stem Cell Factor, 100 ng/µl aqueous solution with 0.1% BSA	*Miltenyi Biotec GmbH*, Bergisch Gladbach
StemSpan™ SFEM	Serum free medium for culture and expansion of hematopoietic cells	*Stemcell Technologies*, Köln
StemSpan™ SFEM II	Serum free medium for culture, expansion and differentiation of hematopoietic cells	*Stemcell Technologies*, Köln
Trypsin-EDTA	0.05% Trypsin-EDTA	*GIBCO*, Eggenstein

6.2 Bacterial Culture

***Table 6.3**: Bacteria, bacterial growth media and antibiotics*

Name	Specification
DH5α	supE44 lacU169 (80lacZM15) hsdR17 recA1 endA1 gyrA96 thi-1 relA1
LB medium	1% (w/v) bacto-trypton 0.5% (w/v) yeast extract 172 mM NaCl pH 7.5
LB agar plates	LB medium 1% (w/v) bacto-agar
Ampicillin stock solution	50 mg/ml, *AppliChem GmbH*, Darmstadt
Spectinomycin D stock solution	10 mg/ml, *Sigma-Aldrich Chemie GmbH*, Steinheim

6.3 Plasmids

***Table 6.4**: Lentiviral plasmids*

Plasmid	Description	Source
p8.91	encapsidation plasmid for the production of lentiviral particles	M. Grez *Georg-Speyer-Haus,* Frankfurt
pGIPZ	Lentiviral backbone for the expression of shRNAs ampicillin- and puromycin-resistance *CMV* promoter	*Open Biosystems,* Huntsville
pGIPZ ctrl	*pGIPZ* backbone expression of non-targeting control shRNA (ATCTCGCTTGGGCGAGAGTAAG)	AG Zörnig *Georg-Speyer-Haus,* Frankfurt
pGIPZ shAven 1	*pGIPZ* backbone expression of shRNA 1 (position hg38 chr15:33867586-33867605, AACTAGATCTGTTGCTTAA) directed against *AVEN* mRNA	AG Zörnig *Georg-Speyer-Haus,* Frankfurt
pGIPZ shAven 5	*pGIPZ* backbone expression of shRNA 5 (position hg38 chr15:34003181-34003200, CGGTTGAAGATGACAGCGA) directed against *AVEN* mRNA	AG Zörnig *Georg-Speyer-Haus,* Frankfurt
pLeGO iG2	Lentiviral vector for the overexpression of mammalian genes *SFFV* promoter *IRES eGFP* expression	*Addgene* Cambridge, MA USA
pLeGO iG2 hAven	*pLeGO iG2* backbone expression of *hAVEN* cDNA	AG Zörnig *Georg-Speyer-Haus,* Frankfurt
pLKO.1 puro	Lentiviral backbone for the expression of shRNAs ampicillin- and puromycin resistance	*Sigma-Aldrich Chemie GmbH*, Steinheim
pLKO.1 puro ctrl	*pLKO.1 puro* backbone expression of non-targeting control shRNA (CAACAAGATGAAGAGCACCAA)	AG Zörnig *Georg-Speyer-Haus,* Frankfurt
pLKO.1 puro shAven 5	*pLKO.1* puro backbone expression of shRNA 5 (position hg38 chr15:34003153-34003173) GAGAATGATGAACAGGGAAAT) directed against *AVEN* mRNA	AG Zörnig *Georg-Speyer-Haus,* Frankfurt
pMD2.G	VSV-G envelope proteins expressing plasmid for the production of lentiviral particles	M. Grez *Georg-Speyer-Haus,* Frankfurt
pSIEW	Lentiviral vector for the expression of shRNAs *SFFV* promoter	M. Grez *Georg-Speyer-Haus,* Frankfurt

	GFP expression	
pSIEW ctrl	*pSIEW* backbone Expression of scrambled shRNA (TAACGACGCGACGACGTAA)	Uta Rabenhorst et al., (2009)
pSIEW shFUBP1 4	*pSIEW* backbone Expression of shRNA 4 against *hFUBP1* (position hg38 chr1:77964877-77964897, GATTACAGGAGACCCATATAA)	cloned during this thesis
pSuper	Lentiviral vector for the expression of shRNA under the control of the *H1* promoter	*Oligoengine* Seattle, WA USA

***Table 6.5**: Expression plasmids for transfection*

Plasmid	Description	Source
pcDNA 3.1	mammalian expression system ampicillin- and neomycin-resistance *CMV* promoter	*Invitrogen GmbH*, Darmstadt
pcDNA E47	*pcDNA 3.1* backbone expression of human *E47*	J. Lausen *DRK Blood Donation Service*, Frankfurt
pcDNA TAL1-HA	*pcDNA 3.1* backbone expression of HA-tagged human *TAL1*	J. Lausen *DRK Blood Donation Service*, Frankfurt
pCMV β-Gal	Expression vector encoding *β-Galactosidase* under the control of the *CMV* promoter	AG Zörnig *Georg-Speyer-Haus,* Frankfurt
pGL4.10	Vector encoding the luciferase reporter gene *luc2* with no promoter	J. Lausen *DRK Blood Donation Service*, Frankfurt
pGL4.10 0.5 kb FUBP1	Expression of *luc2* under the control of a fragment of the h*FUBP1* promoter (0.5kb upstream of the *FUBP1* transcription start)	AG Zörnig *Georg-Speyer-Haus,* Frankfurt
pGL4.10 0.5 kb FUBP1 E-box M1	*pGL4.10 0.5 kb FUBP1* with a point mutation within the E-box 340 bp upstream of transcription start	Jasmin Yillah AG Lausen *DRK Blood Donation Service*, Frankfurt
pGL4.10 0.5 kb FUBP1 E-box M2	*pGL4.10 0.5 kb FUBP1* with a point mutation within the E-box 340 bp upstream of transcription start	Jasmin Yillah AG Lausen *DRK Blood Donation Service*, Frankfurt
pGL4.10 0.5 kb FUBP1 GATA M1	*pGL4.10 0.5 kb FUBP1* with a point mutation within the *GATA* site 329 bp upstream of transcription start	Generated during this thesis

pGL4.10 0.5 kb FUBP1 GATA M2	*pGL4.10 0.5 kb FUBP1* with a point mutation within the *GATA* site 329 bp upstream of transcription start	Generated during this thesis

***Table 6.6**: Conditional Knockout First Vector for the generation of Knockout mice*

Plasmid	Description	Source
PG00228.z.8.H08 Fubp1	*Conditional knockout first* vector targeting the *Fubp1* locus	*International Mouse Phenotyping Consortium (IMPC)*, via *Helmholtz Zentrum*, Munich

6.4 Enzymes

***Table 6.7**: Restriction Enzymes*

Enzyme	Concentration	Manufacturer
BglII	20,000 U/ml	*New England Biolabs GmbH*, Frankfurt
Biozym Red HS Taq Master Mix	100 rxn/20µl	*Biozym*, Oldendorf
EcoNI	20,000 U/ml	*New England Biolabs GmbH*, Frankfurt
EcoRI-HF	20,000 U/ml	*New England Biolabs GmbH*, Frankfurt
HincII	20,000 U/ml	*New England Biolabs GmbH*, Frankfurt
HindIII-HF	20,000 U/ml	*New England Biolabs GmbH*, Frankfurt
NdeI	20,000 U/ml	*New England Biolabs GmbH*, Frankfurt
PacI	20,000 U/ml	*New England Biolabs GmbH*, Frankfurt
Rnase A	100 mg/ml	*Roche*, Mannheim
SacI-HF	20,000 U/ml	*New England Biolabs GmbH*, Frankfurt
SmaI	20,000 U/ml	*New England Biolabs GmbH*, Frankfurt
SnaBI	20,000 U/ml	*New England Biolabs GmbH*, Frankfurt

***Table 6.8**: Other Enzymes*

Enzyme	Concentration	Manufacturer
Antarctic Phosphatase	5,000 U/ml	*New England Biolabs GmbH*, Frankfurt
T4 ligase	1 Weiss U/µl	*Fermentas GmbH*, St. Leon-Rot
T4 PNK	10 U/µl	*Thermo Fisher Scientific*, Bonn

6.5 Oligonucleotides

***Table 6.9**: Oligonucleotides for gene expression analysis*

Primer	Sequence from 5´ to 3´
hAFP for	CAGCTTGGTGGTGGATGAAA
hAFP rev	GAGCTTGGCACAGATCCTTATG
hCD235a for	CCCTCCAGAAGAGGAAACCGGAGA
hCD235a rev	GGCACGTCTGTGTCAGGTGAGG
hCD71 for	AGGACGCGCTAGTGTTCTTC
hCD71 rev	CCAGGCTGAACCGGGTATATG
hCDK18 for	AACCTGAAGCACGCCAATA
hCDK18 rev	GTCACTGTCCAGGTACTCAAAC
hCYBB for	CAGTAGCACTCTCTGAACTTGG
hCYBB rev	GCCTCCTTCAGGGTTCTTTATT
hEIF4A1 for	GTTCTGGCTCTAGCAGAGTTT
hEIF4A1 rev	GTTGGTGGGAAGGTCATAGTT
hER1 for	CCTGATGATTGGTCTCGTCTG
hER1 rev	AATGTGTAGAGGGCATGGTG
hFUBP1 for	ACTCCAATGGGACCATACAACCCT
hFUBP1 rev	CAGCCCAAGCTGCTGAATTTGGAT
hGAPDH for	TCTTTTGCGTCGCCAGCCGAGC
hGAPDH rev	TGACCAGGCGCCCAATACGACC
hHEPACAM2 for	TTCCAGCCTCTGATTGTGTATC
hHEPACAM2 rev	AAGTTCACTCTGGATGGTCTTG
hHID for	ATCCATCGTGAGGAGGACTT
hHID rev	CTGGTGGAACTGGATCTTCTTG
hHPRT1 for	CCTAAGATGAGCGCAAGTTGAA
hHPRT1 rev	CCACAGGACTAGAACACCTGCTAA
hINO80D for	GTGAACAGTGCGCTAACAAAG
hINO80D rev	CTGCTGAGAGTGGTTCAAGAG
hITGAV for	CTCGGACTGCACAAGCTATT
hITGAV rev	CTGCTCTTGGAACTCCTGAAA
hp21 for	TGGAGACTCTCAGGGTCGAAA
hp21 rev	CCGGCGTTTGGAGTGGTA
hREN for	TCCGTGATCCTCACCAACTA
hREN rev	GGACGAACCAGTGTCAAAGA
hRICTOR for	CTGTTGTGACTGAGGAGTTCATAG
hRICTOR rev	CTGGCACGATGAGGAAGAATAG
hSLCO2B1 for	TCTACCTCGGGATCCTGTTT

hSLCO2B1 rev	ACCTTCTGGCATCTGGTTAATG
hSOX5 for	GCTGTATCTCCTACCAGCATTC
hSOX5 rev	CCATCAGAGGTCTTGGGTTTAG
hTCF4 for	CACTTTCCCTAGCTCCTTCTTC
hTCF4 rev	TGCCCAACATTCCTGCATAG
mAven Exon 1 for	GGCGCTGGCGAGAGGAG
mAven Exon 1 rev	CGGCCTCCAGGCTCCCA
mAven Exon 3/4 for	CTGAGGAGAAAGAATGGGATGG
mAven Exon 3/4 rev	ATTAAGCCGGACTGCAAGAG
mAven Exon 5/6 for	GAAGGCAATATCTCTCCAGACC
mAven Exon 5/6 rev	CTGCTCAGGTTCCACATTCT
mFubp1 Exon 1 for	CCGCCATCTTCTTCCTTTCT
mFubp1 Exon 1 rev	TGTGGAGTAGTCGGCCATA
mFubp1 Exon 12/13 for	CTGGTGTTCGCATTCAGTTTAAG
mFubp1 Exon 12/13 rev	GGTCTGGAGGTCCTGTTATTTG
mFubp1 Exon 14/15 for	GGCACTCCACAGCAAATAGA
mFubp1 Exon 14/15 rev	CAGGTGGCCCTAAAGGATTT
mFubp1 Exon 19/20 for	GGCTGCTTATTACGCTCACTAT
mFubp1 Exon 19/20 rev	CTGCTGATCTCCTTGTCCATTAG
mFubp1 Exon 2-4 for	AGACCCTTAGAAGATGGAGATCA
mFubp1 Exon 2-4 rev	CTGCTGATGCATTGGAGGTA
mFubp1 Exon 3-5 for	GACAAGTCCGAGCAGTACAA
mFubp1 Exon 3-5 rev	ATCGGTGGTAACTGTGTTCC
mFubp1 Exon 3-8 for	AGCCAGATGCTAAGAAAGTACC
mFubp1 Exon 3-8 rev	GTGAACAGATCTCACGCATACA
mFubp1 Exon 5-7 for	CAGATGGGATGGTCGGATTTA
mFubp1 Exon 5-7 rev	CCACCACTATCAGGTGCTATC
mFubp1 Exon 9/10 for	CGGGAAATGCAGTTCAAGAAATC
mFubp1 Exon 9/10 rev	CCCGTTCCTGAAGCTGTTTAATA

***Table 6.10**: Oligonucleotides for sequencing*

Primer	Sequencing of	Sequence from 5´ to 3´
pGL-RV3 for	*pGL4.10* constructs	CTAGCAAAATAGGCTGTCCC
pGL-RV4 rev	*pGL4.10* constructs	GACGATAGTCATGCCCCG
T7	*pcDNA 3.1* and *pSuper* constructs	TAATACGACTCACTATAGGG
WPRE down	*pSIEW* constructs	ACGAGTCGGATCTCCCTTTGGGC
3´arm/pUC for	*Fubp1* targeting vector	GAAATGGAAGAGTAGTTGGACTTTG
3´arm/pUC rev	*Fubp1* targeting vector	GTGGGCTCTATGGCTTCTG

FRT1 for	*Fubp1* targeting vector	TGTGTGCCTTGCCATACTC
FRT1 rev	*Fubp1* targeting vector	ACAACGGGTTCTTCTGTTAGTC
FRT2/loxP2 for	*Fubp1* targeting vector	GGATCTCATGCTGGAGTTCTTC
FRT2/loxP2 rev	*Fubp1* targeting vector	CTAGACATTTGCCGCCTACT
LacZ PA for	*Fubp1* targeting vector	CGACTTCCAGTTCAACATCAG
LacZ PA rev	*Fubp1* targeting vector	CCCTGCCCGGTTATTATTATTT
loxP1 for	*Fubp1* targeting vector	CTGGATCCGGAATAACTTCGTATAG
loxP1 rev	*Fubp1* targeting vector	TCCTAGGTGTGGACATCTCTT
loxP3 for	*Fubp1* targeting vector	GGTAACCAACCAGCTAACACTA
loxP3 rev	*Fubp1* targeting vector	GCCTTAGAATTGAGTGGAAGAGA
*PUC/5´*arm for	*Fubp1* targeting vector	CGGCGGATAACAATTTCACAC
*PUC/5´*arm rev	*Fubp1* targeting vector	AGCCTAACAACTTACACCTGAC
SA for	*Fubp1* targeting vector	TGCGTTGGTTGTGGATAAGTAG
SA rev	*Fubp1* targeting vector	CCGCTGCTCTGTCAGGTA

***Table 6.11**: Oligonucleotides for ChIP analysis*

Primer	**Sequence form 5´ to 3´**
FUBP1 P1 for	TCCTCACGATTCCTGGAGCTTAC
FUBP1 P1 rev	TCTGGCATTACTTGGTAACTGAAGT
FUBP1 P2 for	CACCACCCAAACACAGTCGC
FUBP1 P2 rev	GCGGAGAGGAGGTGCCAAAA
FUBP1 P3 for	AGCAGCCTTTTTCTGGGCGG
FUBP1 P3 rev	TCTGCCTCTCAGTTCAGAGTCG
FUBP1 P4 for	TGTACTAGGTGCTGGGCATTTTT
FUBP1 P4 rev	TTACCGGGACAGTTGAAGGAAC
Chr18 for	ACTCCCCTTTCATGCTTCTG
Chr18 rev	AGGTCCCAGGACATATCCATT

***Table 6.12**: Oligonucleotides for genotyping*

Identification of	**Primers**	**Sequence from 5´ to 3´**
AvenLacZ	for	TGGGCATCATGTGTGTCAT
	rev 1	AGTGGAGTCCTGACCTAGAA
	rev 2	CCGACTTGGAATGGGTTCAT
Cre expression (in *CamkIIα*- and *Nestin-Cre* mice)	for	GACCAGGTTCGTTCACTCATGG
	rev	AGGCTAAGTGCCTTCTCTACAC
Deletion of *Aven* Exon 2	for	TGGGCATCATGTGTGTCAT
	rev 1	AGTGGAGTCCTGACCTAGAA
	rev 2	CTAAAGGAGCTGTGCTGTGT

Deletion of *Fubp1* exons 4-7	for 1	CTGTGCTTGGACTAAGGATGT
	for 2	GCATTTAGGTGCTTGCCTTC
	rev	GTTCAGAGACAGTCAGCTATGG
ErGFP-Cre expression	for	GTGTGGCTGCCCCTTCTGCCA
	rev 1	GGCAGCCTGGGCACCTTCAC
	rev 2	CAGGAATTCAAGCTCAACCTCA
Floxed *Aven* Exon 2	for	TGGGCATCATGTGTGTCA
	rev	AGTGGAGTCCTGACCTAGAA
Floxed *Fubp1* exons 4-7	for 1	CAAAGCCACACCACAACTATAAG
	for 2	GGATCTCATGCTGGAGTTCTTC
	rev	CAGGAAAGGGACACACAGATTA
Fubp1LacZ	for 1	GGTAACCAACCAGCTAACACTA
	for 2	CTGGATCCGGAATAACTTCGTATA
	rev	GCCTTAGAATTGAGTGGAAGAGA
MMTV-PyVT expression	Tg for	GGAAGCAAGTACTTCACAAGGG
	Tg rev	GGAAAGTCACTAGGAGCAGGG
	Int. ctrl for	CAAATGTTGCTTGTCTGGTG
	Int. ctrl rev	GTCAGTCGAGTGCACAGTTT
Vav-Cre expression	for	CCATGGCACCCAAGAAGAAG
	rev	GCTTAGTTTTCCTGCAGCGG

6.6 Molecular mass markers for electrophoresis

***Table 6.13**: Molecular mass markers for electrophoresis*

Name	Manufacturer
BenchMark™ Pre-stained Protein Ladder	*Life Technologies GmbH*, Darmstadt
Invitrogen™ 1 kb Plus DNA Ladder	*Life Technologies GmbH*, Darmstadt
2-Log DNA ladder	*New England Biolabs GmbH*, Frankfurt

6.7 Kits

***Table 6.14**: Kits*

Name	Manufacturer
Amersham ECL Western Blotting Detection	*GE Healthcare*, Munich
CD34 MicroBead Kit, human	*Miltenyi Biotec GmbH*, Bergisch Gladbach
ChIP DNA Clean&Concentrator™ Kit	*Zymo Research*, Freiburg

DNeasy Blood & Tissue Kit	*Qiagen GmbH*, Hilden
Expand™ Long Template PCR System	*Roche*, Mannheim
Omniscript Reverse Transcription Kit	*Qiagen GmbH*, Hilden
Phusion Site-directed Mutagenesis Kit	*Thermo Fisher Scientific*, Bonn
Plasmid Maxi Kit	*Qiagen GmbH*, Hilden
QIAquick® Gel Extraction Kit	*Qiagen GmbH*, Hilden
Random Primers DNA Labeling System	*Life Technologies GmbH*, Darmstadt
RNase-Free DNase Set	*Qiagen GmbH*, Hilden
RNeasy Mini Kit	*Qiagen GmbH*, Hilden
SuperSignal™ West Pico PLUS Chemiluminescent Substrate	*Thermo Fisher Scientific*, Bonn

6.8 Antibodies

***Table 6.15**: Primary antibodies for immunoblotting*

Antibody	Species	Dilution	Manufacturer
Anti-β-Actin (C11)	goat	1:2,000	*Santa Cruz Biotechnology*, Heidelberg
Anti-Aven	rabbit	1:3,000	*Inc.*, Poway, CA, USA
Anti-Cytokeratin 18 (CD10)	mouse	1:100	*Thermo Fisher Scientific*, Bonn
Anti-Ezrin (3C12)	mouse	1:500	*Thermo Fisher Scientific*, Bonn
Anti-FUBP1 (ab181111)	rabbit	1:2,000	*Abcam*, Cambridge, UK
Anti-FUBP1 (N-15)	rabbit	1:1,000	*Santa Cruz Biotechnology*, Heidelberg
Anti-Lamin B1 (ab16048)	rabbit	1:1,000	*Abcam*, Cambridge, UK

***Table 6.16**: Secondary antibodies for immunoblotting*

Antibody	Species	Dilution	Manufacturer
Anti-goat-HRP	rabbit	1:10,000	*Invitrogen GmbH*, Darmstadt
Anti-mouse-HRP	sheep	1:2,000	*GE Healthcare Europe GmbH*, Munich
Anti-rabbit-HRP	donkey	1:2,000	*GE Healthcare Europe GmbH*, Munich

***Table 6.17**: Antibodies for ChIP*

Antibody	Species	Dilution	Manufacturer
Anti-GATA-1 (ab181544)	rabbit	5 µg/IP	*Abcam*, Cambridge, UK
Anti-RNA Pol II (ab26721)	rabbit	2.4 µg/IP	*Abcam*, Cambridge, UK

Anti-TAL1 (TA-590662)	rabbit	5 µg/IP	*Origene*, Rockville, MD, USA
IgG (2028)	rabbit	5 µg/IP	*Santa Cruz Biotechnology*, Heidelberg

***Table 6.18**: Antibodies for flow cytometry*

Antibody	Clone	Manufacturer
Anti-hB220-Biotin	RA3-6B2	*BioLegend*, London, UK
Anti-hB220 Brilliant Violet 421™	RA3-6B2	*BioLegend*, London, UK
Anti-hCD235a APC	HIR2/GA-R2	*eBioscience*, Frankfurt
Anti-mCD117 (c-Kit) PE-Cy7	2B8	*eBioscience*, Frankfurt
Anti-mCD11b PE-Cy7	M1/70	*eBioscience*, Frankfurt
Anti-mCD11b Biotin	M1/70	*BioLegend*, London, UK
Anti-mCD150 PE	TC15-12F12.2	*BioLegend*, London, UK
Anti-mCD16/32 BD Horizon™ V450	2.4G2	*BD Biosciences*, Franklin Lakes, NJ, USA
Anti-mCD16/32 uncoupled (FcR Block)	93	*eBioscience*, Frankfurt
Anti-mCD19 Biotin	1D3	*eBioscience*, Frankfurt
Anti-mCD34 eFluor® 660	RAM34	*eBioscience*, Frankfurt
Anti-mCD3e Biotin	145-2C11	*eBioscience*, Frankfurt
Anti-mCD3e Brilliant Violet 510™	17A2	*BioLegend*, London, UK
Anti-mCD3 V450	500A2	*BD Biosciences*, Franklin Lakes, NJ, USA
Anti-mCD4 PerCP-Cy5.5	RM4-5	*BD Biosciences*, Franklin Lakes, NJ, USA
Anti-mCD41 Biotin	MWReg30	*eBioscience*, Frankfurt
Anti-mCD45.2 Brillian Violet 711™	104	*BioLegend*, London, UK
Anti-mCD48 FITC	HM48.1	*BioLegend*, London, UK
Anti-mCD71 PE	RI7217	*BioLegend*, London, UK
Anti-CD8-APC	53-6.7	*eBioscience*, Frankfurt
Anti-mc-Kit PE-Cy7	2B8	*BioLegend*, London, UK
Anti-mGr-1 Alexa Fluor® 700	RB6-8C5	*BioLegend*, London, UK
Anti-mGr-1 Biotin	RB6-8C5	*eBioscience*, Frankfurt
Anti-mSca-1 Brilliant Violet 510™	D7	*BioLegend*, London, UK
Streptavidin APC-eFluor® 780	–	*eBioscience*, Frankfurt
Anti-mTer119 Alexa Fluor® 647	TER-119	*BioLegend*, London, UK
Anti-mTer119 Biotin	TER-119	*eBioscience*, Frankfurt
Fixable Viability Dye eFluor® 780	–	*eBioscience*, Frankfurt

6.9 Mouse lines

***Table 6.19**: Mouse Lines*

Line	Description	Source
Alb-Cre	*Cre* expression under the control of the *Alb* promoter	AG Greten, *Georg-Speyer-Haus*, Frankfurt
Aven_CamkIIαCre	CRE-mediated deletion of *Aven* Exon 2 in *CamkIIα* expressing cells (forebrain, specifically to the CA1 pyramidal cell layer in the hippocampus)	established during this thesis
Aven_CMVCre	CRE-mediated constitutive deletion of *Aven* Exon 2	M. Zörnig, *Georg-Speyer-Haus*, Frankfurt generated from conditional mice derived from the IMPC
Aven _Flp	*LoxP* sites flanking *Aven* Exon 2	M. Zörnig, *Georg-Speyer-Haus*, Frankfurt generated from conditional mice derived from the IMPC
AvenLacZ	Replacement of *Aven* Exon 2 by a *LacZ* reporter gene	M. Zörnig, *Georg-Speyer-Haus*, Frankfurt generated from conditional mice derived from the IMPC
Aven_MMTVCre	CRE-mediated deletion of *Aven* Exon 2 in *MMTV* expressing cells (mammary gland)	established during this thesis
Aven_MMTVCrePyVT	CRE-mediated deletion of *Aven* Exon 2 and *Polyoma virus middle tumor antigen* (*PyVT*) expression in *MMTV* expressing cells (mammary gland)	established during this thesis
Aven_NestinCre	CRE-mediated deletion of *Aven* Exon 2 in *Nestin* expressing cells (the central and peripheral nervous system, including neuronal and glial cell precursors and in a few isolated kidney and heart cells)	established during this thesis
Aven_VavCre	CRE-mediated deletion of *Aven* Exon 2 in *Vav* expressing cells (hematopoietic system and endothelial cells)	established during this thesis
C57BL/6J (B6)	Inbred mouse strain; used for backcrossing of the other mouse lines	*Charles River*, Sulzfeld
CamkIIα-Cre (T29-1)	*Cre* expression under the control of the mouse *calcium/calmodulin-*	*The Jackson laboratories*,

	dependent protein kinase II alpha (*CamkIIα*) promoter (active in the forebrain, specifically to the CA1 pyramidal cell layer in the hippocampus)	Bar Harbor, ME USA Stock No: 005359
CMV-Cre	*Cre* expression under the control of the human *cytomegalovirus* (*CMV*) minimal promoter	M. Zörnig, *Georg-Speyer-Haus*, Frankfurt
ErGFP-Cre	*Cre* and *GFP* expression under the control of the EPO receptor promoter	U. Klingmüller, *German Cancer Research Center*, Heidelberg
FLPeR	*FLPe* expression under the control of the *Gt(ROSA)26Sor* promoter	M. Zörnig, *Georg-Speyer-Haus*, Frankfurt
Fubp1	Mice with potential of conditional deletion of *Fubp1* exons 4-7.	generated during this thesis Vector with conditional knockout first potential purchased from the *IMPC*
Fubp1_AlbCre	CRE-mediated deletion of *Fubp1* exons 4-7 in *Albumin* expressing cells (liver cells)	established during this thesis
Fubp1_CMVCre	CRE-mediated constitutive deletion of *Fubp1* exons 4-7	established during this thesis
Fubp1_ErGFPCre	CRE-mediated deletion of *Fubp1* Exons 4-7 and *GFP* expression in *EPO receptor* (*Er*) expressing cells	established during this thesis
Fubp1_Flp	*loxP* sites flanking *Fubp1* exons 4-7	established during this thesis
Fubp1LacZ	Replacement of *Fubp1* exons 4-7 by a *lacZ* reporter gene cassette	established during this thesis
Fubp1_VavCre	CRE-mediated deletion of *Fubp1* Exons 4-7 in *Vav* expressing cells (hematopoietic system and endothelial cells)	established during this thesis
MMTV-Cre	*Cre* expression under the control of the *mouse mammary tumor virus* (*MMTV*) promoter (in the mammary gland)	L. Hennighausen, *National Institutes of Health*, Bethesda, ME USA
MMTV-PyVT	*Polyoma virus middle tumor antigen* (*PyVT*) expression in *MMTV* expressing cells (mammary gland)	M. Rieger *Goethe University Hospital,* Frankfurt
Nestin-Cre	Expression of *Cre* recombinase under the control of the *Nestin* promoter (active in the central and peripheral nervous system, including neuronal and glial cell precursors and in a few isolated kidney and	*The Jackson laboratories*, Bar Harbor, ME USA Stock No: 003771

	heart cells)	
Vav-Cre	*Cre* expression under the control of the *Vav* promoter	C. Stocking-Harbers, *Heinrich-Pette-Institute* Hamburg

6.10 Buffers

***Table 6.20**: Buffers*

Agarose gel electrophoresis	
Running buffer (0.5x TBE)	44.5 mM Tris 44.5 mM boric acid 1 mM EDTA pH 8.0
DNA loading buffer (10x)	100 mM EDTA 1% (w/v) SDS 0.25% (w/v) bromophenol blue 0.25% (w/v) xylenecyanol 20% (v/v) glycerol
Chromatin immunoprecipitation (ChIP)	
Lysis buffer	50 mM Tris-HCl pH 8.0 140 mM NaCl 1% (v/v) Triton X-100 1 mM EDTA pH 8.0 0.1% (w/v) sodium deoxycholate 0.1% (w/v) SDS 1 tablet *Complete Mini* protease inhibitor cocktail (*Roche*, Mannheim) for 10 ml buffer
RIPA/RIPA$^+$ buffer	50 mM Tris-HCl pH 8.0 150 mM NaCl 1% (v/v) NP-40 2 mM EDTA pH 8.0 0.5% (w/v) sodium deoxycholate (0.1% (w/v) SDS for RIPA$^+$) 1 tablet *Complete Mini* protease inhibitor cocktail (*Roche*, Mannheim) for 10 ml buffer
Wash Buffer	20 mM Tris-HCl pH 8.0 150 mM NaCl 1% (v/v) Triton X-100 2 mM EDTA pH 8.0 0.1% (w/v) SDS
Final Wash Buffer	20 mM Tris-HCl pH 8.0 500 mM NaCl 1% (v/v) Triton X-100 2 mM EDTA pH 8.0 0.1% (w/v) SDS
Elution Buffer	100 mM $NaHCO_3$ 1% (w/v) SDS
Flow cytometry	

DPBS	*GIBCO*, Eggstein
FACS buffer	DPBS 10% (v/v) FBS 0.1% (w/v) NaN_3 1mM EDTA pH 8.0
BD Horizon™ Brilliant Stain Buffer	*BD Biosciences*, Franklin Lakes, NJ, USA
Genomic DNA isolation	
Alkaline lysis buffer	25 mM NaOH 0.2 mM EDTA pH 8.0
Neutralization buffer	40 mM Tris-HCl pH 5.0
Isolation of hCD34$^+$ cells	
Equilibration and Rinse Buffer	DPBS 2 mM EDTA 0.5% (w/v) BSA sterile filtered
Luciferase assay	
Lysis Buffer	50 mM Tris-HCl pH 8.0 50 mM NaCl 1% (v/v) Triton X-100
Luciferase Buffer	21.625 mM glycylglycine 1 mM ATP 10 mM $MgCl_2$ 0.075 mM Luciferin
β-Galactosidase Buffer	11.1 mM $MgCl_2$ 50 mM β-mercaptoethanol 3.25 mM ONPG (*ortho*-Nitrophenyl-β-galactoside 74.4 mM sodium phosphate
Plasmid mini preparation	
GTE resuspension buffer	50 mM glucose 25 mM Tris-HCl pH 8.0 10 mM EDTA
Lysis buffer	200 mM NaOH 1% SDS freshly prepared
Neutralization buffer	3 M KOAc pH 5.2
Quantitative real-time PCR and PCR arrays	
Applied Biosystems™ SYBR® Select Master Mix	*Life Technologies GmbH*, Darmstadt
TaqMan® Gene Expression Master Mix	*Life Technologies GmbH*, Darmstadt
SDS polyacrylamide gel electrophoresis	
RIPA lysis buffer	50 mM Tris-HCl, pH 7.5 150 mM NaCl 5 mM EDTA, pH 8.0 1% (v/v) NP-40 0.5% (w/v) sodium deoxycholate

	0.1% (w/v) SDS 1 tablet *Complete Mini* protease inhibitor cocktail (*Roche*, Mannheim) for 10 ml buffer
SDS sample buffer (5x)	62.5 mM Tris-HCl, pH 6.8 2% (w/v) SDS 20% (v/v) glycerol 0.1% (w/v) bromophenol blue 50 mM DTT
SDS PAGE running buffer	50 mM Tris 200 mM glycine 0.15% (w/v) SDS
Southern blotting	
20x SSC (saline sodium citrate)	175.3 g NaCl 88.2 g NaCitrate ddH_2O ad 1 l
Pre-Hybridization Buffer	4 ml 20x SSC 4 ml 10% (w/v) SDS 0.2 g milk powder 4 g Dextran Sulphate 29 ml ddH_2O 3 ml herring sperm DNA (10 mg/ml, denatured at 95°C for 5 min), freshly added
Hybridization Buffer	4 ml 20x SSC 4 ml 10% (w/v) SDS 0.2 g milk powder 29 ml ddH_2O 3 ml herring sperm DNA (10 mg/ml, denatured at 95°C for 5 min), freshly added
Wash Buffer I	2x SSC 0.1%)w/v) SDS
Wash Buffer II	0.2x SSC 0.1% (w/v) SDS
Western blotting	
Blotting buffer	48 mM Tris 39 mM Glycine 20% (v/v) methanol
TBS/TBS-T	25 mM Tris 150 mM NaCl (0.1% (v/v) Tween-20 for TBS-T) pH 8.1
Blocking buffer	3% non-fat milk powder in TBS-T
X-Gal staining	
Wash buffer	DPBS 2 mM $MgCl_2$ 0.1% (v/v) Triton X-100
Staining solution	Wash Buffer 5 mM potassium hexacyanoferrate(III) 5 mM potassium hexacyanidoferrate(II) 4 mg/ml X-Gal

6.11 Laboratory equipment

***Table 6.21**: Flow cytometry*

Device	Manufacturer
BD FACSCalibur™	*BD Biosciences*, Franklin Lakes, NJ, USA
BD FACSCanto™ II	*BD Biosciences*, Franklin Lakes, NJ, USA
BD LSRFortessa™ II	*BD Biosciences*, Franklin Lakes, NJ, USA

***Table 6.22**: Microscopy*

Device	Manufacturer
Fluorescence Microscope *Nikon Eclipse Te300*	*Nikon*, Düsseldorf
Microscope for Cell Culture	*Helmut Hund GmbH*, Wetzlar

***Table 6.23**: Electrophoresis*

Device	Manufacturer
BioRad *Power Pac 300*	*BioRad Laboratories*, Munich
DNA Mini-Subcell for Agarose Gels	*BioRad Laboratories*, Munich
Electrophoresis Power Supply *EPS 301*	*Amersham Pharmacia Biotech*
Gel-Chamber Model *Hoefer HE 33* for Mini Gels	*Amersham Pharmacia Biotech*
Mini-Protean 3 Cell Gel Chamber	*BioRad Laboratories*, Munich
Semidry Blotting Unit *Semiphor Transphor*	*Hoefer Pharmacia Biotech*, Holliston, MA, USA

***Table 6.24**: Centrifuges*

Device	Manufacturer
Biocentrifuge *J2-21M/E* (JA-10, JA-20 rotors)	*Beckman*, Munich
Centrifuge *Megafuge 1.0 R*	*Heraeus*, Munich
Centrifuge *Mikro 220 R*	*Hettich GmbH & Co. KG*, Tuttlingen
Centrifuge *Minifuge GL*	*Heraeus*, Munich
Tabletop Centrifuge *Biofuge pico*	*Heraeus*, Munich
Ultracentrifuge *Optima L-90K* (SW32 Ti rotor)	*Beckman Coulter*, Pasadena, CA, USA

***Table 6.25**: Incubators*

Device	Manufacturer
Bacterial Incubator *Function Line* (37 °C)	*Heraeus*, Munich
Bacterial-Shaker-Incubator *Multitron* (37 °C)	*Infors AG*, Bottmingen, Switzerland
Cell culture Incubator *MCO 17 AI* (37 °C, 5% CO2)	*Sanyo Component Europe GmbH*, Ingolstadt

***Table 6.26**: Heatblocks*

Device	Manufacturer
Dri. Block DB-2D	*Techne Dexford*, Cambridge, England
Thermomixer Compact for 1.5 ml tubes	*Eppendorf AG*, Hamburg

***Table 6.27**: Other laboratory equipment*

Device	Manufacturer
38.5 ml open-top thinwall polypropylene tubes	*Beckman Coulter GmbH*, Krefeld
Autoclave Tuttnauer Systec 2540 EL	*Systec*, Wettenberg
BD Falcon™ FACS tubes with cell strainer	*BD Biosciences*, Franklin Lakes, NJ, USA
BIORUPTOR®	*Diagenode SA*, Seraigne, Belgium
Bunsen Burner *1230/1*	*Carl Friedrich Usbeck KG*, Radevormwald
Dynal® MPC-S	*Thermo Fisher Scientific*, Bonn
FACS tubes (sterile, polypropylene)	*Greiner Bio-One*, Frickenhausen
Freezer (-20 °C)	*Liebherr*, Ochsenhausen
Freezer CFC Free (-80 °C)	*Sanyo*, Wiesbaden
Frigocut 2800	*Reichert-Jung* (Leica Microsystems), Heerbrug, Schweiz
Hybridization Oven	*Biometra*, Göttingen
Hypercassette	*Amersham Pharmacia Biotech*
Integra Pipetboy	*Integra Biosciences*, Fernwald
Laminar Air Flow (*NSF 49 BS 5726 DIN (1-4)*)	*Clean Air*, Woerden, Netherlands
LightCycler® 480	*Roche*, Mannheim
LS Columns	*Miltenyi Biotec GmbH*, Bergisch Gladbach
LUMIstar Galaxy microplate reader	*BMG Labtech, Ortenberg*
Microcentrifuge tubes, low retention	*VWR International GmbH*, Darmstadt
Microwave *MW 7873*	*Severin Elektrogeräte GmbH*, Sundern
Mortar and pestle	*Carl Roth GmbH & Co. KG*, Karlsruhe
NanoDrop™ 1000 Spectrophotometer	*Thermo Fisher Scientific*, Bonn
Neubauer Improved Hemocytometer	*Marienfeld Superior*, Darmstadt
NICK-Column	*Amersham Pharmacia Biotech*
pH-Meter *PHM 83 autocal*	*Radiometer*, Copenhagen, Denmark
Pipettes *Transferpette® S*	*Brand GmbH & Co. KG*, Wertheim

Pipetus® with Storage Battery	*Hirschmann*, Neckartenzlingen
Plastic cuvettes	*Sarstedt AG & Co*, Nümbrecht
Real-time PCR 96-well plates	*4titude*, Berlin
Refrigerator (4°C)	*Bosch* GmbH, Gerlingen
Roller *RM5 Assistant 348*	*Karl Hechst GmbH & Co. KG*, Sondheim
Rotate roller	*Gerlinde Kister*, Mühlhausen
Scale *Kern EMB 200-2*	*Kern & Sohn GmbH*, Balingen
SmartSpec™ 3000 Spectrophotometer	*Bio-Rad Laboratories GmbH*, Munich
SPECTRAmax™ 340	*Molecular Devices, Biberach*
StepOne Plus™ System	*Thermo Fisher Scientific*, Bonn
Stratalinker® 1800 UV Crosslinker	*Stratagene (Agilent),* Santa Clara, CA, USA
Super RX Fuji Medical X-Ray Film	*FUJIFILM Corporation*, Tokyo, Japan
UV-Transluminator with video camera	*UVP Inc.*, San Gabriel, USA
Vacuum pump	*KNF Neuberger LABOPORT*, Freiburg
Vortex Genie 2	*Bender & Hobein AG*, Zürich, Switzerland
Water-Bath	*GFL*, Burgwedel
X-Ray Film Processor *XR 24 Pro*	*Dürr Dental AG*, Bietigheim-Bissingen

6.12 Chemicals

***Table 6.28**: Chemicals*

Name	Manufacturer
Acrylamide solution (*Rotiphorese Gel 30*)	*Carl Roth GmbH & Co. KG*, Karlsruhe
Agarose *UltraPure™ Agarose*	*Invitrogen GmbH*, Darmstadt
Ampicillin	*AppliChem GmbH*, Darmstadt
APS (Ammonium persulfate) 10% in H2 0	*Sigma-Aldrich Chemie GmbH*, Steinheim
Boric acid	*Carl Roth GmbH & Co. KG*, Karlsruhe
Bradford Reagent (*Roti*® *-Quant*)	*Carl Roth GmbH & Co. KG*, Karlsruhe
BrdU (Bromodeoxyuridine)	*BD Biosciences*, Franklin Lakes, NJ, USA
Bromophenol blue	*Carl Roth GmbH & Co. KG*, Karlsruhe
$CaCl_2$ (Calcium chloride)	*Merck*, Darmstadt
Complete Mini Protease Inhibitor Cocktail	*Roche*, Mannheim
DTT (Dithiothreitol)	*Sigma-Aldrich Chemie GmbH*, Steinheim
Dynabeads™ Protein G	*Invitrogen GmbH*, Darmstadt

EDTA (Ethylenediaminetetraacetic acid)	*Sigma-Aldrich Chemie GmbH*, Steinheim
Ethanol	*Carl Roth GmbH & Co. KG*, Karlsruhe
Ethidium bromide	*Carl Roth GmbH & Co. KG*, Karlsruhe
Formaldehyde solution (Formalin) 37%	*Carl Roth GmbH & Co. KG*, Karlsruhe
Glucose	*Carl Roth GmbH & Co. KG*, Karlsruhe
Glycerol	*Carl Roth GmbH & Co. KG*, Karlsruhe
Glycine	*Carl Roth GmbH & Co. KG*, Karlsruhe
Heparin	*Sigma-Aldrich Chemie GmbH*, Steinheim
HEPES (4-(2-Hydroxyethyl)piperazine-1-ethanesulfonic acid)	*Carl Roth GmbH & Co. KG*, Karlsruhe
Illustra^{TM} dNTP Set	*GE Healthcare Europe GmbH*, Munich
Isofluran	*Abbott*, Wiesbaden
Isopropanol (2-propanol)	*Carl Roth GmbH & Co. KG*, Karlsruhe
KOAc (Potassium acetate)	*Carl Roth GmbH & Co. KG*, Karlsruhe
Luciferin	*Sigma-Aldrich Chemie GmbH*, Steinheim
2-Mercaptoethanol	*Sigma-Aldrich Chemie GmbH*, Steinheim
Methanol	*Carl Roth GmbH & Co. KG*, Karlsruhe
$MgCl_2$ (magnesium chloride)	*Sigma-Aldrich Chemie GmbH*, Steinheim
Na_2HPO_4 (Disodium hydrogen phosphate)	*Carl Roth GmbH & Co. KG*, Karlsruhe
NaCl (Sodium chloride)	*Carl Roth GmbH & Co. KG*, Karlsruhe
$NaHCO_3$ (sodium hydrogen carbonate)	*Carl Roth GmbH & Co. KG*, Karlsruhe
NaN_3 (Sodium azide)	*Carl Roth GmbH & Co. KG*, Karlsruhe
NaOH (Sodium hydroxide)	*AppliChem GmbH*, Darmstadt
Non-fat dried milk powder	*AppliChem GmbH*, Darmstadt
NP-40 (*Ipegal CA-630*)	*Sigma-Aldrich Chemie GmbH*, Steinheim
ONPG (*o*-Nitrophenyl β-D-galactopyranoside)	*Sigma-Aldrich Chemie GmbH*, Steinheim
Pierce™ 16% Formaldehyde (w/v), Methanol-free	*Thermo Fisher Scientific*, Bonn
Ponceau S Solution	*Sigma-Aldrich Chemie GmbH*, Steinheim
Potassium hexacyanoferrate (III)	*Sigma-Aldrich Chemie GmbH*, Steinheim
Potassium hexacyanoferrate (II) trihydrate	*Carl Roth GmbH & Co. KG*, Karlsruhe
SDS (Sodium dodecyl sulfate)	*Carl Roth GmbH & Co. KG*, Karlsruhe
Sodium deoxycholate	*Sigma-Aldrich Chemie GmbH*, Steinheim
TEMED (N,N,N',N'-Tetramethylethane-1,2-Diamine)	*Carl Roth GmbH & Co. KG*, Karlsruhe
Thermo ScientificTM RiboLockTM RNase Inhibitor	*Life Technologies GmbH*, Darmstadt
Thermo ScientificTM Random Hexamer Primer	*Life Technologies GmbH*, Darmstadt

Oligo-dT Primer	*Qiagen GmbH*, Hilden
Tris (2-Amino-2-(hydroxymethyl)propane-1,3-diol)	*Carl Roth GmbH & Co. KG*, Karlsruhe
Triton X-100	*Sigma-Aldrich Chemie GmbH*, Steinheim
Trypan Blue Stain 0.4%	*GIBCO* , Eggenstein
Tween-20	*Carl Roth GmbH & Co. KG*, Karlsruhe
Xylenecyanol	*Carl Roth GmbH & Co. KG*, Karlsruhe

7 Methods

7.1 Cell Culture and Cellular Assays

7.1.1 Thawing and freezing cells

Frozen cells stored at -80°C or in liquid nitrogen were thawed in a 37°C water bath and resuspended in 5 ml medium. After pelleting the cells at 1,500 g for 5 min at 4°C, cells were resuspended in medium and seeded in dishes or flasks of appropriate volume. Cells were incubated at 37°C in a 5% CO_2 atmosphere.

For long term storage, adherent cells were detached and singularized. Cells were pelleted at 1,500 g for 5 min at 4°C and washed with 5 ml PBS. The pellet was resuspended in 1ml freezing medium (FCS with 10% (v/v) DMSO). Cells were frozen at a cooling rate of -1°C/min in freezing containers in a -80°C freezer and stored in liquid nitrogen.

7.1.2 Cell passaging

Cells were cultured in medium at densities listed in **table 7.1**. For the passage of adherent cells, medium was aspirated, cells were washed with 5 ml PBS/10cm dish and detached by adding 1 ml trypsin/10cm dish. After incubation for 2-5 min at 37°C, trypsin digestion was stopped by adding at least three volumes of medium. Cells were counted using a *Neubauer* chamber and seeded as indicated in **table 7.1**. Suspension cells were counted and kept at concentration indicated in **table 7.1** by addition of fresh medium.

***Table 7.1**: Conditions for the culture of cell lines and primary hCD34$^+$ cells*

Cell line	Medium	Supplements	Seeding concentration	Splitted at
HEK293T	DMEM	10% FCS 4 mM Glutamine 1% Pen/Strep	3 x 10^6 cells per 10 cm dish	90% confluence
MCF-7	RPMI 1640	10% FCS 4 mM Glutamine 1% Pen/Strep	3 x 10^6 cells per 10 cm dish	90% confluence
MDA-MB 453	DMEM	10% FCS 4 mM Glutamine 1% Pen/Strep	6 x 10^6 cells per 10 cm dish	90% confluence

K562	RPMI 1640	10% FCS 2 mM Glutamine 1% Pen/Strep	1 x 10^5 cells/ml	5-10 x 10^5 cells/ml
HEL	RPMI 1640	10% FCS 2 mM Glutamine 1% Pen/Strep	1 x 10^5 cells/ml	5-10 x 10^5 cells/ml
Primary hCD34$^+$ cells	SFEM I	100 nM SCF 100 nM Flt3-L 20 nM IL-3 20 nM IL-6	5 x 10^5 cells/ml	1-2 x 10^6 cells/ml

7.1.3 Cell quantification with the *Neubauer* chamber

Cells were detached by trypsin digestion if necessary and mixed at a ratio of 1:1 with trypan blue. Trypan blue only enters and stains a cell in case of a damaged cell membrane in dead or apoptotic cells [212]. 10 µl of the sample were loaded into *Neubauer* chambers, and unstained viable cells were counted using a light microscope. The number of counted cells within 16 squares (one quarter of the complete sectioned field) corresponds to the number of cells in the sample per ml.

7.1.4 Isolation of primary hCD34$^+$ cells

Peripheral blood stem cells from G-CSF-treated healthy donors, collected by apharesis, were provided by the DRK blood donation service (Frankfurt). Up to 5 mL of stem cell apharesis were mixed with PBS to a final volume of 30 ml in a 50 ml tube. The mixture was carefully laid on 15 ml Ficoll and subsequently centrifuged at 400 x g and RT, stopped without break after 40 min. The whitish layer of mononuclear cells was transferred into another 50 ml tube, PBS was added to a final volume of 30 ml. Cells were pelleted at 300 x g for 10 min at 4°C and then washed in 20 ml PBS at 300 x g and 4°C for 5 min. Cells were counted and resuspended in PBS at a concentration of 10^8 cells/300 µl. 100 µl FcR block and 100 µl anti-CD34 magnetic microbeads (*Miltenyi Biotec*) were added per 300 µl cell suspension and carefully mixed. After 30 min of incubation at 4°C in the dark, 3 ml PBS were added, and bead-labeled cells were pelleted at 300 x g for 5 min at 4°C. Beads were resuspended in 500 µl buffer and transferred to FACS tubes through a strainer. LS columns (*Miltenyi Biotec*) were placed on a magnetic rack and equilibrated by rinsing them two times with 3 ml buffer. The sample was added and the columns were rinsed two times with 5 ml buffer. The columns were removed from the magnetic rack, and bead-bound selected cells were eluted with 5 ml buffer.

Enrichment of $CD34^+$ cells was tested via flow cytometry using anti-CD45.2-FITC and anti-CD34-PE antibodies at concentrations recommended by the manufacturer. Pelleted cells (5 min at 2,400 rpm, RT) were resuspended in supplemented SFEM I (**table 7.1**) and seeded in a 24-well plate with 2.5 x 10^5 cells in 500 µl medium per well.

7.1.5 Erythroid differentiation of primary human $CD34^+$ cells

After four days of expansion in supplemented SFEM I medium, erythroid differentiation of $hCD34^+$ cells was induced by transferring them into SFEM II medium supplemented with 1 U/ml EPO, 5 ng/ml IL-3, 20 ng/ml SCF, 2 µM Dexamethasone, 0.2 µM 17β-estradiol and 100 U/ml penicillin/streptomycin. Cells were maintained at a concentration of 2.5 x 10^5 cells per 500 µl medium in 24 well plates for up to 12 days. Cell surface marker expression of glycophorin A (CD235a) was tested by flow cytometry (anti-CD235a-APC, 5 µl per 1 x 10^6 cells), and GPA and CD71 mRNA expression was quantified via RT-qPCR to confirm successful differentiation.

7.1.6 Transient Transfection

By transient transfection, foreign DNA is transferred into a host cell without usage of viral vectors and integration of the exogenous DNA into the genome. The uptake of foreign DNA can be achieved by different methods, among them the usage of positively charged chemicals like polyethyleneimine (PEI) that complex with negatively charged DNA. Endocytosis and Phagocytosis are thought to play a role in the uptake of the complex, but the exact process of cell membrane passage as well as the delivery to the nucleus are still unknown [213].

For Luciferase assays, 1 x 10^5 HEK293T cells per well were seeded into 24-well plates. 24 hours after seeding, 100 µl transfection solution were added per well. Transfection solution was prepared as follows: Per well, 100 µl supplemented DMEM without FSC, 4 µl of PEI and a total amount of 1 µg plasmid (0.25 µg reporter plasmid containing luciferase, 0.25 µg *TAL1* and *E47* expression plasmids each, 0.25 µg *β-Galactosidase* plasmid for normalization and empty *pcDNA3.1* vector to adjust DNA amount if necessary) were mixed thoroughly by vortexing for one minute and then incubated at RT for 15 minutes. Cells were harvested for promoter activity assays after 48 hours.

For the production of lentiviral particles, 3 x 10^6 HEK293T cells were seeded in 7 ml medium per 10 cm dish. After 24 hours, 1 ml of transfection solution was added.

Transfection solution was prepared as follows: per dish, 1 ml supplemented DMEM without FCS, 40 µl PEI, 10 µg of transfer vector, 3.5 µg *pMD2.G* and 6.5 µg *p8.91* as packaging plasmids were mixed thoroughly by vortexing for one minute and then incubated at RT for 15 minutes. The supernatant containing the viral particles was harvested after 48 and 72 hours.

7.1.7 Production and concentration of lentiviral particles

Foreign DNA can be introduced in the genome of both dividing and non-dividing cells by lentiviral particles. The infection of non-dividing cells relies on the expression of a lentiviral protein called matrix which promotes the passage of the viral pre-integration complex through the nuclear membrane. Lentiviral particles are produced in a so-called packaging cell line which is transiently transfected with three plasmids. The transgene is encoded by the transfer plasmid. It is flanked by long terminal repeats (LTRs) that are required for the integration into the host genome. The signal sequence Ψ at the 5´-end of the transgene mediates the packaging of the transgene mRNA into the viral particles. A second plasmid contains the *Gag* gene which encodes proteins binding the viral RNA genome and forming the viral core structure as well as the *Pol* gene which encodes the proteins for reverse transcription of the viral genome. A third plasmid encodes an envelope protein which interacts with receptors of the surface of host cells to induce infection. By splitting the viral genome into three plasmids, the chance of recombination events that might result in the production of replication-competent viruses is minimized [214].

HEK293T cells were transiently transfected with transfer and packaging plasmids as described above. 48 and 72 hours after transfection, the supernatant was centrifuged for 5 min at 1,000 rpm and 4°C to remove cells and debris. All subsequent steps were performed on ice. The supernatant was filtered through 0.2 µm syringe filters. Viral particles were concentrated by ultracentrifugation at 20,500 rpm and 4°C for 2 h 20 min. The pellet was resuspended in 150 µl medium and aliquoted for storage at -80°C.

7.1.8 Titration of lentiviral particles

In case lentiviral vectors contained fluorescent markers, the infectious potential of the lentiviral particles was determined by titration. 6 x 10^4 MCF-7 or K562 cells per well were seeded into 24-well plates. After 24 hours, 10 µl of concentrated viral particles were added in different dilutions (undiluted, 1:10, 1:100, and 1:1,000). 72 hours after

transduction, cells were harvested and washed with PBS (5 min at 1,500 rpm and 4°C). The cells were resuspended in 300 µl PBS and tested for fluorescence marker expression by flow cytometry. The virus titer in transducing units (TU) per ml was calculated using the following equation:

$$\text{titer [TU/ ml]} = \frac{\frac{F}{100} \cdot Cn}{DF}$$

F = percentage of fluorescence positive cells
Cn = number of seeded cells
DF = virus dilution factor
V = volume in ml of added viral particles

7.1.9 Gene knockdown and overexpression via lentiviral transduction

The expression of mRNA can be down-regulated by a naturally occurring mechanism called RNA interference (RNAi). Small hairpin RNAs (shRNAs) are used in laboratories to induce this process artificially. Viral vectors allow the stable expression of shRNAs in cells. This kind of genetic manipulation, the integration of non-viral DNA in the genome of a host cell via viral particles, is denoted transduction. The introduced shRNA comprises a hairpin-like stem-loop structure and is processed by the Drosha/DGCR8 complex to become the so-called pre-shRNA. This pre-shRNA, characterized by 2 nucleotide overhangs at the 3´-end, is transported into the cytoplasm, where it is bound by the DICER/TRBP/PACT complex. By cutting the hairpin loop, a double stranded mature shRNA is formed. This shRNA is subsequently integrated in the RNA-interfering silencing complex (RISC) and guides this complex to mRNA with complementary sequence. Depending on the extent of complementarity and the resulting strength of mRNA binding, the mRNA is either degraded or its translation is arrested [215].

For knockdown or overexpression of *AVEN* in adherent cells, 1 x 10^5 cells per well were seeded in 6-well plates. After 24 hours, a minimum of two infectious viral particles per cell (MOI, multiplicity of infection = 2) were added for transduction.

$$\text{MOI} = \frac{\text{titer} \cdot V}{Cn}$$

V = added volume of concentrated viral particles
Cn = number of seeded cells

For knockdown of suspension cells, 1 x 10^5 K562 cells in 1.5 ml medium were seeded per well of a 6-well plate, or 5 x 10^5 hCD34$^+$ cells in 500 µl medium were seeded per well of a 24-well plate. 100 µl of concentrated viral particles were mixed with 30 µl of 0.4 mg/ml protaminesulfate and added to one well. Cells were centrifuged at 2200 x g and 32°C for 90 min.

7.1.10 Multicolor Flow Cytometry

By multicolor flow cytometry, large numbers of cells can be analyzed regarding their size, granularity and fluorescence emission. Within the cytometer, the sample is focused by sheath streams allowing that single cells pass a cuvette flow cell. In the flow cell, laser beams excite fluorochromes at different wave lengths. The passing cells scatter light and emit fluorescence depending on their size, granularity and fluorescent marker expression. Scattered light that is detected in a low angle (<10°) is called FCS (forward light scatter) and represents the size of cells. Scattered light which is detected rectangular is called SSC (sideward light scatter) and constitutes a measure for cell granularity. The concomitant detection of fluorescence at different wave lengths is enabled by systems of band-pass filters and photoelectric tubes.

7.1.10.1 Transduction efficiency

The expression of GFP or VENUS encoded by lentiviral vectors was measured in transduced cells to assess transduction efficiency. Transduced cells were detached and singularized if necessary, washed once in PBS and pelleted (1,500 x g, 5 min at RT). 1 x 10^6 cells were resuspended in 500 µl PBS and analyzed with a *BD FACSCalibur (BD Biosciences)*.

7.1.10.2 Differentiation of hCD34$^+$ cells

The expression of glycophorin A (CD235a) at the surface of hCD34$^+$ cells cultured in differentiation medium was analyzed to confirm erythroid differentiation. Cells were pelleted (1,500 x g, 5 min at RT) and resuspended in 100 µl FACS buffer. 5 µl of anti-CD235a-APC antibody were added per 10^6 cells, followed by an incubation period of 30 min in the dark on ice. APC-labeled cells were counted using a *BD FACSCanto II (BD Biosciences)*.

7.1.10.3 Viability dye staining

Dead cells can be distinguished from viable cells via the integrity of the cell membrane. Fluorescent dyes that react with free amine residues within the cytoplasm are excluded from viable cells with an intact membrane, while dead cells become positively stained. As the reaction between the viability dye and the amines is irreversible, the staining is stable over time [216].

To assess the number of dead cell cells in transduced and/or treated breast cancer cell lines, 3.5 x 10^5 detached singularized cells were transferred into FACS tubes and pelleted by centrifugation at 1,500 x g and 4°C for 5 min. Cells were resuspended in 50 µl FACS buffer and stained with 0.2 µl Viability Dye eFluor® 780 (*eBioscience*) for 20 min on ice in the dark. Cells were washed with 3 ml PBS, pelleted at 1,500 x g and 4°C for 3 min and resuspended in 300 µl FACS buffer. Stained cells were recorded at a *BD FACSCanto II* (*BD Biosciences*).

7.1.10.4 Lineage staining of murine primary cells

To isolate bone marrow cells, tibia, femora and acetabula were dissected and flushed with ice cold PBS until the bones were completely whitened. Cells were suspended to generate a homogenous solution of singularized cells and pelleted by centrifugation at 1,200 rpm, 4°C for 7 min. The pellet was resuspended in 3 ml ice cold PBS, and viable cells were counted with trypan blue in a *Neubauer* chamber.

Spleens and thymi were carefully squeezed through a 100 µm cell strainer into a dish filled with ice-cold PBS. Cells were suspended to generate a homogenous solution of singularized cells. After centrifugation at 1,200 rpm and 4°C for 7 min, the cell pellet was resuspended in 3 ml ice-cold PBS, and viable cells were counted with trypan blue in a *Neubauer* chamber.

To analyze T cell- and lineage-differentiation of BM cells, spleenocytes, thymocytes and peripheral blood, 5 x 10^6 of the respective cells were pelleted (5,000 rpm, 7 min at RT) and resuspended in 20 µl Block solution (19 µl brilliant stain buffer + 1 µl Fc-Block). After an incubation period of 10 min on ice, 20 µl lineage- or T cell-staining master mix **(table 7.2**) were added and cells were incubated with the antibody master mix for at least 30 min on ice in the dark. After incubation, cells were washed with 1 ml PBS at 5,000 rpm for 5 min at RT. The stained cells were resuspended in 500 µl FACS buffer and analyzed using a *BD FACSFortessa (BD Biosciences)*.

7.1.10.5 HSPC staining of murine primary cells

Bone marrow cells were isolated as described above. *Histopaque®-1077* (*Sigma*) was pre-warmed to RT. To isolate bone marrow mononuclear cells (BMMNCs), 3 ml bone marrow cells were loaded carefully on top of 3 ml *Histopaque®-1077* and centrifuged for

30 min at RT and 1,400 rpm without break. The white cloudy interphase containing the mononuclear cells was transferred to a fresh 15 ml tubes. The BMMNCs were washed twice with 10 ml ice cold PBS, centrifuging at 1,200 rpm and 4°C for 7 min. Cells were resuspended in 1 ml PBS and counted with trypan blue in a *Neubauer Chamber*.
To quantify the number of stem and progenitor cells in BMMNCs of *Fubp1VaCre* mice, 1-2 x 10^7 BMMNCs were pelleted at 5,000 rpm and RT for 7 min. The pellet was resuspended in 40 µl of HSPC-staining master mix (**table 7.2**) and incubated for 30 min on ice in the dark. After washing the cells with 1 ml PBS (5,000 rpm, 7min, RT), cells were resuspended in 40 µl FACS buffer with 10 µl Strep-APC-eF780. After incubation for 30 min on ice in the dark, cells were washed as described above and resuspended in 800 µl FACS buffer. The cells were then analyzed with the *BD FACSFortessa (BD Biosciences)*.

For compensation, cells were incubated with single antibodies (single staining). 5 x 10^6 bone marrow cells (for lineage and HSPC staining) or thymocytes (for T cell staining) in 50 µl FACS buffer were stained with one single antibody each. Incubation periods, washing and analyses with the *BD FACSFortessa* were performed as described for the multicolor staining.

Recorded flow cytometry data were analyzed with the software interphases *BC FACSDiva™ V8* (*BD Biosciences*) and *FlowJo* (*Tree Star, Inc.*).

***Table 7.2**: Composition of staining master mixes used for flow cytometry analysis*

master mix	cells	composition
T cell staining	*Fubp1VavCre* thymocytes *AvenVavCre* thymocytes	47 µl FACS buffer 1 µl anti-CD3-V450 1 µl anti-CD4-PerCP-Cy5.5 1 µl anti-CD8-APC 50 µl per 5 x 10^6 cells
Lineage staining	*Fubp1VavCre* BM and spleenocytes *Fubp1ErGFPCre* BM, spleenocytes and peripheral blood	13.9 µl BV stain buffer 0.5 µl anti-CD71-PE 1 µl anti-CD45.2-BV711 1 µl anti-B220-BV421 1 µl anti-CD11b-PE-Cy7 1 µl anti-Gr1-AF700 1 µl anti-CD3-BV511 0.5 µl anti-Ter119-AF647 0.2 µl viability dye eF780 20 µl per 5 x 10^6 cells
HSPC staining	*Fubp1VavCre* BMMNCs	20 µl BV stain buffer 1 µl anti-CD19-Biotin 1 µl anti-B220-Biotin

	1 µl anti-Mac1-Biotin 1 µl anti-Gr1-Biotin 1 µl anti-CD41-Biotin 1 µl anti-Ter119-Biotin 1 µl anti-CD3-Biotin 2 µl anti-Sca1-BV510 2 µl anti-CD48-FITC 3 µl anti-cKIT-PE-Cy7 3 µl anti-CD150-PE 3 µl anti-CD16/32-V450
	40 µl per 2 x 10^7 cells

7.1.11 Nicoletti assay

The Nicoletti assay allows the concomitant assessment of cell cycle phases and cell viability by flow cytometry. For analysis cells are permeabilized to allow the fluorescent dye propidium iodide (PI) to enter the cells. PI stoichiometrically intercalates into DNA, so that the measured fluorescence correlates with the amount of DNA within the cells. As the DNA is doubled during the cell cycle, the measured amount of fluorescence/DNA reflects the different phases G_0/G_1 (single chromosome set), G_2/M (doubled chromosome set) and S (intermediate amount of DNA). Dead cells appear as a population with reduced fluorescence, as their DNA is partially degraded and/or diffusing out of the cells [161], [217].

To assess the cell cycle and viability of MCF-7 and MDA-MB 453 cells, 2.5 x 10^5 cells were seeded per 3 cm dish. After 48 hours, cells were UV-irradiated at the indicated doses. 24 hours after irradiation, cells were harvested: they were detached and singularized by adding 200 µl trypsin (0.05%) for five minutes, before 2 ml medium were added and cells were scraped off the dishes and transferred into FACS tubes. After addition of 2 ml PBS, cells were centrifuged for 5 min at 1,800 rpm and 4°C. The supernatant was aspired and the pellet was resuspended in 1 ml ice cold 70% EtOH, which was added in drops under simultaneous vortexing. Cells were stored for at least 24 hours at 4°C to allow complete fixation. For PI staining, sample tubes were filled with 3 ml sodium citrate (38 mM, pH 7.4) and centrifuged for 5 min at 1,800 rpm and 4°C. The cell pellet was resuspended in 200 µl staining buffer and incubated for 20 min in the dark. After addition of 1 ml sodium citrate, cells were analyzed with a *BD FACSCalibur* (*BD Biosciences*).

7.1.12 Fluorescence activated cell sorting (FACS)

Flow cytometry assesses light scattering and fluorescence of cells. Droplets containing single cells can be electrically charged dependent on the scattering and fluorescent characteristics of the included cell and subsequently diverted into specific tubes. This way, defined cell populations can be isolated. Successfully transduced MCF-7 cells expressing GFP were sorted prior to alamar blue assays. 7 days after transduction, cells were detached, singularized by trypsin digestion and transferred into FACS tubes. Cells were washed with 3 ml PBS and pelleted by centrifugation at 1,500 x g and 4°C for five minutes. The cell pellet was resuspended in FACS buffer with a maximal concentration of 1 x 10^7 cells/ml. Subsequently, GFP expressing cells were sorted into round-bottomed PP tubes. Sorting was performed in the institute´s intern FACS core unit.

7.1.13 Alamar Blue assay

The alamar blue assay assesses cell viability and metabolic activity by measuring the reduction of resazurin. Resazurin is a blue non-fluorescent, non-toxic compound that in presence of electron-donors is reduced to the pink fluorescent resorufin. Production of resorufin in cultured cells (that is colorimetrically detected) is the result of either reductive metabolites (NADPH, NADH, FADH, FMNH) or cytochromes within enzymes (mostly dehydrogenases) and thus reflects metabolic activity and viability of the cells [218].

To test the viability of *AVEN* knockdown, overexpressing and control cells, 6 x10^3 transduced MCF-7 cells per well were seeded into a 96-well plate in medium without phenol red. 24 hours after seeding, 10 µl alamar blue solution were added per well, and absorbance of 420 nm was measured hourly using an elisa reader (*SPECTRAmax™ 340*, *Molecular Devices*). To analyze the effect of estrogen on cell viability, cells were grown in medium supplemented with charcoal-stripped FCS to deprive exogenous hormones. Seeded cells were allowed to adhere and then treated with 17β-estradiol (10nM). Alamar blue reduction was measured 24 hours after estrogen treatment. Cell viability under apoptosis-inducing conditions was tested by irradiating the cells (20mJ/cm^2) one hour prior to alamar blue addition or by Mitomycin C treatment (4 µg/ml) 24 hours prior to alamar blue addition.

7.2 Molecular Biology

7.2.1 Transformation

Plasmid DNA is cloned by transferring it into competent bacteria, in which it is duplicated during bacterial proliferation. The process of this DNA transfer is termed transformation. Bacteria used for cloning need to be competent, meaning they have to be able to take up foreign DNA. Competence occurs both naturally and can be induced by chemicals and electric pulses.

For the amplification of plasmids, 20 ng plasmid DNA were mixed with 50 µl DH5α *E. coli* bacteria chemically rendered competent. The bacteria were incubated for 30 min on ice and then placed on a 43°C heat block for 45 s to activate heat-shock-induced uptake of plasmid DNA. Subsequently, the bacteria were placed on ice for one additional minute. 600 µl LB medium were added, and samples were shaken at 37°C and 300 rpm for at least 30 min. Bacterial cells were pelleted by centrifugation for 1 min at 8,000 rpm. The pellet was resuspended in 50-150 µl of LB medium and plated on LB agar plates containing the appropriate antibiotic for selection. The plates were incubated over night at 37°C.

7.2.2 Mini Plasmid DNA Extraction

Single colonies grown on LB agar plates after transformation were picked and transferred into 3 ml LB medium containing the appropriate antibiotic for selection. Bacteria were grown over night at 37°C, shaking at 130 rpm. 1.5 ml of the overnight culture were transferred into 1.5 ml tubes, and bacteria were pelleted at 13,000 rpm for 2 min. The pellet was resuspended in 100 µl ice-cold GTE buffer. 200 µl freshly prepared lysis buffer were added and then mixed by inverting five times. After addition of 150 µl ice-cold neutralization buffer, the samples were thoroughly mixed by vortexing and incubated for 5 min on ice. Cell debris was pelleted at 13,000 rpm for 5 min. The supernatant was transferred into fresh 1.5 ml tubes, and 1 ml 100% EtOH was added to precipitate DNA. Precipitated DNA was pelleted at 13,000 rpm for 10 min. The pellet was washed with 1 ml 70% EtOH, and DNA was again pelleted at 13,000 rpm for 10 min. After removal of the supernatant, the DNA pellet was shortly air dried and then resuspended in 30 µl ddH_2O containing 50 µg/ml RNAse A.

7.2.3 Large scale (Maxi) Plasmid DNA Extraction

Single colonies of transformed bacteria were picked and transferred in 250 ml LB medium containing the appropriate antibiotic for selection. Bacteria were grown over night at 37°C, shaking at 130 rpm. Plasmid DNA was extracted using the *QIAGEN Plasmid Purification* Kit according to the manufacturer´s manual. DNA yield was quantified by UV spectrophotometry using the *Nanodrop™ 1000*.

7.2.4 Agarose Gel Electrophoresis

Agarose gel electrophoresis separates DNA molecules according to size. The agarose gels consist of a polymerized agarose grid, with spacing dependent on the particular agarose concentration. The phosphate backbone confers a negative charge to DNA. Consequently, DNA that is placed into the wells of an agarose gel within a electrophoresis chamber filled with buffer will move to the anode. As small DNA fragments pass the agarose grid more easily than large fragments, the position of the DNA within the gel corresponds to the size of the molecule. The size in base pairs (BP) can be determined by comparing the position of the DNA sample with a DNA ladder marker which contains DNA fragments of distinct size. DNA in an agarose gel can be visualized using ethidium bromide (EtBr). Intercalation of EtBr in DNA significantly increases fluorescence of EtBr after excitation with UV light. Thus, EtBr-stained DNA lights up when exposed to UV light [219].

For the preparation of agarose gels, 0.8 – 2% agarose were dissolved in TAE buffer under heating, and 0.5 µg/ml EtBr were added. Electrophoresis was performed in TAE-filled chambers at 90-120 V for a time period sufficient for clear DNA separation.

7.2.5 Analytical DNA restriction digest

Bacterial restriction endonucleases recognize and cut foreign DNA at specific sites – a mechanism that protects bacteria from infection. As the cleavage by restriction endonucleases creates specific DNA fragments of distinct size, the enzymes are used in the laboratory to test DNA for the presence and integrity of a sequence of interest [220].

1 µg plasmid DNA was digested for 90 min at 37°C in a total reaction volume of 20 µl. After addition of DNA loading dye, DNA fragments were separated by agarose gel

electrophoresis.

7.2.6 Sequencing

Sequence integrity of cloned plasmids and the purchased conditional *FUBP1* "knockout first" vector were confirmed by sequencing. Sequencing was performed by *GATC Biotech AG*, and a premix of plasmid DNA and primers was prepared according the companies instructions.

7.2.7 Cloning of lentiviral *FUBP1* knockdown plasmids

The sequences of oligonucleotides encoding shRNA directed against human *FUBP1*, including *AgeI* and *EcoRI* restriction site overhangs, were obtained from *The RNAi Consortium* (TRC) library available at *Sigma-Aldrich Chemie GmbH*. 5 µl of 100 µM forward and reverse oligonucleotides were mixed with 40 µl annealing buffer and subjected to the following temperature program:

***Table 7.3**: Temperature protocol for oligonucleotide annealing*

temperature	time
95 °C	4 min
75 °C	4 min
70 °C	10 min
37 °C	20 min
10 °C	15 min
4 °C	∞

2 µl of annealed oligonucleotides were phosphorylated using 1 µl of T4 PNK, 1 µl of T4 PNK buffer, and 1 µl of 1 mM ATP in a total volume of 10 µl. Samples were incubated for 30 min at 37°C. T4 PNK was subsequently inactivated at 70°C for 10 min.
30 µg *pSuper* were linearized with 1 µl *HindIII*-HF in a total volume of 30 µl, incubated for 2 hours at 37°C. The digestion buffer was eliminated using the *QIAqick gel extraction kit* according to the manufacturer´s manual. The purified linearized vector was digested with *BglII* in a total volume of 50 µl and incubated for 2 hours at 37°C. To avoid auto-ligation of the vector backbone, 1 µg of digested vector were dephosphorylated with 1 µl of Antarctic Phosphatase in a total volume of 20 µl. Dephosphorylation was performed at 37°C for 30 min, and subsequently, the phosphatase was inactivated at 80°C for 2 min.

100 ng of phosphorylated, annealed oligonucleotides and 50 ng of dephosphorylated, digested *pSuper* were ligated using 1 µl of T4 ligase in a total volume of 10 µl and incubated at RT for 1 hour. The whole ligation preparation was transferred in DH5α *E. coli* bacteria for transformation as described in **7.2.1**.
Plasmid mini DNA preparations from transformed bacteria colonies were tested for correct ligation by analytical restriction digest using *EcoRI* and *HindIII*. DNA fragments were separated by agarose gel electrophoresis (2% agarose gel, 290 bp fragments for correctly ligated plasmids). Positively tested clones were used for large scale plasmid preparation.
20 µg of *pSuper*-containing shRNA insert were digested with *SmaI* in a total volume of 50 µl for three hours at 25°C. The samples were cleared from reaction buffer using the *QIAquick gel extraction* kit according to the manufacturer´s manual. The purified DNA was digested using 2 µl *HincII* in a total volume of 50 µl, followed by an incubation for 2 hours at 37°C. The digested plasmid DNA was electrophoretically separated on a 2% agarose gel. The 316 bp fragment containing the shRNA coding sequence under the control of the *pSuper* encoded *H1* promoter was isolated with the *QIAquick gel extraction* kit according to the manufacturer´s manual.
10 µg *pSIEW* were digested with 1 µl *SnaBI* in a total volume of 20 µl for 2 hours at 37°C. The linearized vector was dephosphorylated as described above. The 316 bp fragment was ligated into the *pSIEW* backbone using T4 ligase as described above. The ligation preparation was transferred into DH5α *E. coli* bacteria for transformation. Mini plasmid DNA preparations from transformed bacteria were tested by analytical restriction digest using *EcoRI*. Positively tested preparations were additionally sequenced to confirm plasmid sequence integrity and then used for large scale plasmid preparations.

7.2.8 Genomic DNA extraction

Genomic DNA from mice was extracted from mouse tail tips for genotyping using the *DNeasy Blood and Tissue Kit* according to the manufacturer´s instructions.
For quick DNA extraction, tissue samples were transferred in 80 µl lysis buffer and incubated for 20 min at 95°C. Samples were placed on ice for 1 min, then 80 µl of neutralization buffer were added. The mixture was transferred to *DNeasy Mini spin columns*, and DNA was isolated according to the *DNeasy blood and tissue* kit manual.

7.2.9 Polymerase Chain Reaction (PCR)

The polymerase chain reaction (PCR) allows the amplification of specific DNA

sequences. The reaction starts with the denaturation of double stranded DNA at high temperatures. When the temperature decreases, short DNA molecules with a sequence complementary to the ends of the forward and backward strand of the DNA fragment of interest, the so called primers, anneal at the specific complementary sites. The annealed primer serves as a starting point for the synthesis of a new DNA strand complementary to the template, which is catalyzed by a heat-stable polymerase. This elongation is performed at the temperature of optimal polymerase activity. Repeating this reaction cycle leads to the exponential amplification of a specific DNA fragment [221].

PCR conditions are shown in **table 7.4**. If two reverse primers but only one forward primer were used, concentrations would be reversed. In case only one forward and backward primer were used, 2 µl of each and 3 µl ddH_2O were added. PCR products were analyzed by gel electrophoresis after addition of DNA loading dye.

***Table 7.4**: Master mix composition and temperature protocol for PCR*

Reaction Mix		**Temperature Cycle**		
Substance	**Volume**	**Temperature**	**Time**	**Repeats**
Template DNA	5 µl	94 °C	2 min	1
Primer for 1	0.8 µl	94 °C	15 sec	35
Primer for 2	0.8 µl	60 °C	15 sec	
Primer rev	1.2 µl	72 °C	2 sec	
Red HS Taq Master Mix	10 µl	72 °C	1 min	1
ddH_2O	2.2 µl	4 °C	∞	

7.2.10 RNA isolation

To prepare cells for RNA extraction, cells were detached by trypsin digestion if necessary, washed with PBS once and then pelleted at 1,500 x g and 4°C for 5 min. The cell pellet was stored at -80°C if RNA extraction was not performed subsequently.
To extract RNA from mouse organs, the tissue was shock frozen and then crushed to powder using a mortar filled with liquid nitrogen. The tissue powder was stored at -80°C if RNA extraction was not performed subsequently.
RNA was isolated from pelleted cells or tissue powder using the *RNeasy Mini Kit* (*Qiagen*) according to the manufacturer´s instructions. Cells were homogenized on *QIAshredder* columns (*Qiagen*), and DNA was eliminated from the samples by an on-column DNase I digest using the *RNAse-Free DNase Set* (*Qiagen*). RNA was eluted in

30 µl RNase-free water and its yield was determined with the *NanoDrop™ 1000* spectrophotometer. RNA was stored at -80°C.

7.2.11 cDNA synthesis

To quantify mRNA levels, isolated RNA was reversely transcribed to cDNA using the *Omniscript Reverse Transcription Kit* (Qiagen): 1.5 µg RNA were transcribed in a total reaction volume of 20 µl, including 0.5 mM of each dNTP, 1 µM *Oligo-dT primer* (*Qiagen*), 5 µM *Thermo Scienrific™ Random Hexamer Primer* (Lifer Technologies), 10 units *Thermo Scientific™ RiboLock™ RNase Inhibitor* (*Lifer Technologies*) and 4 units *Omniscript Reverse Transcriptase*. Reverse transcription was performed at 37°C for one hour. To test for DNA contamination, one sample containing ddH_2O instead of reverse transcriptase was prepared for each experiment. cDNA was stored at -20°C.

7.2.12 Gene expression analysis by quantitative real-time PCR (qPCR)

To quantify the amount of a specific DNA sequence within a sample, PCRs can be performed in the presence of specific fluorescent dyes like SYBR® Green. These dyes are integrated in the newly synthesized DNA, which changes their fluorescent performance. The fluorescence of integrated dyes is detected simultaneously with the PCR reaction. At the beginning of the PCR, DNA synthesis and thus the measured fluorescence increase exponentially, mostly independent of external factors such as substrate availability. In this phase, the reaction cycle at which the fluorescence exceeds a certain threshold (CT value) reflects the amount of template DNA: the more template was present at the beginning of the reaction, the earlier the threshold is reached.
To analyze gene expression, mRNA that was transcribed to cDNA is quantified by qPCR. To compensate variations in the quality and yield of isolated RNA and synthesized cDNA, a reference gene that is supposed to be stably expressed is amplified along with the gene of interest. Target gene expression is then quantified relative to the reference gene [222].

For gene expression analysis, cDNA derived from isolated RNA was amplified using *SYBR® Select Master Mix* (*Life Technologies*) and primers at concentrations shown in **table 7.5**. cDNA was diluted 1:2 to 1:3 to keep CT values between 15 and 30. The reaction mix was filled in 96-well qPCR plates (*4titude*); the plates were sealed with adhesive covers and shortly centrifuged prior to the measurement at the *LightCacler 480* (*Roche*). Melting curves were recorded as quality control, and qPCRs were performed in

technical duplicates. The temperature program is shown in **table 7.5**.

Measured CT values were used to calculate the relative abundance of the target gene according to the $2^{-\Delta\Delta CT}$ method as described by Livak and Schmittgen [223]. The relative abundance was calculated as follows:

$$\text{relative abundance} = 2^{-[\Delta C_T \text{sample} - \Delta C_T \text{mock}]}$$
$$\text{with } \Delta C_t = \Delta C_T(\text{taget gene}) - \Delta C_T(\text{reference gene})$$

***Table 7.5**: Master mix composition and temperature protocol for qPCR*

Reaction Mix		**Temperature Cycle**			
Substance	**Volume**	**Step**	**Temperature**	**Time**	**Repeats**
cDNA (diluted)	2 µl	UDG activation	50 °C	2 min	–
Primer for (10 µM)	0.6 µl	Initial denaturation	95 °C	2 min	–
Primer rev (10 µM)	0.6 µl	Quantification	95 °C	15 sec	40
SYBR® Select Master Mix (2x)	10 µl		57 °C	15 sec	
Nuclease-free H_2O	6.8 µl		72 °C	1 min	
total	20 µl	Melting curve	50 °C	10 sec	–
			+ 2.2 °C until 95 °C	10 sec per step	
			4°C	∞	

7.2.13 Photometric determination of DNA, RNA and protein concentration and purity

Proteins and nucleic acids absorb ultraviolet (UV) light with absorption maxima at different wavelengths. Light absorption of proteins is based on light absorption by aromatic amino acid residues, mainly tyrosine and tryptophan, which results in an absorption maximum at 280 nm. In DNA and RNA, purine and pyrimidine bases absorb light at 260 nm. The extent of light absorption in a sample correlates with the amount of proteins and DNA/RNA. Thus, absorption measurement can be used to determine DNA, RNA and protein concentrations. Furthermore, the ratio of absorption at 260 nm and 280 nm gives information obout the purity of isolated proteins or DNA and RNA.
UV absorption of isolated RNA, DNA and protein was measured using the *NanoDrop™*

1000 spectrophotometer (*Thermo Fischer Scientific*) according to the manufacturer´s manual.

7.2.14 PCR based site-directed mutagenesis

Point mutations, deletions and insertions can be introduced at specific sites of plasmid DNA using PCR. The desired modification is encoded in the primers that are used for the amplification of the whole plasmid. Mismatching will not inhibit primer annealing as long as a sufficient number of correctly matched nucleotides (24-30 nt) is present. Thus, PCR amplification produces DNA with the primer-encoded mutations. Primers are designed to bind back to back to the template plasmid and they have phosphorylated 5´ends. Thus, mutated linearized PCR products can be directly ligated to complete plasmid molecules. Prior to ligation, initial DNA without mutation and molecules with only one mutated strand can be eliminated by *DpnI* digestion. This enzyme digests DNA marked by the methylation pattern of most *E. coli* strains, in which plasmids have been cloned (*Phusion Site-directed mutagenesis* manual, *Thermo Fisher Scientific*).

Point mutations within the *FUBP1* promoter in the luciferase reporter vector were introduced using the *Phusion Site-directed Mutagenesis Kit* (*Thermo Scientific*) with the following primers:

***Table 7.6**: Sequences of primers used to introduce site-specific mutations*

Mutation	Primer	Sequence from 5´to 3´
GATA M1	Primer for	CCTGCAGGAACAATTACCCAGC
	Primer rev (mutated)	GTGGTGGGT**A**A**TA**GTGGCCAGTTGA
GATA M2	Primer for	CCTGCAGGAACAATTACCCAGC
	Primer rev (mutated)	GTGGTGGGT**GCTA**GTGGCCAGTTGA

Mutated plasmids were used for transformation as described in section **7.2.1**. Maxi plasmid preparations were sent to sequencing to confirm the intended mutation.

7.2.15 Luciferase assay

Luciferase from the firefly *Photinus pyralis* catalyzes the light emitting two-step reaction of luciferin to oxyluciferin in the presence of ATP and Mg^{2+}. If the luciferase gene is cloned under the control of a promoter of interest, promoter activation can be measured by detecting light emission: the enzymatic activity of the reporter protein is approximately

proportional to the activity of the promoter [224].

Luciferase assays were used to test the effect of point mutations within the *FUBP1* promoter on TAL1 mediated promoter activation. 1 x 10^5 HEK293T cells per well were seeded into a 24-well plate and cultured for 24 hours. Cells were transfected with luciferase reporter plasmids, *TAL1* and *E47* expression plasmids and β-Galactosidase reporter plasmids as described in section **7.1.6**. 48 hours after transfection, cells were harvested in 500 µl PBS and pelleted by centrifugation at 2,000 rpm and RT for 3 min. Cell pellets were resuspended in 110 µl lysis buffer II and incubated on ice for 15 min. After centrifugation at 2,000 rpm and RT for 2 min, the supernatant was transferred in fresh reaction tubes. 10 µl of lysate per well were pipetted into a 96-well plate and mixed with 90 µl luciferin buffer. Bioluminescence was detected using a *LUMIstar Galaxy* microplate reader (*BMG Labtech*). Every measurement was performed in technical duplicates.
Recorded luminescence was normalized to the activity of the co-transfected β-Galactosidase, thereby taking transfection efficiency into account. To assess β-Galactosidase activity, 5 µl of cell lysate per well were filled into a 96-well plate and mixed with 95 µl substrate buffer. Lysates were incubated at RT for 5 to 30 min. As soon as a yellow stain of the sample was observed, absorbance at 420 nm was measured with a *SPECTRAmax™ 340* (*Molecular Devices*).

7.2.16 Differential gene expression analysis with *TaqMan® Array 96-Well Fast Plates*

TaqMan® Array 96-Well Fast Plates (*Applied Biosystems*) provide gene-specific primers spotted in wells of a 96-well plate. By applying cDNA and reaction master mix, expression of 92 target genes and 4 housekeeping genes can be quantified.
K562 cells were transduced with control shRNA or shRNA targeting *FUBP1* mRNA as described in **7.1.9**. 9 days after transduction, protein and RNA were isolated as described in **7.2.10** and **7.3.1**. Efficient knockdown (>80%) of FUBP1 expression was confirmed by western blotting. Isolated RNA was transcribed in cDNA (section **7.2.11**) and used with *TaqMan® Array 96-Well Fast Plates* for analysis of the human erythropoietin pathway according to the manufacturer´s instructions. The qPCR reactions were run on a *StepOne Plus™* system (*Applied Biosystems*) under standard cycling conditions. Gene expression was calculated relative to the mean of *18S*, *GUSB* and *HPRT1* expression. Expression of *GAPDH* was excluded from normalization as it seemed to be affected by *FUBP1* expression levels.

7.2.17 Differential gene expression analysis by RNA sequencing

K562 cells were transduced with control shRNA or shRNA directed against *FUBP1* as described in **7.1.9**. 9 days after transduction, cells were harvested. 3 x 10^5 cells were pelleted by centrifugation at 1,200 x g and 4°C for 5 min. The pellet was resuspended in 1 ml *TRIzol™ Reagent* (*Invitrogen*) and stored at -80°C. 1 x 10^6 cells were used for protein isolation as described in **7.3.1**. Efficient *FUBP1* knockdown (>80%) was confirmed by western blotting. Cells dissolved in trizol were sent to the *Transcriptome and Genome Analysis Laboratory (TAL)* in Göttingen for sequencing. Sequence data analysis was performed independently by *TAL* and Birgitta Michels (GSH, AG Farin).

7.3 Protein biochemistry

7.3.1 Protein extraction

To isolate proteins, cells were harvested and pelleted by centrifugation at 1,500 x g and 4°C for 5 min. The cell pellet was resuspended in 150 µl RIPA lysis buffer per 1 x 10^6 cells and incubated on ice for 40 min. Cell debris was pelleted at 13,000 rpm and 4°C for 10 min. The supernatant containing proteins was transferred in fresh tubes, and the protein concentration was quantified (sections **7.2.13**, **7.3.2**). Protein lysates were stored at -80°C.

7.3.2 Bradford Assay

The absorption maximum of Coomassie brilliant blue shifts from 365 nm to 595 nm upon binding to proteins. Thus, an absorption measurement at 595 nm can be used to determine protein concentrations [225].
5 µl of protein lysate were diluted in 800 µl ddH_2O. 200 µl Bradford reagent were added and samples were mixed thoroughly. The mixture was transferred in cuvettes and incubated for 5 min at RT. Absorption at 595 nm was measured with a *SmartSpec™ 3000* spectrophotometer (*BioRad Laboratories*). The protein concentration was calculated by the device according to a BSA standard curve.

7.3.3 SDS-PAGE

Sodium dodecyl sulfate (SDS) polyacrylamide gel electrophoresis (PAGE) separates proteins according to their stokes radius, which reflects their size. SDS binds to proteins, leading to the interruption of protein interactions and denaturation of protein structure. As SDS has a strong negative charge, the protein inherent charge is covered and has no significant impact on the movement through the gel to the anode. Differences in the running speed result from different protein sizes, as small proteins pass the gel grid more easily. Thus, the position on the gel can be correlated to protein size [226].
12% running gels and 2.5% stacking gels with a thickness of 1.0 mm were used for SDS-PAGE (**table 7.7**). Protein lysates were diluted with ddH_2O and SDS sample buffer to a concentration of 5 µg/ml and heated for 5 min at 95°C. 30 to 50 µg protein were loaded per pocket. 18 µl protein marker (*BenchMark Pre-Stained Protein Ladder*, *Invitrogen*) were loaded as size reference. Electrophoresis was performed in SDS running buffer filled *Protean II System* (*Biorad*) chambers. A voltage of 80 V was applied until the samples reached the running gel, then the voltage was increased to 130 V. When the protein marker showed the desired band separation, electrophoresis was stopped and the gels were used for western blotting.

***Table 7.7**: Protocol for the preparation of SDS stacking and running gels. Preparations are sufficient for two gels*

Component	2.5% stacking gel	12% running gel
ddH_2O	5.52 ml	5.25 ml
Tris-HCl pH 6.8 (1.5 M)	925 µl	–
Tris-HCl pH 8.8 (1 M)	–	3.75 ml
Acrylamide/Bisacrylamide (37.5 : 1)	1.25 ml	6 ml
SDS (20% w/v)	37.5 µl	75 µl
APS (10% w/v)	100 µl	100 µl
TEMED	10 µl	10 µl

7.3.4 Western blotting

7.3.4.1 Blotting

The transfer of proteins within an SDS gel onto an adsorbing membrane is termed

blotting. Negatively charged proteins move to the anode within a blotting chamber until they reach the membrane which adsorbs them via hydrophobic interactions [227]. Blotting was performed in a semi-dry manner. In blotting buffer activated nitrocellulose membranes were placed on three blotting buffer-soaked whatman filter papers on the anode face of a *Keutz* blotting chamber. The SDS gel containing the separated proteins was laid on top of the membrane, and air bubbles were carefully removed. Another three blotting buffer-soaked whatman filter papers were placed on top of the gel. Blotting was performed at 55 mA per membrane for 2 hours. After blotting, the membrane was stained with PonceauS solution to confirm successful protein transfer. The membranes were destained in distilled water before immunodetection of proteins.

7.3.4.2 Immunodetection of blotted proteins

Blotted proteins were detected by antibodies recognizing specific antigens within the protein. Antigen-bound primary antibodies are visualized by reporter-tagged secondary antibodies, which interact with the constant part of primary antibodies of a distinct species. A commonly used reporter tag is horse radish peroxidase (HRP). HRP catalyzes the oxidation of luminol under release of luminescence. Luminescence is detected on photosensitive films [227].

Membranes were incubated in 3% milk solution for 1.5 hours at RT to block unspecific binding sites. Primary antibodies were diluted in milk solution as indicated in *Materials*. Blocked membranes were incubated in primary antibody solution for 1 h at RT or overnight at 4°C. Free antibodies were removed by washing the membranes three times in TBS-T for 10 min. Secondary antibodies were diluted in milk solution (*Materials*), and membranes were incubated in secondary antibody solution for one hour at RT. After three washes in TBS-T for 10 min, 500 µl of chemiluminescence reagent were applied per membrane. After 2 min of incubation in case of *Amershan ECL* (*GE Healthcare*), and 5 min of incubation in case of *SuperSignal™ West Pico PLUS* (*Thermo Fisher*), chemiluminescence was detected on photosensitive films. Housekeeping proteins were detected as loading control.
For the quantification of protein expression, chemiluminescence was detected and quantified with the *Fusion Fx* system (*Vilber Lourmat*). Quantified signals of target proteins were normalized to the signals of housekeeping proteins.

7.3.5 Chromatin immunoprecipitation (ChIP)

Using chromatin immunoprecipitation (ChIP), interactions between proteins and genomic

DNA can be analyzed. Protein-DNA interactions are captured by cross-linking. Subsequently, chromatin is fragmented and isolated, and antibodies are used to precipitate the proteins of interest. If the protein was close enough to or interacting with DNA, the cross-linked DNA fragment is precipitated along with the protein. After purification of the precipitated protein-DNA adducts, crosslinks are reversed by heating, and proteins are removed by proteinase K digest. Isolated DNA fragments can then be identified and quantified by PCR. Thus, the sites of DNA binding and the frequency of DNA binding of proteins can be determined [228].

24 hours before cells were harvested for ChIP, the medium was exchanged to allow optimized growth of the cells. The crosslinking and immunoprecipitation procedure based on the ChIP (X-ChIP) protocol provided by *abcam* was used as described in the following. 467 µl formalin (*PierceTM 16% Formaldehyde*, *Thermo Fisher,* final concentration 0.75%) were added in drops to 10^7 cells in 10 ml medium under shaking. After incubation for 10 min at RT under gentle rotation, cross-linking was stopped by adding glycine to a final concentration of 125 mM to the medium (1,275 µl 1 M glycine). After another incubation period of 5 min at RT under gentle rotation, cells were pelleted by centrifugation at 1,200 x g and 4°C for 5 min. Cells were washed three times with 10 ml ice-cold PBS and centrifuged at 1,200 x g, 4°C for 5 min. The pellet was resuspended in 600 µl lysis buffer (supplemented with protease inhibitors). 300 µl aliquots were transferred into 1.5 reaction tubes and incubated on ice for 1 hour. During the incubation time, the tubes were vortexed several times. Chromatin was fragmented by sonication via a *Bioruptor® Plus* device (*diagenode*). 10 to 15 cycles of sonication (high setting) were performed, each with 30 s sonication followed by a 30 s break. Large DNA fragments and cell debris were removed by centrifugation at 8,000 x g and 4°C for 10 min. The supernatant was transferred in fresh tubes. The size of DNA fragments was tested by electrophoresis on a 1.5% agarose gel. If a considerable amount of DNA fragments exceeded the desired fragment size of 200 to 1,000 bp, further cycles of sonication were performed. Chromatin fragments were stored at -80°C.

Proteins were precipitated using specific antibodies and magnetic protein G beads (*Dynabeads*, *Invitrogen*). 50 µl protein G beads were resuspended in 300 µl RIPA buffer and placed on a magnetic rack. The supernatant was removed, and beads were resuspended in 270 µl RIPA buffer and 30 µl *Roti®-Block* (*Roth*). Beads were rotated at 20 rpm and 4°C for one hour. After blocking, beads were washed twice with 300 µl RIPA buffer and then resuspended in 300 µl RIPA buffer. Beads were stored for up to three days at 4°C.

60 to 80 µl of chromatin were used per precipitation. In each experiment, one aliquot of chromatin was used for IgG precipitation as the isotype-matched negative control. One

aliquot of chromatin was stored as the input sample. Specific antibodies and IgG were diluted in RIPA$^+$ buffer (RIPA buffer supplemented with 0.1% SDS) at concentrations indicated in *Materials*. Diluted antibodies and IgG were mixed with chromatin, protease inhibitors and 25 µl blocked protein G beads in low attachment 1.5 ml tubes. RIPA$^+$ buffer was added to a final volume of 500 µl. Precipitation was performed over night at 4°C under rotation.

Tubes were placed on a magnetic rack and the supernatant was carefully removed. Beads were equilibrated in 600 µl ChIP wash buffer for one minute and subsequently washed three times for 10 min in 600 µl ChIP wash buffer at 4°C under rotation. The beads were then equilibrated in 600 µl Final ChIP Wash Buffer for one minute, followed by three washes for 10 min in 600 µl Final ChIP wash buffer at 4°C under rotation. Residual Final Wash Buffer was carefully removed, and beads were resuspended in 120 µl elution buffer. Bound proteins were eluted by incubating the cells for 30 min at 30°C and 1,000 rpm. Tubes were placed on the magnetic rack, and the supernatant containing the eluted proteins was transferred in fresh 1.5 ml tubes. Potentially co-precipitated RNA was removed by adding RNase A (final concentration 50 µg/ml) and 10 min of incubation at 37°C and 750 rpm. 5 µl of proteinase K (20 mg/ml) were added, and cross-linking was reversed and proteins degraded for 4 to 5 hours at 65°C and 750 rpm.

DNA fragments were isolated in 40 µl elution buffer using the *ChIP DNA Clean & Concentrator* kit (*Zymo Research*) according to the manufacturer´s instructions. The isolated DNA and the input sample were analyzed by qPCR in technical duplicates as described above. Enrichment of DNA fragments was calculated relative to the input according to the following equation:

$$\text{enrichment as \% Input} = 100 \cdot 2^{(CT(\text{Input})-CT(\text{Precipitate}))}$$

7.4 Histology

7.4.1 Embryo and organ dissection

Mice were killed by cervical dislocation under isoflurane anesthesia. Organs and mammary tumors were dissected from surrounding tissue and washed in ice-cold PBS before freezing or fixing for X-Gal staining and immunohistochemistry as described below. For embryo dissection, uteri from pregnant mice were dissected and washed in ice-cold PBS. Embryos were isolated from the uterus and yolk sac and washed in ice-cold PBS to remove maternal blood. One forepaw and one hind paw were removed for

genotyping. Embryos were frozen for X-Gal staining or fixed for immunohistochemistry as described below.

7.4.2 X-Gal staining

X-Gal staining is a common method to detect expression of the *lacZ* gene-encoded reporter β-Galactosidase. This bacterial enzyme displays different catalytic activities: it cleaves lactose and allolactose and it transfers galactosyl units to lactose and allolactose. To visualize β-Galactosidase activity, the artificial glycoside X-Gal (5-Bromo-4-chloro-3-indoyl-galactopyranoside) is applied as substrate. Cleavage of the colorless chemical releases the indole compound, which dimerizes and oxidases subsequently to the blue insoluble 5,5-dibromo-4,4-dichloro-indigo [229].

Dissected mouse organs and embryos were rinsed shortly in PBS and carefully dried on paper tissue. *Cryomolds* (*Sakura*) were filled to one third with *Tissue-Tek® O.C.T.™ Compound* (*Sakura*), and embryos and organs were placed on top. Embryos and organs were completely covered with *Tissue-Tek® O.C.T.™ Compound* and placed on dry ice for freezing. After one hour, embedded tissues were stored at -20°C for 24 hours and at -80°C afterwards. 5 µm cryosections were prepared at a *Frigocut 2800* (*Reichert-Jung*) and stored at -20°C. For X-Gal staining, cryosections were fixed in 4% formalin for 5 min at RT. After two washes in Rinse Buffer for 10 min, cryosections were placed in X-Gal staining solution and incubated at 37°C for 24-72 hours. X-Gal-stained sections were counter-stained with Eosin by the institute´s histology core facility.

7.4.3 Immunohistochemistry

Dissected embryos and mammary glands were fixed in 4% formalin at 4°C for 48 hours. Paraffin embedding, immuno-staining with anti-AVEN antibody, anti-cleaved Caspase 3 antibody and anti-Ki67 antibody and counterstaining with hematoxylin were performed by the institute´s histology core facility. Single cells were identified using the *Aperio ImageScope* software (*Leica Biosystems*) and discriminated into unstained cells (blue cells), weakly stained cells (faint brown/yellow color), moderately stained cells (brown/orange color) and strongly stained cells (deep brown/dark red color). Staining was quantified by calculating the percentage of stained cells (weakly, moderately and strongly) of all identified single cells.

7.5 Generation of conditional *Fubp1* knockout mice

7.5.1 Vector preparation

The targeting vector was linearized by endonuclease digestion: 20 µg vector were digested with 5 µg *PacI* (*NEB*) in diluted *CutSmart* buffer (*NEB*) in a total volume of 50 µl. The digestion was performed for 4.5 hours at 37°C. 5 µl sodium acetate (3 M, pH 5.2) were added, and the sample was mixed thoroughly by vortexing. 137 µl pure ethanol were added and the sample was vortexed. Precipitated DNA was pelleted by centrifugation at 13,000 rpm for 15 min. The DNA pellet was washed twice in 400 µl 80% EtOH and centrifuged at 13,000 rpm for 10 min. The DNA was stored in 80% EtOH.

7.5.2 Embryonic stem cell (ESC) culture and electroporation

Murine embryonic stem cells (JM8A3) were grown on feeder cells (murine embryonic fibroblasts, inactivated by γ-irradiation, neomycin resistant). ESCs were cultured by the Transgene-Service W450 of the *German Cancer Research Center* (Heidelberg).
For electroporation, a 10 cm dish with 10^7 ESCs (65% confluent ESC colonies) was washed twice with 5 ml PBS, and cells were singularized by trypsin digestion (3 ml, 0.25% trypsin) for 2 min at 37°C. Digestion was stopped by adding 10 ml medium, and cells were centrifuged at 1,000 rpm for 5 min at RT. The cell pellet was resuspended in 1 ml PBS.
20 µg precipitated linearized target vector were resuspended in 250 µl PBS and mixed with 500 µl of the singularized ESCs. The mixture was transferred into a *Gene Pulser Cuvette* (*Bio-Rad*) and electroporized at 240 V and 500 µF using a *Gene Pulser Electroporator* (*Bio-Rad*). After electroporation, cells were incubated on ice for 20 min and then diluted in 80 ml medium. Cells were seeded on 8 x 10 cm plates with feeder cells. After 24 hours, the selection of transfected cells was started by adding G-418 at a final concentration of 300 µg/ml to the medium. The medium was changed every 24 to 48 hours, depending on the extent of cell death. After 7 to 9 days of selection, 288 ESC colonies were picked and transferred into the wells of a 48 well-plate with feeder cells. One ESC clone was seeded per well. After three days of culture, medium was soaked off the wells, and cells were carefully washed with 500 µl PBS. 150 µl trypsin (0.25%) were added per well, and cells were digested for 70 to 90 s at 37°C. Cells were singularized by pipetting up and down 6 - 10 times before adding 800 µl medium. Singularized ESCs were transferred to a new 48-well plate with feeder cells. After three

days of culture, cells were trypsinized as described above, but instead of 800 µl medium, 200 µl solution A (70% ESC medium, 30% FCS) were added. 100 µl of singularized ESCs were transferred into 1 ml medium in gelatin-coated wells of a 24-well plate. The remaining ESCs were placed on ice, 200 µl solution B (50% ESC medium, 30% FCS, 20% DMSO) were added and cells were frozen and stored at -80°C.

ESCs grown on gelatin-coated plates were cultured until they reached 80-100% confluence. To lyse cells, ESCs were carefully washed with PBS, before 500 µl lysis buffer were added per well. Cells were incubated in lysis buffer at 37°C for at least 3 hours.

To isolate DNA, 500 µl ESC lysate were transferred into 1.5 reaction tubes. 250 µl of 5 M NaCl were added, and samples were shaken vigorously by hand for 1 min. Cell debris was removed by centrifugation at 13,000 rpm and RT for 10 min. The supernatant was transferred into fresh tubes and 450 µl isopropanol were added. To precipitate the DNA, the samples were shaken vigorously by hand for 1 min. DNA was pelleted by centrifugation at 13,000 rpm and RT for 10 min and washed with 500 µl 70% ethanol. The pellet was air-dried for 3 min and then dissolved in 200 µl ddH_2O.

7.5.3 Long-range PCR

To test the isolated DNA for correct target vector integration, a long range PCR was performed using the *Expand™ Long Template PCR System* (*Roche*) with the concentrations and temperature protocol shown in **table 7.8**. Only samples that were positively tested for correct integration at the 3´-end were subsequently tested for correct integration at the 5´end.

Primers used to test the intended integration at the 5´-end and the 3´-end of the vector, respectively, are given in **table 7.9**.

***Table 7.8**: Master mix composition and temperature protocol for long-range PCR*

Master mix		**Temperature protocol**		
Component	**Volume**	**Temperature**	**Time**	**repeats**
ddH_2O	13.25 µl	94°C	2 min	–
Buffer 1	2.5 µl	94°C	10 s	10
Primer for 1	1 µl	64°C	30 s	
Primer for 2	1 µl	68°C	4 min	
Primer rev	1.5 µl	94°C	15 s	18
dNTPs	3 µl	64°C	30 s	
Enzyme mix	0.75 µl	68°C	4 min plus 20 s for each successive cycle	

DNA	2 µl	68°C	7 min	–
Total volume	25 µl	4°C	∞	–

***Table 7.9**: Sequence of primers used to detect vector integration into genomic DNA*

Primer sequences to test integration at the 5´end of the vector	
Primer for	5´-CTGGCAGGTCTCTTGAGTTT-3´
Primer rev 1	5´-GACTAACAGAAGAACCCGTTGT-3´
Primer rev 2	5´-TCTCTTCCACTCAATTCTAAGGC-3´
Primer sequences to test integration at the 3´end of the vector	
Primer for 1	5´-TGTGTGCCTTGCCATACTCAA-3´
Primer for 2	5´-CGCGTCGAGAAGTTCCTATT-3´
Primer rev	5´-CTGCACCTTACAATCCAGGAC-3´

7.5.4 Southern Blotting

Southern blotting denotes the transfer and associated immobilization of electrophoretically separated DNA fragments to a membrane. Specific DNA fragments on the gel can be visualized when a labeled probe is applied which binds complementary sequences. A commonly used protocol comprises three stages: in the first step, the DNA within the agarose gel is depurinated, denatured and neutralized by acidic and alkaline solutions. The second stage is the transfer of the DNA to a membrane via capillary forces. In the last step, the DNA is immobilized on the membrane [230].

7.5.4.1 Restriction digest of genomic DNA

To further test the integration of the target vector into the *Fubp1* locus of the ESC genome, DNA isolated from ESCs was fragmented in a restriction digest. 5 µg DNA were digested over night with 1 µl *SacI* (NEB) in a total volume of 30 µl. As the targeted region within the vector contains an additional cleavage site, correct integration of the vector results in a distinct fragmentation of the *Fubp1* locus. The digested DNA and a DNA ladder were loaded onto a 0.8% agarose gel, and electrophoresis was performed at 100 V. The position of the bands, visualized by EtBr, was recorded.

7.5.4.2 Blotting

The gel was incubated in 0.25 M HCl for 20 min and subsequently in 0.4 M NaOH for another 20 min. For blotting, a glass plate was placed on a basin filled with 0.4 M NaOH. Two wetted whatman papers were laid over the glass plate with the ends hanging into

the buffer. The agarose gel was placed on top followed by the wetted nylon membrane. Air bubbles were carefully removed and three sheets of dry whatman paper and a stack of paper tissues were added on top. The stack was finished with another glass plate and a filled 1 l flask was placed on top as weight. The transfer was performed overnight and the membrane was washed in saline sodium citrate (SSC) buffer and dried on a sheet of Whatman Paper.

7.5.4.3 Crosslinking and Hybridization

DNA was cross-linked to the membrane by UV irradiation using a *Stratalinker® 1800 UV Crosslinker* (*Stratagene*). The membrane was transferred into a hybridization tube which was filled with 20 ml pre-hybridization buffer. The membrane was incubated in the buffer at 65°C for 2.5 hours. The pre-hybridization buffer was poured off and the tube was refilled with 20 ml hybridization buffer containing the radioactive labeled probe (see below). Subsequently, the membrane was hybridized over night at 65°C.
After hybridization, the membrane was washed twice in wash buffer 1 for 20 min at 65°C. The membrane was tested for radioactivity using a Geiger counter. Depending on the extent of radioactivity, the membrane was washed for another 5 to 30 min in wash buffer 2 at 68°C. An X-Ray film was exposed to the membrane for 24-72 hours at -80°C to detect the hybridized probe.

7.5.4.4 Probe generation by preparative restriction digest

1 µg targeting vector were digested with 1 µl *EcoNI* and 1 µl *NdeI* in a total volume of 30 µl. Digest was performed for 2 hours at 37°C. The DNA fragments were electrophoretically separated in a 1.5 % agarose gel. The 604 bp fragment was isolated using the *QIAquick gel extraction kit* (*Qiagen*) according to the manufacturer´s manual.
25 ng of the isolated fragment were heated for 5 min at 95°C and then immediately cooled on ice. The fragment was used as template to generate an α-^{32}P-labelled probe. Labeling was performed with the *Random Primers DNA Labeling System* (*Life Technologies*) according to the manufacturer´s instructions. [α-^{32}P]dCTP was used for labeling. The labeled probe was purified on *NICK columns* (*Amersham*) as described in the manufacturer´s manual. TE buffer was used for equilibration, washing and elution. The purified probe was heated for 5 min on 95°C, then immediately cooled on ice and subsequently used for hybridization.

7.5.5 Injection and transplantation of targeted ESCs

ESC clones that were positively tested for the correct integration of the targeting vector

were thawed and cultured for a sufficient expansion. ESCs were then injected into blastocysts and transplanted into the uteri of pseudo pregnant foster mice. As ESCs were derived from the *C57BL/6N-A^{tm1Brd}* strain with agouti fur color and injected into *C57BL/6N* mice with black fur color, chimeric offspring was identified by a mixed agouti/black coat. ESC injection, transplantation and breeding of chimeric offspring was performed by the Transgene-Service W450 of the *German Cancer Research Center* (Heidelberg).

7.5.6 Breeding of mice with conditional *Fubp1* knockout potential

Offspring showing >70% agouti fur color were transferred to the Georg-Speyer-Haus and bred with *C57Bl/6J* mice. Germline transmission of the targeted DNA, identified in offspring with agouti fur color, was observed for animals derived from two different ESC clones. The modification of the *Fubp1* locus in these animals was confirmed by genotyping. Offspring carrying the targeted *Fubp1* allele were mated with *FLP1* recombinase-expressing deleters (*FLPeR*) to generate mice with floxed *Fubp1* exons 4 to 7. They were also mated with *Cre* expressing deleters (*CMV-Cre*) to generate mice with a constitutive *Fubp1* knockout and *lacZ* reporter gene expression.

7.6 Animal husbandry conditions

Mouse breeding and husbandry was performed under specific pathogen-free conditions in filter-top or isolated individually ventilated cages (IVCs) according to the German Animal Welfare Law. The general health status of the mice was checked daily by animal caretakers or the veterinarian. Randomly selected mice were sent to the *mfd Diagnostics GmbH* (Wendelsheim) at regular intervals for a complete health monitoring according to the *Federation of European Laboratory Animal Science Associations* (FELASA).

7.7 Statistics

The results of experiments performed in at least three replicates were statistically analyzed using *GraphPad Prism* software. Data not fulfilling normal distribution were tested for statistical significance using the non-parametric two-tailed Mann-Whitney u-test. If data passed normality test, unpaired and parametric two-tailed student's t-test

was used to calculate statistical significance. Significance calculated by both tests was defined as ***P < 0.0001, **P < 0.01, *P < 0.05.

8 Literature

1. Clarke, P.G. and S. Clarke, *Nineteenth century research on cell death.* Exp Oncol, 2012. **34**(3): p. 139-45.
2. Kerr, J.F., A.H. Wyllie, and A.R. Currie, *Apoptosis: a basic biological phenomenon with wide-ranging implications in tissue kinetics.* Br J Cancer, 1972. **26**(4): p. 239-57.
3. Elmore, S., *Apoptosis: a review of programmed cell death.* Toxicol Pathol, 2007. **35**(4): p. 495-516.
4. Galluzzi, L., et al., *Molecular mechanisms of cell death: recommendations of the Nomenclature Committee on Cell Death 2018.* Cell Death Differ, 2018. **25**(3): p. 486-541.
5. Bratton, S.B. and G.S. Salvesen, *Regulation of the Apaf-1-caspase-9 apoptosome.* J Cell Sci, 2010. **123**(Pt 19): p. 3209-14.
6. Burlacu, A., *Regulation of apoptosis by Bcl-2 family proteins.* J Cell Mol Med, 2003. **7**(3): p. 249-57.
7. Yang, J.K., *Death effecter domain for the assembly of death-inducing signaling complex.* Apoptosis, 2015. **20**(2): p. 235-9.
8. Chau, B.N., et al., *Aven, a novel inhibitor of caspase activation, binds Bcl-xL and Apaf-1.* Mol Cell, 2000. **6**(1): p. 31-40.
9. Figueroa, B., Jr., et al., *Aven and Bcl-xL enhance protection against apoptosis for mammalian cells exposed to various culture conditions.* Biotechnol Bioeng, 2004. **85**(6): p. 589-600.
10. Kutuk, O., et al., *Aven blocks DNA damage-induced apoptosis by stabilising Bcl-xL.* Eur J Cancer, 2010. **46**(13): p. 2494-505.
11. Melzer, I.M., et al., *The Apaf-1-binding protein Aven is cleaved by Cathepsin D to unleash its anti-apoptotic potential.* Cell Death Differ, 2012. **19**(9): p. 1435-45.
12. Hawley, R.G., et al., *An Integrated Bioinformatics and Computational Biology Approach Identifies New BH3-Only Protein Candidates.* Open Biol J, 2012. **5**: p. 6-16.
13. Guo, J.Y., et al., *Aven-dependent activation of ATM following DNA damage.* Curr Biol, 2008. **18**(13): p. 933-42.
14. Awasthi, P., M. Foiani, and A. Kumar, *ATM and ATR signaling at a glance.* J Cell Sci, 2015. **128**(23): p. 4255-62.
15. Zou, S., et al., *Identification of dAven, a Drosophila melanogaster ortholog of the cell cycle regulator Aven.* Cell Cycle, 2011. **10**(6): p. 989-98.
16. Gross, A., *A new Aven-ue to DNA-damage checkpoints.* Trends Biochem Sci, 2008. **33**(11): p. 514-6.
17. Thandapani, P., et al., *Aven recognition of RNA G-quadruplexes regulates translation of the mixed lineage leukemia protooncogenes.* Elife, 2015. **4**.
18. Rhodes, D. and H.J. Lipps, *G-quadruplexes and their regulatory roles in biology.* Nucleic Acids Res, 2015. **43**(18): p. 8627-37.
19. Esmaili, A.M., et al., *Regulation of the ATM-activator protein Aven by CRM1-dependent nuclear export.* Cell Cycle, 2010. **9**(19): p. 3913-20.
20. O'Shea, L.C., C. Hensey, and T. Fair, *Progesterone regulation of AVEN protects bovine oocytes from apoptosis during meiotic maturation.* Biol Reprod, 2013. **89**(6): p. 146.
21. Laurentino, S., et al., *Apoptosis-inhibitor Aven is downregulated in defective spermatogenesis and a novel estrogen target gene in mammalian testis.* Fertil Steril, 2011. **96**(3): p. 745-50.
22. Ina, S., et al., *Expression of the mouse Aven gene during spermatogenesis, analyzed by subtraction screening using Mvh-knockout mice.* Gene Expression Patterns, 2003. **3**(5): p. 635-638.
23. Cai, Z., H. Liu, and X. Wu, *Forkhead-box transcription factor 1 affects the apoptosis of natural regulatory T cells by controlling Aven expression.* BMC

Immunology, 2017. **18**(1).
24. Hanahan, D. and R.A. Weinberg, *Hallmarks of cancer: the next generation.* Cell, 2011. **144**(5): p. 646-74.
25. Paydas, S., et al., *Survivin and aven: two distinct antiapoptotic signals in acute leukemias.* Ann Oncol, 2003. **14**(7): p. 1045-50.
26. Choi, J., et al., *Aven overexpression: association with poor prognosis in childhood acute lymphoblastic leukemia.* Leuk Res, 2006. **30**(8): p. 1019-25.
27. Eissmann, M., et al., *Overexpression of the anti-apoptotic protein AVEN contributes to increased malignancy in hematopoietic neoplasms.* Oncogene, 2013. **32**(20): p. 2586-91.
28. Ouzounova, M., et al., *MicroRNA miR-30 family regulates non-attachment growth of breast cancer cells.* BMC Genomics, 2013. **14**: p. 139.
29. Baranski, Z., et al., *Aven-mediated checkpoint kinase control regulates proliferation and resistance to chemotherapy in conventional osteosarcoma.* J Pathol, 2015. **236**(3): p. 348-59.
30. Han, K.Y., et al., *Akt regulation of Aven contributes to the sensitivity of cancer cells to chemotherapeutic agents.* Mol Med Rep, 2015. **11**(5): p. 3866-71.
31. Chakrabarti, M., D.J. Klionsky, and S.K. Ray, *miR-30e Blocks Autophagy and Acts Synergistically with Proanthocyanidin for Inhibition of AVEN and BIRC6 to Increase Apoptosis in Glioblastoma Stem Cells and Glioblastoma SNB19 Cells.* PLoS One, 2016. **11**(7): p. e0158537.
32. Duncan, R., et al., *A sequence-specific, single-strand binding protein activates the far upstream element of c-myc and defines a new DNA-binding motif.* Genes Dev, 1994. **8**(4): p. 465-80.
33. Duncan, R., et al., *A unique transactivation sequence motif is found in the carboxyl-terminal domain of the single-strand-binding protein FBP.* Mol Cell Biol, 1996. **16**(5): p. 2274-82.
34. Davis-Smyth, T., et al., *The far upstream element-binding proteins comprise an ancient family of single-strand DNA-binding transactivators.* J Biol Chem, 1996. **271**(49): p. 31679-87.
35. Michelotti, G.A., et al., *Multiple single-stranded cis elements are associated with activated chromatin of the human c-myc gene in vivo.* Mol Cell Biol, 1996. **16**(6): p. 2656-69.
36. Vindigni, A., et al., *Identification of human DNA helicase V with the far upstream element-binding protein.* Nucleic Acids Res, 2001. **29**(5): p. 1061-7.
37. Benjamin, L.R., et al., *Hierarchical mechanisms build the DNA-binding specificity of FUSE binding protein.* Proc Natl Acad Sci U S A, 2008. **105**(47): p. 18296-301.
38. Braddock, D.T., et al., *Structure and dynamics of KH domains from FBP bound to single-stranded DNA.* Nature, 2002. **415**(6875): p. 1051-6.
39. Liu, J., et al., *The FBP interacting repressor targets TFIIH to inhibit activated transcription.* Mol Cell, 2000. **5**(2): p. 331-41.
40. Liu, J., et al., *Defective interplay of activators and repressors with TFIH in xeroderma pigmentosum.* Cell, 2001. **104**(3): p. 353-63.
41. Hsiao, H.H., et al., *Quantitative characterization of the interactions among c-myc transcriptional regulators FUSE, FBP, and FIR.* Biochemistry, 2010. **49**(22): p. 4620-34.
42. Zhang, J. and Q.M. Chen, *Far upstream element binding protein 1: a commander of transcription, translation and beyond.* Oncogene, 2013. **32**(24): p. 2907-16.
43. Gerlach, K., *Characterization of FUSE-Binding Protein 1 as a Hematopoietic Stem Cell Self-Renewal Factor.* 2015.
44. Rabenhorst, U., et al., *Overexpression of the far upstream element binding protein 1 in hepatocellular carcinoma is required for tumor growth.* Hepatology, 2009. **50**(4): p. 1121-9.
45. Liu, J., et al., *JTV1 co-activates FBP to induce USP29 transcription and stabilize p53 in response to oxidative stress.* EMBO J, 2011. **30**(5): p. 846-58.
46. Hauck, S., *Mechanistic studies on FUSE binding protein 1 (FUBP1) inhibition in cancer cells.* 2016.

47. Irwin, N., et al., *Identification of two proteins that bind to a pyrimidine-rich sequence in the 3'-untranslated region of GAP-43 mRNA.* Nucleic Acids Res, 1997. **25**(6): p. 1281-8.
48. Weber, A., et al., *TFIIH operates through an expanded proximal promoter to fine-tune c-myc expression.* Mol Cell Biol, 2005. **25**(1): p. 147-61.
49. Olanich, M.E., et al., *Identification of FUSE-binding protein 1 as a regulatory mRNA-binding protein that represses nucleophosmin translation.* Oncogene, 2011. **30**(1): p. 77-86.
50. Zheng, Y. and W.K. Miskimins, *Far upstream element binding protein 1 activates translation of p27Kip1 mRNA through its internal ribosomal entry site.* Int J Biochem Cell Biol, 2011. **43**(11): p. 1641-8.
51. Chien, H.L., C.L. Liao, and Y.L. Lin, *FUSE binding protein 1 interacts with untranslated regions of Japanese encephalitis virus RNA and negatively regulates viral replication.* J Virol, 2011. **85**(10): p. 4698-706.
52. Zhang, Z., D. Harris, and V.N. Pandey, *The FUSE binding protein is a cellular factor required for efficient replication of hepatitis C virus.* J Virol, 2008. **82**(12): p. 5761-73.
53. Huang, P.N., et al., *Far upstream element binding protein 1 binds the internal ribosomal entry site of enterovirus 71 and enhances viral translation and viral growth.* Nucleic Acids Res, 2011. **39**(22): p. 9633-48.
54. Dixit, U., et al., *FUSE Binding Protein 1 Facilitates Persistent Hepatitis C Virus Replication in Hepatoma Cells by Regulating Tumor Suppressor p53.* J Virol, 2015. **89**(15): p. 7905-21.
55. Jacob, A.G., et al., *The splicing factor FUBP1 is required for the efficient splicing of oncogene MDM2 pre-mRNA.* J Biol Chem, 2014. **289**(25): p. 17350-64.
56. Miro, J., et al., *FUBP1: a new protagonist in splicing regulation of the DMD gene.* Nucleic Acids Res, 2015. **43**(4): p. 2378-89.
57. Hwang, I., et al., *Far Upstream Element-Binding Protein 1 Regulates LSD1 Alternative Splicing to Promote Terminal Differentiation of Neural Progenitors.* Stem Cell Reports, 2018. **10**(4): p. 1208-1221.
58. Steiner, M., et al., *FUSE Binding Protein 1 (FUBP1) expression is upregulated by T-cell acute lymphocytic leukemiea protein 1 (TAL1) and required for efficient erythroid differentiation.* 2018.
59. Kim, M.J., et al., *Downregulation of FUSE-binding protein and c-myc by tRNA synthetase cofactor p38 is required for lung cell differentiation.* Nat Genet, 2003. **34**(3): p. 330-6.
60. Ko, H.S., et al., *Identification of far upstream element-binding protein-1 as an authentic Parkin substrate.* J Biol Chem, 2006. **281**(24): p. 16193-6.
61. Atanassov, B.S. and S.Y. Dent, *USP22 regulates cell proliferation by deubiquitinating the transcriptional regulator FBP1.* EMBO Rep, 2011. **12**(9): p. 924-30.
62. Ma, J., et al., *Prostaglandin E2 promotes liver cancer cell growth by the upregulation of FUSE-binding protein 1 expression.* Int J Oncol, 2013. **42**(3): p. 1093-104.
63. He, L., et al., *Loss of FBP function arrests cellular proliferation and extinguishes c-myc expression.* EMBO J, 2000. **19**(5): p. 1034-44.
64. Jang, M., et al., *Far upstream element-binding protein-1, a novel caspase substrate, acts as a cross-talker between apoptosis and the c-myc oncogene.* Oncogene, 2009. **28**(12): p. 1529-36.
65. Quinn, L.M., *FUBP/KH domain proteins in transcription: Back to the future.* Transcription, 2017. **8**(3): p. 185-192.
66. Dixit, U., et al., *Fuse binding protein antagonizes the transcription activity of tumor suppressor protein p53.* BMC Cancer, 2014. **14**: p. 925.
67. Zhou, W., et al., *Far Upstream Element Binding Protein Plays a Crucial Role in Embryonic Development, Hematopoiesis, and Stabilizing Myc Expression Levels.* Am J Pathol, 2016. **186**(3): p. 701-15.
68. Wesely, J., et al., *Delayed Mesoderm and Erythroid Differentiation of Murine*

Embryonic Stem Cells in the Absence of the Transcriptional Regulator FUBP1. Stem Cells Int, 2017. **2017**: p. 5762301.
69. Gabay, M., Y. Li, and D.W. Felsher, *MYC activation is a hallmark of cancer initiation and maintenance.* Cold Spring Harb Perspect Med, 2014. **4**(6).
70. Green, D.R. and G. Kroemer, *Cytoplasmic functions of the tumour suppressor p53.* Nature, 2009. **458**(7242): p. 1127-30.
71. Iwakuma, T. and G. Lozano, *MDM2, an introduction.* Mol Cancer Res, 2003. **1**(14): p. 993-1000.
72. Matsushita, K., et al., *An essential role of alternative splicing of c-myc suppressor FUSE-binding protein-interacting repressor in carcinogenesis.* Cancer Res, 2006. **66**(3): p. 1409-17.
73. Malz, M., et al., *Overexpression of far upstream element (FUSE) binding protein (FBP)-interacting repressor (FIR) supports growth of hepatocellular carcinoma.* Hepatology, 2014. **60**(4): p. 1241-50.
74. Weber, A., et al., *The FUSE binding proteins FBP1 and FBP3 are potential c-myc regulators in renal, but not in prostate and bladder cancer.* BMC Cancer, 2008. **8**: p. 369.
75. de Oliveria Andrade, L.J., et al., *Association between hepatitis C and hepatocellular carcinoma.* J Glob Infect Dis, 2009. **1**(1): p. 33-7.
76. Singer, S., et al., *Coordinated expression of stathmin family members by far upstream sequence element-binding protein-1 increases motility in non-small cell lung cancer.* Cancer Res, 2009. **69**(6): p. 2234-43.
77. Bettegowda, C., et al., *Mutations in CIC and FUBP1 contribute to human oligodendroglioma.* Science, 2011. **333**(6048): p. 1453-5.
78. Matsushita, K., et al., *c-myc suppressor FBP-interacting repressor for cancer diagnosis and therapy.* Front Biosci (Landmark Ed), 2009. **14**: p. 3401-8.
79. Jia, M.Y. and Y.J. Wang, *Far upstream element-binding protein 1(FUBP1) expression differs between human colorectal cancer and non-cancerous tissue.* Neoplasma, 2014. **61**(5): p. 533-40.
80. Ding, Z., et al., *Expression of far upstream element (FUSE) binding protein 1 in human glioma is correlated with c-Myc and cell proliferation.* Mol Carcinog, 2015. **54**(5): p. 405-15.
81. Baumgarten, P., et al., *Loss of FUBP1 expression in gliomas predicts FUBP1 mutation and is associated with oligodendroglial differentiation, IDH1 mutation and 1p/19q loss of heterozygosity.* Neuropathol Appl Neurobiol, 2014. **40**(2): p. 205-16.
82. Zubaidah, R.M., et al., *2-D DIGE profiling of hepatocellular carcinoma tissues identified isoforms of far upstream binding protein (FUBP) as novel candidates in liver carcinogenesis.* Proteomics, 2008. **8**(23-24): p. 5086-96.
83. Malz, M., et al., *Overexpression of far upstream element binding proteins: a mechanism regulating proliferation and migration in liver cancer cells.* Hepatology, 2009. **50**(4): p. 1130-9.
84. Weber, K., et al., *A multicolor panel of novel lentiviral "gene ontology" (LeGO) vectors for functional gene analysis.* Mol Ther, 2008. **16**(4): p. 698-706.
85. Shen, L., Q. Shi, and W. Wang, *Double agents: genes with both oncogenic and tumor-suppressor functions.* Oncogenesis, 2018. **7**(3): p. 25.
86. Hoang, V.T., et al., *The transcriptional regulator FUBP1 influences disease outcome in murine and human myeloid leukemia.* 2018.
87. Chung, H.J., et al., *FBPs are calibrated molecular tools to adjust gene expression.* Mol Cell Biol, 2006. **26**(17): p. 6584-97.
88. Gau, B.H., et al., *FUBP3 interacts with FGF9 3' microsatellite and positively regulates FGF9 translation.* Nucleic Acids Res, 2011. **39**(9): p. 3582-93.
89. Gherzi, R., et al., *The role of KSRP in mRNA decay and microRNA precursor maturation.* Wiley Interdiscip Rev RNA, 2010. **1**(2): p. 230-9.
90. Orkin, S.H. and L.I. Zon, *Hematopoiesis: an evolving paradigm for stem cell biology.* Cell, 2008. **132**(4): p. 631-44.
91. Metcalf, D., *The molecular control of hematopoiesis: progress and problems with*

gene manipulation. Stem Cells, 1998. **16 Suppl 2**: p. 1-9.
92. Antoniani, C., O. Romano, and A. Miccio, *Concise Review: Epigenetic Regulation of Hematopoiesis: Biological Insights and Therapeutic Applications.* Stem Cells Transl Med, 2017. **6**(12): p. 2106-2114.
93. Parekh, C. and G.M. Crooks, *Critical differences in hematopoiesis and lymphoid development between humans and mice.* J Clin Immunol, 2013. **33**(4): p. 711-5.
94. Palis, J., *Primitive and definitive erythropoiesis in mammals.* Front Physiol, 2014. **5**: p. 3.
95. Mosaad, Y.M., *Hematopoietic stem cells: an overview.* Transfus Apher Sci, 2014. **51**(3): p. 68-82.
96. Heinig, K., et al., *Development and trafficking function of haematopoietic stem cells and myeloid cells during fetal ontogeny.* Cardiovasc Res, 2015. **107**(3): p. 352-63.
97. Potocnik, A.J., C. Brakebusch, and R. Fassler, *Fetal and adult hematopoietic stem cells require beta1 integrin function for colonizing fetal liver, spleen, and bone marrow.* Immunity, 2000. **12**(6): p. 653-63.
98. Mikkola, H.K., et al., *Haematopoietic stem cells retain long-term repopulating activity and multipotency in the absence of stem-cell leukaemia SCL/tal-1 gene.* Nature, 2003. **421**(6922): p. 547-51.
99. Ichikawa, M., et al., *Runx1/AML-1 ranks as a master regulator of adult hematopoiesis.* Cell Cycle, 2004. **3**(6): p. 722-4.
100. Purnell, B.A., *How to maintain hematopoietic stem cells.* Science, 2016. **354**(6316): p. 1114-1115.
101. Tusi, B.K., et al., *Population snapshots predict early haematopoietic and erythroid hierarchies.* Nature, 2018. **555**(7694): p. 54-60.
102. Rodriguez-Fraticelli, A.E., et al., *Clonal analysis of lineage fate in native haematopoiesis.* Nature, 2018. **553**(7687): p. 212-216.
103. Zheng, S., et al., *Molecular transitions in early progenitors during human cord blood hematopoiesis.* Mol Syst Biol, 2018. **14**(3): p. e8041.
104. Attar, A., *Changes in the Cell Surface Markers During Normal Hematopoiesis: A Guide to Cell Isolation*. Vol. 1. 2014. 20-28.
105. Iwasaki, H., et al., *The order of expression of transcription factors directs hierarchical specification of hematopoietic lineages.* Genes Dev, 2006. **20**(21): p. 3010-21.
106. Ng, F.S., F.J. Calero-Nieto, and B. Gottgens, *Shared transcription factors contribute to distinct cell fates.* Transcription, 2014. **5**(5): p. e978173.
107. Sive, J.I. and B. Gottgens, *Transcriptional network control of normal and leukaemic haematopoiesis.* Exp Cell Res, 2014. **329**(2): p. 255-64.
108. Bonavita, O., et al., *Regulation of hematopoiesis by the chemokine system.* Cytokine, 2018. **109**: p. 76-80.
109. Smith, B.R., *Regulation of hematopoiesis.* Yale J Biol Med, 1990. **63**(5): p. 371-80.
110. Chen, K., et al., *Resolving the distinct stages in erythroid differentiation based on dynamic changes in membrane protein expression during erythropoiesis.* Proc Natl Acad Sci U S A, 2009. **106**(41): p. 17413-8.
111. Dzierzak, E. and S. Philipsen, *Erythropoiesis: development and differentiation.* Cold Spring Harb Perspect Med, 2013. **3**(4): p. a011601.
112. Nandakumar, S.K., J.C. Ulirsch, and V.G. Sankaran, *Advances in understanding erythropoiesis: evolving perspectives.* Br J Haematol, 2016. **173**(2): p. 206-18.
113. Keerthivasan, G., A. Wickrema, and J.D. Crispino, *Erythroblast enucleation.* Stem Cells Int, 2011. **2011**: p. 139851.
114. Klei, T.R., et al., *From the Cradle to the Grave: The Role of Macrophages in Erythropoiesis and Erythrophagocytosis.* Front Immunol, 2017. **8**: p. 73.
115. Perreault, A.A., et al., *Epo reprograms the epigenome of erythroid cells.* Exp Hematol, 2017. **51**: p. 47-62.
116. Ingley, E., P.A. Tilbrook, and S.P. Klinken, *New insights into the regulation of erythroid cells.* IUBMB Life, 2004. **56**(4): p. 177-84.

117. Suzuki, N., et al., *Erythroid-specific expression of the erythropoietin receptor rescued its null mutant mice from lethality.* Blood, 2002. **100**(7): p. 2279-88.
118. Zeigler, B.M., et al., *A mouse model for an erythropoietin-deficiency anemia.* Dis Model Mech, 2010. **3**(11-12): p. 763-72.
119. Grover, A., et al., *Erythropoietin guides multipotent hematopoietic progenitor cells toward an erythroid fate.* J Exp Med, 2014. **211**(2): p. 181-8.
120. Hattangadi, S.M., et al., *From stem cell to red cell: regulation of erythropoiesis at multiple levels by multiple proteins, RNAs, and chromatin modifications.* Blood, 2011. **118**(24): p. 6258-68.
121. Perry, C. and H. Soreq, *Transcriptional regulation of erythropoiesis. Fine tuning of combinatorial multi-domain elements.* Eur J Biochem, 2002. **269**(15): p. 3607-18.
122. Cantor, A.B. and S.H. Orkin, *Transcriptional regulation of erythropoiesis: an affair involving multiple partners.* Oncogene, 2002. **21**(21): p. 3368-76.
123. Love, P.E., C. Warzecha, and L. Li, *Ldb1 complexes: the new master regulators of erythroid gene transcription.* Trends Genet, 2014. **30**(1): p. 1-9.
124. Porcher, C., H. Chagraoui, and M.S. Kristiansen, *SCL/TAL1: a multifaceted regulator from blood development to disease.* Blood, 2017. **129**(15): p. 2051-2060.
125. Li, Y., et al., *Dynamic interaction between TAL1 oncoprotein and LSD1 regulates TAL1 function in hematopoiesis and leukemogenesis.* Oncogene, 2012. **31**(48): p. 5007-18.
126. Jayapal, S.R., et al., *Down-regulation of Myc is essential for terminal erythroid maturation.* J Biol Chem, 2010. **285**(51): p. 40252-65.
127. Capellera-Garcia, S., et al., *Defining the Minimal Factors Required for Erythropoiesis through Direct Lineage Conversion.* Cell Rep, 2016. **15**(11): p. 2550-62.
128. Singh, V.K., A. Saini, and R. Chandra, *Role of Erythropoietin and Other Growth Factors inEx VivoErythropoiesis.* Advances in Regenerative Medicine, 2014. **2014**: p. 1-8.
129. Singh, V.K., A. Saini, and R. Chandra, *Role of Erythropoietin and Other Growth Factors in Ex Vivo Erythropoiesis.* Advances in Regenerative Medicine, 2014. **2014**: p. 8.
130. Sung, Y.H., et al., *Mouse genetics: catalogue and scissors.* BMB Rep, 2012. **45**(12): p. 686-92.
131. Skarnes, W.C., et al., *A conditional knockout resource for the genome-wide study of mouse gene function.* Nature, 2011. **474**(7351): p. 337-42.
132. Brown, S.D.M., et al., *High-throughput mouse phenomics for characterizing mammalian gene function.* Nat Rev Genet, 2018. **19**(6): p. 357-370.
133. Capecchi, M.R., *Gene targeting in mice: functional analysis of the mammalian genome for the twenty-first century.* Nat Rev Genet, 2005. **6**(6): p. 507-12.
134. Wright, W.D., S.S. Shah, and W.D. Heyer, *Homologous recombination and the repair of DNA double-strand breaks.* J Biol Chem, 2018. **293**(27): p. 10524-10535.
135. Hall, B., A. Limaye, and A.B. Kulkarni, *Overview: generation of gene knockout mice.* Curr Protoc Cell Biol, 2009. **Chapter 19**: p. Unit 19 12 19 12 1-17.
136. Tzimagiorgis, G., et al., *Introduction of the negative selection marker into replacement vectors by a single ligation step.* Nucleic Acids Res, 1996. **24**(17): p. 3476-7.
137. Kanellopoulou, C., et al., *Reprogramming of Polycomb-Mediated Gene Silencing in Embryonic Stem Cells by the miR-290 Family and the Methyltransferase Ash1l.* Stem Cell Reports, 2015. **5**(6): p. 971-978.
138. Marin, T.M., et al., *Rapamycin reverses hypertrophic cardiomyopathy in a mouse model of LEOPARD syndrome-associated PTPN11 mutation.* J Clin Invest, 2011. **121**(3): p. 1026-43.
139. Bouabe, H. and K. Okkenhaug, *Gene targeting in mice: a review.* Methods Mol Biol, 2013. **1064**: p. 315-36.

140. Friedel, R.H. and P. Soriano, *Gene trap mutagenesis in the mouse.* Methods Enzymol, 2010. **477**: p. 243-69.
141. Komor, A.C., A.H. Badran, and D.R. Liu, *CRISPR-Based Technologies for the Manipulation of Eukaryotic Genomes.* Cell, 2017. **168**(1-2): p. 20-36.
142. Yang, H., et al., *One-step generation of mice carrying reporter and conditional alleles by CRISPR/Cas-mediated genome engineering.* Cell, 2013. **154**(6): p. 1370-9.
143. Smalley, E., *CRISPR mouse model boom, rat model renaissance.* Nat Biotechnol, 2016. **34**(9): p. 893-4.
144. Tang, L., et al., *CRISPR/Cas9-mediated gene editing in human zygotes using Cas9 protein.* Mol Genet Genomics, 2017. **292**(3): p. 525-533.
145. Batzoglou, S., et al., *Human and mouse gene structure: comparative analysis and application to exon prediction.* Genome Res, 2000. **10**(7): p. 950-8.
146. Yue, F., et al., *A comparative encyclopedia of DNA elements in the mouse genome.* Nature, 2014. **515**(7527): p. 355-64.
147. Doetschman, T., *Influence of genetic background on genetically engineered mouse phenotypes.* Methods Mol Biol, 2009. **530**: p. 423-33.
148. Eisener-Dorman, A.F., D.A. Lawrence, and V.J. Bolivar, *Cautionary insights on knockout mouse studies: the gene or not the gene?* Brain Behav Immun, 2009. **23**(3): p. 318-24.
149. El-Brolosy, M.A. and D.Y.R. Stainier, *Genetic compensation: A phenomenon in search of mechanisms.* PLoS Genet, 2017. **13**(7): p. e1006780.
150. Rabenhorst, U., et al., *Single-Stranded DNA-Binding Transcriptional Regulator FUBP1 Is Essential for Fetal and Adult Hematopoietic Stem Cell Self-Renewal.* Cell Rep, 2015. **11**(12): p. 1847-55.
151. Schwenk, F., U. Baron, and K. Rajewsky, *A cre-transgenic mouse strain for the ubiquitous deletion of loxP-flanked gene segments including deletion in germ cells.* Nucleic Acids Res, 1995. **23**(24): p. 5080-1.
152. Wang, X., et al., *Distribution of CaMKIIalpha expression in the brain in vivo, studied by CaMKIIalpha-GFP mice.* Brain Res, 2013. **1518**: p. 9-25.
153. Mignone, J.L., et al., *Neural stem and progenitor cells in nestin-GFP transgenic mice.* J Comp Neurol, 2004. **469**(3): p. 311-24.
154. Georgiades, P., et al., *VavCre transgenic mice: a tool for mutagenesis in hematopoietic and endothelial lineages.* Genesis, 2002. **34**(4): p. 251-6.
155. Germain, R.N., *T-cell development and the CD4-CD8 lineage decision.* Nat Rev Immunol, 2002. **2**(5): p. 309-22.
156. Koulnis, M., et al., *Identification and analysis of mouse erythroid progenitors using the CD71/TER119 flow-cytometric assay.* J Vis Exp, 2011(54).
157. *The Human Protein Atlas*, (08/2018); Available from: https://www.proteinatlas.org/ENSG00000169857-AVEN/tissue.
158. Liaudet-Coopman, E., et al., *Cathepsin D: newly discovered functions of a long-standing aspartic protease in cancer and apoptosis.* Cancer Lett, 2006. **237**(2): p. 167-79.
159. Fluck, M.M. and B.S. Schaffhausen, *Lessons in signaling and tumorigenesis from polyomavirus middle T antigen.* Microbiol Mol Biol Rev, 2009. **73**(3): p. 542-63, Table of Contents.
160. Fantozzi, A. and G. Christofori, *Mouse models of breast cancer metastasis.* Breast Cancer Res, 2006. **8**(4): p. 212.
161. Nicoletti, I., et al., *A rapid and simple method for measuring thymocyte apoptosis by propidium iodide staining and flow cytometry.* J Immunol Methods, 1991. **139**(2): p. 271-9.
162. Ford, C.H., et al., *Reassessment of estrogen receptor expression in human breast cancer cell lines.* Anticancer Res, 2011. **31**(2): p. 521-7.
163. Jia, M., K. Dahlman-Wright, and J.A. Gustafsson, *Estrogen receptor alpha and beta in health and disease.* Best Pract Res Clin Endocrinol Metab, 2015. **29**(4): p. 557-68.
164. Perillo, B., et al., *17beta-estradiol inhibits apoptosis in MCF-7 cells, inducing bcl-*

2 expression via two estrogen-responsive elements present in the coding sequence. Mol Cell Biol, 2000. **20**(8): p. 2890-901.
165. Endoh, T., Y. Kawasaki, and N. Sugimoto, *Stability of RNA quadruplex in open reading frame determines proteolysis of human estrogen receptor alpha.* Nucleic Acids Res, 2013. **41**(12): p. 6222-31.
166. Yillah, J., *Die Regulation von FUBP1 durch TAL1 während der Erythropoiese.* 2017.
167. Rodriguez, P., et al., *GATA-1 forms distinct activating and repressive complexes in erythroid cells.* EMBO J, 2005. **24**(13): p. 2354-66.
168. Wu, W., et al., *Dynamic shifts in occupancy by TAL1 are guided by GATA factors and drive large-scale reprogramming of gene expression during hematopoiesis.* Genome Res, 2014. **24**(12): p. 1945-62.
169. Moriguchi, T. and M. Yamamoto, *A regulatory network governing Gata1 and Gata2 gene transcription orchestrates erythroid lineage differentiation.* Int J Hematol, 2014. **100**(5): p. 417-24.
170. Zhang, M.Y., et al., *NF-kappaB transcription factors are involved in normal erythropoiesis.* Blood, 1998. **91**(11): p. 4136-44.
171. Sivertsen, E.A., et al., *PI3K/Akt-dependent Epo-induced signalling and target genes in human early erythroid progenitor cells.* Br J Haematol, 2006. **135**(1): p. 117-28.
172. Abbey, J.L. and H.C. O'Neill, *Expression of T-cell receptor genes during early T-cell development.* Immunol Cell Biol, 2008. **86**(2): p. 166-74.
173. Seshacharyulu, P., et al., *Targeting EGF-receptor(s) - STAT1 axis attenuates tumor growth and metastasis through downregulation of MUC4 mucin in human pancreatic cancer.* Oncotarget, 2015. **6**(7): p. 5164-81.
174. Modjtahedi, H., et al., *Anti-EGFR monoclonal antibodies which act as EGF, TGF alpha, HB-EGF and BTC antagonists block the binding of epiregulin to EGFR-expressing tumours.* Int J Cancer, 1998. **75**(2): p. 310-6.
175. Bai, L. and S. Wang, *Targeting apoptosis pathways for new cancer therapeutics.* Annu Rev Med, 2014. **65**: p. 139-55.
176. O'Doherty, A.M., et al., *Expression of granulosa cell microRNAs, AVEN and ATRX are associated with human blastocyst development.* Mol Reprod Dev, 2018.
177. Blaschke, A.J., K. Staley, and J. Chun, *Widespread programmed cell death in proliferative and postmitotic regions of the fetal cerebral cortex.* Development, 1996. **122**(4): p. 1165-74.
178. Penaloza, C., et al., *Cell death in development: shaping the embryo.* Histochem Cell Biol, 2006. **126**(2): p. 149-58.
179. Saftig, P., et al., *Mice deficient for the lysosomal proteinase cathepsin D exhibit progressive atrophy of the intestinal mucosa and profound destruction of lymphoid cells.* EMBO J, 1995. **14**(15): p. 3599-608.
180. Nie, J., et al., *Post-transcriptional Regulation of Nkx2-5 by RHAU in Heart Development.* Cell Rep, 2015. **13**(4): p. 723-732.
181. Li, M., et al., *WAP-TAg transgenic mice and the study of dysregulated cell survival, proliferation, and mutation during breast carcinogenesis.* Oncogene, 2000. **19**(8): p. 1010-9.
182. J, W., *Analyse der zellulären Immunantwort gegen SV40 T-Antigen-induzierte Mammakarzinome im transgenen Mausmodell.* 2011.
183. Andersen, J.L. and S. Kornbluth, *The tangled circuitry of metabolism and apoptosis.* Mol Cell, 2013. **49**(3): p. 399-410.
184. Yi, C.H., H. Vakifahmetoglu-Norberg, and J. Yuan, *Integration of apoptosis and metabolism.* Cold Spring Harb Symp Quant Biol, 2011. **76**: p. 375-87.
185. Cheng, E.H., et al., *Bax-independent inhibition of apoptosis by Bcl-XL.* Nature, 1996. **379**(6565): p. 554-6.
186. Pietrocola, F., et al., *Acetyl coenzyme A: a central metabolite and second messenger.* Cell Metab, 2015. **21**(6): p. 805-21.
187. Liu, R., et al., *Overexpression of Bcl-x(L) promotes chemotherapy resistance of*

mammary tumors in a syngeneic mouse model. Am J Pathol, 1999. **155**(6): p. 1861-7.
188. Maji, S., et al., *Bcl-2 Antiapoptotic Family Proteins and Chemoresistance in Cancer.* Adv Cancer Res, 2018. **137**: p. 37-75.
189. Pecot, J., et al., *Tight Sequestration of BH3 Proteins by BCL-xL at Subcellular Membranes Contributes to Apoptotic Resistance.* Cell Rep, 2016. **17**(12): p. 3347-3358.
190. Nuessler, V., et al., *Bcl-2, bax and bcl-xL expression in human sensitive and resistant leukemia cell lines.* Leukemia, 1999. **13**(11): p. 1864-72.
191. Kassouf, M.T., et al., *Differential use of SCL/TAL-1 DNA-binding domain in developmental hematopoiesis.* Blood, 2008. **112**(4): p. 1056-67.
192. Han, G.C., et al., *Genome-Wide Organization of GATA1 and TAL1 Determined at High Resolution.* Mol Cell Biol, 2016. **36**(1): p. 157-72.
193. Tripic, T., et al., *SCL and associated proteins distinguish active from repressive GATA transcription factor complexes.* Blood, 2009. **113**(10): p. 2191-201.
194. Suzuki, M., et al., *GATA factor switching from GATA2 to GATA1 contributes to erythroid differentiation.* Genes Cells, 2013. **18**(11): p. 921-33.
195. McGahon, A.J., et al., *Downregulation of Bcr-Abl in K562 cells restores susceptibility to apoptosis: characterization of the apoptotic death.* Cell Death Differ, 1997. **4**(2): p. 95-104.
196. Quentmeier, H., et al., *JAK2 V617F tyrosine kinase mutation in cell lines derived from myeloproliferative disorders.* Leukemia, 2006. **20**(3): p. 471-6.
197. Haider, S. and R. Pal, *Integrated analysis of transcriptomic and proteomic data.* Curr Genomics, 2013. **14**(2): p. 91-110.
198. Manzoni, C., et al., *Genome, transcriptome and proteome: the rise of omics data and their integration in biomedical sciences.* Brief Bioinform, 2018. **19**(2): p. 286-302.
199. Kumar, D., et al., *Integrating transcriptome and proteome profiling: Strategies and applications.* Proteomics, 2016. **16**(19): p. 2533-2544.
200. Wilson, A., et al., *c-Myc controls the balance between hematopoietic stem cell self-renewal and differentiation.* Genes Dev, 2004. **18**(22): p. 2747-63.
201. Ohmori, Y., et al., *Role of c-Myc on erythroid differentiation.* Tohoku J Exp Med, 1992. **168**(2): p. 203-10.
202. Dang, C.V., *MYC, metabolism, cell growth, and tumorigenesis.* Cold Spring Harb Perspect Med, 2013. **3**(8).
203. Rylski, M., et al., *GATA-1-mediated proliferation arrest during erythroid maturation.* Mol Cell Biol, 2003. **23**(14): p. 5031-42.
204. Debaize, L., et al., *Two hematopoietic transcription factors, RUNX1 and FUBP1, control the expression of KIT oncogene in pre-B lymphoblasts.* Experimental Hematology, 2017. **53**: p. S112.
205. Munugalavadla, V., et al., *Repression of c-kit and its downstream substrates by GATA-1 inhibits cell proliferation during erythroid maturation.* Mol Cell Biol, 2005. **25**(15): p. 6747-59.
206. Simon, M.M., et al., *A comparative phenotypic and genomic analysis of C57BL/6J and C57BL/6N mouse strains.* Genome Biol, 2013. **14**(7): p. R82.
207. Kafri, R., M. Springer, and Y. Pilpel, *Genetic redundancy: new tricks for old genes.* Cell, 2009. **136**(3): p. 389-92.
208. Zheng, Y., *FUBP1 and FUBP2: A "Buddy System" Essential for Cell Survival.* 2017.
209. Khageh Hosseini, S., *Targeting FUBP1 in Hepatocellular Carcinoma.* 2014.
210. Yi, H., et al., *Gene expression atlas for human embryogenesis.* FASEB J, 2010. **24**(9): p. 3341-50.
211. Garnis, C., T.P. Buys, and W.L. Lam, *Genetic alteration and gene expression modulation during cancer progression.* Mol Cancer, 2004. **3**: p. 9.
212. Strober, W., *Trypan blue exclusion test of cell viability.* Curr Protoc Immunol, 2001. **Appendix 3**: p. Appendix 3B.
213. Reed, S.E., et al., *Transfection of mammalian cells using linear polyethylenimine*

is a simple and effective means of producing recombinant adeno-associated virus vectors. J Virol Methods, 2006. **138**(1-2): p. 85-98.
214. Amado, R.G. and I.S. Chen, *Lentiviral vectors--the promise of gene therapy within reach?* Science, 1999. **285**(5428): p. 674-6.
215. Rao, D.D., et al., *siRNA vs. shRNA: similarities and differences.* Adv Drug Deliv Rev, 2009. **61**(9): p. 746-59.
216. Perfetto, S.P., et al., *Amine-reactive dyes for dead cell discrimination in fixed samples.* Curr Protoc Cytom, 2010. **Chapter 9**: p. Unit 9 34.
217. Riccardi, C. and I. Nicoletti, *Analysis of apoptosis by propidium iodide staining and flow cytometry.* Nat Protoc, 2006. **1**(3): p. 1458-61.
218. Munshi, S., R.C. Twining, and R. Dahl, *Alamar blue reagent interacts with cell-culture media giving different fluorescence over time: potential for false positives.* J Pharmacol Toxicol Methods, 2014. **70**(2): p. 195-8.
219. Voytas, D., *Agarose gel electrophoresis.* Curr Protoc Immunol, 2001. **Chapter 10**: p. Unit 10 4.
220. Loenen, W.A., et al., *Highlights of the DNA cutters: a short history of the restriction enzymes.* Nucleic Acids Res, 2014. **42**(1): p. 3-19.
221. Chuang, L.Y., Y.H. Cheng, and C.H. Yang, *Specific primer design for the polymerase chain reaction.* Biotechnol Lett, 2013. **35**(10): p. 1541-9.
222. VanGuilder, H.D., K.E. Vrana, and W.M. Freeman, *Twenty-five years of quantitative PCR for gene expression analysis.* Biotechniques, 2008. **44**(5): p. 619-26.
223. Livak, K.J. and T.D. Schmittgen, *Analysis of relative gene expression data using real-time quantitative PCR and the 2(-Delta Delta C(T)) Method.* Methods, 2001. **25**(4): p. 402-8.
224. Smale, S.T., *Luciferase assay.* Cold Spring Harb Protoc, 2010. **2010**(5): p. pdb prot5421.
225. Bradford, M.M., *A rapid and sensitive method for the quantitation of microgram quantities of protein utilizing the principle of protein-dye binding.* Anal Biochem, 1976. **72**: p. 248-54.
226. Rehm, H.L., T, *Der Experimentator Proteinbiochemie/Proteomics*. 7 ed. 2016.
227. Ni, D., P. Xu, and S. Gallagher, *Immunoblotting and Immunodetection.* Curr Protoc Protein Sci, 2017. **88**: p. 10 10 1-10 10 37.
228. Carey, M.F., C.L. Peterson, and S.T. Smale, *Chromatin immunoprecipitation (ChIP).* Cold Spring Harb Protoc, 2009. **2009**(9): p. pdb prot5279.
229. Juers, D.H., B.W. Matthews, and R.E. Huber, *LacZ beta-galactosidase: structure and function of an enzyme of historical and molecular biological importance.* Protein Sci, 2012. **21**(12): p. 1792-807.
230. Brown, T., *Southern blotting.* Curr Protoc Immunol, 2001. **Chapter 10**: p. Unit 10 6A.

9 Abbreviations

°C	Degree Celsius
µg	Microgram
µl	Microliter
µm	Micrometer
µM	Micromolar
A	Ampere
AAAA	Polyadenylation signal
aa	Amino acid(s)
AGM region	Aorta-gonad mesonephros region
AKT	A serine-threonine protein kinase
Amp	Ampicillin
APS	Ammonium persulfate
ARS	Aminoacyl-tRNA synthetase
ATP	Adenosine triphosphate
AT-rich	Adenine-thymine-rich
B cell	Bursa-derived cell
β2M	Gene symbol of β_2 microglobulin
Bl/6	C57BL/6J inbred mouse line
BCL-2	B-cell lymphoma 2
BCL-x_L	B-cell lymphoma-extra large
BFU-E	Burst forming unit-erythroid
BIK	Bcl-2-interacting killer
BM	Bone marrow
BMMNC	Bone marrow mononuclear cell
bp	Base pairs
BrdU	Bromodeoxyuridine
BSA	Bovine serum albumin
$CaCl_2$	Calcium chloride
CaMKIIα	Calcium/calmodulin-dependent protein kinase Type II alpha chain
CASP	Gene symbol for Caspase
CCND2	G1/S-specific cyclin-D2
CD	Cluster of differentiation
cDNA	Complementary DNA
CFU-E	Colony forming unit-erythroid
c-Kit	A tyrosine-protein kinase, SCF receptor
CLP	Common lymphoid progenitor
cm	Centimeter
CMP	Common myeloid progenitor
CMV	Cytomegalovirus
c-MYC	Proto-oncogene originally isolated from an avian myelocytomatosis virus
CRE	Cre recombinase
C-terminal	Carboxy-terminal
Cy5.5	Cyanine 5.5
Cy7	Cyanine 7
dATP	Deoxyadenosine triphosphate
DMEM	Dulbecco's modified eagle medium
DMSO	Dimethyl sulfoxide
DNA	Deoxyribonucleic acid
DNase I	Deoxyribonuclease I
dNTP	Deoxynucleotide triphosphate
DPBS	Dulbecco's phosphate buffered saline
DTT	Dithiothreitol
E2	17β-Estradiol
E. coli	*Escherichia coli*
ECL	Enhanced chemiluminescence
EDTA	Ethylenediaminetetraacetic acid
EPO	Erythropoietin
EPOR	Erythropoietin receptor
ER1	Estrogen receptor alpha

ESC	Embryonic stem cell
e	Exon
FACS	Fluorescence-activated cell sorting
FBS	Fetal bovine serum
FcR	Fc (*Fragment, crystallizable*) receptor
Fig.	Figure
FIR	FUBP interacting repressor
FITC	Fluorescein isothiocyanate
FLP	Flippase recombinase
FLT3-L	Fms-related tyrosine kinase 3 ligand
for	Forward
FRT	Flippase recognition target
FUBP1	*FUSE*-binding protein 1
FUBP2	*FUSE*-binding protein 2
FUBP3	*FUSE*-binding protein 3
FUSE	Far upstream element
G4	G-quadruplex secondary structure
GAPDH	Gene symbol of the glyceraldehyde-3-phosphate dehydrogenase
GATA-1	GATA-binding protein 1
GATA-2	GATA-binding protein 2
GFP	Green fluorescent protein
GMP	Granulocyte/macrophage pogenitor
GT	Gene trap
GTE	Glucose/Tris-HCl/EDTA buffer
h	Hour(s)
h	human
H_2O	Water
HCC	Hepatocellular carcinoma
HCl	Hydrochloric acid
HCV	Hepatitis C virus
HEPES	4-(2-Hydroxyethyl)piperazine-1-ethanesulfonic acid
HPRT1	Gene symbol of the hypoxanthine phosphoribosyltransferase 1
HRP	Horseradish peroxidase
HSC	Hematopoietic stem cell
HSPC	Hematopoietic stem and progenitor cell
IL-3	Interleukin-3
IL-6	Interleukin-6
IL-9	Interleukin-9
IRES	Internal ribosomal entry site
IT	Intermediate-term repopulating
kb	Kilobase(s)
kDa	Kilodalton
KH	K-homology
KOAc	Potassium acetate
KSL	c-Kit^+ $Sca\text{-}1^+$ lin^- cell population
LB	Lysogeny broth
L-glu	L-glutamine
Lin^-	Lineage-negative cells
Lin^+	Lineage-positive cells
loxP	Locus of X-over P1
LT	Long-term repopulating
LT-HSCs	Long-term (repopulating) hematopoietic stem cells
m	murine
M	Molar
mA	Milliamper
MCS	Multiple cloning site
MDM2	Murine double minute 2
MEP	Megakaryocyte/erythroid progenitor
mg	Milligram
$MgCl_2$	Magnesium chloride
min	Minute(s)
ml	Milliliter
mM	Millimolar

MMTV	Mouse mammary tumor virus
MOI	Multiplicity of infection
MPP	Multipotent progenitor
mRNA	Messenger RNA
NA	Not available
Na_2HPO_4	Disodium hydrogen phosphate
NaCl	Sodium chloride
NaN_3	Sodium azide
NaOH	Sodium hydroxide
NFκB	Nuclear factor kappa-light-chain-enhancer of activated B cells
ng	Nanogram
NK	Natural killer cell
NLS	Nuclear localization signal
nm	Nanometer
NOXA	Pro-apoptotic protein belonging to the Bcl-2 family
NP-40	Igepal CA-630
N-terminal	Amino-terminal
Oligo dT	Oligonucleotide composed of deoxythymidines
p21	Also known as cyclin-dependent kinase inhibitor 1A (CDKN1A)
p27	Also known as cyclin-dependent kinase inhibitor 1B (CDKN1B)
p38/JTV-1	Also known as AIMP2 (aminoacyl tRNA synthase complex-interacting multifunctional protein 2)
p53	Tumor protein p53
PAGE	Polyacrylamide gel electrophoresis
PB	Peripheral blood
PBS	Phosphate buffered saline
PCR	Polymerase chain reaction
PE	Phycoerythrin
Pen	Penicillin
PerCP	Peridinin chlorophyll
PGE_2	Prostaglandin E_2
PI3K	Phosphatidylinositol-4,5-bisphosphate 3-kinase
POL II	RNA Polymerase II complex
PyVT	Polyoma Virus middle T antigen
qPCR	Quantitative real-time PCR
rev	Reverse
RIPA	Radioimmunoprecipitation assay buffer
RNA	Ribonucleic acid
RNase	Ribonuclease
ROS	Reactive oxygen species
rpm	Revolutions per minute
RPMI	Roswell Park Memorial Institute cell culture medium
RT	Reverse transcriptase
RUNX1	Runt-related transcription factor 1
s	Second(s)
Sca-1	Stem cell antigen-1
SCF	Stem cell factor
SCL	Stem cell leukemia, also known as TAL1
SD	Standard deviation
SDS	Sodium dodecyl sulfate
SFEM	Serum-free expansion medium
shRNA	Short hairpin RNA
ST	Short-term repopulating
ST-HSC	Short-term repopulating hematopoietic stem cell
Strep	Streptomycin
T cell	Thymus-derived cell
TAL1	T-cell acute lymphocytic leukemia 1
TBE	Tris/boric acid/EDTA buffer
TBS	Tris-buffered saline
TBS-T	Tris-buffered saline with 0.1% Tween-20
TCTP	Translationally controlled tumor protein
TEMED	N,N,N',N'-Tetramethylethane-1,2-Diamine
TFIIH	Transcription factor II H

TGF-β	Transforming growth factor-β
TNF	Tumor necrosis factor
TPO	Thrombopoietin
TRC	*The RNAi Consortium*
Tris	2-Amino-2-hydroxymethyl-propane-1,3-diol
TU	Transducing units
Txnip	Gene symbol of the Thioredoxin interacting protein
U	Unit
USP22	Ubiquitin-specific protease 22
USP29	Ubiquitin-specific peptidase 29
UTR	Untranslated region
UV	Ultraviolet
V	Volt
VSV	Vesicular stomatitis virus
VSV-G	Glycoprotein G of VSV
w/v	Weight/volume
Wnt	Wingless-type MMTV integration site protein family
x g	Times gravity
X-Gal	5-bromo-4-chloro-3-indolyl-β-D-galactopyranoside
YM motif	Tyrosine-rich motif
β-Gal	β-Galactosidase